



**Universidad de Valladolid**

SCHOOL OF INDUSTRIAL ENGINEERING

DEPARTMENT OF SYSTEMS ENGINEERING AND  
AUTOMATIC CONTROL

PHD THESIS:

Energy generation and recovery by Pressure  
Retarded Osmosis (PRO): Modeling and  
experiments.

Thesis submitted by Khaled Touati for the degree of Doctor  
of Industrial Engineering in the University of Valladolid.

Supervised by:

Fernando Tadeo

2015





# Acknowledgements

I would like to express my appreciation to the following persons, who have helped me during the years of my PhD candidature.

To my supervisor, Professor Fernando Tadeo, for his kind help, advices, patience, supervision, and this important opportunity he gave me.

To the reviewers of the thesis, Professors Mohamed Safi, Hamza Elfil and Joon Ha Kim, for their time, feedback and nice comments.

To the members of the jury, for their willingness and feedback.

To my colleagues from the H2Ocean project for their support.

To my colleagues from the department of Systems Engineering and Automatic Control of the University of Valladolid (Spain).

To my colleagues from Fraunhofer Institute for Interfacial Engineering and Biotechnology, especially Dr. Thomas Schiestel and Christopher Haenel.

To my colleagues from the center of researches and water technologies (CeRTE) – BorjCedria (Tunisia) for their support and encouragements.

To my parents for their patience and support during my entire career.

To my wife Zainab for the support, care and patience.

To all the members of my family.

To my friends, Haithem, Walid, Borhane, Saber, Klai, Mohamed SBS, Hassan, Seddik, Rochdi, and others for their help and advices.

To the person who changed my life, Abdullah Al Harari.



# Contenu

## Aknowledgements

## Contents

### Chapter 1 : Introduction

1. Problem statement .....	1
2. Pressure Retarded Osmosis (PRO).....	1
3. Objectives of the thesis .....	2
4. Organization of the dissertation.....	3

### Chapter 2: Pressure Retarded Osmosis: State of the art

1. Introduction.....	7
2. Salinity gradient energy.....	7
3. Gibbs free energy of mixing .....	9
4. Pressure Retarded Osmosis .....	10
4.1 Osmotic processes.....	10
4.1.1 Reverse Osmosis.....	10
4.1.2 Forward Osmosis.....	11
4.1.3 Pressure Retarded Osmosis .....	11
4.2 Basic concept of Pressure Retarded Osmosis .....	11
4.2.1 Water and salt fluxes across a PRO membrane.....	12
4.2.2 Concentration polarization.....	15
4.2.3 PRO power density .....	17
4.3 Developments of PRO .....	19
4.3.1 Temporal sequence of the PRO development.....	19
4.3.2 PRO models development.....	22
4.3.3 PRO membrane development .....	25
4.4 Integration of PRO with desalination systems .....	31
4.5 PRO limitations and suggested solutions.....	42
4.5.1 Membrane fouling.....	42
4.5.2 Membrane scaling .....	45
4.5.3 Concentration polarization.....	47
4.5.4 Membrane deformation.....	47
4.6 PRO cost.....	47

4.7	Environmental impact.....	51
5.	Final consideration and Conclusions .....	53

### **Chapter 3: Water flux and power density in PRO**

1.	Problem statement .....	65
1.	Problem statement .....	66
2.1	Basic models for water and salt fluxes.....	66
2.2	Concentration polarization.....	67
2.2.1	Internal concentration polarization (ICP).....	68
2.2.2	External concentration polarization (ECP).....	69
2.3	Model of the water flux $J_w$ .....	71
2.4	Model of the temperature profile through the membrane.....	72
3.	Materials and methods.....	77
3.1	Model validation.....	77
3.1	Model validation.....	77
3.1	Model validation.....	77
4.	Results and discussion .....	79
4.1	Model validation.....	79
4.2	Effect of the concentrations of feed and draw solutions .....	82
4.3	Effect of the flow rate velocity.....	84
4.4	Effect of the bulk temperatures on the membrane temperature distribution.....	85
4.5	Effect of the bulk temperatures on the membrane parameters.....	86
4.5.1	Effect of the temperatures on the water permeability coefficient A .....	86
4.5.2	Effect on the salt permeability coefficient B.....	88
4.5.3	Effect on the structure parameter $s$ .....	89
4.6	Study of the reverse solute diffusion.....	91
5	Conclusions .....	94

### **Chapter 4: Effect of the Reverse Salt Flux on PRO**

1.	Introduction.....	100
2.	Theory .....	101
2.1	Modeling the reverse salt flux .....	101
2.2	Reverse salt flux $J_s$ .....	107
3.	PRO bench-scale and membranes .....	108

4.	Effect of the operating conditions on the reverse salt flux.....	109
4.1	Effect of the osmotic pressure difference .....	109
4.2	Effect of the cross flow velocity .....	113
4.3	Effect of the membrane orientation.....	115
4.5	Effect of the draw solution composition .....	118
4.6	Effect of the solutions temperature .....	120
5.	Theoretical discussion of the ratio $J_s/J_w$ .....	123
6.	Implications of the Reverse salt flux for full-scale power plants.....	125
7.	Conclusion .....	127

## **Chapter 5: Effect of the temperature on hydrodynamics and PRO membrane parameters**

1.	Introduction.....	135
2.	PRO background .....	136
3.	Experimental .....	139
3.1	Membranes.....	139
3.2	PRO bench-scale.....	139
3.3	Chemicals .....	140
4.	Effect of the operating temperature on the feed and draw solution chemistry.....	140
4.1	The Osmotic Pressure.....	140
4.2	The diffusion coefficient D .....	142
5.	Effect of the operating temperature on the hydrodynamic parameters .....	143
5.1	Reynolds, Schmidt and Sherwood numbers.....	143
5.2	The boundary layer thickness $\delta$ .....	148
6.	Effect of the operating temperature on the membrane parameters.....	150
6.1	<i>Effect of the temperature on the solute resistivity K</i> .....	152
6.2	Effect of the temperature on the water flux $J_w$ .....	154
7.	CONCLUSION .....	157

## **Chapter 6: Integration of PRO in desalination processes**

1.	Introduction.....	164
2.	Motivation.....	164
3.	Energy consumption of the desalination processes.....	166
4.	Energy recovery from MED system .....	169

4.1	Methodology .....	169
4.2	Application to a case study .....	169
5.	PRO integration in Reverse Osmosis .....	174
5.1	Description of the case study .....	175
5.2	First RO-PRO configuration .....	177
5.2.1	Methodology .....	177
5.2.2	RO-PRO modeling .....	178
5.3	Second RO-PRO configuration .....	191
5.3.1	Methodology .....	191
5.4	RO model results .....	191
5.5	PRO model results .....	193
5.5.	RO-PRO model results .....	196
6.	Conclusions .....	199
	Final Conclusions and further work .....	204
	Spanish abstract .....	207
	List of Acronyms .....	210
	List of Tables .....	212
	List of Figures .....	214
	List of Publications .....	217





# Chapter 1: Introduction

## 1. Problem statement

Due to economic development and the continuous rise in population, the demand for energy is increasing [1]. The world is facing unprecedented challenges for energy supply because of the decrease in oil and gas reserves, aggravated by the emissions of greenhouse gases [2]. Many researchers are focusing on alternative energy sources to fulfill this demand [3]: solar, wind, tidal wave, and biomass, have been studied to provide safe and sustainable energy sources. However, high installation costs, coupled with the uneven availability distribution, are still preventing them from being widely used. Affordable, clean, safe, and adequate energy sources remain one of the world's biggest challenges.

Water and energy are intrinsically linked; both are required to maintain an adequate standard of living [4]. Today, energy is not yet sufficiently abundant in any form that may be used sustainably to increase water supplies. Reuse of water makes great technical sense, and this approach must be explored and applied to its greatest practical extent. The desalination of seawater is the second largest method, after fresh water treatment, for water supply to communities and cities [5]. Reverse osmosis (RO), and thermal desalination processes like multi-effect distillation (MED), are the most common processes for seawater desalination. Unfortunately, the major problem in these processes is the high energy requirements for seawater desalination [5]. Consequently, it becomes a necessity to find technologies that have a low environmental impact to fulfill the need of water and energy.

## 2. Pressure Retarded Osmosis (PRO)

Pressure Retarded Osmosis (PRO) is the process through which osmotic energy can be harnessed and power generated [6]. In a typical PRO process, water molecules are spontaneously transported through a semi-permeable membrane from a low salinity stream (such as river water, brackish or waste water) at ambient pressure into a pressurized high salinity stream (seawater or brine), with the aid of the osmotic pressure gradient across the membrane. Power is then obtained by depressurizing a

portion of the diluted seawater through a hydro-turbine [7]. It has been estimated that up to 0.8 kWh can be generated when 1 m<sup>3</sup> of river water flows into seawater. Thus, it is estimated that the global energy production potential of PRO is around 2,000 TWh per year [8].

A review of published material and experimental data on pressure retarded osmosis (PRO) showed increasing interest in PRO for power generation in two time periods, the 1970s -for 20 years-, and significant attention over the past decade- the 2000s-, with increasing oil prices. Although the concept of PRO was first reported by Pattle in 1954 [9], the method has been improving over the years, particularly after the opening of the first osmotic power plant prototype by the Norwegian state-owned power company, Statkraft, in 2009. The plant followed the proposal plant by Loeb and was designed to generate 10 kW [10]. Work is currently being done to overcome some of the difficulties of the technology, such as the high price of the membrane and its durability, the fouling and scaling, and the concentration polarization.

### **3. Objectives of the thesis**

The main objectives of this investigation are:

1. To develop a model of the water flux for a PRO flat sheet membrane that includes all the limitation factors of the PRO process, such as the concentration polarization and the salt leakage. This model will be validated using lab-scale experiments. The model will be extended to a large-scale PRO membrane.
2. To develop a model for salt flux diffusion in PRO that reproduces the behavior of the reverse salt diffusion across the membrane, in order to understand the decrease in performance, and to suggest solutions for better PRO membranes. This model will also be validated using lab-scale experiments.
3. To study the effect of the operating conditions (concentrations, temperature, pressure, etc.) on the performance of the PRO in realistic conditions.
4. To develop a model to quantify the temperature distribution inside a PRO membrane as a function of the solution temperatures.
5. To study the feasibility of integrating PRO within desalination units to improve their performance.

#### 4. Organization of the dissertation

This document contains 6 chapters distributed as follows:

- ❖ The first chapter (the current one) contains a brief introduction presenting the motivation, a brief discussion of the PRO process (that will be extended further in the second chapter), and the objectives of this thesis.
- ❖ The second chapter presents the state of the art of PRO, since the discovery of the process to the present.
- ❖ The third chapter deals with the development of a model reproducing the water flux. The model is also validated and used to study the effect of the operating conditions on the water flux and, subsequently, on the power density.
- ❖ The fourth chapter contains the development of a model reproducing the salt flux diffusion. After being validated, the model was used to study the effect of the operating conditions on reverse salt diffusion and its impact on power plants.
- ❖ The fifth chapter deals with the effect of temperature on the hydrodynamics and the membrane parameters in PRO based on the models developed in the previous chapters.
- ❖ The sixth chapter contains a study of the integration of PRO within desalination units (MED and RO) and the feasibility of this integration.

## REFERENCES OF CHAPTER 1

- [1] T.S. Chung, X. Li, R.C. Ong, Q.C. Ge, H.L. Wang, G. Han, Emerging forward osmosis (FO) technologies and challenges ahead for clean water and clean energy applications, *Curr Opin Chem Eng* 1 (2012) 246–257.
- [2] A. Lewis, S. Estefen, J. Huckerby, W. Musial, T. Pontes, J. Torres-Martinez, Ocean energy, in: O. Edenhofer, R. Pichs-Madruga, Y. Sokona, K. Seyboth, P. Matschoss, S. Kadner, T. Zwickel, P. Eickemeier, G. Hansen, S. Schlömer, C. von Stechow (Eds.), *IPCC Special Report on Renewable Energy Sources and Climate Change Mitigation*, Cambridge University Press, Cambridge and New York, 2011.
- [3] J.W. Post, J. Veerman, H- V.M. Hamelers, G- J.W. Euverink, S.J. Metz, K. Nymeyer, J.N.C. Buisman, Salinity-gradient power: Evaluation of pressure-retarded osmosis and reverse electrodialysis, *J. Membr. Sci.* 288 (2007) 218–230.
- [4] M. D. Bartos, M. V. Chester, The Conservation Nexus: Valuing Interdependent Water and Energy Savings in Arizona, *Environ. Sci. Technol.* 48(2014) 2139–2149.
- [5] A. Altaee, G. Zaragoza, A. Sharif, Pressure retarded osmosis for power generation and seawater desalination: Performance analysis, *Desalination* 344 (2014) 108–115.
- [6] S. Loeb, Osmotic power plants, *Science*, 189(1975) 654–655.
- [7] S. Loeb, F. Van Hessen, D. Shahaf, Production of energy from concentrated brines by pressure retarded osmosis. II. Experimental results and projected energy costs, *J. Membr. Sci.* 1 (3) (1976) 249–69.
- [8] A.T. Jones, W. Finley, Recent Developments in Salinity Gradient Power, *OCEANS 2003 Proceedings* 4 (2003) 2284–2287.
- [9] R.E. Pattle, Production of electric power by mixing fresh and salt water in the hydroelectric pile. *Nature* 174 (1954) 660–660.
- [10] Statkraft Press Centre, Crown princess of Norway to open the world's first osmotic Powerplant, 2009 <http://www.statkraft.com/>.





## Chapter 2:

# Pressure Retarded Osmosis: State of the art

### 1. Introduction

The global primary energy demand has doubled between 1971 and 2012, mainly relying on fossil fuels [1]. This affects the world's environment in aspects such as climate change, and other long term effects mainly caused by the increase in quantity of greenhouse gases (GHGs) emissions [2]. Moreover, the present use of fossil fuels such as oil and natural gas will result in an expected depletion in 2050 onwards [3]. Each of these concerns should provide enough motivation for drastically reducing the use of fossil fuels. Therefore, the need of renewable energy sources has increased during the last decades in order to meet the world energy demand and progressively divert fossil energy sources [4]. One of these new renewable energy sources is the so-called 'Blue Energy' or 'Salinity Gradient Power' (SGP).

### 2. Salinity gradient energy

Salinity gradient power is the energy created from the difference in salt concentration between two fluids, commonly fresh and salt water. When a river runs into a sea, spontaneous mixing of fresh and salt water occurs. This natural process is irreversible; no work is attained from it. However, if the mixing is done (partly) reversibly, work can be obtained from the mixing process [4]. Approximately 0.70–0.75 kWh (2.5–2.7 MJ) is dissipated when 1m<sup>3</sup> of freshwater flows into the sea [5], meaning that 1m<sup>3</sup>.s<sup>-1</sup> of freshwater can potentially generate 2.5–2.7 MW. Helfer et al. [2] gave some estimation about the maximum energy that could be theoretically produced the energy from the mixing of freshwater with saline water from five different sources (summarized in Table 2.1). The total technical potential for salinity gradient power is estimated to be around 647 gigawatts (GW) globally (compared to a global power capacity in 2011 of 5456 GW), which is equivalent to 5177 terawatt-hours (TWh), or 23% of electricity

consumption in 2011 [5]. The report [6] by Kachan& Copointed out that the osmotic power generation is potentially worth three times more than solar and wind power generation combined. Osmotic power reportedly could generate up to 1,700 TWh of electricity each year by 2030 that is around 50% of Europe's total energy demand.

Table 2.1: Theoretical extractable energy from the mixing of fresh water with saline water from different sources [2].

<i>Saline water source</i>	<i>Concentration (g/l)</i>	<i>Theoretical energy (kWh/m<sup>3</sup>)</i>
Seawater	35	2.7
SWRO brine	70	5.4
Great Salt Lake	485	37.5
Dead Sea	657	50.7

Renewable energy could reduce global greenhouse gas emissions by 2741 Mt by 2030 under accelerated environmental policies, according to the International Energy Agency [7]. EU leaders have agreed on a binding target of cutting emissions 40% on 1990 levels by 2030. Annual coal-fired generation is projected to double from 7,400 TWh in 2006 to 9,500 TWh in 2015 and 13,600 TWh in 2030 [7]. Replacing current and planned coal-fired power plants with salinity power plants (40% of energy conversion) could reduce global greenhouse gas emissions by 10 Pg CO<sub>2</sub>-eq/year (~ 1010 tonnes/year). This means a potential reduction of 40% of current global energy-related greenhouse gas emissions [8].

The most investigated techniques to generate energy from SGP are Pressure Retarded Osmosis (PRO) and Reversed Electrodialysis (RED) where, respectively, transport of water or ions through semi-permeable membranes takes place [9,10,11]. Both PRO and RED have a large potential for producing energy for the coming years and they could be used for different applications [4,11]. This dissertation concentrates on PRO because it could achieve greater efficiencies and higher power densities than RED [11]. PRO is more suitable to extract energy from a range of salinity gradients.

### 3. Gibbs free energy of mixing

The Gibbs energy of mixing  $\Delta_{mix}G = \Delta H_{mix} - T\Delta S_{mix}$  is the theoretical non-expansion work that can be produced from mixing. It determines whether mixing at constant temperature and pressure is a spontaneous process. This quantity combines two physical effects: the enthalpy of mixing  $\Delta H_{mix}$ , which is a measure of the energy change, and the entropy of mixing  $\Delta S_{mix}$ :

$$\Delta_{mix}G = \Delta H_{mix} - T\Delta S_{mix} \quad (2.1)$$

For an ideal gas mixture or an ideal solution, there is no enthalpy of mixing ( $\Delta H_{mix} = 0$ ); the expression of the free Gibbs energy of mixing a concentrated and a diluted solutions is [4,12]:

$$\Delta_{mix}G = \Delta G_b - (\Delta G_c + \Delta G_d) = -(n_c + n_d)T\Delta_{mix}S_b + (n_cT\Delta_{mix}S_c + n_dT\Delta_{mix}S_d) \quad (2.2)$$

where:

The subscript *c*: corresponds to the concentrated solution.

The subscript *d*: corresponds to dilute solution.

The subscript *b*: corresponds to the resulting brackish solution.

*n*: the amount (moles).

*T*: the absolute temperature.

$\Delta_{mix}S$ : the contribution of the molar entropy of mixing (J/mol/K) to the total molar entropy of the corresponding electrolyte solution, according to:

$$\Delta_{mix}S = -R \sum_i x_i \ln x_i \quad (2.3)$$

where *R* is the universal gas constant (8.314 J/mol/K), and *x* the mole fraction of component *i* (For simulated seawater, *i* = Na, Cl, H<sub>2</sub>O). Vermaas et al. [10] showed that the theoretically Gibbs free energy obtained by mixing simulated seawater (30 g/l NaCl) and simulated river water (1g/l NaCl), both at a flow rate of 1 m<sup>3</sup>/s, is 1.39 MJ. Post et al. [4] presented some results of the theoretically available amount of energy (MJ) from mixing 1 m<sup>3</sup> of a diluted and 1 m<sup>3</sup> of a concentrated sodium chloride solution (Fig. 2.1).

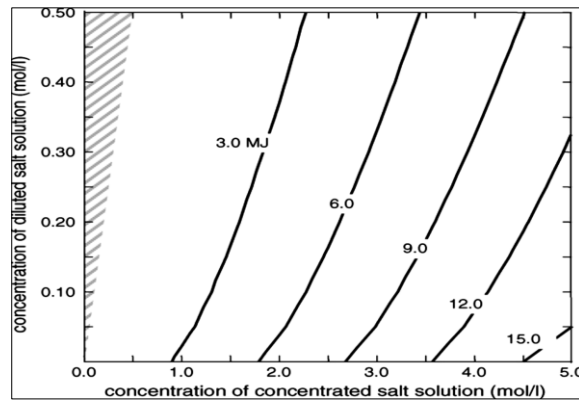


Fig. 2.1: Theoretically available amount of energy (MJ) from mixing  $1\text{m}^3$  of a diluted and  $1\text{m}^3$  of a concentrated sodium chloride solution ( $T = 293\text{ K}$ ). [4]

## 4. Pressure Retarded Osmosis

### 4.1 Osmotic processes

The Osmosis phenomenon was already observed by Nollet in 1748 [13]. When two solutions of different concentration are separated by a semipermeable membrane (i.e. one which is permeable to the solvent but impermeable to the solute), osmotic pressure  $\pi$  arises due to the difference in the chemical potential. Water flows from the high chemical potential side to the low one until equilibrium is reached. The increased volume of water in the low chemical potential side builds up a hydrodynamic pressure difference, which is called the osmotic pressure difference  $\Delta\pi$ . Osmotic processes include Reverse Osmosis (RO), Forward Osmosis (FO), and Pressure Retarded Osmosis (PRO).

#### 4.1.1 Reverse Osmosis

Reverse Osmosis (RO) is a process that uses semipermeable membrane to separate dissolved salt from water. It is the process of Osmosis in reverse. Whereas Osmosis occurs naturally without energy required, to reverse the process of osmosis energy has to be applied to the most saline solution [14]. A reverse osmosis membrane is then a semi-permeable membrane that allows the passage of water molecules. However the water has to be pushed through the RO membrane by applying pressure  $\Delta P$  greater than the naturally occurring osmotic pressure, in order to migrate pure water from the saline solution while holding back the majority of salt (Fig. 2.2).

#### 4.1.2 Forward Osmosis

Forward Osmosis uses the osmotic pressure differential ( $\Delta\pi$ ) across a semi-permeable membrane, that separates two solutions with different concentration, as the driving force for transport of water from low concentrated solution to high concentrated solution (Fig. 2.2) [14].

#### 4.1.3 Pressure Retarded Osmosis

Pressure Retarded Osmosis can be viewed as an intermediate process between FO and RO, where hydraulic pressure is applied in the opposite direction of the osmotic pressure gradient (similar to RO). However, the net water flux is still in the direction of the concentrated draw solution (Fig. 2.2) [14].

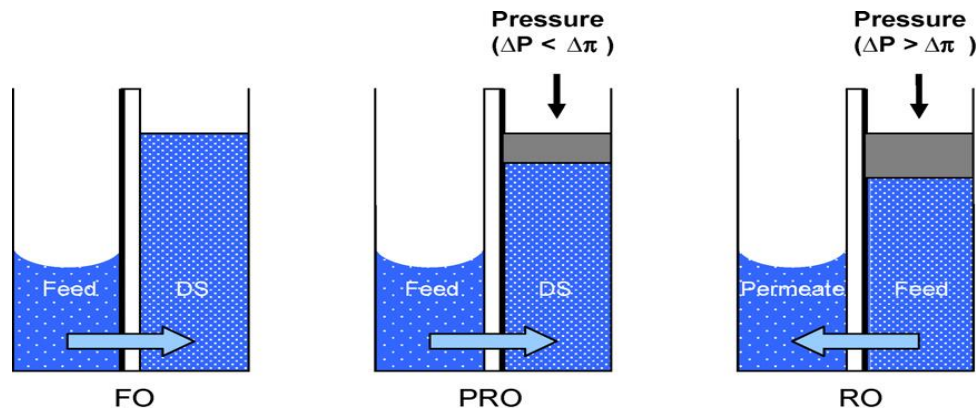


Fig. 2.2: Representation of water flow in FO, PRO, and RO (The thick black line represents the membrane active layer).

#### 4.2 Basic concept of Pressure Retarded Osmosis

As it has been seen, Pressure Retarded Osmosis is a membrane-based process that generates energy from salinity gradients [15]. The principle of power generation by PRO is illustrated in Fig. 2.3. When concentrated seawater and diluted fresh water (i.e. river water) are separated by a semipermeable membrane, water will diffuse from the feed side into the draw solution side (i.e. seawater side), that is pressurized. To recover the hydraulic energy generated the pressurized diluted seawater is then split into two streams: one going through a hydro-turbine to generate electric power, and the other one passing through a pressure exchanger to assist in pressuring the inlet seawater, and thus maintaining the circulation [16]. The main variables of the process are now discussed in detail.

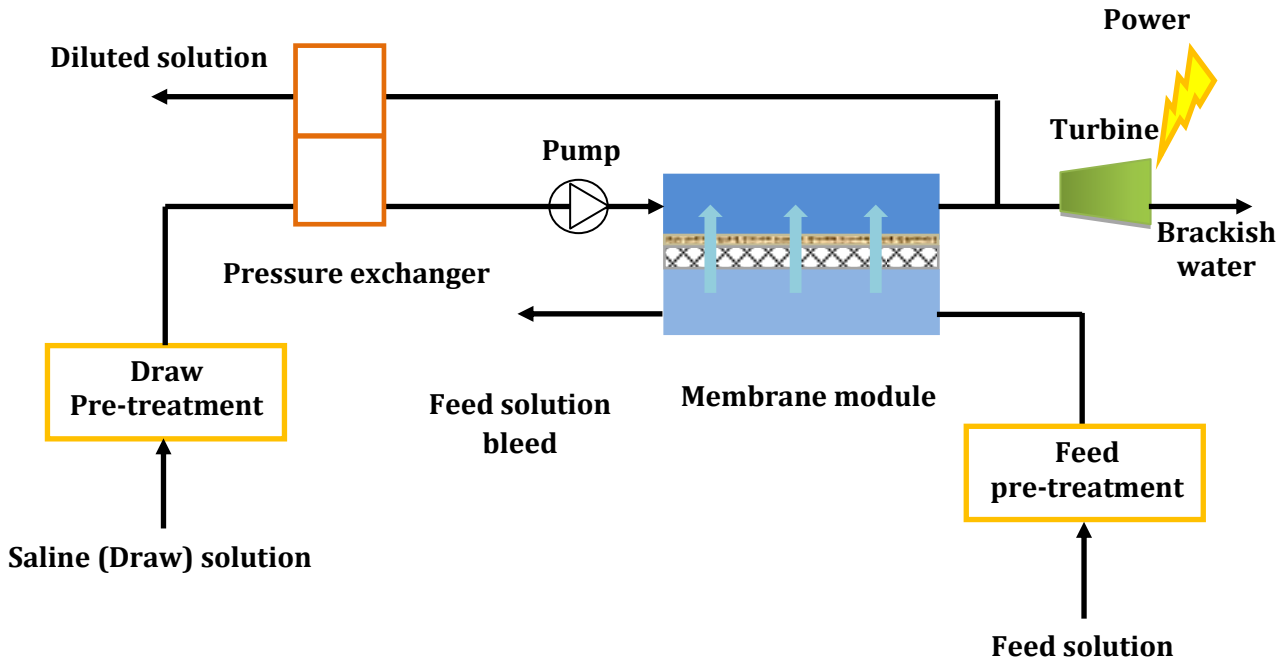


Fig. 2.3: Schematic of a PRO power plant.

#### 4.2.1 Water and salt fluxes across a PRO membrane

##### a. Ideal membrane with perfect hydrodynamics

Theoretically, the water permeation flux  $J_w$  across an ideal semi-permeable thin film that allows water passage but fully rejects all other solute molecules or ions can be expressed in terms of water permeability coefficient  $A$ , the osmotic pressure difference  $\Delta\pi$  and the trans-membrane hydraulic pressure difference  $\Delta P$  as follows [17]:

$$J_w = A(\Delta\pi - \Delta P) = A(\pi_{Draw} - \pi_{Feed} - \Delta P) \quad (2.4)$$

where  $\pi_{Draw}$  and  $\pi_{Feed}$  are the bulk osmotic pressures of the draw and feed solutions, respectively. This equation is valid in an ideal system with a perfectly selective membrane (the membrane allows only the passage of water molecules but rejects all solutes) and perfect hydrodynamics in the draw and feed channels so that the concentrations at the membrane surface are equal to the bulk concentrations.

*b. Realistic membrane with reverse salt flux and concentration polarization.*

With a realistic membrane and hydrodynamics, an amount of salt permeates the membrane from the draw solution to the feed solution due to the concentration gradient across the membrane, and the effect of hydrodynamics is present. A schematic presentation of a PRO membrane at steady state is shown in Fig. 2.4.

Three phenomena occur to reduce the trans-membrane water flux:

- ❖ First, the porous support layer induces Internal Concentration Polarization (ICP): this effect takes place within the porous support, increasing the local concentration at the active-support interface, from  $C_{F,b}$  to  $C_{F,m}$ , which detrimentally enhances  $\pi_{F,m}$  (the osmotic pressure of the feed solution at the interface active-support layers) by increasing the solute concentration at the feed membrane interface reducing the transmembrane driving force.
- ❖ Second, without perfect hydrodynamics in the draw solution flow channel, dilutive External Concentration Polarization (*ECP*) occurs in the mass transfer boundary layer of the draw solution, reducing the local concentration at the active layer from  $C_{D,b}$  to  $C_{D,m}$ , which lowers  $\pi_{D,m}$  (the osmotic pressures of the draw active layer surface membrane).
- ❖ Lastly, because the membrane is no longer perfectly selective, reverse salt flux takes place, resulting in uncontrolled mixing and therefore reducing the energy extraction in the process.

As consequences of these effects, mass transfer kinetics of water across the semipermeable membrane under applied hydraulic pressure,  $\Delta P$  is more precisely described as:

$$J_w = A(\Delta\pi_m - \Delta P) = A(\pi_{D,m} - \pi_{F,m} - \Delta P) \quad (2.5)$$

The reverse salt flux,  $J_s$ , is described as [18]: (2.6)

$$J_s = B(C_{D,m} - C_{F,m}) \quad (2.7)$$

where,  $B$  is the salt permeability coefficient of the membrane active layer and  $C_{D,m}$  and  $C_{F,m}$  are the solute concentrations at the interface of the active and support

layers, respectively. A typical concentration profile through the membrane is shown in Fig. 2.4.

The salt permeability coefficient  $B$  of a semi-permeable membrane can be obtained from RO experiments [17] and is given by:

$$B = \frac{A(1-R_S)(\Delta\pi - \Delta P)}{R_S} \quad (2.8)$$

where  $R_S$  is the salt rejection defined as:

$$R_S = 1 - \frac{C_P}{C_F} \quad (2.9)$$

with  $C_P$  the salt concentration in the permeate solution obtained in the RO experiments and  $C_F$  the one of the feed solution.

The salt reverse flux can be expressed as a function of  $J_w$  using van't Hoff factor  $\beta$  as [19]:

$$J_s = \frac{B}{\beta RT} \left( \frac{J_w}{A} + \Delta P \right) \quad (2.10)$$

where  $R$  is the universal gas constant, and  $T$  is the absolute temperature.

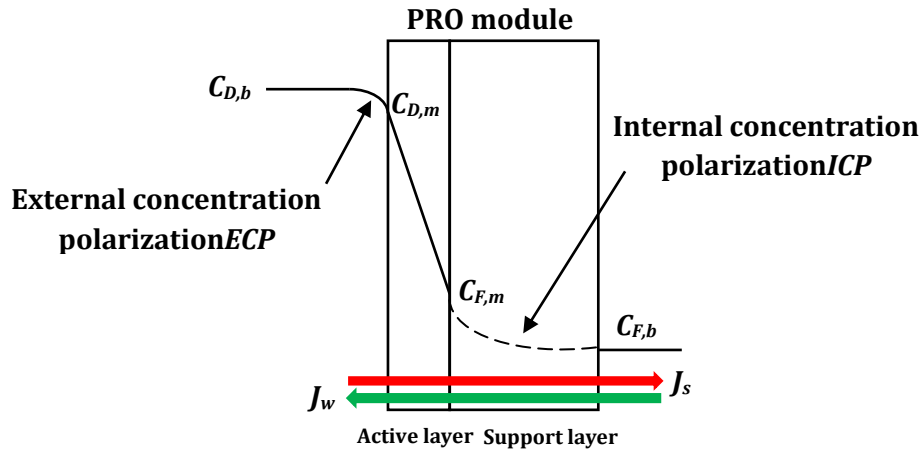


Fig. 2.4: Schematic representation of the concentration profile over the membrane, and the directions of the water flux  $J_w$  and the salt flux  $J_s$  across a PRO membrane at steady state. Concentrative ECP in the feed solution is assumed to be negligible.

#### 4.2.2 Concentration polarization

Concentration polarization is a phenomenon that can severely reduce the effective osmotic pressure difference across the membrane, due to the accumulation or depletion of solutes near an interface [20]. As a result of water crossing the membrane, in PRO process the solute concentrates on the feed side of the membrane surface and dilutes on the permeate side. Because the membranes used in PRO are typically asymmetric (comprised of a thin dense layer on top of a porous support layer), concentration polarization occurs externally on the dense layer side and internally in the support layer side. Both internal and external concentration polarization reduce the effective osmotic pressure difference across the membrane.

##### 4.2.2.1 Internal Concentration Polarization

When a non-ideal composite membrane is operated in a standard PRO process (with the active layer facing the draw solution), water flows from the fresh water through the support and active layers into the draw solution, while salt permeates from the salty water across the membrane skin and the support layer into the fresh water. Therefore, there exists a salt gradient in the membrane support (see Fig. 2.4). This gradient will result in concentrative Internal Concentration Polarization ICP, lowering the osmotic force driving the water across the membranes [19, 20].

ICP occurs when the thin film is supported by a porous substrate: based on the mass balance in the porous substrate layer, Lee et al. developed a theoretical model for the PRO process which suggested that membranes with high water permeation and high salt rejection are essential for high PRO performance [17]. The mass transport of salt in the membrane support, and in each of the boundary layers, will balance the sum of the convective salt transport and the diffusive salt transport due to the gradient in salt concentration. Hence, this balance of transport of salt can be described by:

$$\frac{\varepsilon D}{\tau} \frac{dC}{dx} - J_w C = J_s \quad (2.11)$$

where  $C$  is the salt concentration at position  $x$ ,  $D$  is the diffusion coefficient,  $\varepsilon$  is the porosity and  $\tau$  is the tortuosity of the support layer. Lee et al. [17] derived an expression for modeling this phenomenon in PRO, which Loeb et al. [21] later related to water flux and other membrane constants:

$$K = \left( \frac{1}{J_w} \right) L n \frac{B + A\pi_{D,m} - J_w}{B + A\pi_{F,m}} \quad (2.12)$$

where  $K$  is the solute resistivity for diffusion within the porous support layer, defined by:

$$K = \frac{\tau t_s}{\varepsilon D} \quad (2.13)$$

where  $t_s$  is the thickness of the support layer.

#### 4.2.2.2 External Concentration Polarization

##### a. Concentrative ECP

In PRO process, concentrative ECP occurs when the support layer of the membrane faces the feed solution [22]. The water flow transports the solute from the bulk solution to the surface of the active layer. Water permeates this layer leaving the solute behind with higher concentrations. Thus, the feed solutes would be expected to accumulate at the surface of the active layer and cause the increase of

the feed concentration ( $C_{F,b} \rightarrow C_{F,m}$ ) (Fig. 2.4). The driving force must overcome this increased concentration, in order for water flux to occur. As a result, the effective osmotic pressure difference would reduce ( $\pi_{F,b} \rightarrow \pi_{F,m}$ ). McCutcheon et al. proved that  $\pi_{F,m}$  is related to  $\pi_{F,b}$  by what is called the concentrative ECP modulus assuming that the ratio of the membrane surface concentration of feed solute to the bulk concentration is equal to the corresponding ratio of osmotic pressures [23]:

$$\frac{\pi_{F,m}}{\pi_{F,b}} = \exp\left(\frac{J_w}{k}\right) \quad (2.14)$$

where  $k$  is the mass transfer coefficient defined as:

$$k = \frac{ShD}{d_h} \quad (2.15)$$

with  $Sh$  the Sherwood number and  $d_h$  the hydraulic diameter of the flow channel. It should be pointed out that when the feed solution concentration is negligible, the concentrative ECP can also be considered negligible.

#### *b. Dilutive ECP*

Dilutive *ECP* occurs on the draw side of the membrane in *PRO* mode. It is a phenomenon similar to the concentrative *ECP*: on the draw side, solutes are diluted at the surface, as water enters from the feed side, giving rise to dilutive *ECP*. As a result, the effective osmotic pressure difference would reduce ( $\pi_{D,b} \rightarrow \pi_{D,m}$ ). Dilutive *ECP* is expressed using the dilutive *ECP* modulus [23]:

$$\frac{\pi_{D,m}}{\pi_{D,b}} = \exp\left(-\frac{J_w}{k}\right) \quad (2.16)$$

#### 4.2.3 *PRO power density*

In terms of energy production, the power density  $W$  is defined as osmotic energy output per unit of membrane area, which can be calculated by the product of the trans-membrane pressure  $\Delta P$  and the water flux  $J_w$  permeating across the membrane [24]:

$$W = J_w \Delta P = A(\Delta\pi - \Delta P)\Delta P \quad (2.17)$$

By differentiating Eq. (2.15) with respect to  $\Delta P$ , the maximum power density can be obtained: this corresponds to a hydrostatic pressure difference equal to half of the osmotic pressure difference across the membrane,  $\Delta\pi/2$ . Then, the maximum of energy that can be produced is:

$$W_{max} = A \frac{\Delta\pi^2}{4} \quad (2.18)$$

Fig. 2.5 shows the variation of the water flux  $J_w$  and the power density  $W$  as a function of  $\Delta P$  for FO ( $P = 0$ ) PRO ( $\Delta P < \Delta\pi$ ), and RO (where  $\Delta P > \Delta\pi$ ) under ideal conditions.

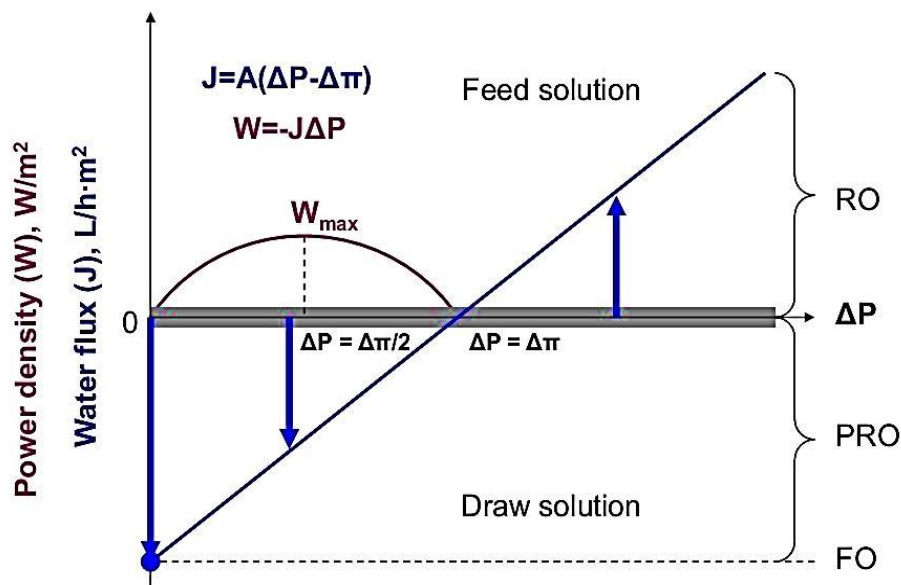


Fig. 2.5: Magnitude and direction of  $J_w$  for FO, PRO, and RO and magnitude of  $W$  for PRO in an ideal case.

### *4.3 Developments of PRO*

In our point of view, the development of the PRO process was a result of two fundamental factors. The first one is the membrane fabrication progress which allowed reaching higher values of power density and proved the feasibility of the process. The second one is the good understanding of the process by developing mathematical models reproducing fluxes and power densities. In this section, a brief description of the history of PRO is presented concentrating on the development of the membranes and models.

#### *4.3.1 Temporal sequence of the PRO development*

Pressure Retarded Osmosis is a novel technology, although it already has a long history, starting from the first article that was published by Pattle in 1954 [26]. Pattle described how to use osmotic energy and semi-permeable membrane to produce power by mixing freshwater and saltwater in a Nature article, describing that when a volume  $V$  of a pure solvent mixes with a much larger volume of a solution of osmotic pressure  $\pi$ , the free energy released is equal to  $\pi V$ . No work was then published on PRO for around 20 years. Since then, the concept of PRO has received spasmodic attention, mainly in the form of design studies and economic viability evaluations, it has not been yet fully developed due to the inadequate separation capabilities of current semi-permeable membranes, the expected high cost and the relatively low trans-membrane water flux [16,17,18].

After the oil crisis in 1973, the subject of renewable energies was opened, so, from 1974 to 1976, four investigation papers were published about the feasibility of using PRO to produce energy [15,24,25,43]. The PRO process subject started to appear as a feasible solution. The challenge in PRO began with the schematic diagram of an osmotic energy convertor proposed by Norman [25] in 1974. He suggested that after freshwater permeated through a selective permeable membrane into a pressurized seawater chamber, the spill-over water would turn a water wheel to power a generator. One year later, Loeb and Norman [24] proposed PRO based on osmotic driven membrane process. The first experimental PRO data were published by Loeb et al. in 1976 [15] where hollow fiber seawater RO membrane were tested using freshwater in bore and pressurized brine in shell.

The principle was validated, although the performance was small due to the use of a RO membrane.

In 1978, Loeb and Mehta [27] published a paper introducing the role of the internal concentration polarization and discussing the strong adverse effect on the power generation by PRO. One year later, Loeb and Mehta [28] published an article investigating various operating conditions to prove the PRO concept and developed a model to predict flux in PRO; the measured power densities up to 3.27 W/m<sup>2</sup>, using a hypersaline draw solution. The result of the study showed that osmotic power could produce renewable energy if the design and production of a specific semi-permeable membrane was addressed. Jellinek and Masuda [29] proposed a construction of a cost-comparative PRO power plant in 1981. Lee et al. [17] developed a model considering the effect of the internal concentration polarization and neglecting the external concentration polarization, in order to evaluate the power density and water flux, from FO and RO experiments. Low water flux and power density, due to internal concentration polarization of RO membrane, were obtained in experimental results by Lee et al. and Mehta. Despite that, the model developed by Lee et al. [17] was a reference model for further developments. In 1990, the theoretical mechanical efficiency of several configurations of PRO plants was investigated by Loeb et al. [30]. It was found that the alternating-flow terrestrial PRO plant had the highest efficiency but required the use of two pressure vessels in addition to the usual PRO equipment. In parallel, Reali et al. [31] used numerical techniques to compute the profile of salt concentration in the porous support layer in PRO system showing the effect of membrane characteristics, such as the water permeability coefficient  $A$ , the salt permeation coefficient  $B$ , the effective salt diffusivity  $D$  and the support layer thickness  $t_s$ , on the water and salt permeation flux through an anisotropic membrane.

In 1998, Loeb studied the possibility of producing water using the Dead Sea [32]: depending on various configurations of the PRO system, the cost of produced electrical energy would be from 0.058 to 0.07 \$/KWh. During the same year, Seppälä et al. realized a theoretical study to optimize PRO [33]. They suggested that the system can be optimized either by maximizing the net power or maximizing the ratio between the net power and entropy generation. At the

beginning of the 2000s, Loeb continued his investigation on PRO applications now in the Great Salt Lake and found that the cost of the produced electrical energy would be 0.15 \$/KWh at this location [34]. Then, the pressure exchanger device (originally developed for RO applications) was then introduced to reduce internal power consumption, providing a cost-effective PRO system by Loeb in 2002 [35]. In 2004, Seppälä published a work suggesting that there is no proof that the apparent non-linearity of the osmotic pressure is caused by concentration polarization phenomena [36].

After that, the development of osmotic power has been promoted by Statkraft and executed by research groups in Germany, Norway, Netherlands, USA, Canada, Japan and Korea, increasing the power density of PRO membranes from less than 0.1 W/m<sup>2</sup> up to 3 W/m<sup>2</sup> [37]. The first prototype PRO installation was opened in Norway by Statkraft in 2009. The plant configuration followed the proposed schematic of plant by Loeb and was designed to generate 10 kW of power, firstly to confirm that the designed system can produce power on a reliable 24 h/d, and secondly to use the plant for further tests [38] (see Fig. 2.6).

Achilli et al. [39] expanded on the model developed by Lee et al. [17] by considering the external concentration polarization in an experimental and theoretical investigation into PRO system: power density that exceeded 5.1 W/m<sup>2</sup> was observed with a flat sheet cellulose triacetate (CTA) FO membrane. In 2011, Yip et al. fabricated a thin film composite PRO membrane with a polysulfone support layer and a polyamide active layer; they also developed a model for the water flux considering internal and external concentration polarizations, and salt flux leakage. Experimental results lead to a projected peak power density of 6.1W/m<sup>2</sup>. Since that time, several investigations have been published studying the parameters optimizing the PRO power density [39,40,41,46]. In parallel, several membranes had been fabricated for PRO, like spiral wound membranes and hollow fiber membranes. The progress of PRO membrane is studied in details in Section 4.3.2. Also, several works investigating the integration of PRO were published (this subject is left for Section 4.4.)

Unfortunately, in 2014, the Statkraft Company declared that it was discontinuing its efforts and leaving the PRO technology development to “other players in the global market”. *“Our main challenge has been to make the technology efficient*

enough to achieve energy production costs on par with competing technologies. With the current market conditions, we see that we cannot achieve this in the foreseeable future. There are other technologies which have developed enormously in recent years. These are more competitive and relevant investments for us in the future”, said Statkraft department manager Stein Erik Skilhagen [42]. However, research in PRO has not been suspended; many researchers are now carrying on developing the process and improving its performance [76,78,79,80]. In addition, other interesting PRO projects were launched such as “Mega-ton RO-PRO” in Fukuoka City- Japan (Fig. 2.10) that are starting to give results [72,97].

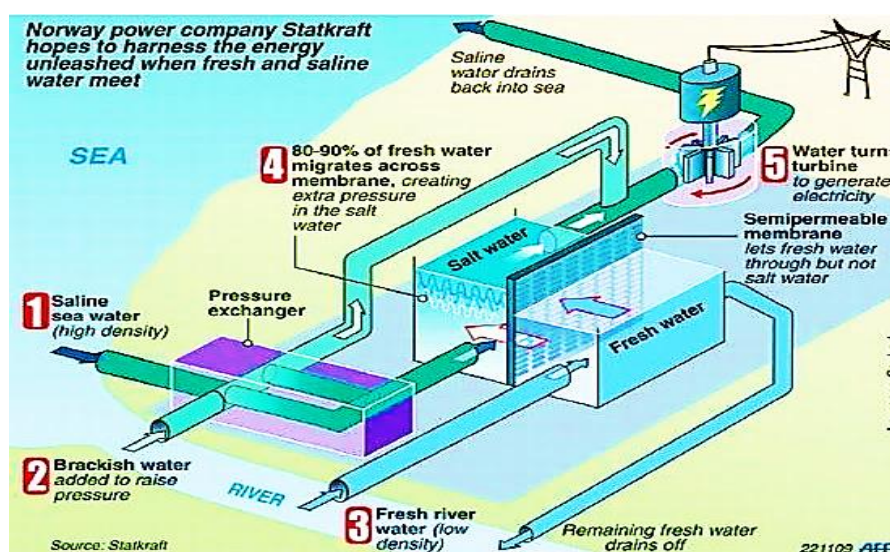


Fig. 2.6: Schematic diagram of the pilot PRO plant, constructed by Statkraft [38].

### 4.3.2 PRO models development

#### 4.3.2.1 Loeb model

The first PRO model was developed by Sidney Loeb in 1976 [43]. It was developed for a RO asymmetric hollow fiber membrane. Loeb considered that the porous substructure have the character of a boundary layer, in which water flux is a function of concentrations and of concentration gradients. Assuming that the salt flux,  $J_s$ , is negligible, the transport of water in the porous substructure is by diffusion only, the concentration is proportional to the osmotic pressure, and there is no external concentration polarization, the expression of the water flux developed was:

$$J_w = A \left( \pi_{Draw} - \pi_{Feed} \exp\left(\frac{\Delta X}{D_{sp}}\right) - \Delta P \right) \quad (2.19)$$

where  $\pi_{Draw}$  and  $\pi_{Feed}$  are the osmotic pressures of the draw and feed bulks, respectively,  $\Delta X$  is the thickness of the membrane and  $D_{sp}$  is the diffusion coefficient in the support layer.

#### 4.3.2.2 Lee model

The model developed by Lee et al. in 1981 was the first to consider concentration polarization in PRO [17]. Assuming that the external concentration polarization has been reduced to negligible levels by efficient stirring, and the ratio of salt concentrations is equal to the ratio of osmotic pressures, they derived an expression to model the effect of internal concentration polarization that gave the following PRO water flux model:

$$J_w = A \left( \pi_{D,m} \frac{1 - \frac{C_{F,b}}{C_{D,m}} \exp(J_w K)}{1 + \frac{B}{J_w} [\exp(J_w K) - 1]} \right) \quad (2.20)$$

where  $\pi_{D,m}$  is the osmotic pressure at the active layer in the draw bulk side,  $C_{F,b}$  and  $C_{D,m}$  are, respectively, the feed solution and the solute concentrations in the active layer of the draw bulk side, and  $K$  is the solute resistivity. The effect of the ICP corresponds to the term  $\exp(J_w K)$  in the water flux equation.

#### 4.3.2.3 Achili model

Achili et al. [39] expanded on the model developed by Lee et al. [17] by considering the external concentration polarization. Using the external concentration polarization modulus developed by [22], and assuming that  $C_{F,b}/C_{D,m} = \pi_{F,b}/\pi_{D,m}$ , Eq. (20) becomes:

$$J_w = A \left( \pi_{D,b} \exp(-J_w/k) \frac{1 - \frac{\pi_{F,b}}{\pi_{D,b}} \exp(J_w K) \exp(J_w/k)}{1 + \frac{B}{J_w} [\exp(J_w K) - 1]} \right) \quad (2.21)$$

where  $k$  is the mass transfer coefficient.

#### 4.3.2.4 Yip model

The previous models did not take into consideration the effect the reverse salt flux. In 2011, Yip et al. [18] modified the existing Lee model to incorporate the effect of ECP and the reverse permeation of the salt. Assuming that the osmotic pressure is linearly proportional to the salt concentration and neglecting the concentrative ECP, the water flux expression is:

$$J_w = \left( \frac{\pi_{D,b} \exp\left(-\frac{J_w}{k}\right) - \pi_{F,b}(J_w K)}{1 + \frac{B}{J_w} \left[ \exp(J_w K) - \exp\left(-\frac{J_w}{k}\right) \right]} \right) \quad (2.22)$$

where  $\pi_{D,b}$  and  $\pi_{F,b}$  are the osmotic pressures of the draw and feed bulks, respectively, and  $k$  is the mass transfer coefficient in the draw water side. The term  $\exp\left(-\frac{J_w}{k}\right)$  condenses the effect of the external concentration polarization. The effect of the reverse permeation of the salt gives the denominator of Eq. (2.22).

#### 4.3.2.5 Sivertsen model (for a hollow fiber PRO membrane)

The previous models are only applicable to flat sheet membranes. So, they should be modified according to the new spatial parameters when the geometry of the membrane changes. For example, Sivertsen et al. [44] developed a model for water transport in PRO asymmetric hollow fiber membranes. A structure parameter similar to the one for flat sheet membranes has been defined. Assuming a cylindrical geometry of a single hollow fiber, the equation describing the effective concentration difference in the active layer is presented as:

$$\Delta C_{skin} = \frac{C_s - C_f (r_0 + d_s / r_0)^{J_{vm} r_0 / D} (r_0 - \Delta x_{mem} / r_0 - \Delta x_{mem} - d_f)^{J_{vm} r_0 / D} (r_0 / r_0 - \Delta x_{mem})^{J_{vm} r_0 / D \phi}}{(r_0 + d_s / r_0)^{J_{vm} r_0 / D} + (B / J_{vm}) \left[ (r_0 + d_s / r_0)^{J_{vm} r_0 / D} (r_0 - \Delta x_{mem} / r_0 - \Delta x_{mem} - d_f)^{J_{vm} r_0 / D} (r_0 / r_0 - \Delta x_{mem})^{J_{vm} r_0 / D \phi} - 1 \right]} \quad (2.23)$$

where  $\Delta C_{skin}$  the concentration difference of salt over the membrane active layer,  $C_s$  and  $C_f$  are the draw and feed bulk solute concentrations, respectively,  $J_{vm}$  is the volume flux,  $d_s$  and  $d_f$  are the film thicknesses at the draw side and the feed side, respectively,  $D$  is the diffusion coefficient,  $\Delta x_{mem}$  is the membrane thickness,  $\phi$  is the porosity and  $r_0$  is the radial distance between the center of the hollow fiber and the active layer.

### 4.3.3 PRO membrane development

Pressure retarded osmotic and forward osmosis are similar technics, but differ in the purpose of each process: PRO is generally used to produce energy and FO to produce freshwater. The performance of both technics is strongly dependent on the membrane. The earlier studies on PRO were developed using reverse osmosis membranes. Severe internal concentration polarization was found due to the thick support layer, which leads to a very low permeate flow rate. The development of specific PRO membrane becomes a necessity to overcome the limitations of the process. Desalination using FO is less energetic comparing to RO process, which stimulated an interest to develop forward osmosis desalination. The rapid progress in forward osmosis membranes [45] opened up new perspectives for the development of PRO membranes. Suitable membranes are being developed following the information extracted from the mathematical models to improve the energy production.

The best characteristics of membranes for PRO should be:

- High density of the active layer for high solute rejection; a thin membrane with minimum porosity of the support layer for low ICP, and therefore, higher water flux.
- Hydrophobicity for enhanced flux and reduced membrane fouling.
- High mechanical strength to sustain hydraulic pressure.

Two main families of membrane are being developed for PRO: flat-sheet membranes and hollow-fiber membranes. Several studies carried out to improve the performance of both membranes families are now discussed.

#### 4.3.3.1 Flat-sheet membrane development

##### a. Cellulose acetate membrane

Cellulose is considered one of the most abundant natural polymers [46]. Cellulose acetate (CA) Cellulose is considered one of the most abundant natural polymers. It was first prepared in 1865 by heating cotton with acetic anhydride [47]. Cellulose acetate-based membranes have been used widely in the PRO process for power generation [39,58,59]. These membranes have several advantages such as high hydrophilicity, which promotes water flux and reduces membrane fouling, good mechanical strength, and relatively high tolerance to chlorine [48]. The hydrophilic

nature of cellulose acetate is desirable in osmotically driven membrane processes: wetting of the membrane reduces ICP and increases the water flux [49]. Based on the Preferential Sorption-Capillary Flow Model, Loeb and Sourirajan [61] developed cellulose acetate membrane for seawater desalination. The announcement of Loeb-Sourirajan membrane in 1960 opened up the golden era of R&D activities on membrane technologies [50]. During the 1990s, a special membrane for FO was developed by Osmotek Inc. (Albany, Oregon) (Hydration Technologies Inc. (HTI)). This membrane has been tested in a wide variety of applications by different research groups [39,51,52]. It is also used successfully in commercial applications of water purification for military, emergency relief, and recreational purposes. The HTI membrane revealed a good performance in PRO bench scale test [39]. However, Statkraft, the first PRO prototype plant, obtained in practice power densities of less than  $1.5 \text{ W/m}^2$  using these conventional cellulose acetate flat sheet membranes [53]. This value is far below the target power density of  $5 \text{ W/m}^2$  for the process to be commercially viable. Schiestel et al. [54] developed a cellulose acetate membrane with better performance than HTI membrane, with highly porous support layers with pressure stability up to 20 bar (Fig. 2.7). Table 2.2 presents some experimental results using flat sheet -based cellulose acetate membranes.

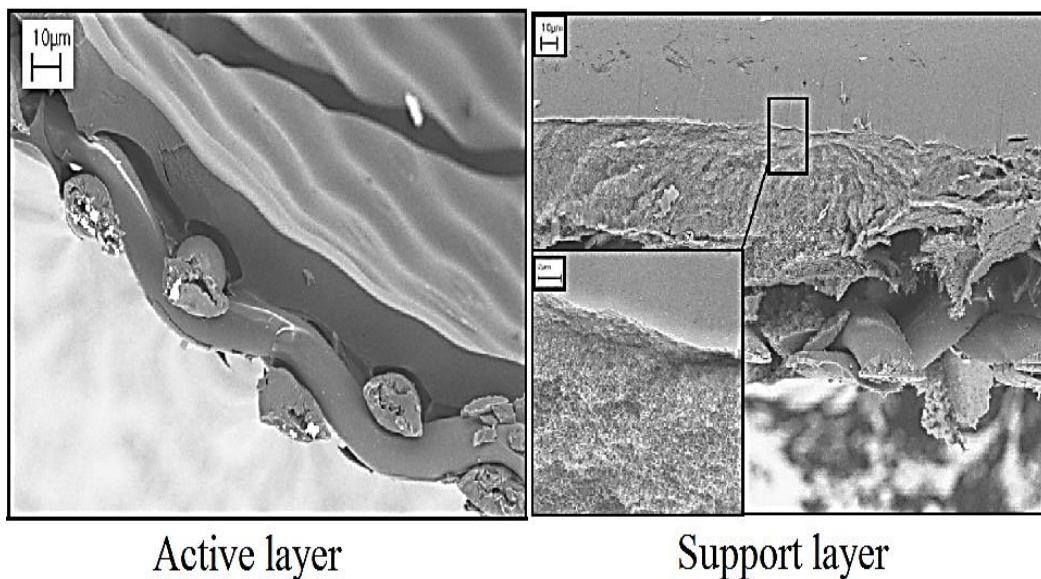


Fig. 2.7: Scanning Electron Microscope (SEM) photos of Cellulose acetate PRO membrane developed by Schiestel [54].

*b. Thin film composite PRO membrane*

Thin-film composite (TFC) membranes usually consist of layers of dissimilar materials joined together to form a single membrane. This layered construction permits using material combinations that optimize the performance and durability of the membrane. Contrary to CTA membrane, TFC membranes are characterized by a wide range of feed pH; however they have low tolerance to oxidants and chlorine chemicals [69]. Yip et al. [17] were the first to use a Polysulfone (PSF)-Polyamide TFC membrane supported by mesh spacers in PRO bench scale tests. The study of the membrane revealed that a less porous sponge-like morphology is present in the top skin portion of the PSf support layer that is capable of minimizing the detrimental effects of ICP while allowing the formation of a polyamide layer that possesses high water permeability and salt rejection properties. The active layer (modified polyamide Surface) was characterized by sponge-like skin layer forming on top of a layer containing macrovoids. Yip claimed that the presence of macrovoids is capable to minimize ICP; however, this suggestion was rejected by other researchers [55,56]. Han et al. prepared a new modified surface single layer TFC membrane with so called "Matrimid" support layer [21]. The membrane revealed a good robustness, high water permeability and sufficient power density. Zhang et al. fabricated a Polyamide /Polyacrylonitrile (PAN) composite membrane with enhanced mechanical properties and water permeability for osmotic power (Fig. 2.8) [56]. It was shown that the membrane treatment by alcohol leads to higher water fluxes and mechanical stability. Also, ethanol treatment swells up the polymeric chains and extracts unreacted monomers and low molecular weight polymer chains. Consequently, a thinner and smoother polyamide layer with a larger free volume is therefore produced, which leads to a higher water flux, better mechanical stability and greater power density. For the first time, Bui et al. introduced the use of nanofiber TFC membrane in PRO power production [57]. Two different selective layers were formed, each from different precursors and having different permselectivity. One was generated from Trimesoylchloride (TMC) and m-phenylene diamine (MPD) (mTFC), while the other was produced from Isophthaloyl chloride (IPC) and Polyethyleneimine (PEI) (pTFC). These membranes employ an extremely thin selective layer forming on a highly porous, interconnected, low tortuosity nanofiber mat electro-spun onto a

nonwoven polyester backing. This nanofiber structure is tiered, meaning the nanofibers decrease in diameter as they approach the selective layer. Both the pTFC and mTFC membranes exhibited much higher water fluxes and power densities, than the HTI-CTA membrane. Some experimental results using flat sheet TFC membranes are presented in Table 2.2.

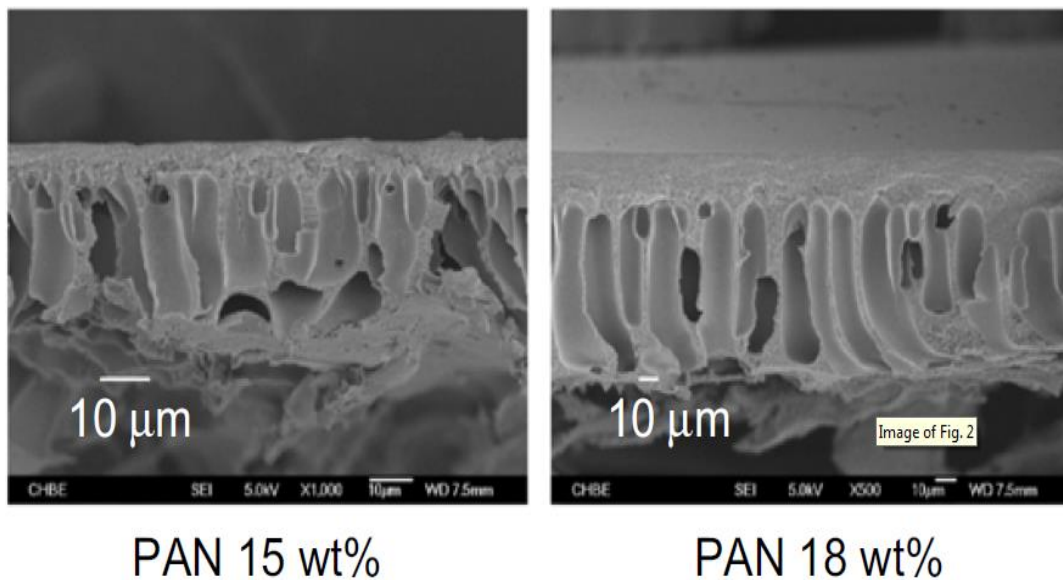


Fig. 2.8: SEM cross-section of the Polyamide/polyacrylonitrile (PAN) substrates made from two polymer concentrations developed in [56].

#### 4.3.3.2 Hollow fiber PRO membrane

A hollow fiber membrane is a tubular, self-supporting membrane with a fiber diameter less than 500 μm [60]. These membranes are prepared by phase inversion in a hollow fiber spinning setup. A viscous polymer solution (dope solution) is pumped through a spinneret and the bore solution fluid is pumped through the inner tube of the spinneret. After a short residence time in air or a controlled atmosphere, the fiber is soaked in a coagulation bath.

As with flat sheet membranes, the hollow fiber membranes have shown a remarkable development since its first use in PRO [61]. A hollow fiber membrane was first used in PRO by Chou et al. [62]. The support layer of the membrane was a commercial polymer polyethersulfone (PES) and the active layer was prepared using polyamide. According to Chou et al., the membrane performance was the best in term of energy production and mechanical strength compared to results

published for other types of PRO membranes. One year after, Chou et al. introduced another hollow fiber PRO membrane by adopting the Polyetherimide as the material for the substrate layer and the polyamide RO-like as the active layer [63]. The newly developed TFC hollow fiber membrane was characterized by high mechanical strength, high power density and low reverse salt diffusion. Han et al. [64] fabricated a robust hollow fiber membrane supports for high performance thin-film composite PRO membranes. Han et al. claimed that the desirable hollow fiber supports should possess high stretch resistance and acceptable ductility. The developed TFC PRO hollow fiber revealed a very low specific reverse salt flux value.

A fundamental study of polyamide-based thin film composite hollow fiber membranes over a PES support for PRO through chemical modification was carried out by Ingole et al. [65]. The characterization of the membrane revealed that a thinner and smoother polyamide layer with a larger free volume was produced, which led to a higher water flux, better mechanical stability and greater power density than existing membranes. A thin-film composite TFC hollow fiber membrane via dual-layer co-extrusion technology has been designed and manufactured by Li et al. [66]. The proposed membrane support resisted high burst pressures (up to 24 bar). Zhang et al. [67] used an advanced co-extrusion technology to fabricate the PES hollow fiber supports with diversified structures from macrovoid to sponge-like. The TFC hollow fiber fabricated showed high asymmetry, high porosity, and a thick skin layer with a small and narrow pore size distribution underneath the TFC layer; it produced a maximum power density of 24.3 W/m<sup>2</sup> at 20.0 bar using 1M NaCl, as the draw, and deionized water as feed (See Fig. 2.9).

A summary of some experimental results using hollow fiber PRO membrane are illustrated in Table 2.3.

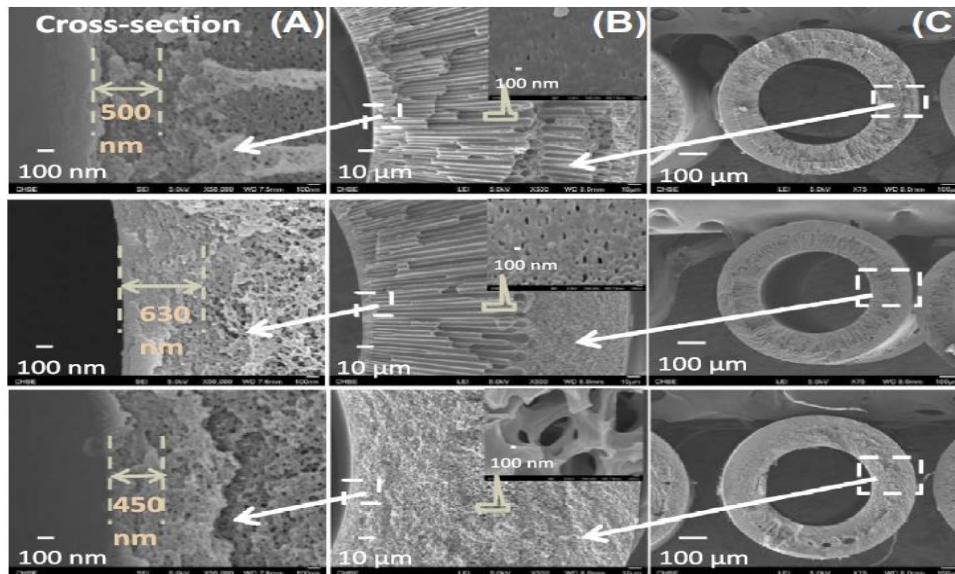


Fig. 2.9: SEM of the cross-section and surface morphologies of the PES hollow fiber supports developed in [67].

Table 2.2: Summary of experimental results in the literature using flat-sheet PRO membranes.

<i>Membrane</i>	<i>Feed solution</i>	<i>Draw solution</i>	<i>Pressure (bar)</i>	<i>Power density (W/m<sup>2</sup>)</i>	<i>Ref</i>	<i>Year</i>
CTA	*DI	1M	9.7	5.1	[39]	2009
CTA	0.04M	1M	9.7	4	[39]	2009
CTA	DI	1M	9.7	5.1	[39]	2009
CA	DI	1M	8.2	1.6	[51]	2009
CA	0.1M	1M	13	3.8	[59]	2012
CA	0.1M	2M	13	6.7	[59]	2012
CA	DI	1M	8	2.25	[54]	2012
CTA	0.5M	1M	9.3	0.73	[58]	2013
CTA	0.5M	2M	21.6	2.1	[58]	2013
TFC	DI	0.5M	12	10	[18]	2011
Matrimid TFC	DI	1M	15	12	[21]	2013
PAN-TFC	DI	0.6M	10	2.6	[56]	2013
Matrimid TFC	DI	0.6M	13	9	[21]	2013
PAN-mTFC	DI	0.6M	10	8.0	[57]	2014
PAN-pTFC	DI	0.6M	8.3	6.2	[57]	2014
TFC (FO)	DI	0.6M	48	57	[68]	2014

\*DI: deionized water

Table 2.3: Summary of experimental results in the literature using hollow fiber PRO membranes.

<i>Membrane</i>	<i>Feed water</i>	<i>Draw water</i>	<i>Pressure (bar)</i>	<i>Power density (W/m<sup>2</sup>)</i>	<i>Ref</i>	<i>Year</i>
PES-TFC	0.04M	1M	9.0	10.6	[62]	2012
PEI-TFC	0.001M	1M	15	20.9	[63]	2013
Matrimid-TFC	*DI	1M	15	16.5	[64]	2014
PES TFC	DI	0.6M	6	1.62	[65]	2014
P84 TFC	DI	1M	21	12	[66]	2014
Modified PES-TFC	DI	1M	20	24.3	[67]	2014

\*DI: deionized water

#### 4.4 Integration of PRO with desalination (hybrid PRO)

The PRO process can be applied to various sources of feed and draw solutions, not only fresh and seawater, but also pretreated seawater and concentrated brine (SWRO-PRO hybrid process), or wastewater effluents and concentrated brine (SWRO-PRO-WWT hybrid process) [70]. PRO hybridization with desalination technologies, especially FO and RO, has been found to be very promising, with the potential of reducing the cost of seawater desalination as well as the environmental impact due to brine discharge [71]. In many countries, especially in the United States, the combination of PRO with other types of desalination processes is being actively investigated, with the RO-PRO hybrid process getting the most attention.

In 2010, Japan launched the Megaton water system (see Fig. 2.10). As part of the project, a prototype RO-PRO hybrid plant was built and operated. Recycled water was supplied from a regional sewage treatment facility and concentrated brine from a seawater reverse osmosis [SWRO] plant, using PRO Toyobo hollow fiber modules. Studied by Saito et al. [72], the prototype PRO plant got the maximum output power density of 13.8W/m<sup>2</sup> at 30 bars of hydraulic pressure difference, corresponding to a 38% permeation of pure water into the brine. Saito et al. tested the possibility of decreasing the concentration polarization by increasing the number of orifices of the membrane module: they were increased from 3 (feed inlet, concentrated brine outlet, and the permeate outlet) to 4. The fourth orifice, was used as purge for feed water discharge, decreasing the effect of internal

concentration polarization by enhancing leaked salt flushing away from the membrane surface.

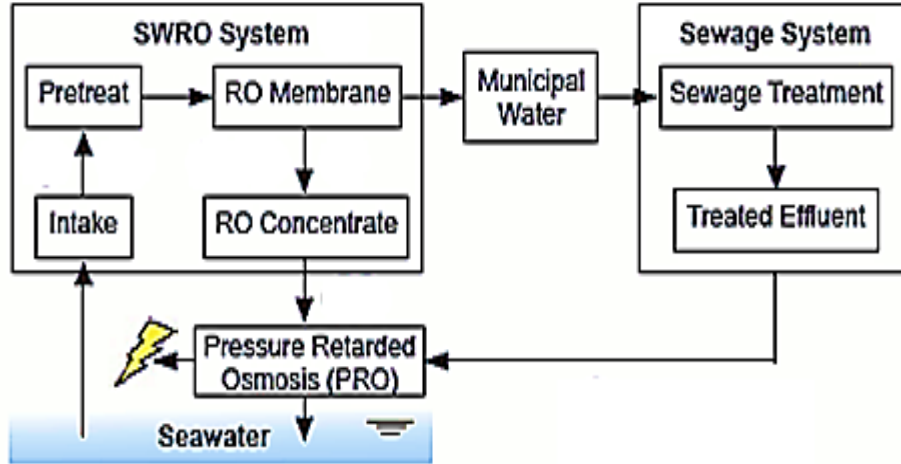


Fig. 2.10: Schematic of Mega-ton RO-PRO hybrid [84].

In another study realized by Feinberg et al. [73], a theoretical comparison of RO-PRO and RO-RED system was performed. However this study considered only thermodynamically reversible PRO and did not consider effects due to concentration polarization and pressure drops along the membrane module. An investigation was presented by Kim et al. discussing four RO-PRO hybrid configurations systems for power generation and seawater desalination using different salinity gradient resources [74]. These configurations are illustrated in Fig. 2.11. According to Kim et al. RO and PRO are operated for different purposes (to produce water and energy, respectively) and one requires a proper criterion to compare the different processes. Thus, Kim et al. introduced a new indicator named the water and energy return rate (WERR) to evaluate these hybrid systems, as follows:

$$WERR = \text{Price}_{\text{Electricity}}(W_{PRO} - W_{RO}) + \text{Price}_{\text{Water}}Q_{p,RO} \quad (2.24)$$

where  $\text{Price}_{\text{Electricity}}$  and  $\text{Price}_{\text{Water}}$  are the electricity and water prices, respectively,  $W_{PRO}$  and  $W_{RO}$  are the energy generated by PRO and the energy consumed by RO, respectively, and  $Q_{p,RO}$  is the RO permeate flow. The WERR unit is \$/min: a higher WERR value indicates a higher benefit obtained by the hybrid processes. Based on a previously validated RO process model and modified a model of a pressure-

retarded osmosis PRO process to properly consider the spatial distribution of concentration and velocity based on a mass balance principle, Kim et al. claimed that hybrid systems that use seawater as a feed water for RO are more energy price sensitive. Also, the decrease in the size of RO plant decreases the WERR value while the size of PRO plant has no significant impact on the WERR value.

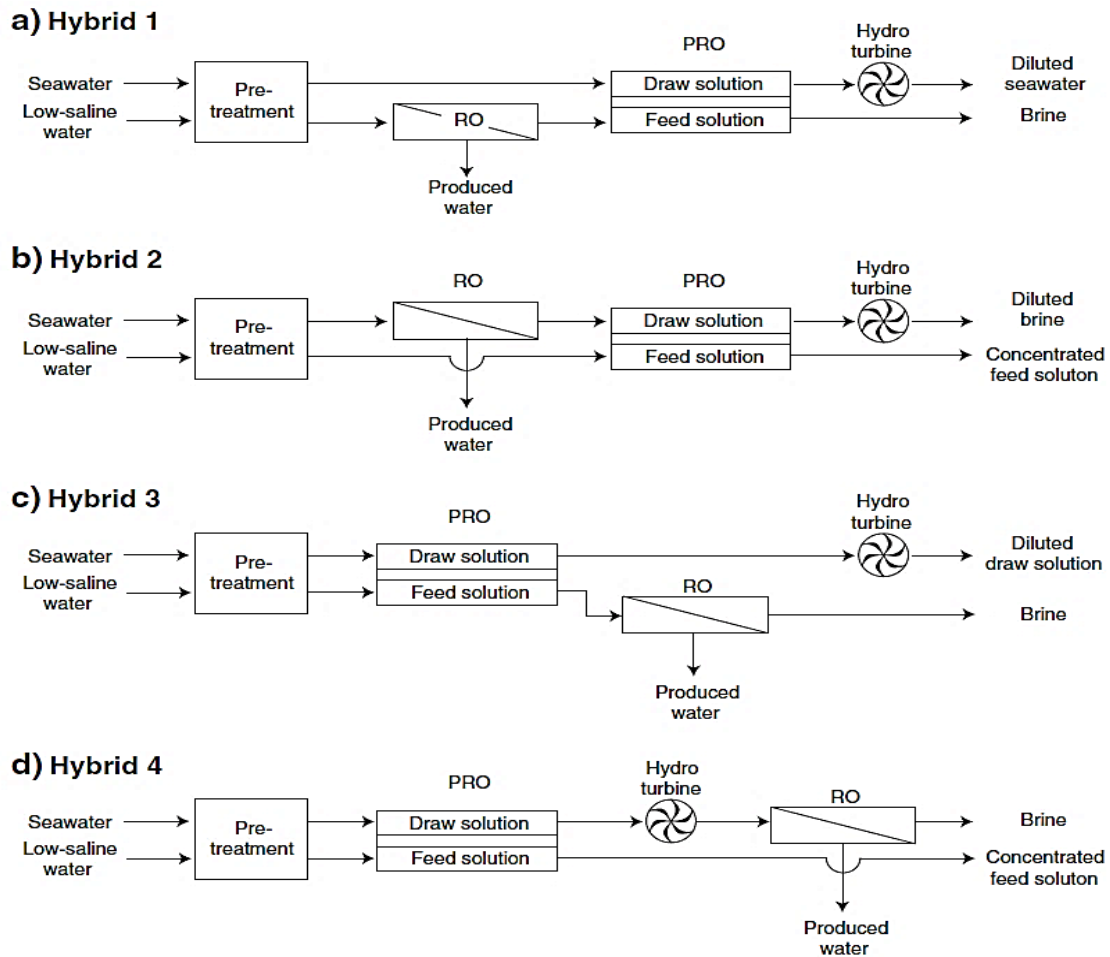


Fig. 2.11: Schematic of four RO-PRO hybrid systems proposed by Kim et al. [74]

Next, Achili et al. investigated the feasibility of a coupled RO-PRO system using a pilot-scale RO-PRO system [75]. Three spiral-wound RO membrane modules were installed into high-pressure vessels in the small-scale pilot system. Each module had an active membrane surface area of 2.8 m<sup>2</sup>. The membrane modules were arranged in series so that the concentrated brine leaving the first module was the feed solution for the subsequent module. The hybrid system is presented in Fig. 2.12. A spiral-wound TFC PRO membrane module was used. The module has an active membrane surface area of approximately 4.18 m<sup>2</sup> and was installed into a

high-pressure vessel in the small-scale pilot system. Seawater is pressurized in a pressure exchanger (PX) before going to the RO system for desalination. In the RO system, seawater feed splits into two flows: a freshwater permeate and brine concentrate. The pressurized brine concentrate goes first to Energy Recovery Device (ERD) to reduce its pressure to a desirable level for the PRO process. After leaving the EDR, brine concentrate enters the PRO system as the high salinity or the draw solution flow while a low flow stream or feed flow is wastewater effluent. In the PRO module, freshwater permeates across the membrane from the low salinity to the pressurized high salinity stream as a result of osmotic pressure gradient. A pressure exchanger is installed on the discharge side of the diluted draw solution to exchange energy with the seawater feed to the RO membrane system. According to Achili, the RO-PRO system has several advantages: compared to a standard RO-PX system, RO energy consumption is further reduced with energy production by PRO, the brine generated during the RO process is diluted back to seawater concentration. RO brine is good draw solution compared to other draw solution sources for three reasons: first, among other readily available draw solutions, RO brine is an abundantly available, low-cost residual from existing commercial systems, second, RO brine has production, and third, the brine entering the PRO subsystem is relatively free of foulants because it receives prior treatment by the RO pretreatment system, which eliminates additional energy expenditure. Without the ERD the measured energy consumption of the RO membrane system was 3.82 kWh/m<sup>3</sup> (with 20% of recovery) that decreased to 2 kWh/m<sup>3</sup> with the ERD (with 30% recovery).

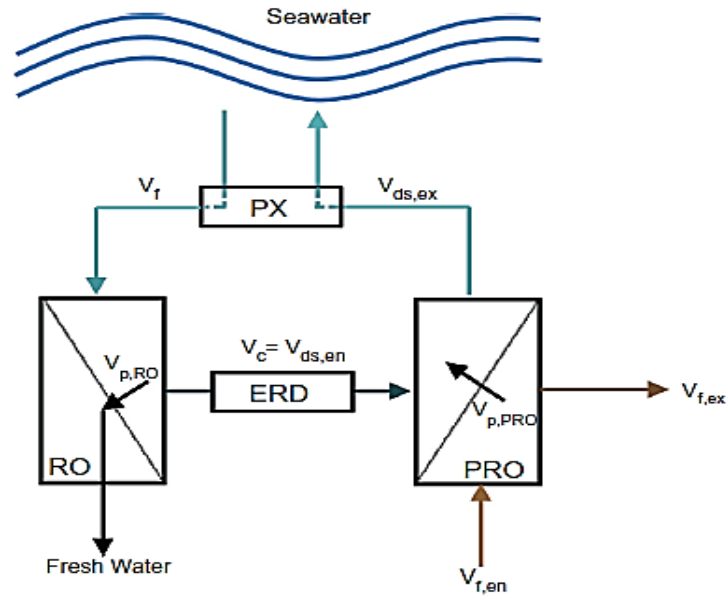


Fig. 2.12: Schematic of RO-PRO hybrid adopted by Achili et al. [75]

Using the same RO-PRO system adopted by Achili et al. [75], Prante developed a model the specific energy consumption of a RO-PRO system using RO conditions at the thermodynamic restriction and a novel module-based PRO model [76]. The minimum net specific energy consumption of the modeled system was  $1.2 \text{ kWh/m}^3$  for a 50% RO recovery. Under an RO specific energy consumption of  $2.0 \text{ kWh/m}^3$ , the RO-PRO system could achieve theoretically a 40% of energy reduction.

Lin et al. investigated a closed-loop system that combines membrane distillation (MD), which generates concentrated and fresh water streams by thermal separation, and PRO, which converts the energy of mixing to electricity by a hydro-turbine [77]. Fig. 2.13 shows the different compounds of PRO-MD hybrid system. Results indicate that the hybrid PRO-MD system can theoretically achieve an energy efficiency of 9.8% (81.6% of the Carnot efficiency) with hot and cold working temperatures of 60 and 20 °C, respectively, and a working solution of 1M NaCl. Of course, when mass and heat transfer kinetics are limited, conditions that more closely represent actual operating conditions, the practical energy efficiency will be lower than the theoretically achievable efficiency.

Streams S10 and S13 enter the PRO module as the high concentration draw solution and distilled water feed solution streams ("D" and "F" in Fig. 2.13, respectively) in co-current mode with the draw solution chamber under a constant



was investigated by Altaee et al. [79] that combined Forward Osmosis with Pressure Retarded Osmosis. Two configurations were studied: the PRO-FO and FO-PRO systems shown in Fig. 2.15, using hypersaline solution as draw solution and wastewater effluent as feed. The study showed that the efficiency of the PRO-FO design was higher than that of the FO-PRO design in terms of the power generation. They also tested the effect of the feed solution flow rate, and the results revealed that in this specific case its effect on the performance of FO membrane was negligible.

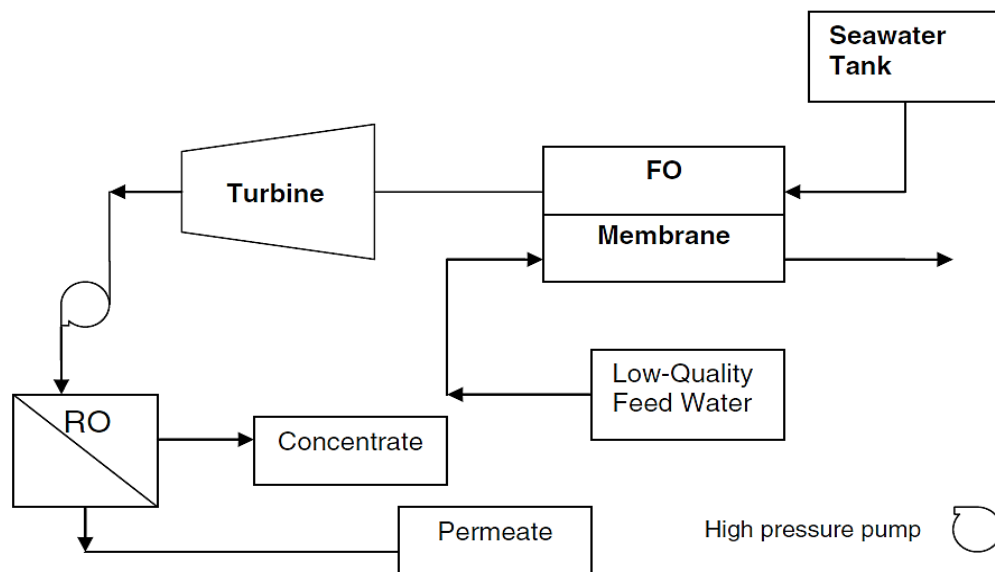


Fig. 2.14: Schematic diagram of the PRO-RO system for combined power generation and seawater desalination studied by Altaee et al. [78]

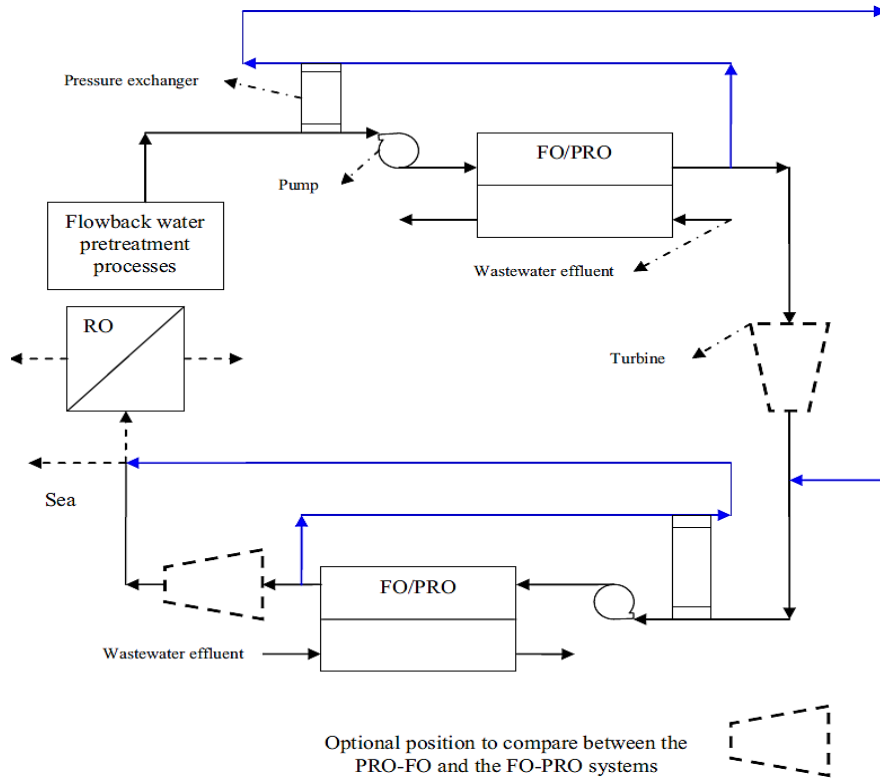


Fig. 2.15: Schematic diagram of the FO-PRO system for combined power generation and water treatment desalination studied by Altaee et al. [79]

He et al. investigated the feasibility of a reverse osmosis desalination system powered by a stand-alone pressure retarded osmosis unit [81] (Fig. 2.16). A Feasible Condition number (FC) was introduced to study the feasibility of the system. This number takes into consideration the efficiency of the components in the hybrid RO-PRO:

$$FC = \frac{\Delta P_{PRO} \left[ (1-Y) \left( \eta_{HT} - \frac{\eta_{ERD}}{\eta_{HP}} \right) + Y_P \right]}{\Delta P_{PRO} \left[ \frac{1 - \eta_{ERD}(1-Y)}{\eta_{HP}} \right]} \quad (2.25)$$

where  $\eta_{HP}$ ,  $\eta_{ERD}$  and  $\eta_{HT}$  are the efficiencies of HP, ERD, and HT, respectively and  $Y$  is the RO water recovery rate. A high value of FC means better feasibility of the system. The results obtained showed that lower RO water recovery rates and higher ratio of the PRO feed volumetric flow rate to the combined PRO feed and draw flow rates improved the feasibility of the hybrid system. To achieve the optimum FC numbers at low water permeation rates higher applied hydraulic pressure is required, but lower membrane area. Unfortunately the study did not

take into consideration the effect of the concentration polarization and the salt reverse flux on the performance of the RO-PRO system, which would affect the results.

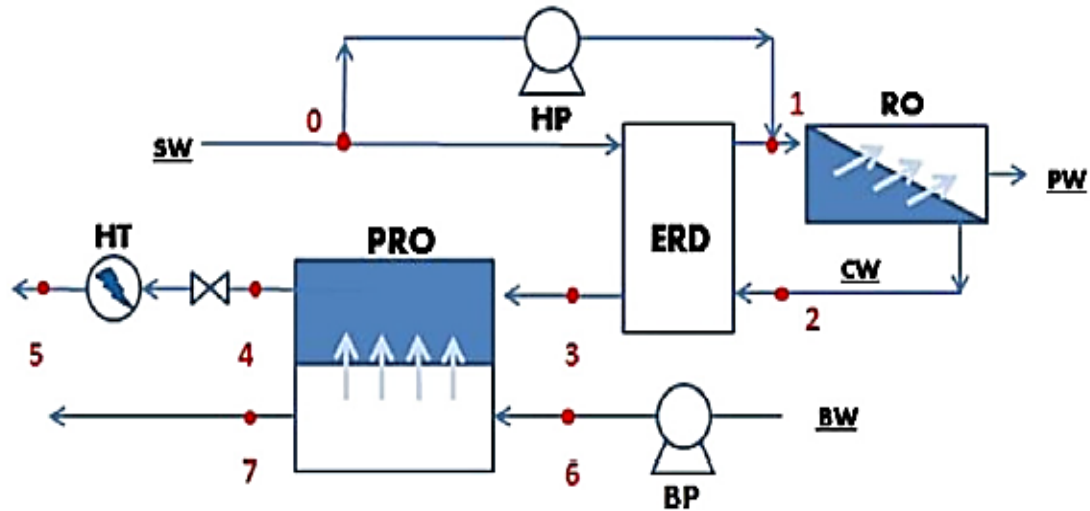


Fig.2.16: Schematic diagram of a RO-PRO hybrid system adopted by He et al. [81]

In another study, He et al. [82] discussed the performance of a two-stage PRO design. Four configurations were studied and compared to a single-stage PRO performance. According to different flow schemes between the two PRO stages in a “TwoPRO”, the four configurations were defined as: CDCF, DDDF, CDDF and DDCF (Fig. 2.17) in which ‘D’ and ‘F’ in each PRO module represent the draw and feed solutions flow channel, respectively, ‘C’ correspondsto continuous treatment (which means the solution is treated continuously by the two stages), and ‘D’ to divided treatment (in which the solution is divided before it flows into the first stage and treated separately in each stage).

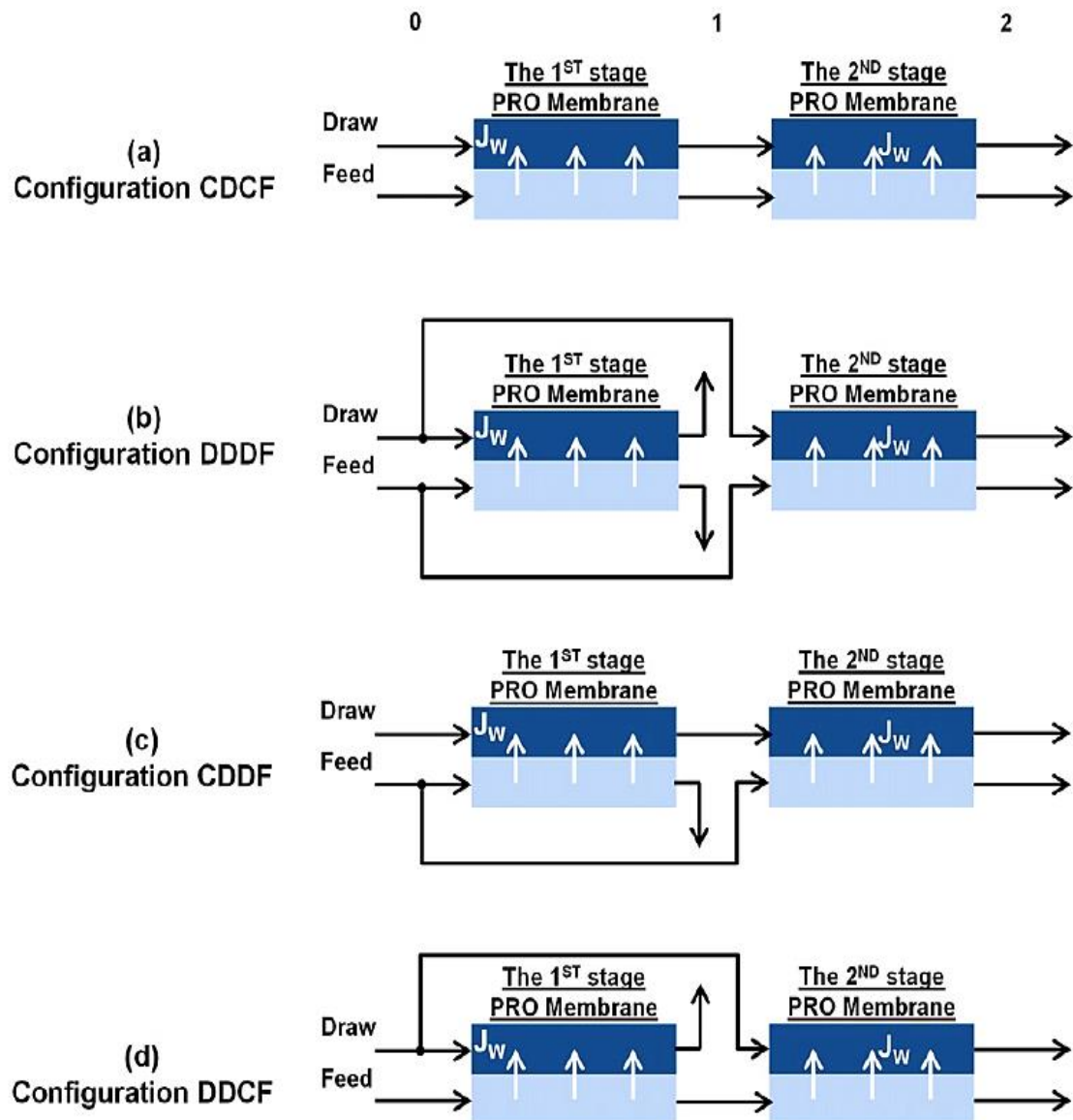


Fig. 2.17: Schematic diagram of the four possible configurations of the "TwoPRO" process proposed by He et al. [82].

For example, in the configuration DDCF, the draw solution is first divided into two branches that flow separately into the two stages. In the case of CDCF, both feed and draw solutions are connected in series, and the salinity gradients are continuously treated in two stages. It was found that CDCF has advantageous energy capacity in all flow rates. The maximum energy surplus of the configuration CDCF was reached between the flow ratios of 0.5 and 0.6.

For the configuration DDDF, two streams of draw and feed solutions are divided from the beginning and treated separately in two independent PRO modules. It was shown that this configuration had worse performance than that of the single-stage PRO plant in terms of extractable energy.

In the configurations CDDF and DDCF, only one stream, either the draw or feed solutions needs to be considered in the flow distribution. Results showed that CDDF and DDCF have advantageous energy capacity under fixed dimensionless flow rate compared to that of the single PRO.

Lee et al. [83] investigated the integration of PRO with a multi-stage vacuum membrane distillation (MVMD) to produce power and freshwater. Fig. 2.18 shows the configuration adopted by them. The MVMD system employs a recycling flow scheme (MVDM-R) for the continuous production of both distillate water and highly concentrated brine. The concentrated brine that is produced from the MVMD-R system is then used as a draw solution for power generation in the PRO system, with river water as feed. A power density of  $9.7\text{W}/\text{m}^2$  was achieved under feed and draw solutions flow rates of  $0.5\text{ kg}/\text{min}$  and a constant hydraulic pressure difference of 13 bars.

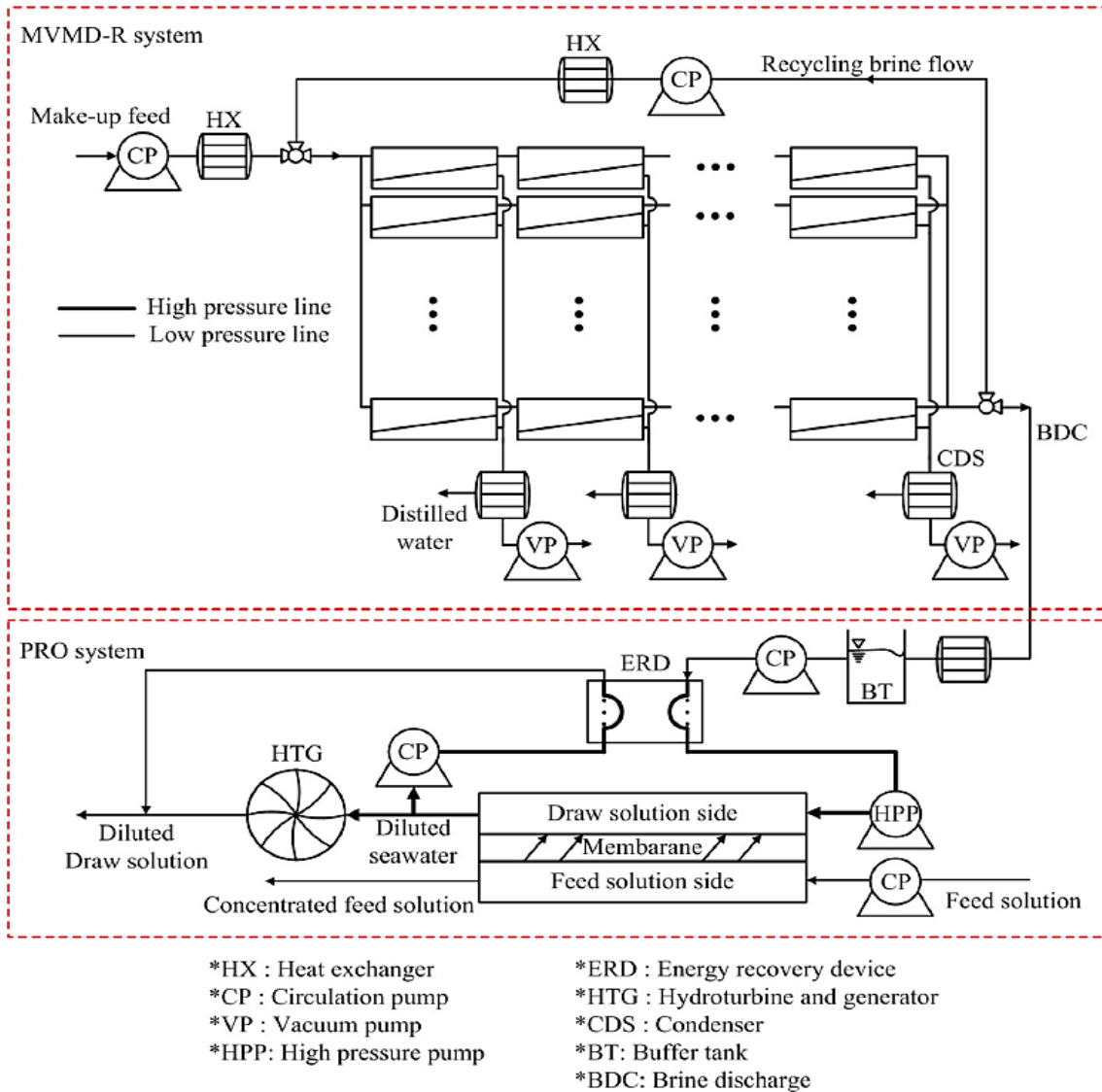


Fig. 2.18: Schematic of the hybrid MVMD-R-PRO system proposed by Lee et al. [83].

#### 4.5 PRO limitations and suggested solutions

As other pressure-driven processes, PRO is limited by concentration polarizations, reverse salt diffusions, and other factors that reduce the water flux and the membrane durability. They are now discussed.

##### 4.5.1 Membrane fouling

Membrane fouling is caused by convective or diffusive transport of suspended or colloidal matter or by biological growth (so-called bio-fouling). An existing fouling layer increases the overall resistance to mass transfer, so the overall performance

decreases significantly. In addition, membrane fouling increases pressure losses along the membrane[85].

The first published study of PRO membrane fouling was realized by She et al. [86] in 2013. The investigation showed the important effect of the bivalent salts flux diffusion on the membrane fouling. In fact, the diffusion of calcium and magnesium from the draw solution to the feed solution increases the fouling process due to the fact that those ions form interactions with organic foulants, which enhance the fouling. The increase of the draw solution concentration leads to an increase of the salt diffusion, and therefore it increases the fouling. For that, She et al. claimed that the concept known in RO as “the critical flux” can be used in PRO as “the critical draw solution concentration”.

A study made by Thelin et al. [87] has experimentally shown that the decline of water flux does not correlate with the accumulated Natural Organic Matter (NOM) and was independent of the concentration of NOM in the feed. Also, it was noted that the rate of flux decline as a function of accumulated NOM load depends on the type of membrane. The study of the effect of the ionic strength revealed that although it has an impact on the fouling propensity, the ionic strength effects werenot enough to explain the differences in fouling propensity for different membrane types. Thus, Thelin et al. claimed that there is a strong correlation between PRO membrane characteristics and the fouling propensity. Therefore, they proposed that the mechanism of fouling is due to NOM accumulation within the porous support and the cake formation at the surface of the support membrane (Fig. 2.19). To face the problem of organic fouling, the authors suggested reducing the fouling potential of the feed water by pretreatment, mitigating the fouling propensity of the membrane by improving structural properties and reducing its affinity towards foulants in the feed water, and mitigating the development of fouling backwashing and chemical cleaning.

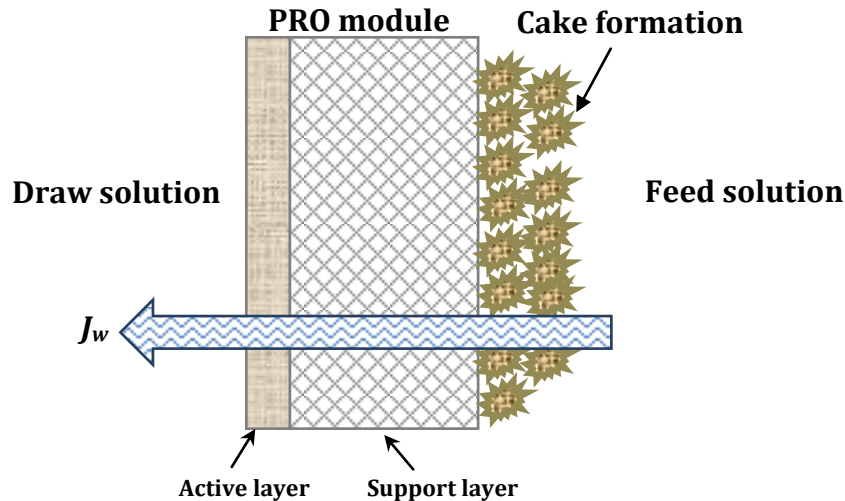


Fig. 2.19: NOM Cake layer formation in the surface of PRO membrane porous layer.

Later, Yip and Elimelech studied the effect on PRO performance of the Natural Organic Matter fouling (NOM) and backwashing [88]. They claimed that NOM is able to pass through the porous layer and to be blocked in the active-porous interface. Thus, two cake layers can be formed: i) in the surface of the support layer, ii) in the active-porous interface. Results revealed that the NOM deposited in the membrane cause a severe increase in hydraulic resistance, thus lowering water permeability and detrimentally reducing productivity of PRO. The study of backwashing showed that this operation restores part of the initial membrane performance thanks to its ability to remove the NOM deposited in the active-porous layer (Fig. 2.20).

Chen et al. [89] investigated the effect of the hydraulic pressure on PRO fouling by gypsum scalants, sodium alginate, and the combined foulants, using hollow fiber membrane. Significant alginate fouling was observed under ultrahigh hydraulic pressures ( $\Delta P > 18$  bars), whereas the gypsum scaling was inhibited. Results indicated that the reverse salt flux resulted in a faster rate of alginate fouling but a limited gypsum scaling. Combined fouling was severe with the co-existence of gypsum crystals and alginate under 0 bars. Chen et al. attributed this behavior to the fact that the fouling could be enhanced by a high reverse salt flux under 18 bars because the reverse sodium ions induced significant concentration polarization near the membrane surface and calcium ions bridged alginate gelation. In the combined fouling experiments, the membranes were conditioned by one of

foulants followed by the other; Chen et al. suggested that such conditioning could increase the rate of combined fouling because of the change in membrane surface chemistry. The study of the co-existence of gypsum crystals and alginate under 0 bars led to the synergistic combined fouling and resulted in a greater flux decline than the sum of individual foulings. However, under high pressure PRO tests, gypsum-alginate synergistic fouling was not observed, because the increased reverse salt flux inhibited the formation of gypsum crystals. Consequently, Chen et al. concluded that alginate fouling could be the dominant fouling mechanism for both alginate conditioning and then scalants fouling, and scalants conditioning and then alginate fouling PRO processes under 8 bars and 18 bars. Thus, the removal of alginate type foulants from the feed water stream may become necessary for good PRO performance under high pressures. We must point out that a recent study revealed that the use of thick feed spacers reduces biofouling of a FO membrane [90]: The result could be extended to PRO membranes.

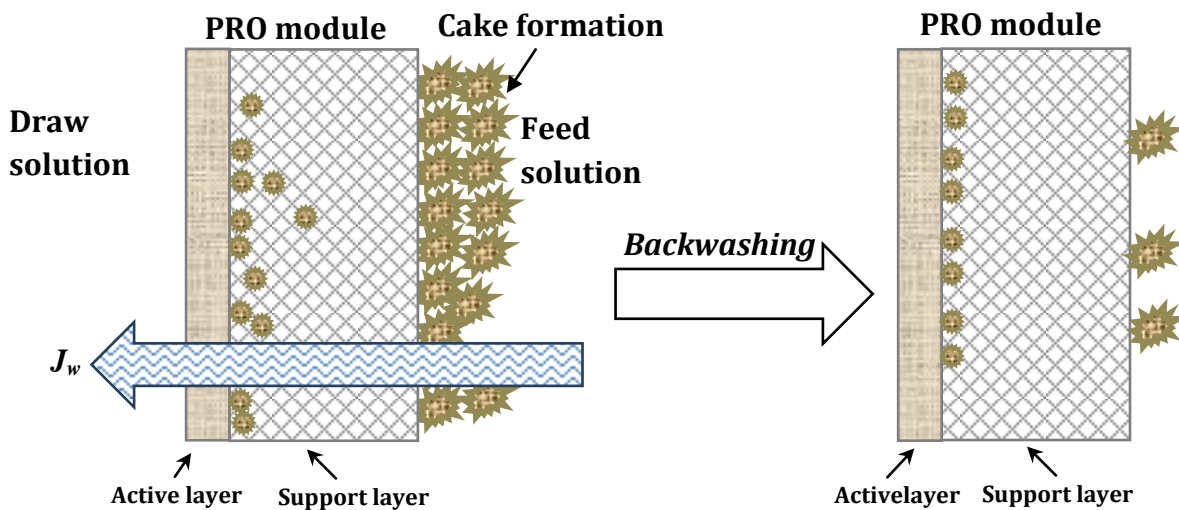


Fig. 2.20: Effect of the backwashing on reducing the NOM fouling in PRO membrane.

#### 4.5.2 Membrane scaling

Scaling of the membrane is caused by super-saturation of inorganic compounds concentrated on the feed side: Super-saturated salts precipitate on the membrane surface building a thin layer, which hinders mass transfer through the membrane [85].

PRO membrane scaling is not yet well studied: only one published paper was found treating this subject: Zhang et al. [91] investigated the role of membrane scaling in reducing the PRO performance. It was found that the chemistries of the feed and draw solutions play a determinant role in membrane scaling. The existence of precursor ions (i.e.,  $\text{Ca}^{2+}$  and  $\text{SO}_4^{2-}$ ) may trigger the gypsum precipitation because of the migration of these ions from the draw solution to the feed solution by means of salt reverse flux. Hence, the increase of operating pressure leads to the increase of salt reverse diffusion; therefore, the risk of gypsum precipitation increases. They suggested that if scaling precursors enter the porous support layer either by convection from the bulk feed solution or by diffusion from the draw solution, the internal concentration polarization of both convected and reverse diffused scaling precursors would lead to an elevated saturation index inside the porous support layer, generating internal scaling. Moreover if the bulk feed solution were oversaturated, external scaling can also occur (See Fig. 2.21). As a solution, the authors claimed that the orientation -active layer facing the feed solution- can reduce the concentration of scaling precursor. However, it is not clear how this will affect the power density and the overall performance. As an alternative, controlling the salt reverse diffusion by providing a good mechanical stability of the PRO membranes can reduce the risk of scaling.

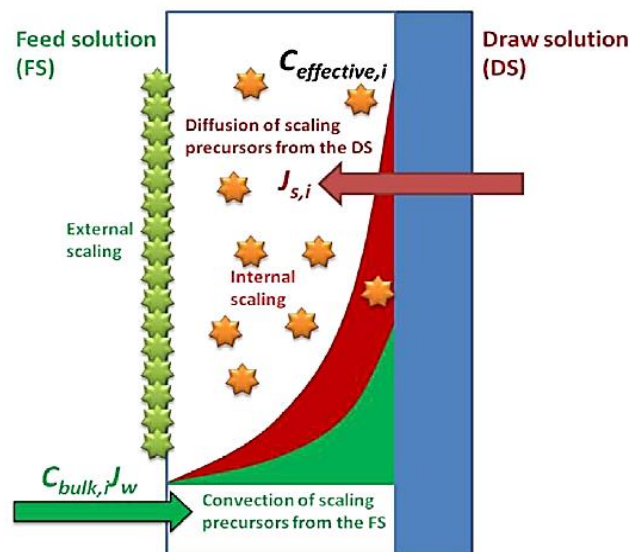


Fig. 2.21: PRO scaling mechanisms. The subscript ( $i$ ) refers to the precursor ( $i$ ) [91].

#### *4.5.3 Concentration polarization*

As mentioned before, Concentration Polarization is one of the major factors that affect the performance of PRO process. Several works had been realized to study the impact of this phenomenon on the water flux and the power density [17,39,58,59]. It was noted that the concentration polarization depends on the hydrodynamics, the membrane orientation, the membrane design, and the operating conditions (temperature, pressure, solutions concentrations, solution composition, etc.). In general the internal concentration polarization ICP is more severe than the external concentration polarization ECP. To reduce the effect of the ICP, it is necessary to build membranes with the thinner support layer that is possible. ECP can be mitigated by increasing the cross flow velocity and the operating temperature.

#### *4.5.4 Membrane deformation*

One of the main causes of reduced performance of the PRO process is the membrane deformation caused by the hydraulic pressure. Some investigations have shown that the membrane deformation reduces significantly the water flux [40,59], with some membranes collapsing at high pressures. Using spacers with high opening size aggravates the membrane deformation. As presented in the previous section, several researches are working in the development of robust PRO membranes that withstand high pressures. In general, the use of moderated opening size of thick spacers can reduce membrane deformation.

#### *4.6 PRO cost*

Theoretically, PRO can be a competitive source of energy compared to other renewable energies; for example, compared with other forms of ocean energy, osmotic power cost is similar to ocean energy sources, such as tidal energy [92]. In fact, under a constant supply of feed and draw solutions, osmotic power plants could operate continuously for more than 8000 h annually (24 hours/day, 7days/week) [93]. Experimental results at laboratory scale have shown a good performance. However, the cost perspective for full-scale PRO power plants is still uncertain due to the absence of large-scale plants to validate cost assumptions. It is therefore only possible to make projections of costs based on current knowledge

and suppositions about the development of the key components of these technologies. Key components affecting the capital, operation, and maintenance costs are the membranes (including replacement over the life-time of the project), the pre-treatments and the pumping of water. It has been estimated that membranes would account for up to 30% of total capital costs because the PRO membrane would cost three times more than other commercial membranes [94]. Other study has shown that the intake and outfall systems, pre-treatment facilities, and membranes all combined would account for around 75% of the cost [90].

Nowadays, the price of the commercialized membranes is high, affecting viability of the process. The current cost of the membranes is around 5€/m<sup>2</sup> but perspectives reported that this price would decrease to 2 €/m<sup>2</sup> within a few years. Fig. 2.22 shows the decrease of membranes price since early 1990's till now. However, the membrane price is not only the factor that should be taking into consideration; its performance and durability should be important factors. Cheap membranes with low durability and performance are not beneficial for the process. As a comparison, Achili et al. [96] showed that if the membrane durability were 10 years, the revenue would be almost 10 times than that of a membrane of only 1 year of durability. Concerning the membrane performance, the difference between the membrane costs for a 1W/m<sup>2</sup> PRO plant and for a 5W/m<sup>2</sup> PRO plant would be approximately 500 million\$ for a 20MW capacity power plant, assuming a cost per unit area of installed membrane of 30\$.

Another important factor that is able to affect the energy production price is the power plant capacity. Kleiterp [95] analyzed the capital and unit energy costs for both 25 and 200MW osmotic power plants in the Netherlands using a membrane output of 2.4W/m<sup>2</sup>. Perspectives revealed that a unit energy cost of 1.21\$ / kWh resulted from the 25MW osmotic power plant analysis, and 1.0\$/kWh from the 200 MW plant.

Several studies revealed that the energy production is affected by the nature of the sources used [95,97,98]. As an example: Tanioka et al. [97] reported that the energy cost using freshwater vs brine is 0.16€/kWh, whereas, Dinger et al. [98] reported a cost of 0.18\$/kWh using freshwater vs seawater.

It should be noted that the cost depends also on the nature of the installation: stand-alone PRO plant cost should be higher compared to hybrid installation. Cost

projections for the year 2020, vary between 0.08 €/kWh and 0.15 /kWh [99]. On the other hand, costs for hybrid installations are estimated to be 0.11€/kWh [99]. A detailed cost calculations made by Stenzel [100] based on simulations of plants near existing installations in Germany, demonstrate that besides the costs of membranes and pre-treatment of water, of particular relevance are the local site conditions, for example to what extent the plant can use the already available infrastructure.

The performance of PRO membranes is constantly improving: Researchers are producing membrane with high performance under bench-scale tests [56,57,67,68]. Without doubt, this improvement will decrease the energy cost due to considerable contribution of the membrane cost in the energy production cost. The development of desalination processes enhances the development of PRO process because of the resemblance between the two techniques in terms of principles and components. Consequently, the development of desalination process and equipment (pressure exchangers, spacers, pumps, vessels, etc.) can be useful for PRO with small modifications for process adaptation.

Other important factors are the pre-treatment and pumping: they could require a relatively large amount of energy, with a high cost. These costs need to be brought down to make the installations more efficient: Hydro-Quebec Canada and Statkraft concluded a memorandum of understanding with the purpose to reduce these costs.

The Levelized Cost Of Energy(LCOE)primary metric for utilities to evaluate the cost of produced electricity. It is calculated by accounting for all of a system's expected lifetime costs (including construction, financing, fuel, maintenance, taxes, insurance and incentives), which are then divided by the expected power output (kWh) during its lifetime [101]. As a financial tool, LCOE is very valuable for the comparison of various generation options. A relatively low LCOE means that electricity is being produced at a low cost, with higher likely returns for the investor [101]. Statkraft estimated that the future LCOE for salinity gradients power may fall in the same range as other more mature renewable technologies, such as wind, based on their current hydropower knowledge, general desalination (reverse osmosis) engineering and a specific membrane technology [3]. Achieving competitive costs will, however, be dependent on the development of reliable,

large-scale and low-cost membranes. Statkraft estimated that investment costs will be much higher than other RE technologies, but that capacity factors could be very high, with 8,000 hours of operation annually [3]. A recent study developed by Naghiloo et al. [109] investigating the feasibility of 25 MW osmotic power plant installation on Bahmanshir River (Iran), found that the capital cost to build the plant was 117.6 M€ for a net energy production is 138.75 GWh/yr, assuming an efficiency of 63.3%. Naghiloo et al. found that modeling results indicate that for a 15 year return on investment, an annual increase in purchase price of electricity 10% and constant interest rate of 6%, the sale price of electricity should be 0.41 €/kWh, quite expensive compared to other renewable sources (0.09€/kWh). According to Naghiloo et al., this high price was due to the high capital cost of the intake and outfall system (61.5% of the cost), and the pre-treatment (28.4%). Thus, to make this installation commercially viable, intake and outfall systems costs, pretreatment system costs should be reduced.

Table 2.4 summarizes the energy production costs for different PRO power plants developed in the literature.

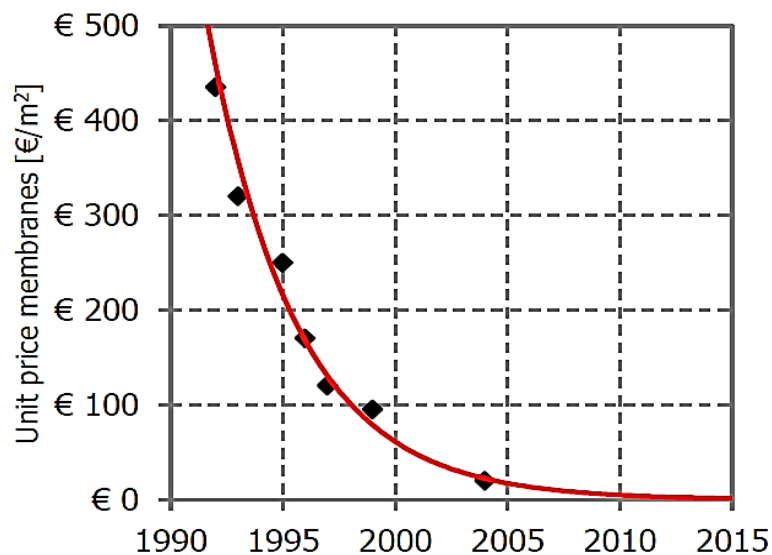


Fig. 2.22: Decrease of membrane price [95].

Table 2.4: Estimated energy production cost for different PRO power plants.

<i>Feed solution</i>	<i>Draw solution</i>	<i>Energy cost (\$/kWh)</i>	<i>Ref</i>
RO Desalination brine	brine from Dead Sea	0.07	[32]
river water	brine from Great Salt Lake	0.09	[34]
freshwater	Seawater	0.18	[98]
freshwater	seawater	0.09–0.16	[92]
freshwater	brine from desalination	0.16	[97]
freshwater	seawater	0.07–0.12	[95]
freshwater	seawater	0.06	[107]
freshwater	seawater	0.045	[93]
freshwater	brine from desalination	0.13	[100]
freshwater	seawater	0.33	[100]
freshwater	seawater	0.13-0.26	[104]
river water	Persian Gulf	0.47	[109]

#### 4.7 Environmental impact

PRO is a renewable energy source that does not produce emissions of CO<sub>2</sub> during operation. Mono nitrogen oxides (NO<sub>x</sub>) and carbon monoxide (CO) emissions are also absent and the installations are not noisy [94]. The mixing of seawater and freshwater is a process that occurs in nature all over the world. Interestingly, most rivers around the globe run into the ocean in a city or an industrial area. This means that most of the osmotic power potential can be utilized without constructing power plants in natural areas.

It was demonstrated in previous study that the cumulative rejection of the desalination units brine into the sea can induce bad effects on the local aquatic environment [102,103]. As shown in the previous section, PRO process can be coupled to desalination plant by using the desalination plants brine as a draw solution. Thus, this brine will be diluted before being released into the sea, which mitigates its impact on the nature. On the other hand, in heavily industrialized areas, it is possible that an osmotic power plant can improve the environmental conditions by the use of industrial rejected brines [94]. In addition, osmotic power

plants are usually described as requiring a relatively small footprint area and can be constructed partly or completely underground and would thus fit very well into the local environment [94]. The environmental impact of power plants located at the mouths of rivers can be minimized, thereby respecting the ecological conditions of estuaries and rivers. An environmental optimization and pre-environmental impact assessment of an osmotic power plant located at a river outlet has compensated by a combination of environmental flow requirements for the river and the osmotic power plant and environmental engineering of intake and outlet of brackish water.

Nonetheless, some studies have pointed out that PRO power plants could have some effects on the local environment. In fact, like RO plants, the problems of concentration polarization, fouling and scaling require chemical cleaning that affects the properties of the brackish water released into the environment. Hopefully, a biological investigation made by Statkraft during the last 3 years has shown no impact of the discharge water of their prototype on the local benthic communities [104]. Another study showed a small effect on the surface temperature of the water where the PRO brackish will be released due to differences in temperatures [105]. Another important environmental impact that should be taken into account: the large amount of fresh water that can be used by PRO power plants. Investigation reports said that only around 2.5% of the water glob is a freshwater when only 1.5% is directly accessible for human uses, and 70% of it is used for agricultural issues [106]. The intensive use of fresh water for power generation can enhance water scarcity in the future.

Fortunately, PRO could reduce global greenhouse gas emissions by 2741 megatons by 2030 under accelerated environmental policies, according to the International Energy Agency [2]. European Union leaders agreed on a binding target of cutting emissions 40% on 1990 levels by 2030 [8]. Annual coal-fired generation is projected to double from 7,400 TWh in 2006 to 9,500 TWh in 2015 and 13,600 TWh in 2030 [2,80]. Replacing current and planned coal-fired power plants with salinity power plants (40% of energy conversion) could reduce global greenhouse gas emissions by 10 Pg CO<sub>2</sub>-eq/year (~ 1010 tonnes/year). This means a potential reduction of 40% of current global energy-related greenhouse gas emissions [109].

## 5. Final consideration and Conclusions

The world is facing the economical and environmental effects of fossil fuels, so the development of alternative energy sources is a necessity. This chapter has shown that Pressure Retarded Osmosis can be part of the solution thanks to its ability to generate a constant supply of power and its low environmental impact.

Since 1974 until now, PRO technology has been rapidly improving and has become the interest of several research groups. In the theoretical level, the process is being extensively studied: basic mathematical models have already been developed to imitate the power density produced by PRO, presenting good correlation with experimental results at laboratory level. Experimentally, the technique is improving especially with the development of membrane fabrication: Different types of membranes are being used such as cellulose-based flat-sheet membrane, thin film composite membrane, and hollow fiber membrane.

PRO is financially viable when minimum power density of  $5\text{W}/\text{m}^2$  is produced. This value is reachable at laboratory scale, but, unfortunately this minimum of power density is not yet accessible for large scale power plant due to the fact that PRO membranes with required characteristics are not commercialized.

Like any other osmotic membrane process, many operation problems can be faced in PRO such as fouling, scaling and membrane deterioration. Several precautions should be taken to mitigate these problems such as the optimization of operating conditions and the improvement of the membrane characteristics.

Many reports focused on the perspectives of the energy cost using pressure retarded osmosis. In fact, the absence of operating full scale PRO power plant made the estimation of energy cost uncertain. The published studies reported that the energy cost is affected by several factors such as the membrane cost and performance, the plant capacity and location, the chemical solutions required, and the cost of pretreatment and pumping. Reducing the energy cost is one of the important challenges to make PRO competitive with other renewable energies.

Ecological studies have revealed that PRO has a low impact on the environment. Moreover, PRO can be also useful to reduce the environmental impact of brine rejected by the desalination units and industrial zones. A good political strategy to reduce the cost and control the environmental impact can make PRO the energy source of the future.

## REFERENCES OF CHAPTER 2

- [1] Chung TS, Li X, Ong RC, Ge QC, Wang HL, Han G. Emerging forward osmosis (FO) technologies and challenges ahead for clean water and clean energy applications. *Curr Opin Chem Eng* 2012;1:246–257.
- [2] IEA. 'CO<sub>2</sub> emissions from fuel combustion – highlights', 2014. Retrieved from:<https://www.iea.org/publications/freepublications/publication/CO2EmissionsFromFuelCombustionHighlights2014>.
- [3] Helfer, F., Lemckert C., & Anissimov, Y. G. Osmotic power with Pressure Retarded Osmosis: Theory, performance and trends – A review. *Journal of Membrane Science*, 453, (2014) 337-358
- [4] Post JW, Veerman J, Hamelers H- VM, Euverink G- JW, Metz S, Nijmeijer K, Buisman JNC. Salinity-gradient power: Evaluation of pressure-retarded osmosis and reverse electro dialysis. *J Membr Sci* 2007;288:218–230.
- [5] Kruyt B, van Vuuren D P, de Vries HGM, Groenenberg H. Indicators for energy security, *Energ Policy* 2009;37(6):2166-2181.
- [6] Kho J. Osmotic Power: A Primer, Examining the opportunities and risks of making baseload power from osmosis. Kachan & Co. report, June 2010.
- [7] EIA, International energy outlook 2009. Office of integrated analysis and forecasting. 2009, Washington D.C.: U.S. Department of energy.
- [8] Olivier JGJ, Van Aardenne JA, Dentener F, Pagliari V, Ganzeveld LN, Peters JAHW. Recent trends in global greenhouse gas emissions: Regional trends, 1970-2000 and spatial distribution of key sources in 2000. *Env Sci* 2005;2(2-3):81–99.
- [9] Kwon K, Han J, Ho Park B, Shin Y, Kim D. Brine recovery using reverse electro dialysis in membrane-based desalination processes. *Desalination* 2015;362 :1–10.
- [10] Vermaas DA, Veerman J, Yip NY, Elimelech M, Saakes M, Nijmeijer K. High Efficiency in Energy Generation from Salinity Gradients with Reverse Electro dialysis. *ACS Sustainable Chem Eng* 2013;1:1295–1302.
- [11] Yip NY, Elimelech M. Comparison of Energy Efficiency and Power Density in Pressure Retarded Osmosis and Reverse Electro dialysis. *Environ Sci Technol* 2014; 48: 11002–11012.
- [12] Alvarez-Silva O, Osorio AF. Salinity gradient energy potential in Colombia considering site specific constraints. *Renew Energy* 2015;74:737–748.

- [13] Jamaly S, Darwish NN, Ahmed I, Hasan SW. A short review on reverse osmosis pretreatment technologies. *Desalination* 2014;354:30–38.
- [14] Cath TY, Childress A E, Elimelech M. Forward osmosis: Principles, applications, and recent developments. *J Membr Sci* 2006;281:70–87.
- [15] Loeb S, Van Hessen F, Shahaf D. Production of energy from concentrated brines by pressure retarded osmosis, II. Experimental results and projected energy costs. *J Membr Sci* 1976;1(3):249–69.
- [16] Skilhagen SE, Dugstad JE, Aaberg RJ. Osmotic power—power production based on the osmotic pressure difference between waters with varying salt gradients. *Desalination* 2008;220:476–482.
- [17] Lee KL, Baker RW, Lonsdale HK. Membrane for power generation by pressure retarded osmosis. *J Membr Sci* 1981;8:141–171.
- [18] Yip NY, Tiraferri A, Phillip WA, Schiffman JD, Hoover LA, Chang Kim Y, Elimelech M. Thin-Film Composite Pressure Retarded Osmosis Membranes for Sustainable Power Generation from Salinity Gradients. *Environ Sci Technol* 2011;45:4360–4369.
- [19] Chou S, Wang R, Shia L, Shea Q, Tanga C, Fane AG. Thin-film composite hollow fiber membranes for pressure retarded osmosis (PRO) process with high power density. *J Membr Sci* 2012;389:25–33.
- [20] Tan CH, Ng HY. Modified models to predict flux behavior in forward osmosis in consideration of external and internal concentration polarizations. *J Membr Sci* 2008;324:209–219.
- [21] Loeb S, Titelman L, Korngold E, Freiman J. Effect of porous support fabric on osmosis through a Loeb-Sourirajan type asymmetric membrane. *J Membr Sci* 1997;129:243–249.
- [22] Han G, Zhang S, Li X, Chung TS. High performance thin film composite pressure retarded osmosis (PRO) membranes for renewable salinity gradient energy generation. *J Membr Sci* 440;2013:108–121.
- [23] McCutcheon JR, Elimelech M. Influence of concentrative and dilutive internal concentration polarization on flux behavior in forward osmosis. *J Membr Sci* 2006;284: 237–247.
- [24] Loeb S, Norman RS. Osmotic power plants. *Science* 1975;189: 654–655.
- [25] Norman RS, Water salination: a source of energy. *Science* 1974;186:350–352.

- [26] Pattle RE. Production of electric power by mixing fresh and salt water in the hydroelectric pile. *Nature* 1954;174:660-660.
- [27] Mehta GD, Loeb S. Internal polarization in the porous substructure of a semipermeable membrane under pressure-retarded osmosis. *J Membr Sci* 1978;4:261-265.
- [28] Loeb S, Mehta GD. A two coefficient water transport equation for pressure retarded osmosis. *J Membr Sci* 1979;4:351-362.
- [29] Jellinek HH, Masuda H. Osmo-power. Theory and performance of an osmo- power pilot plant, *Ocean Engineering* 1981;8:103-128.
- [30] Loeb S, Honda T, Reali M, Comparative mechanical efficiency of several plant configurations using a pressure-retarded osmosis energy converter. *J Membr Sci* 1990;51:323-335.
- [31] Reali M, Dassie G, Jonsson G. Computation of salt concentration profiles in the porous substrate of anisotropic membranes under steady pressure-retarded osmosis conditions. *J Membr Sci* 1990;48:181-201.
- [32] Loeb S. Energy production at the Dead Sea by pressure-retarded osmosis: challenge or chimera?. *Desalination* 1998;120:247-262.
- [33] Seppälä A, Lampinen MJ. Thermodynamic optimizing of pressure-retarded osmosis power generation systems. *J Membr Sci* 1999;161:115-138.
- [34] Loeb S. One hundred and thirty benign and renewable megawatts from Great Salt Lake? The possibilities of hydroelectric power by pressure-retarded osmosis. *Desalination* 2001;141:85-91.
- [35] Loeb S. Large-scale power production by pressure-retarded osmosis, using river water and sea water passing through spiral modules. *Desalination* 2002;143:115-122.
- [36] Seppälä A, Lampinen MJ. On the non-linearity of osmotic flow. *Exp Therm Fluid Sci* 2004;28: 283-296.
- [37] Skilhagen S. Osmotic power- a new, renewable energy source, *Desalination* 2010;15:271-278.
- [38] Statkraft Press Centre. Crown princess of Norway to open the world's first osmotic powerplant2009,<http://www.statkraft.com/presscentre/pressreleases/crownprincess-mettemarit-to-open-the-worlds-first-osmotic-power-plant.aspx>.

- [39] Achilli A, Tzahi YC, Childress AE. Power generation with pressure retarded osmosis: An experimental and theoretical investigation. *J Membr Sci* 2009;343:42–52.
- [40] She Q, Hou D, Liu J, Tan KH, Tang CY. Effect of feed spacer induced membrane deformation on the performance of pressure retarded osmosis (PRO): Implications for PRO process operation. *J Membr Sci* 2013;445:170–182.
- [41] van der Zwan S, Pothof IWM., Blankert B, Bara JI. Feasibility of osmotic power from a hydrodynamic analysis at module and plant scale, *J Membr Sci* 2012;389:324–333.
- [42] Patel S. Statkraft Shelves Osmotic Power Project, *Power Magazine* 2014.<http://www.powermag.com/statkraft-shelves-osmotic-power-project/>.
- [43] Loeb S. Production of energy from concentrated brines by pressure retarded osmosis: I. Preliminary technical and economic correlations. *J Membr Sci* 1976;1:49–63.
- [44] Sivertsen E, Holt T, Thelin W, Brekke G. Modelling mass transport in hollow fibre membranes used for pressure retarded osmosis. *J Membr Sci* 2012;417–418:69–79.
- [45] McCutcheon JR, Elimelech M. Modeling water flux in forward osmosis: implications for improved membrane design. *AIChE J* 2007;53:1736–1744.
- [46] Azzaoui K, Mejdoubi E, Lamhamdi A, Zaoui S, Berrabah M, Elidrissi A, Hammouti, Moustafa B, Fouda MG, S Al-Deyab S. Structure and properties of hydroxyapatite/hydroxyethyl cellulose acetate composite films. *Carbohydr Polym* 2015;115:170–176.
- [47] Starbard N. *Beverage Industry Microfiltration*, John Wiley & Sons 2009;pp 47.
- [48] Wang X, Huang Z, Li L, Huang S, Hao Yu E, Scott K. Energy generation from osmotic pressure difference between the Low and high salinity water by pressure retarded osmosis. *J Technol Innov Renew Energy* 2012;1:122–30.
- [49] McCutcheon JR, Elimelech M. Influence of membrane support layer hydrophobicity on water flux in osmotically driven membrane processes, *J Membr Sci* 2008; 318:458–466.
- [50] Loeb S, Sourirajan S. UCLA Dept. Eng. Report No. 1961;60-60.
- [51] Beaudry EG, Lampi KA. Membrane technology for direct osmosis concentration of fruit juices. *Food Technol.* 1990;44:121.

- [52] Cath TY, Gormly S, Beaudry EG, Adams VD, Childress AE. Membrane contactor processes for wastewater reclamation in space. I. Direct osmotic concentration as pretreatment for reverse osmosis. *J Membr Sci* 2005;257:85–98.
- [53] Thorsen T, Holt T, The potential for power production from salinity gradients by pressure retarded osmosis. *J Membr Sci* 2009;335:103–10.
- [54] Schiestel T, Hänel C, Öxler L, Roelofs K, Walitza E, Cellulose acetate membranes with an optimized internal structure for pressure retarded osmosis. in: *Proceedings of the 3<sup>rd</sup> Osmosis Membrane Summit*, Statkraft, Barcelona; 2012.
- [55] Widjojo N, Chung TS, Weber M, Maletzko C, Warzelhan V. The role of sulphonated polymer and macrovoid-free structure in the support layer for thin-film composite (TFC) forward osmosis (FO) membranes. *J Membr Sci* 2011;383:214–23.
- [56] Zhang S, Fu FJ, Chung TS, Substrate modifications and alcohol treatment on thin film composite membranes for osmotic power, *Chem Eng Sci* 2013;87:40–50.
- [57] Bui N-N, McCutcheon J R. Nanofiber supported thin-film composite membrane for pressure-retarded osmosis. *Environ Sci Technol* 2014;48(7):4129–36.
- [58] Kim YC, Elimelech M. Potential of osmotic power generation by pressure retarded osmosis using seawater as feed solution: analysis and experiments. *J Membr Sci* 429 ;2013:330–37.
- [59] She Q, Jin X, Tang Chuyang Y. Osmotic power production from salinity gradient resource by pressure retarded osmosis: Effects of operating conditions and reverse solute diffusion. *J Membr Sci* 2012;401– 402:262–73.
- [60] Clausi DT, Koros WJ. Formation of defect-free polyimide hollow fiber membranes for gas separations. *J Membr Sci* 2000;167:79–89.
- [61] Mulder M. *Basic Principles of Membrane Technology*; Kluwer Academic Publishers: Dordrecht, The Netherlands; 1996.
- [62] Chou S, Wang R, Shi , She Q, Tang C, Fane AG. Thin-film composite hollow fiber membranes for pressure retarded osmosis (PRO) process with high power density. *J Membr Sci* 2012;389:25–33.
- [63] Chou S, Wang R, Fane A G. Robust and High performance hollow fiber membranes for energy harvesting from salinity gradients by pressure retarded osmosis. *J Membr Sci* 2013;448:44–54.
- [64] Han G, Chung T-S. Robust and high performance pressure retarded osmosis hollow fiber membranes for osmotic power generation, *AIChE J* 2014;60(3):1107–19.

- [65] Ingole PG, Choi W, Kim K-H, Jo H-D, Choi W-K, Park J-S, Lee H-K. Preparation, characterization and performance evaluations of thin film composite hollow fiber membrane for energy generation. *Desalination* 2014;345:136–45.
- [66] Li X, Chung T-S. Thin-film composite P84 copolyimide hollow fiber membranes for osmotic power generation. *Appl Energy* 2014;114:600–10.
- [67] Zhang S, Sukitpaneevit P, Chung T-S. Design of robust hollow fiber membranes with high power density for osmotic energy production. *Chem. Eng. J.* 2014;241:457–65.
- [68] Straub AP, Yip NY, Elimelech M. Raising the Bar: Increased hydraulic pressure allows unprecedented high power densities in Pressure-Retarded Osmosis. *Environ Sci Technol Lett* 2014;1:55–9.
- [69] Xie W, Geise MG, Freeman BD, Lee H-S, Byun G, McGrath James E. Polyamide interfacial composite membranes prepared from m-phenylene diamine, trimesoyl chloride and a new disulfonated diamine. *J Membr Sci* 2012;403–404:152–61.
- [70] Kim J, Lee J, Kim J-H. Overview of pressure-retarded osmosis (PRO) process and hybrid application to sea water reverse osmosis process. *Desal Wat Treat* 2012;43:193–200.
- [71] Altaee A. Forward Osmosis, Potential use in desalination and water reuse, *J Membr Sep Technol* 2012;1:79–93.
- [72] Saito K, Irie M, Zaitso S, Sakai H, Hayashi H, Tanioka A, Power generation with salinity gradient by pressure retarded osmosis using concentrated brine from SWRO system and treated sewage as pure water. *Desal Water Treat* 2012;41:114–21.
- [73] Feinberg BJ, Ramon G, Hoek EMV. Thermodynamic analysis of osmotic energy recovery at a reverse osmosis desalination plant. *Environ Sci Technol* 2013;47:2982–89.
- [74] Kim J, Park M, A-Snyder S, Kim J- H. Reverse osmosis (RO) and pressure retarded osmosis (PRO) hybrid processes: Model-based scenario study. *Desalination* 2013:322 121–30.
- [75] Achilli A, Prante JL, Hancock NT, Maxwell EB, Childress AE, Experimental results from RO-PRO: A next generation system for low-energy desalination. *Environ Sci Technol* 2014;48 (11):6437–43.

- [76] Prante JL, Ruskowitz JA, AE Childress, Achilli A, RO-PRO, desalination: An integrated low-energy approach to seawater desalination. *Appl Energy* 2014;120:104–14.
- [77] Lin S, NY Yip, Cath YT, CO Osuji, Elimelech M. Hybrid Pressure Retarded Osmosis–Membrane Distillation System for Power Generation from Low-Grade Heat: Thermodynamic Analysis and Energy Efficiency. *Environ Sci Technol* 2014;48:5306–13.
- [78] Altaee A, Zaragoza G, Sharif A, Pressure retarded osmosis for power generation and seawater desalination: Performance analysis. *Desalination* 2014;344:108–15.
- [79] Altaee A, Hilal N. Dual-stage forward osmosis/pressure retarded osmosis process for hypersaline solutions and fracking wastewater treatment. *Desalination* 2014;350:79–85.
- [80] Lewis A, Estefen S, Huckerby J, Musial W, Pontes T, Torres-Martinez J, Ocean energy, in: Edenhofer O, Pichs-Madruga R Sokona, Y, Seyboth K, Matschoss P, Kadner S, Zwickel T, Eickemeier P, Hansen G, Schlömer S, von Stechow C (Eds.). *IPCC Special Report on Renewable Energy Sources and Climate Change Mitigation*. Cambridge University Press, Cambridge and New York, 2011.
- [81] He W, Wang Y, Sharif A, Hasan Shaheed M. Thermodynamic analysis of a stand-alone reverse osmosis desalination system powered by pressure retarded osmosis, *Desalination* 2014;352:27–37.
- [82] He W, Wang Y, Shaheed M H. Enhanced energy generation and membrane performance by two-stage pressure retarded osmosis (PRO). *Desalination* 2015;359:186–99.
- [83] Lee J-G, Kim Y-D, Shim S-M, Im B-G, Kim W-S. Numerical study of a hybrid multi-stage vacuum membrane distillation and pressure-retarded osmosis system. *Desalination* 2015, <http://dx.doi.org/10.1016/j.desal.2015.01.043>.
- [84] Mega-ton Project Enters Final Stage, <http://www.desalination.com/wdr /49/16/mega-ton-project-enters-final-stage>; 2014.
- [85] Fritzmann C, Löwenberg J, Wintgens Melin T. State-of-the-art of reverse osmosis desalination. *Desalination* 2007;216:1–76.
- [86] She Q, Wong YKW, Zhao S, Tang CY. Organic fouling in pressure retarded osmosis: Experiments, mechanisms and implications. *J Membr Sci* 2013;428:181–89.

- [87] Thelin WR, Sivertsen E, Holt T, Brekke G. Natural organic matter fouling in pressure retarded osmosis. *J Membr Sci* 2013;438: 46–56.
- [88] Yip NY, Elimelech M. Influence of Natural Organic Matter Fouling and Osmotic Backwash on Pressure Retarded Osmosis Energy Production from Natural Salinity Gradients. *Environ Sci Technol* 2013;47:12607–16.
- [89] Chen SC, Wan C F, Chung T-S. Enhanced fouling by inorganic and organic foulants on pressure retarded osmosis (PRO) hollow fiber membranes under high pressures. *J Membr Sci* <http://dx.doi.org/10.1016/j.memsci.2015.01.037>.
- [90] Valladares Linares R, Bucs Sz S, Li Z, AbuGhdeeb M, Amy G, Vrouwenvelder JS. Impact of spacer thickness on biofouling in forward osmosis, *Wat Res* 57 (2014) 223–33.
- [91] Zhang M, Hou D, She Q, Tang CY. Gypsum scaling in pressure retarded osmosis: Experiments, mechanisms and implications. *Wat Res* 2014;48:383–95.
- [92] Skilhagen SE. Osmotic power: a new, renewable source of energy, in: *Proceedings of the 3<sup>rd</sup> Annual European Renewable Energy Markets*, Platts, Berlin; 2012.
- [93] A. O. Sharif, Ali A. Merdaw, M. Aryafar, P. Nicoll, *Theoretical and Experimental Investigations of the Potential of Osmotic Energy for Power Production*. *Membranes* 2014;4:447–468.
- [94] Kempener R, Neumann F. *Salinitygradient energytechnology brief*. The International Renewable Energy Agency; 2014.
- [95] Kleiterp R. *The Feasibility of a Commercial Osmotic Power Plant*. (Masterthesis), Department of Hydraulic Engineering, Delft University of Technology, Delft–The Netherlands; 2012.
- [96] Achilli A, Childress AE, Pressure retarded osmosis: from the vision of Sidney Loeb to the first prototype installation – review. *Desalination* 2010;261(3):205-11.
- [97] Tanioka A, Saito K, Irie M, Zaitso S, Sakai H, Hayashi H. Power generation by pressure retarded osmosis using concentrated brine from sea water desalination system and treated sewage: review of experience with pilot plant in Japan. in: *Proceedings of the 3<sup>rd</sup> Osmosis Membrane Summit*, Statkraft, Barcelona; 2012.
- [98] Dinger F, Troendle T, Platt U. Osmotic power plants, in: *Proceedings of the 3<sup>rd</sup> Osmosis Membrane Summit*, Statkraft, Barcelona; 2012.

- [99] Genné I, Brauns E. “Energy Generation and Desalination: The REAPOWER project”, in Lienard F, Neumann F., F. (eds.), *Salinity Gradient Power in Europe: State of the Art*, Sustainable Energy Week Brussels; 2011.
- [100] Stenzel P. Potentials of the Osmosis for Generating and Storing of Electricity. *Energy and Sustainability* 2012;4:ISBN: 978-3-643-11271.
- [101] U.S. Energy Information Administration, *Levelized Cost and Levelized Avoided Cost of New Generation Resources in the Annual Energy Outlook 2014*, <http://www.eia.gov/forecasts/aeo/index.cfm>.
- [102] Fernandez Y-T, Sanchez-Lzaso JL, Gonzales-Correa JM. Preliminary results of the monitoring of the brine discharge produced by the SWO desalination plant of Alicante (SESpain). *Desalination* 2005;182:395–402.
- [103] Raventos N, Macpherson E, García-Rubiés A. Effect of brine discharge from a desalination plant on macro benthic communities in the NW Mediterranean. *Mar Environ Res* 2006;62:1–14.
- [104] Kleverud J, Skilhagen SE, Brekke G. Experiences with the Tofte prototype plant. in: *Proceedings of the 3<sup>rd</sup> Osmosis Membrane Summit*, Statkraft, Barcelona; 2012.
- [105] Staalstrom A, Gitmark J. *Environmental Impacts by Running an Osmotic Power Plant*. Norwegian Institute for Water Research, Report no.6307-2012, Prepared for Statkraft Development AS, Oslo, Norway; 2012.
- [106] The United Nations World Water Development Report 3: *Water in a Changing World*; 2009.
- [107] Ramon GZ, Feinberg BJ, Hoek EMV. Membrane-based production of salinity-gradient power. *Energy Environ Sci* 2011;4:4423–34.
- [108] Francisco GM, Maria JA, MA Francisco. Renewable energy production in Spain: A review. *Renew Sust Energ Rev* 2014;33:509–31.
- [109] Naghiloo A, Abbaspour M, M-I Behnam, Bakhtari K. Modeling and design of a 25 MW osmotic power plant (PRO) on Bahmanshir River of Iran. *Renew Energy* 2015;78:51–59.





# Chapter 3: Water flux and power density in PRO

## 1. Introduction

As it has been seen in previous chapters, Pressure Retarded Osmosis is based on the osmotic transport of water across a semi-permeable membrane from a low salinity feed solution (e.g. river water or WWTP effluent) into a high salinity solution (e.g. seawater or brine) [1,2]. The draw solution side is pressurized at a specific value to obtain power by depressurizing the water permeated through the membrane.

This chapter concentrates on developing models that make possible to predict the performance of PRO. The exact description of the mass transport is very important to evaluate the membrane performance, taking into account all negative effects that reduce the performance, such as the Internal Concentration Polarization (ICP), caused by the membrane porous layer, and the External Concentration Polarization (ECP), building up in the fluid boundary layers on both sides of membrane [3].

In PRO salts are transported towards the low concentration solution (due to the chemical potential difference on the two sides of membrane), while water is transported in the opposite direction (due to the osmotic pressure difference). This clearly differs from Reverse Osmosis, where these flows are in the same direction, so PRO models must take this into account: PRO operating conditions and PRO membranes are therefore different from RO.

Several models have been developed to reproduce the water and salt fluxes across the membrane [3,4,5,8,9]. Most of them apply the well-known diffusion-convection water transport equation [6] and neglect the effect of the external concentration polarization that occurs in the feed solution side. This assumption is acceptable when the feed solution is negligible, but not when the concentration of the feed solution is significant (e.g. seawater or WWTP effluents). Moreover, the developed models the effect of the pressure on the reverse salt flux  $J_s$  is neglected; however it has been shown that the applied pressure has a strong effect on the salt diffusion, and therefore the water flux [5].

Thus, in this chapter, a mathematical model is developed to simulate the water flux in PRO. The model was developed by using the minimum of assumptions, so it takes into consideration the effect of the Internal Concentration Polarization (ICP), the External Concentration Polarization on both sides of the membranes, and the effect of pressure on the salt flux diffusion. This model was validated and tested at lab scale, under different operating conditions to show its consistency. An important operating parameter is also studied here in detail: the temperature. For that, a mathematical model was developed to describe the distribution of the temperature inside the membrane depending on the bulk temperatures. After that, the effect of the temperature on the water flux and the power density was studied, using experimental results and the developed models.

## 2. Modeling

### 2.1 Basic models for water and salt fluxes

In an osmotically driven membrane process, the water permeation flux  $J_w$  across an ideal semipermeable thin film that allows water passage but rejects solute molecules or ions is related to the water permeability  $A$ , the effective osmotic pressure difference  $\Delta\pi_m$  and the trans-membrane hydraulic pressure difference  $\Delta P$  as follows[11]:

$$J_w = A (\Delta\pi_m - \Delta P) \quad (3.1)$$

The effective osmotic pressure difference can be evaluated from:

$$\Delta\pi_m = \pi_{D,m} - \pi_{F,m} \quad (3.2)$$

where  $\pi_{D,m}$  and  $\pi_{F,m}$  are the osmotic pressure at the surface of the active and support layers, respectively (see Fig. 3.1).

On the other hand, salts permeate across the membrane from the draw solution into the feed solution, in the opposite direction of the water flux. This so-called reverse salt flux  $J_s$ , is described as follows [12]:

$$J_s = B(C_{D,m} - C_{F,m}) \quad (3.3)$$

where  $B$  is the salt permeability coefficient of the membrane active layer and  $C_{D,m}$  and  $C_{F,m}$  are the solute concentrations at the interface of the active and support layers, respectively. A typical concentration profile through the membrane is shown in Fig. 3.1.

The specific salt flux in PRO, defined as the ratio of salt flux to water flux  $J_s/J_w$ , is affected by the intrinsic transport properties of the membranes, as follows [13]:

$$\frac{J_s}{J_w} = \frac{B}{A\beta RT} \left( 1 + \frac{A\Delta P}{J_w} \right) \quad (3.4)$$

where  $\beta$  is the van't Hoff coefficient,  $R$  is the universal gas constant, and  $T$  is the absolute temperature.

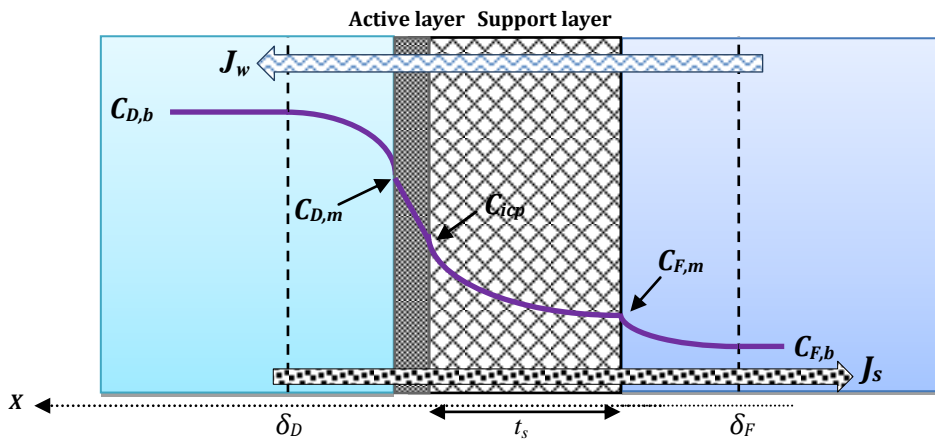


Fig.3.1: Concentration profile through the membrane, with directions of the water flux  $J_w$  and salt flux  $J_s$ . The membrane module is under counter-current cross-flow mode.

## 2.2 Concentration polarization

In osmotically driven membrane processes, concentration polarization is caused by the concentration difference between the feed and draw solutions through an asymmetric membrane, with the profile for a PRO membrane illustrated in Fig. 3.1. Both external concentration polarization (ECP) and internal concentration polarization (ICP) take place in PRO processes [14,20]. Generally, ECP occurs at the surface of the dense active layer of the membrane and ICP occurs within the

porous support layer of the membrane. They are now described following [15,21].

### 2.2.1 Internal concentration polarization (ICP)

When a non-ideal composite membrane is operated in a typical PRO process (with the active layer facing the draw solution), water flows from the feedside through the support and active layers into the draw solution (flux  $J_w$ ), while salts permeate from the draw side across the membrane skin and the support layer into the feed solution (flux  $J_s$ ). Therefore, there exists a salt gradient in the membrane support. This salt gradient will result in concentrative internal concentration polarization ICP and lower the osmotic driving force for water flow across the membranes [16,20]. Internal concentration polarization (ICP) occurs when the thin film is supported by a porous substrate. Based on the mass balance in the porous substrate layer, Lee et al. [17] developed a theoretical model for the PRO process which indicated that membranes with high water permeation and high salt rejection are essential for high PRO performance. Assuming for simplicity a single solute (salt) in the draw side, the mass transport of this salt into the membrane support, and in each of the boundary layers, will equal the sum of the convective and diffusive salt transports due to the gradient in salt concentration. Hence, the transport of salt can be described by [17]:

$$D_{s,l} \frac{dC(x)}{dx} - J_w C(x) = J_s \quad (3.5)$$

where  $C(x)$  is the salt concentration at position  $x$  and  $D_{s,l}$  is the diffusion coefficient of the support layer defined as:

$$D_{s,l} = \frac{\varepsilon D}{\tau} \quad (3.6)$$

where  $D$  is the bulk diffusion coefficient,  $\varepsilon$  is the porosity and  $\tau$  is the tortuosity of the support layer.

Rearrangement of Eq. (3.5) gives:

$$\left(\frac{1}{C + \frac{J_s}{J_w}}\right) dC = \frac{\tau}{\varepsilon D} J_w dx \quad (3.7)$$

Integration of Eq. (3.7) over the support layer using boundary conditions:

$$C(x=0) = C_{F,m}$$

$$C(x=t_s) = C_{icp}$$

where the distance  $x$  is measured from the interface between the support and active layers,  $C_{icp}$  is the solute concentration at the interface between the support and active layers, and  $t_s$  is the thickness of the support layer (Fig. 3.1), gives

$$C_{icp} = \left(C_{F,m} + \frac{J_s}{J_w}\right) \exp(J_w K) - \frac{J_s}{J_w} \quad (3.8)$$

where  $K$  is the solute resistivity for diffusion within the support layer, defined as:

$$K = \frac{\tau t_s}{\varepsilon D} = \frac{s}{D} \quad (3.9)$$

where  $s$  is defined as the structure parameter of the support layer. This is a property of the support structure which provides a length scale of the concentration polarization in the support layer, analogous to the boundary layer thickness in external concentration polarization [18].

Referring to Eq. (3.8),  $C_{icp}$  clearly shows the effect of the external concentration polarization (created by the flux  $J_s$ ) on the feed solution side  $C_{F,m}$ .

## 2.2.2 External concentration polarization (ECP)

### 2.2.2.1 ECP on the draw solution side:

The dilutive external concentration polarization (ECP) is the concentration polarization that results in the solute being diluted on the draw solution side of the membrane. The reverse draw solute flux on the side of the draw solution can also be derived using the same differential equation as in Eq. (3.5), albeit with different boundary conditions, assuming a steady-state condition. Thus, the boundary

conditions for ECP on the draw solution side are:

$$C(x = 0) = C_{D,m}$$

$$C(x = \delta_D) = C_{D,b}$$

where the distance  $x$  is now measured from the membrane surface of the active layer side and  $\delta_D$  is the thickness of the draw boundary layer.

Integration of Eq. (3.7) over the thickness of the draw boundary layer using these boundary conditions gives:

$$C_{D,m} = \left( C_{D,b} + \frac{J_s}{J_w} \right) \exp\left(-\frac{J_w}{k_D}\right) - \frac{J_s}{J_w} \quad (3.10)$$

where  $k_D$  is the mass transfer coefficient in the draw solution, calculated using

$$k_D = \frac{Sh D_D}{d_h} \quad (3.11)$$

where  $D_D$  is the diffusion coefficient of the solute in the draw solution,  $d_h$  is the hydraulic diameter of the flow channel, and  $Sh$  is the Sherwood number, which has been experimentally determined from correlations under several flow conditions as follows [19]:

$$Sh = 0.04 Re^{0.75} Sc^{0.33} \quad (\text{Turbulent flow}) \quad (3.12)$$

$$Sh = 1.85 \left( Re \cdot Sc \frac{d_h}{L} \right) \quad (\text{Laminar flow}) \quad (3.13)$$

Where  $Re$  is the Reynolds number,  $Sc$  is the Schmidt number and  $L$  is the length of the channel. These Reynolds and Schmidt numbers are calculated as follows:

$$Re = \frac{v \cdot d \cdot \rho}{\eta} = \frac{v \cdot d}{\mu} \quad (3.14)$$

$$Sc = \frac{\mu}{\rho D} \quad (3.15)$$

where  $v$  is the velocity of the solution,  $d$  is the diameter of the pipe,  $\rho$  is the density of the solution,  $\eta$  the dynamic viscosity of the solution and  $\mu$  its cinematic viscosity.

### 2.2.2.2 ECP on the feed solution side

To derive a model for the ECP on the feed solution side a similar process can be followed, but using the boundary conditions

$$C(x = 0) = C_{F,b}$$

$$C(x = \delta_F) = C_{F,m}$$

where the distance  $x$  is now measured from the feed boundary layer side and  $\delta_F$  is the thickness of the feed boundary layer.

Integration of Eq. (3.7) over the thickness of the feed boundary layer using these boundary conditions gives:

$$C_{F,m} = \left( C_{F,b} + \frac{J_s}{J_w} \right) \exp\left(\frac{J_w}{k_F}\right) - \frac{J_s}{J_w} \quad (3.16)$$

where  $k_F$  is the mass transfer coefficient in the draw solution, which is calculated using:

$$k_F = \frac{Sh D_F}{d_h} \quad (3.17)$$

where  $D_F$  is the diffusion coefficient of the solute in the feed solution.

### 2.3 Model of the water flux $J_w$

As shown in Eq. (3.1),  $\Delta\pi_m$  is the effective pressure that takes into consideration ICP and ECP on both sides of the membrane. As we have assumed for simplicity that there is only one type of solute in the system, which means that the solute concentration is proportional to the osmotic pressure. Thus, we consider that:

$$\pi_{D,m} = \beta RT C_{D,m} \quad (3.18)$$

$$\pi_{icp} = \beta RT C_{icp} \quad (3.19)$$

$$\pi_{F,m} = \beta RT C_{F,m} \quad (3.20)$$

It was mentioned in Eq. (3.8) that  $C_{icp}$  shows the effect of the external concentration polarization on the feed solution side, so we can consider that the effective osmotic pressure governing the mechanism is as defined in [17]:

$$\Delta\pi_m = \pi_{D,m} - \pi_{icp} \quad (3.21)$$

So, substituting  $C_{D,m}$  in Eq. (3.18) with its expression developed in Eq. (3.10), substituting  $C_{icp}$  in Eq. (19) with its expression developed in Eq. (3.8), and substituting the ratio  $J_s/J_w$  with its expression presented in Eq. (3.4) ,  $J_w$  can be written using Eq. (3.1) as follows:

$$J_w = A \left[ \left( \pi_{D,b} + \frac{B}{A} \left( 1 + \frac{A\Delta P}{J_w} \right) \right) \exp\left(-\frac{J_w}{k_D}\right) - \left[ \pi_{F,b} + \frac{B}{A} \left( 1 + \frac{A\Delta P}{J_w} \right) \right] \exp(J_w K) \exp\left(\frac{J_w}{k_F}\right) - \Delta P \right] \quad (3.22)$$

The power density  $W$ , defined as the osmotic energy output per unit membrane area, can be calculated by the product of the trans-membrane pressure  $\Delta P$  and the water flux  $J_w$  permeating across the membrane, as follows:

$$W = J_w \Delta P = A \left[ \left( \pi_{D,b} + \frac{B}{A} \left( 1 + \frac{A\Delta P}{J_w} \right) \right) \exp\left(-\frac{J_w}{k_D}\right) - \left[ \pi_{F,b} + \frac{B}{A} \left( 1 + \frac{A\Delta P}{J_w} \right) \right] \exp(J_w K) \exp\left(\frac{J_w}{k_F}\right) - \Delta P \right] \Delta P \quad (3.23)$$

#### 2.4 Model of the temperature profile through the membrane

In parallel to the water transport in PRO heat is transferred through the membrane: A temperature difference is created at membrane interfaces due to the difference of temperatures at each side of the membrane. The resultant temperature gradient across the membrane, translates into non-homogenous conditions, which in turn, affect the water transport across the membrane. Heat

transfer also occurs between bulk solutions and membrane surface.

In this section, a model that describes the effect of the different temperatures on the membrane parameters is studied, and therefore its effect on the power density is evaluated. It is important to consider the temperature at each part of the process, so we consider that temperatures in the bulks are not the same ( $T_{F,b} \neq T_{D,b}$ ), with the temperature profile presented in Fig. 3.2. This temperature difference induces heat transfer by convection in the opposite direction. In addition, there are two boundary layers adjoining the membrane and heat is transferred between the bulk and the membrane interface. We also assume that the heat transfer through the membrane is by conduction, that the heat fluxes are unidirectional and perpendicular to the surface of the membrane, that there is no gap between the active and support layers and that there is no discontinuity of temperature at the interfaces.

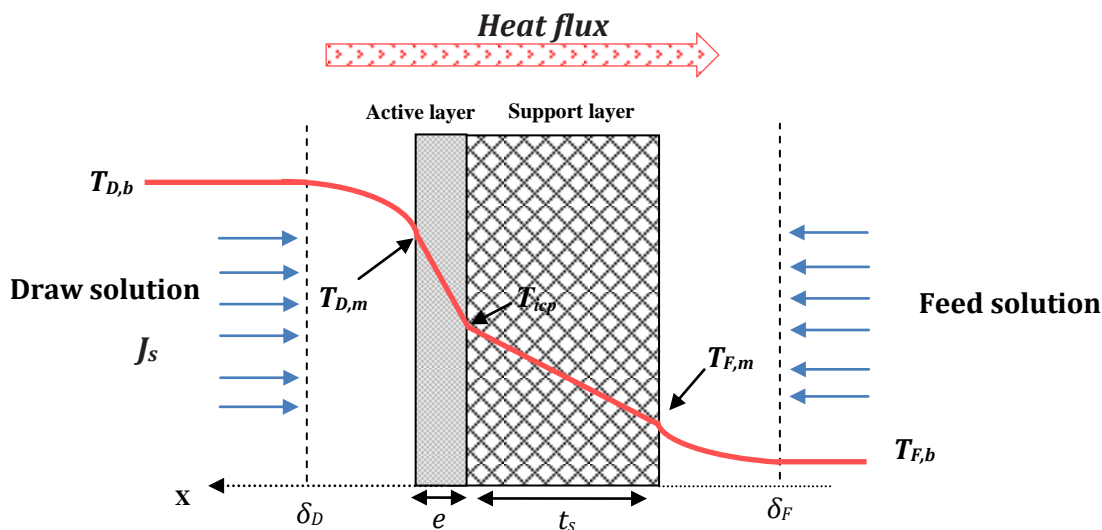


Fig.3.2: temperature profile over the membrane, when  $T_{D,b} > T_{F,b}$ .  $T_{D,m}$ : temperature of the active layer (side in contact with the draw solution),  $T_{icp}$ : temperature of the limit surface between the active and the support layers.  $T_{F,m}$ : the temperature of the support layer (side in contact with the feed solution).

The support layer of the membrane is, in fact, not dense, but it is a porous layer characterised by a porosity which affects the mode of heat transfer across the media. Thus, to calculate the heat transfer rate in the support layer some assumptions are taken into consideration:

We assume that the porous medium is rigid, uniform, isotropic and fully saturated

with the solution. The thermo-physical properties of both solute and solution are constant, that the phases are in local thermal equilibrium, and that the thermal dispersion is negligible.

The equation of energy conservation is then given by [22]:

$$\frac{d(uT)}{dx} = \frac{d}{dx} \left( \frac{\lambda_{s,l}}{\rho c_p} \frac{dT}{dx} \right) \quad (3.24)$$

where  $\rho$  and  $c_p$  are the density and specific heat capacity of the feed solution, respectively. The effective thermal conductivity of the support layer  $\lambda_{s,l}$  is given by [21]:

$$\lambda_{s,l} = (1 - \varepsilon)\lambda_s + \varepsilon\lambda_F \quad (3.25)$$

where  $\lambda_s$  and  $\lambda_F$  are the thermal conductivity of the material that constitutes the support layer and of the feed solution, respectively.

The velocity of the water can be calculated using the Darcy's law in the presence of a pressure gradient. In the axial orientation, the velocity is then [23]:

$$u = \frac{\varphi}{\mu} \frac{\partial P}{\partial x} = \frac{\varphi}{\mu} \frac{\partial(\Delta\pi_m - \Delta P)}{\partial x} \quad (3.26)$$

where the permeability  $\varphi$  is given by [29,31]:

$$\varphi = \frac{\varepsilon^3 d_p^2}{150(1-\varepsilon)^2} \quad (3.27)$$

where  $d_p$  and  $\varepsilon$  represent, respectively, the diameter of the pores and the porosity of the support layer.

As the heat flux is  $Q = -\lambda_{s,l} \frac{\partial T}{\partial x}$  and the boundary conditions for the temperature are

$$T(x=0) = T_{F,m}$$

$$T(x=t_s) = T_{icp}$$

Then, integration of the energy conservation Eq.(3.24) over the support layer gives

$$T_{icp} - T_{F,m} = \frac{Q}{u\rho c_p} \exp\left(\frac{u\rho c_p}{\lambda_{s,l}} t_s\right) \quad (3.28)$$

We then introduce the following parameters [22,24]:

$$Nu = \frac{Q}{(T_{F,m} - T_{icp}) \lambda_{s,l}} \quad (\text{Nusselt number})$$

$$Re_x = \frac{u\rho t_s}{\mu} \quad (\text{Local Reynolds number})$$

$$Pr = \frac{\mu c_p}{\lambda_{s,l}} \quad (\text{Local Prandtl number})$$

Using these parameters Eq. (3.28) can be rearranged to be:

$$T_{F,m} - T_{icp} = -\frac{Q}{RePr \lambda_{s,l}} \exp(Re_x Pr_x) \quad (3.29)$$

Thus, the thermal conductivity of the support layer  $h_{s,l}$  is:

$$h_{s,l} = \frac{\lambda_{s,l}}{t_s} Re Pr \exp(Re_x Pr_x) = Nu_x \frac{\lambda_{s,l}}{t_s} \quad (3.30)$$

where  $Nu_x$  is the local Nusselt number. At steady-state conditions, the heat transfer equation is as follows:

$$\begin{aligned} Q &= h_F(T_{F,b} - T_{F,m}) \\ &= J_w \rho_w C_p (T_{F,b} - T_{D,b}) - h_{s,l} (T_{icp} - T_{F,m}) - J_s \rho_s C_p (T_{D,b} - T_{F,b}) - h_{a,l} (T_{D,m} - T_{icp}) \\ &= h_D (T_{D,m} - T_{D,b}) \end{aligned} \quad (3.31)$$

where  $\rho_w$  and  $\rho_s$  are the densities of the feed and draw solutions, respectively,  $h_D$  and  $h_F$  are the heat transfer coefficients in the feed and in the draw boundary

layer, respectively, defined as:

$$h_D = \frac{\lambda_D}{\delta_D} S \quad (3.32)$$

$$h_F = \frac{\lambda_F}{\delta_F} S \quad (3.33)$$

with  $\lambda_D$  the thermal conductivity coefficient of the draw solution and  $S$  the surface of the membrane.

Finally, the thermal conductivity of the active layer  $h_{a,l}$  is defined as:

$$h_{a,l} = \frac{\lambda_{a,l}}{e} \cdot S \quad (3.34)$$

where  $e$  is the thickness of the active layer.

Rearranging Eq. (3.31) gives explicit expressions for  $T_{D,m}$  and  $T_{F,m}$  :

$$T_{F,m} = \frac{h_F T_{F,b} \left(1 + \frac{h_{a,l}}{h_D}\right) - J_w \rho_w c_p (T_{F,b} - T_{D,b}) + J_s \rho_s c_p (T_{D,b} - T_{F,b}) + (h_{s,l} - h_{a,l}) T_{icp} + h_{a,l} T_{D,b}}{h_F \left(1 + \frac{h_{a,l}}{h_D}\right) + h_{s,l}} \quad (3.35)$$

$$T_{D,m} = \frac{h_D T_{D,b} \left(1 + \frac{h_{s,l}}{h_F}\right) + J_w \rho_w c_p (T_{F,b} - T_{D,b}) - J_s \rho_s c_p (T_{D,b} - T_{F,b}) + (h_{a,l} - h_{s,l}) T_{icp} + h_{s,l} T_{F,b}}{h_D \left(1 + \frac{h_{s,l}}{h_F}\right) + h_{a,l}} \quad (3.36)$$

$T_{icp}$  is not exactly the arithmetic mean of  $T_{D,m}$  and  $T_{F,m}$  because of differences between the characteristics of the material of each layer and its width. Taken these into consideration,  $T_{icp}$  can be reasonably approximated as:

$$T_{icp} = \frac{e \cdot h_{a,l} T_{D,m} + t_s \cdot h_{s,l} T_{F,m}}{e \cdot h_{a,l} + t_s \cdot h_{s,l}} \quad (3.37)$$

Solving the system of equations formed by (3.35), (3.36) and (3.37) gives explicit values of  $T_{D,m}$ ,  $T_{icp}$  and  $T_{F,m}$ .

### 3. Materials and methods

In order to validate the model developed in the last section, results from experiments with two membranes were used. All model parameters and experimental conditions for the verification are summarized in Tables 3.1, 3.2 and 3.3.

#### *3.1 Solution chemistries*

Certified ACS-grade NaCl (Fisher Scientific) was used to prepare both feed and draw solutions. Mass and velocities were obtained from provided Labview software. Operating temperatures, osmotic pressures, viscosities, and diffusion coefficients of solutions were calculated and are shown in Tables 3.1 and 3.2.

#### *3.2 Membranes*

Two flat-sheet cellulose acetate membranes were used in the experiments: Commercial FO membrane (TCA) from Hydration Technology Innovations, Albany OR, called here HTI membrane [27] and a membrane developed by Fraunhofer Institute for Interfacial Engineering and Biotechnology, called here IGB membrane [28]. The physical characteristics of this IGB membrane are similar to other commercially available semi-permeable membranes.

#### *3.3 PRO bench-scale*

The laboratory equipment is reported in Fig. 3.3. The test unit had a channel on the feed side of the membrane to allow the feed solution to flow tangentially to the membrane. This channel was 40mm long, 25mm wide and 2.5mm deep, with an effective membrane area of 18cm<sup>2</sup>. Mesh spacers placed in the feed channel supported the membrane and enhanced the turbulence in the feed stream. The feed solution was contained in a 5 litre reservoir. A high-pressure positive displacement pump was used to recirculate the feed solution at selected velocities. Purge was collected in a 5 litre container. Each container was placed on an analytical balance. Temperatures were controlled using thermostatic baths. The flux through the membrane was calculated based on the change of weight in the containers. The conductivities were also recorded.

Table 3.1: Characteristics of 8.55mM NaCl feed solution at different operating temperatures.

$T_F$ (°C)	$D_F$ (m <sup>2</sup> /s)	$\eta_F$ (Pa.s)	$\pi_{F,b}$ (bar)
20	$3.80 \times 10^{-9}$	$1.02 \times 10^{-3}$	0.38
30	$4.93 \times 10^{-9}$	$7.89 \times 10^{-4}$	0.39
40	$6.23 \times 10^{-9}$	$6.53 \times 10^{-4}$	0.40

Table 3.2: Characteristics of two NaCl draw solutions at different operating temperatures.

$T_D$ (°C)	1.026M			0.6M		
	$D_D$ (m <sup>2</sup> /s)	$\eta_D$ (Pa.s)	$\pi_{D,b}$ (bar)	$D_D$ (m <sup>2</sup> /s)	$\eta_D$ (Pa.s)	$\pi_{D,b}$ (bar)
20	$3.43 \times 10^{-9}$	$1.11 \times 10^{-3}$	45.4	$3.56 \times 10^{-9}$	$1.07 \times 10^{-3}$	26.3
30	$4.33 \times 10^{-9}$	$9.1 \times 10^{-4}$	46.9	$4.78 \times 10^{-9}$	$8.60 \times 10^{-4}$	27.2
40	$5.79 \times 10^{-9}$	$7.02 \times 10^{-4}$	48.5	$5.92 \times 10^{-9}$	$6.95 \times 10^{-4}$	28.1

Table 3.3 :Parameters used for modelling.

Parameter	TCA FO Membrane	IGB membrane
Water permeability coefficient $A$	$3.56 \times 10^{-13}$ m/s/Pa	$1.06 \times 10^{-12}$ m/s/Pa
Salt permeability coefficient $B$	$5.90 \times 10^{-9}$ m/s	$2.62 \times 10^{-8}$ m/s
Solute resistivity $K$	$1.52 \times 10^5$ s/m	$1.52 \times 10^5$ s/m
Mass transfer coefficient (draw side) $k_D$	$1.17 \times 10^{-4}$ m/s	$1.17 \times 10^{-4}$ m/s
Mass transfer coefficient (feed side) $k_F$	$1.19 \times 10^{-4}$ m/s	$1.19 \times 10^{-4}$ m/s
Diffusion coefficient in the draw solution $D_D$	$4.25 \times 10^{-9}$ m <sup>2</sup> /s	$4.25 \times 10^{-9}$ m <sup>2</sup> /s
Diffusion coefficient in the feed solution $D_F$	$4.35 \times 10^{-9}$ m <sup>2</sup> /s	$4.35 \times 10^{-9}$ m <sup>2</sup> /s
Porosity of the support layer $\epsilon$	80 %	80 %
Thickness of the active layer $e$	10-20 $\mu$ m [26]	100 nm
Thickness of the support layer $t_s$	50 $\mu$ m [29]	12 $\mu$ m

Table 3.4: Experimental conditions.

Variable	Values
Temperature	20°C
Concentration of the feed bulk $C_{F,b}$	8.55 mM ( $\approx 0.5$ g/l)
Concentration of the draw bulk $C_{D,b}$	0.6 M ( $\approx 35$ g/l)
Dynamic viscosity of the feed solution $\eta_F$	$8.91 \times 10^{-4}$ Pa.s
Dynamic viscosity of the draw solution $\eta_D$	$9.11 \times 10^{-4}$ Pa.s
Density of the feed solution $\rho_w$	997.4 kg/m <sup>3</sup>
Density of the draw solution $\rho_s$	1034 kg/m <sup>3</sup>
Hydraulic diameter $d_h$	$9.46 \times 10^{-4}$ m
Length of the channel	0.070m

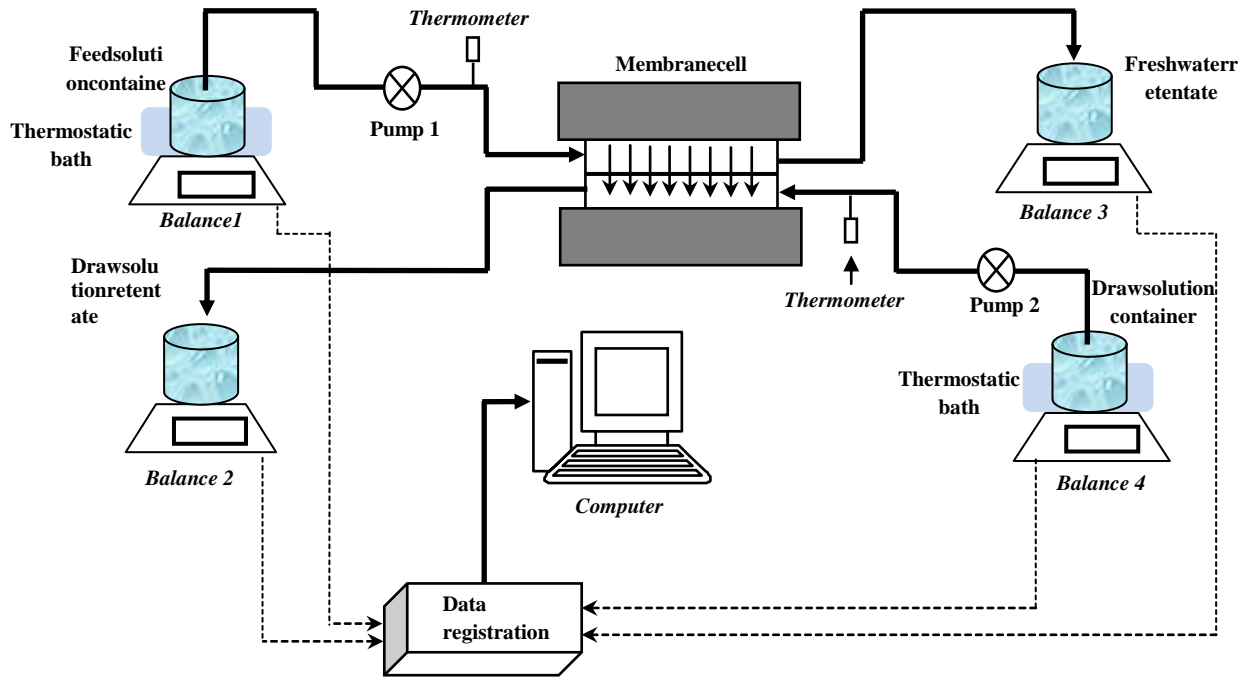


Fig.3.3:Schematic of laboratory bench-scale PRO system.

#### 4. Results and discussion

Using the experimental system and the modelling parameters presented in Section 3, the model developed is now discussed.

##### 4.1 Model validation

In order to validate the model developed in the Section 2, results from experiments on the PRO bench-scale system presented in Section 3 are now discussed. Solutions characteristics, model parameters and experimental conditions are summarized in Tables 3.1, 3.2 and 3.3, respectively.

The predicted results of the model proposed in Eqs. (3.22) and (3.23) is compared with the experimental data in Figs. 3.4, 3.5 and 3.6, that show the comparison for water flux  $J_w$ , power density  $W$  and reverse salt flux  $J_s$ , respectively. It can be seen clearly that the model presented in Eq. (3.22) describes the experimental results closely for both membranes. Effectively, the maximum specific power is obtained for a hydraulic pressure around half of the osmotic pressure, as expected.

Compared to the other models, the model proposed here takes into consideration

the mass transfer coefficient of the feed solution, which can be significant in terms of internal concentration polarization when the concentration of the feed solution is not low (for instance when the feed is seawater and the draw is brine) and the solution temperature is significantly high [37]. Clearly, the model shows that the concentration at the surface of the support layer and the concentration on the feed bulk are different; thus, the effective osmotic pressure will be significantly different from the case when the two concentrations are the same especially in the case of non-fresh water in the feed side.

It can also be appreciated in the experimental results that the performance of the IGB membrane is better than the HTI membrane (as predicted by the proposed models). In fact, the water permeability coefficient  $A$  of the IGB membrane is around four times that of the HTI membrane. Nonetheless, the HTI membrane presents better attenuation of the reverse salt flux (six times smaller). It must be pointed out that the results for the HTI membrane are consistent with previous results when tested in similar conditions (such as the 35g/l as draw solution, 0 g/l as feed solution tested in [8]). The obtained power density is similar, taking into account that the feed solution concentrations are slightly different (a more realistic 0.5 g/l is used as feed solution for the current study, which leads to an internal polarization concentration).

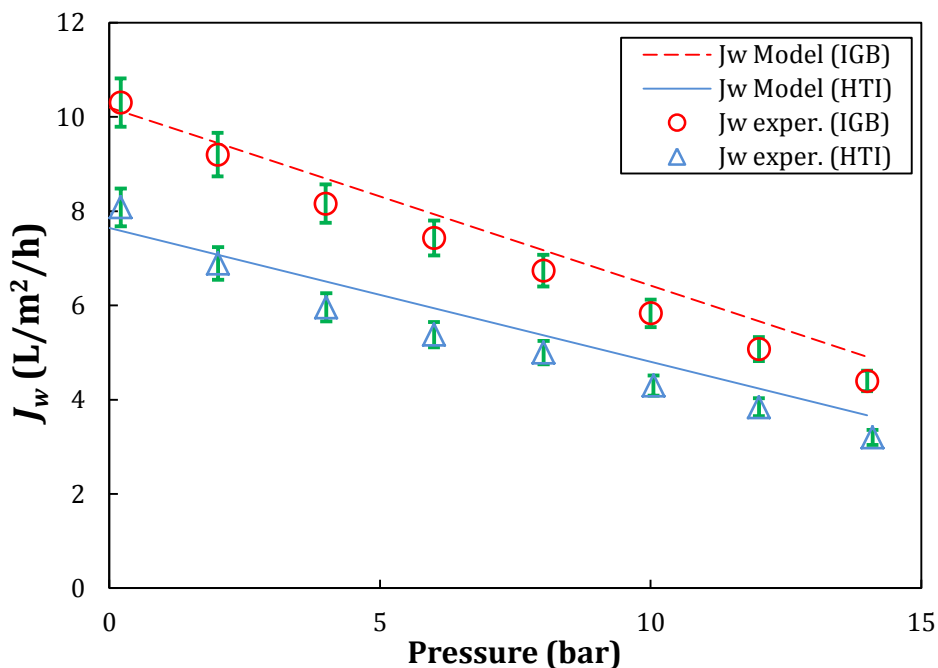


Fig. 3.4: Simulation using Eq. (3.22) and experimental results of the water flux ( $J_w$ ) in PRO process as a function of the applied pressure ( $\Delta P$ ).

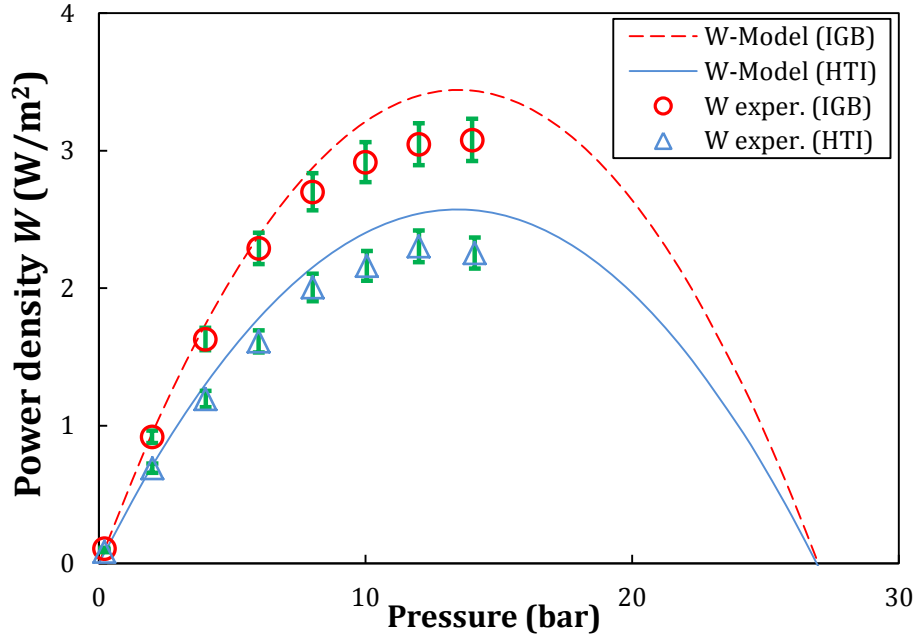


Fig. 3.5: Simulation using Eq. (3.23) and experimental results of the power density ( $W$ ) in the PRO process as a function of the applied pressure ( $\Delta P$ ).

Table 3.5: Comparison of the proposed PRO water flux model with previous models.

<i>Model</i>	<i>Model equation and assumptions</i>
Achilli et al. [8]	$J_w = A \left( \pi_{D,b} \exp\left(-\frac{J_w}{k}\right) \frac{1 - \frac{\pi_{F,b}}{\pi_{D,b}} \exp(J_w K) \exp\left(\frac{J_w}{k}\right)}{1 + \frac{B}{J_w} [\exp(J_w K) - 1]} - \Delta P \right)$ $C_{F,m} = C_{F,b}; k_D = k_F = k; \pi = \beta RTC; \frac{C_{F,b}}{C_{D,m}} = \frac{\pi_{F,b}}{\pi_{D,m}}$
Prante et al. [25]	$J_w = A \left( \frac{\pi_{D,b} \exp\left(-\frac{J_w}{k}\right) - \pi_{F,b} \exp(J_w K)}{1 + \frac{B}{J_w} [\exp(J_w K) - \exp\left(-\frac{J_w}{k}\right)]} - \Delta P \right)$ $C_{F,m} = C_{F,b}; k_D = k_F = k; \pi = \beta RTC$
Proposed model	$J_w = A \left[ \left( \pi_{D,b} + \frac{B}{A} \left( 1 + \frac{A \Delta P}{J_w} \right) \right) \exp\left(-\frac{J_w}{k_D}\right) - \left[ \pi_{F,b} + \frac{B}{A} \left( 1 + \frac{A \Delta P}{J_w} \right) \right] \exp(J_w K) \exp\left(\frac{J_w}{k_F}\right) - \Delta P \right]$ $C_{F,m} \neq C_{F,b}; k_D \neq k_F; \pi = \beta RTC$

#### 4.2 Effect of the concentrations of feed and draw solutions

Several types of draw and feed solutions could be used in PRO, as long as a sufficient osmotic pressure difference is achieved to guarantee the functioning of the process [29]. However, the power produced is not economically viable if it is lower than  $5 \text{ W/m}^2$  [7]. This criterion requires a good choice of feed and draw solution, in order to exceed this minimum value.

Thus, the effect of the concentrations of these solutions is now studied: combinations of four feed solutions with different concentration (8.55mM, 55mM, 0.2M, and 0.3M of NaCl) and two different draw solutions (0.6M and 1.026 M of NaCl) were tested. To reduce the number of experiments, when testing feed solutions the concentration of the draw solution was always 0.6M, whereas for draw solutions tests, the feed solution was maintained at 8.55mM. All solutions were tested under the same flow rate (FR=50ml/min). The water flux model Eq. (3.22) was solved numerically to determine the theoretical water flux  $J_w$  and the corresponding power densities were calculated over a range of hydraulic pressure differences.

Fig. 3.6 and 3.7 present the model and experimental results with the IGB PRO membrane. As expected, the power density values decrease as the concentration of the feed solution becomes higher (Fig. 3.6), due to the decrease of the osmotic pressure difference. Theoretically, the power density reaches a maximum when the applied pressure  $\Delta P$  is half of the osmotic pressure difference [8], and reaches a minimum when the applied pressure is close to the osmotic pressure difference. In reality, maximum power density occurs at  $\Delta P = \frac{\Delta\pi}{2}$ : The ICP effect is accentuated on the surface of the membrane while increasing the concentration of the feed solution.

Fig. 3.6 shows also that increasing the concentration of the feed solution from 8.55mM to 55mM leads to a decrease of the power density of about 60%. On the contrary, Fig. 3.7 shows that when the concentration of draw solution was increased from 0.6 to 1.026M NaCl, the power density significantly increased (about 40 %). With a draw solution concentration around 1M, a significant power density could be produced ( $W > 5 \text{ W/m}^2$ ). Using draw solutions with high

concentration, the water flux increases significantly and therefore the power density also increases.

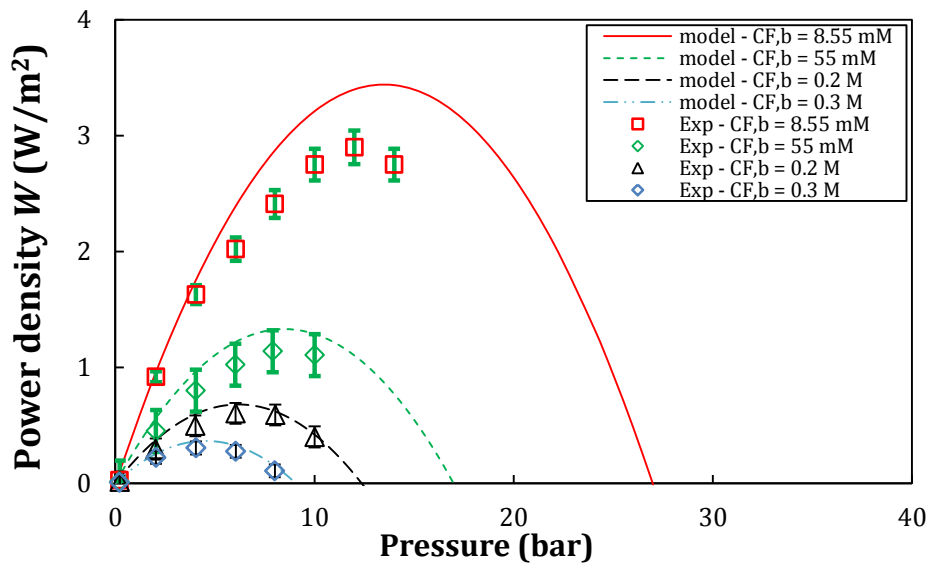


Fig 3.6: Modeled and experimental power density for different feed solution concentrations as a function of applied pressure ( $C_{D,b} = 0.6$  M, temperature  $T = 20^\circ\text{C}$ , flow rate:  $\text{FR} = 50\text{ml}/\text{min}$ ).

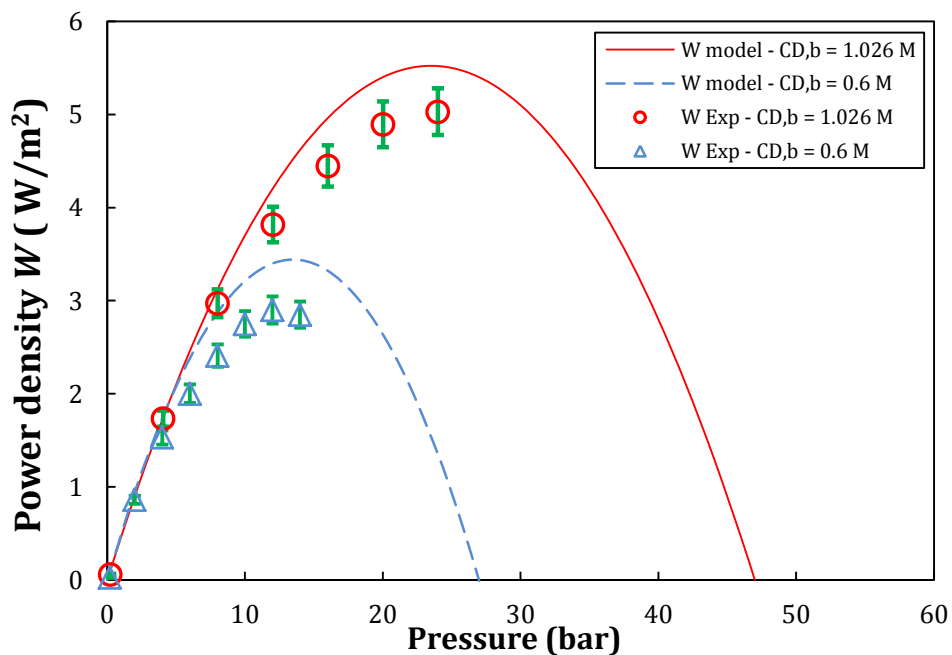


Fig 3.7: Modeled and experimental power density for different draw solution concentrations as a function of applied pressure ( $C_{F,b} = 8.55\text{mM}$ ,  $T = 20^\circ\text{C}$ ,  $\text{FR} = 50\text{ml}/\text{min}$ ).

#### 4.3 Effect of the flow rate velocity

In this section, the effect of the flow rate velocity (FR) is studied. The process was experimentally operated under different flow rates (25, 50, 100, and 150 ml/min): The feed flow rate was the same as the draw during all the experiments. The concentration of the draw solution was 1.026M whereas the concentration of the feed solution was 8.55mM. The experiments were carried out using the IGB membrane. The power density was measured and modeled as shown in Fig. 3.8.

Fig. 3.8 shows that by increasing the operating flow rate, the energy increases remarkably. It can be seen also that the increase of the power density is quite important when the FR was increased from 25 to 50ml/min, compared with the increase of the power density when the FR was raised from 100 to 150ml/min. This power density converges to a limit value for high FR. This behavior can be explained according to film theory: the flow changes the thickness of the mass transfer boundary layer at the surface of the membrane [30]. When the FR is high, the boundary layer is thinner, which results in a higher rate of mass transfer and, consequently, to reduce the external concentration polarization.

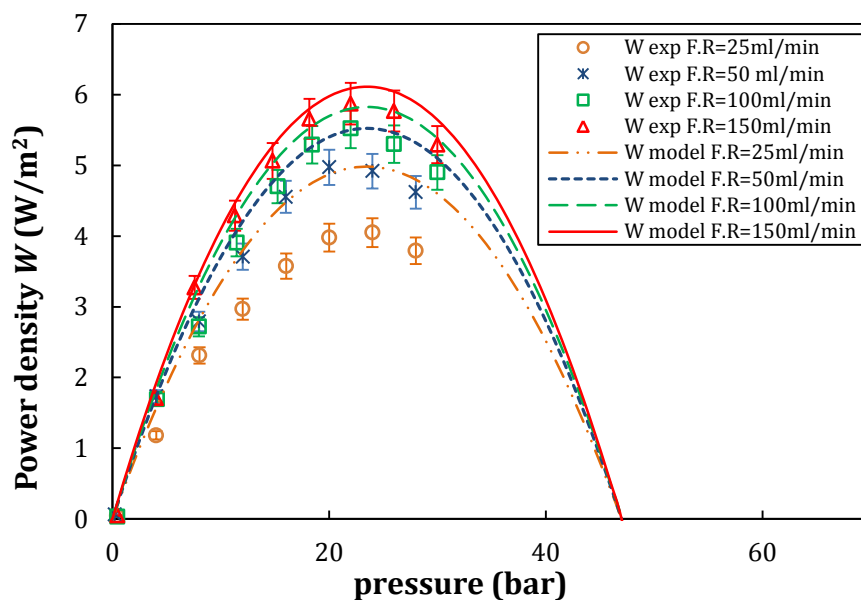


Fig. 3.8: Modeled and experimental power density versus the applied pressure for different flow rates. The draw solution concentration was equal to 1.026M; the feed solution concentration was equal to 8.55mM. The draw solution flow rate was equal to the feed solution flow rate.  $T = 20^{\circ}\text{C}$ .

#### 4.4 Effect of the bulk temperatures on the membrane temperature distribution

In Section 2 a model for the temperature in each part of the membrane was developed. Thus, solving Eqs. (3.35), (3.36) and (3.37) gives the temperature distribution over the membrane. The parameters used to calculate the temperatures are presented in Tables 3.6 and 3.7 obtained from Eqs. (3.25), (3.30), (3.32), (3.33), (3.34), and Table 3.3. Fig. 3.9 presents the variation of the temperature in each part of the membrane for different bulks temperatures. The model was applied to HTI and IGB membranes taking into account the characteristics of each membrane. The concentration of the feed and draw solutions were  $C_{F,b} = 8.55\text{mM}$  and  $C_{D,b} = 0.6\text{M}$ , respectively. The bulks temperatures were swept from  $20^\circ\text{C}$  to  $40^\circ\text{C}$ .

In Fig. 3.9, it can be seen that raising the temperature of the draw solution leads to a remarkable increase of the temperature in the draw boundary layer side and the temperature where the ICP occurs ( $T_{icp}$ ). However, the temperature in the feed boundary side increases slightly. On the other hand, the increase of the feed solution temperature is followed by a prominent increase of the solution temperature at the feed boundary layer and a noticeable increase of  $T_{icp}$ . This result clearly shows that different solutions temperatures on either side of the membrane induce a variation of the temperature distribution, especially in the inner of the membrane. This non-homogenous distribution of temperature should affect the PRO process due to the strong correlation between the temperature, the osmotic pressure and the membrane properties.

The effect of the temperature gradient on the membrane properties is studied in the next section.

Table 3.6: Thermal conductivities of feed and draw solutions and IGB membrane.

$h_D$ (W/m <sup>2</sup> /K)	$h_F$ (W/m <sup>2</sup> /K)	$h_{a,l}$ (W/m <sup>2</sup> /K)	$h_{s,l}$ (W/m <sup>2</sup> /K)
31.6	28.6	4806	3966

Table 3.7: Thermal conductivity coefficients of feed and draw solutions and IGB membrane.

$\lambda_{s,l}$ (W/m/K)	$\lambda_{a,l}$ (W/m/K)	$\lambda_D$ (W/m/ K)	$\lambda_F$ (W/m/ K)
0.526	0.267	0.62	0.60

Table 3.8: Different cases of bulk temperatures and operating scenarios.

<i>Scenario 1</i>	<i>Scenario 2</i>
• Case 1: $T_{D,b} = 20^\circ\text{C}$ , $T_{F,b} = 20^\circ\text{C}$	• Case 1: $T_{D,b} = 20^\circ\text{C}$ , $T_{F,b} = 20^\circ\text{C}$
• Case 2: $T_{D,b} = 20^\circ\text{C}$ , $T_{F,b} = 30^\circ\text{C}$	• Case 2: $T_{D,b} = 30^\circ\text{C}$ , $T_{F,b} = 20^\circ\text{C}$
• Case 3: $T_{D,b} = 20^\circ\text{C}$ , $T_{F,b} = 40^\circ\text{C}$	• Case 3: $T_{D,b} = 40^\circ\text{C}$ , $T_{F,b} = 20^\circ\text{C}$

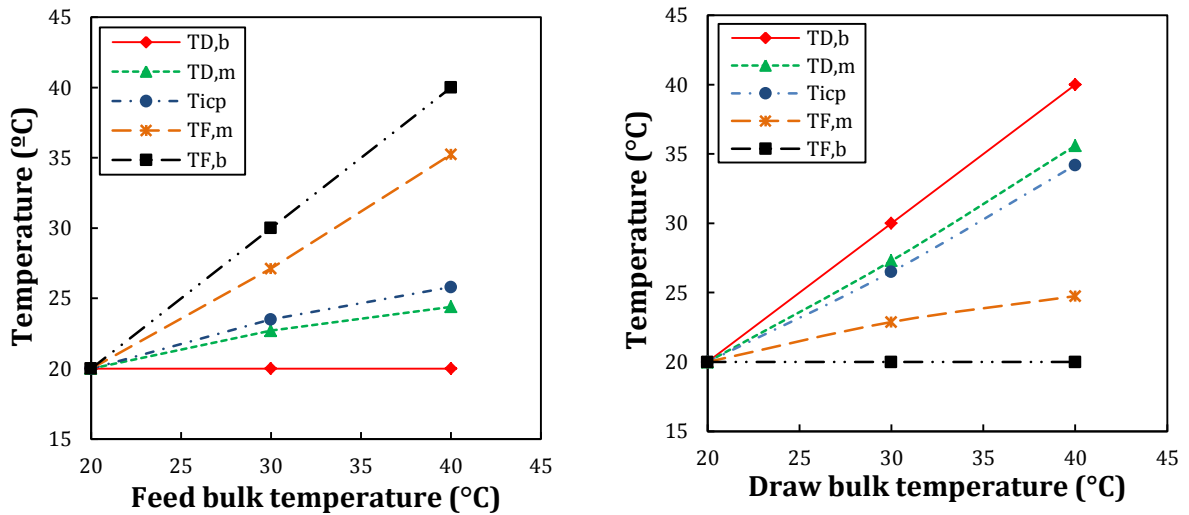


Fig. 3.9: Variation of the IGB membrane temperature with the water bulk temperature under different scenarios presented in Table 3.8.  $FR = 50\text{ml/min}$ ,  $(C_{F,b} = 8.55\text{mM}, C_{D,b} = 0.6\text{M})$ .

#### 4.5 Effect of the bulk temperatures on the membrane parameters

##### 4.5.1 Effect of the temperatures on the water permeability coefficient $A$

The water permeability coefficient is an important parameter to determine the performance of a membrane. To study the effect of the bulks temperatures on  $A$ , experiments were carried out using the IGB membrane. The concentration of the

feed solution was maintained at 8.55mM, the draw solution at 0.6M and the flow rates at 50ml/min for all scenarios. Table 3.8 resumes the different cases studied.

The  $A$  value of the membrane at each  $\Delta P$  was calculated by rearrangement of Eq. (3.22):

$$A = \frac{J_w}{\frac{\pi_{D,b} + \frac{J_s}{J_w} \beta RT}{\exp(J_w/k_D)} - \left( \pi_{F,b} + \frac{J_s}{J_w} \beta RT \right) \exp(J_w K) \exp(J_w/k_F) - \Delta P} \quad (3.38)$$

From Fig. 3.10, it can be clearly seen that increasing the temperature of the bulks increases the water permeability coefficient  $A$ . This result is in coherence with a previous study presented in [35]. However, this study was limited to the effect under the same temperature in both sides of membrane. In the current study, a temperature gradient was created between the two sides to investigate the effect of the temperatures on the membrane properties.

Fig. 3.10 shows the effect of the experimental variation of  $T_{D,b}$  on the water permeability coefficient at different values of the feed bulk temperature  $T_{F,b}$ . There is only a slight increase of  $A$  when the draw bulk temperature  $T_{D,b}$  is increased. Also, it can be seen that the increment of  $T_{F,b}$  leads to a high increase of the water permeability. In fact, when  $T_{F,b} = 20^\circ\text{C}$  the water permeability is  $A = 7.2 \times 10^{-13}$  m/s/Pa at  $T_{D,b} = 30^\circ\text{C}$ , whereas when  $T_{F,b} = 40^\circ\text{C}$  the water permeability increases to  $A = 10.5 \times 10^{-13}$  m/s/Pa at  $T_{D,b} = 30^\circ\text{C}$ .

The results show that the impact of the feed solution temperature on  $A$  is more important than that of draw solution temperature. Also, the modification of the physico-chemical parameters such as the viscosity, the density, the diffusivity and the osmotic pressure leads to better performance of the membrane [36]. The experimental results reinforce the hypothesis which suggests that the PRO membrane is physically modified during the process [10]. It should be pointed out that the use of the membrane at high temperature is limited by the thermal resistance of each manufacturing material. Moreover, rising the temperature of the process increases the osmotic pressure of the treated solutions, thus, the driving force  $\Delta\pi_m$  increases to a maximum, enhances the performance of the process.

In summary, operating at high operating temperatures with good control of the membrane parameters and solution characteristics would result in an improved performance of the PRO process.

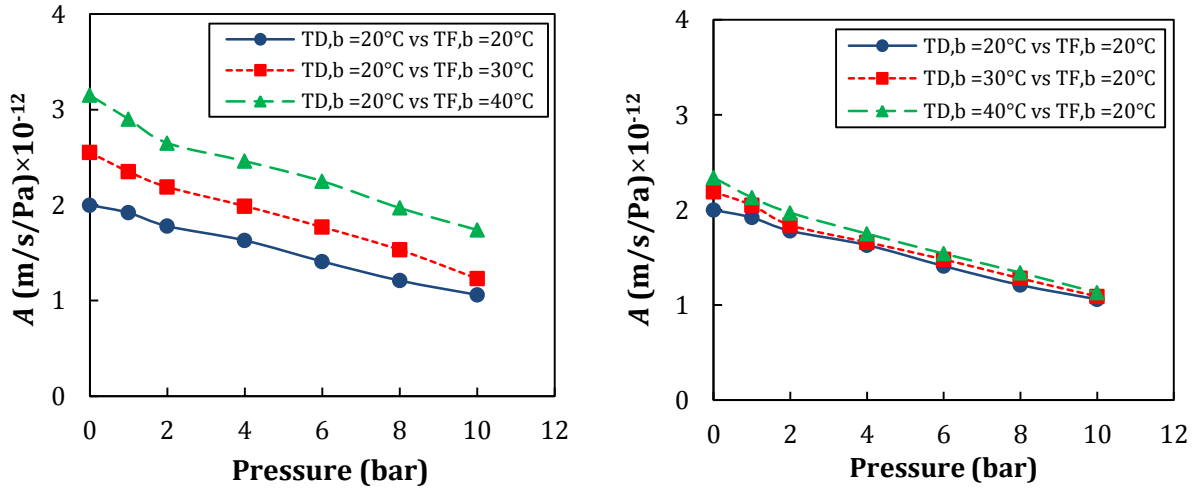


Fig. 3.10: Variation of the water permeability coefficient  $A$  with the bulk temperatures as described in Table 3.8.

#### 4.5.2 Effect on the salt permeability coefficient $B$

The salt permeability coefficient is also a key parameter in PRO, as it reduces the performance of the process. Unfortunately, the preparation of membranes with zero salt permeability is not feasible, so the aim is to keep  $B$  as low as possible. Thus, the effect  $B$  and its dependence with the operating parameters should be taken into account, so in this study the effect of the bulk temperatures on the salt permeability is experimentally studied using the IGB membrane. The concentration of the feed solution is maintained in all the experiments equal to 8.55mM and the draw solution to 0.6M. The  $B$  value of the membrane at each case was calculated by rearrangement of Eq. (3.22):

$$B = \frac{J_s}{\frac{c_{D,b} + \frac{J_s}{J_w}}{\exp(J_w/k_D)} - \left( c_{F,b} + \frac{J_s}{J_w} \right) \exp(J_w K) \exp(J_w/k_F)} \quad (3.39)$$

As shown in Fig. 3.11, the increases in  $T_{D,b}$  or  $T_{F,b}$  are followed by an increase in the value of  $B$ . According to Fig. 3.9,  $T_{F,b}$  has a strong effect on rising the temperature of the separation layer material which causes an improvement of the membrane salt permeability. When the feed solution temperature is high,  $B$  is

high, which can be justified by the fact that for dense selective membranes, the increase of  $A$  is usually accompanied by the increase of  $B$  value, and vice versa, due to the intrinsic tradeoff between permeability and selectivity [41]. Unfortunately, the increased  $B$  value can elevate the reverse solute diffusion and the accumulation of the solute within the membrane support layer and in the bulk feed solution, which will adversely impact the PRO performance due to the enhanced ICP (This will be studied in Section 4.6.)

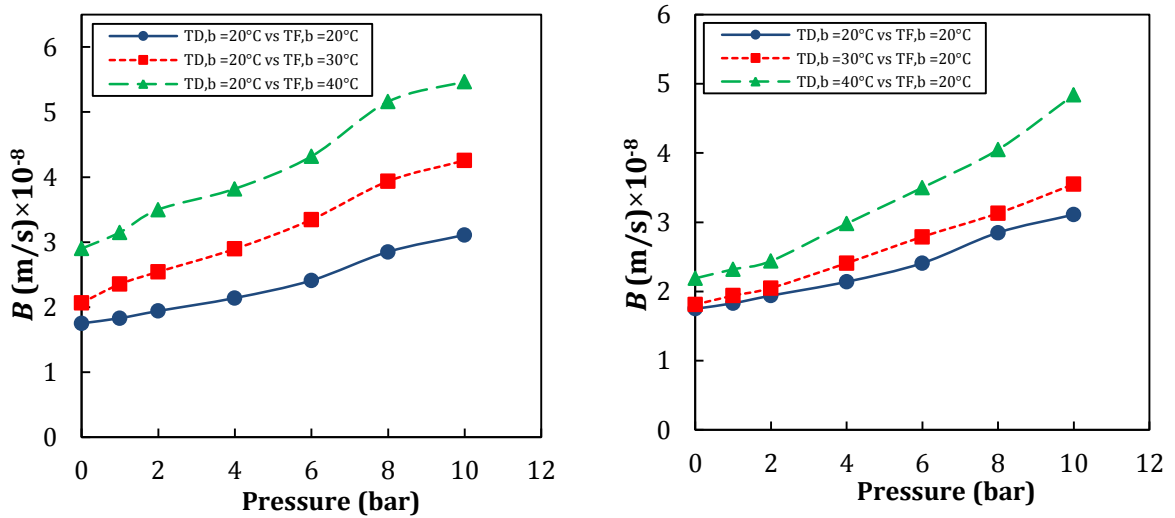


Fig.3.11: Variation of the salt permeability coefficient  $B$  with the bulk temperatures as described in Table 3.9.

#### 4.5.3 Effect on the structure parameter $s$

The structure parameter  $s$  governs the internal concentration polarization in osmotically driven membrane processes and is also an important parameter for membrane manufacturing. In many published papers,  $s$  is considered as a constant [8,11]. However, in practices takes different values depending on operating conditions (Temperature, Pressure, etc). A generalized equation describing the structure parameter is shown below by rearrangement of  $J_w$  in Eq. (3.22):

$$s = \frac{D_F}{J_w} \ln \left[ \frac{\pi_{D,b} + \frac{B}{A} \left(1 + \frac{A\Delta P}{J_w}\right) \frac{J_w - \Delta P}{\exp(J_w/k_D)}}{\left[\pi_{F,b} + \frac{B}{A} \left(1 + \frac{A\Delta P}{J_w}\right)\right] \exp(J_w/k_F)} \right] \quad (3.40)$$

Thus, the structure parameter was experimentally studied at different values of the temperatures and the results are shown in Fig. 3.12. The explanation of the results is based on the fact that the increase of the temperature causes a dilatation of the polymer which constitutes the surface of the membrane: it becomes softer, so the pressure exerts a tangential force on the soft surface, and as a consequence the structure parameter decreases with the increasing of the temperature. Thus, the decrease of parameter  $s$  is due to a mutual and simultaneous action of two parameters: the temperature and the pressure. A similar behavior has been found with the increase of the pressure (only) [12,30]. However the simultaneous action of the temperature and the pressure is more important. In fact, the polymer network may expand due to high pressure, resulting in better connectivity and thus less tortuosity in the sponge-like structure. The increase of the temperature reduces the thickness of the substrate and expands its porosity which decreases the salt resistivity through the support layer, thus, reducing  $s$  leads to decrease the internal concentration polarization. As shown in Fig. 3.12-b, when the draw solution temperature was fixed and the feed solution temperature was varied  $s$  was strongly reduced compared to the opposite case shown in Fig. 12-a: for example, when  $T_{F,b} = 40^\circ\text{C}$  and  $T_{D,b} = 20^\circ\text{C}$ ,  $s$  is around  $5.55 \times 10^{-4}$  m, in the opposite case ( $T_{D,b} = 40^\circ\text{C}$  and  $T_{F,b} = 20^\circ\text{C}$ ),  $s$  is around  $6.15 \times 10^{-4}$  m. This is due to the direct contact between the substrate and the feed solution, so the heat transfer is guaranteed by both convection and conduction. However, in the case of the draw solution, the existence of the active layer establishes a thermal barrier between the draw solution and the support layer, which reduces the thermal effect and minimizes the heating of the substrate by the draw solution.

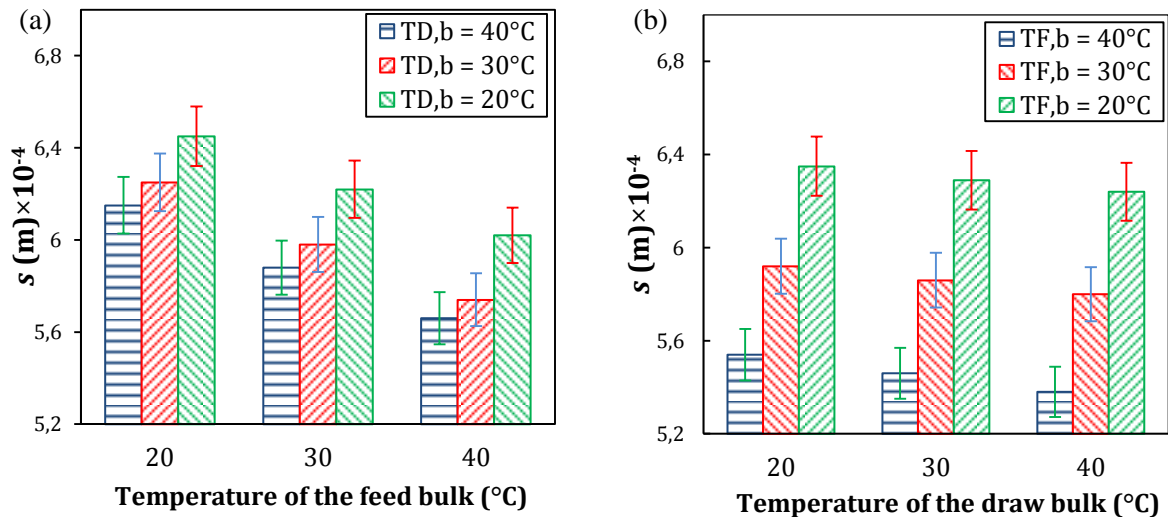


Fig.3.12: Variation of the structure parameter  $s$  with the bulk temperatures, as described in Table 3.8.

#### 4.6 Study of the reverse solute diffusion

This section discusses the effect of the temperatures on the reverse solute diffusion and thus on PRO performance. To guarantee a high flux across the membrane, osmotically driven processes require a high draw concentration to drive water permeation through the membrane. However, this condition induces an undesirable phenomenon that affects the performance of the process: the reverse salt flux occurs simultaneously with the water permeation, but in the reverse direction. It has been shown that this inevitable phenomenon reduces the performance of PRO due to its correlation with the ICP [42]. Moreover, it has been proved that high salt diffusion leads to a severe membrane fouling by enhancement of the ICP[43,44].

The specific salt flux ( $J_s/J_w$ ), theoretically given by Eq. (3.4), can be useful to study the effect of the salt flux diffusion on PRO due to the fact that it is related to the water and salt fluxes. In PRO mode, Eq. (3.4) shows that the increase of the pressure leads to an increment of the ratio  $J_s/J_w$ . Fig. 3.13-a and b present the experimental and simulated  $J_s/J_w$  as a function of effective applied pressure and the temperature for all scenarios presented in Table 3.8. The simulation of  $J_s/J_w$  is based on Eq. (3.4), with  $A$  and  $B$  values are considered variables as presented in Sections 4.5.1 and 4.5.2. The draw and the feed solutions were prepared using NaCl (draw solution concentration: 0.35M, feed solution concentration: 8.55mM). In FO

mode ( $\Delta P = 0$ ), the specific salt flux is always  $J_s/J_w = B/A\beta RT$  [32]. A good correlation between experimental and simulated  $J_s/J_w$  at low and high pressures was observed which confirms the hypothesis of membrane deformation that suggests the dependence of the specific salt flux to the operating conditions and the ratio ( $B/A$ ) and as shown in Eq. (3.4). Experimental and simulated  $J_s/J_w$  increased with temperature in both scenarios. However, a comparison between results from each scenario revealed a net difference when the temperature of the water bulk increases: when the feed solution temperature was increased but the draw solution bulk was maintained at 20°C,  $J_s/J_w$  decrease from 0.017 to 0.012 (around 35% of reduction), whereas in the opposite case,  $J_s/J_w$  decreased from 0.017 to 0.0076 (around 75% of reduction) which proves that the increase of the water flux induces more important diffusion of the salt comparing to the draw solution temperature. It should be pointed out that at that temperatures of scenario 1 (high  $T_{F,b}$ ), the simulation overestimated the water flux (Fig. 3.13-c) which shows the existence of a limiting factor that reduces the performance of the membrane in this case. For scenario 2 (high  $T_{D,b}$ ), the simulation predicts precisely the water flux, so this unknown limiting factor is less severe for low temperatures (Fig. 3.13-d). This is further consistent with experimental and simulated results of the power density that confirms the presence of the ICP due to the diffusion of the salt to the support layer, so the optimal hydraulic pressure to obtain the peak power density was reduced. In fact, diffusion of the draw solution causes the accumulation of the salt on the surface of the support layer, which leads to an increase of the concentration  $C_{icp}$  (Fig. 3.1); consequently, the effective osmotic pressure and the water flux are reduced: see Eqs. (3.19) and (3.21) and thus the performance of PRO is limited.

In summary, the results revealed the strong relationship between the water flux and the salt diffusion: high temperature leads to a higher water flux, which unfortunately induces more severe solute diffusion. We suggest that this behavior is due a modification of the membrane structure: the temperature acts upon the pores of the membrane and tends to enlarge them, followed by an increase of the water and salt fluxes. This seems to be consistent with the results shown in Section 4.5.

It remains to note that the gap between the curves of the power density for the case when the draw solution temperature is increased (Fig. 3.13-f) is due to the increase of the osmotic pressure caused by the increase of temperature which leads to a different applied pressure for each studied case.

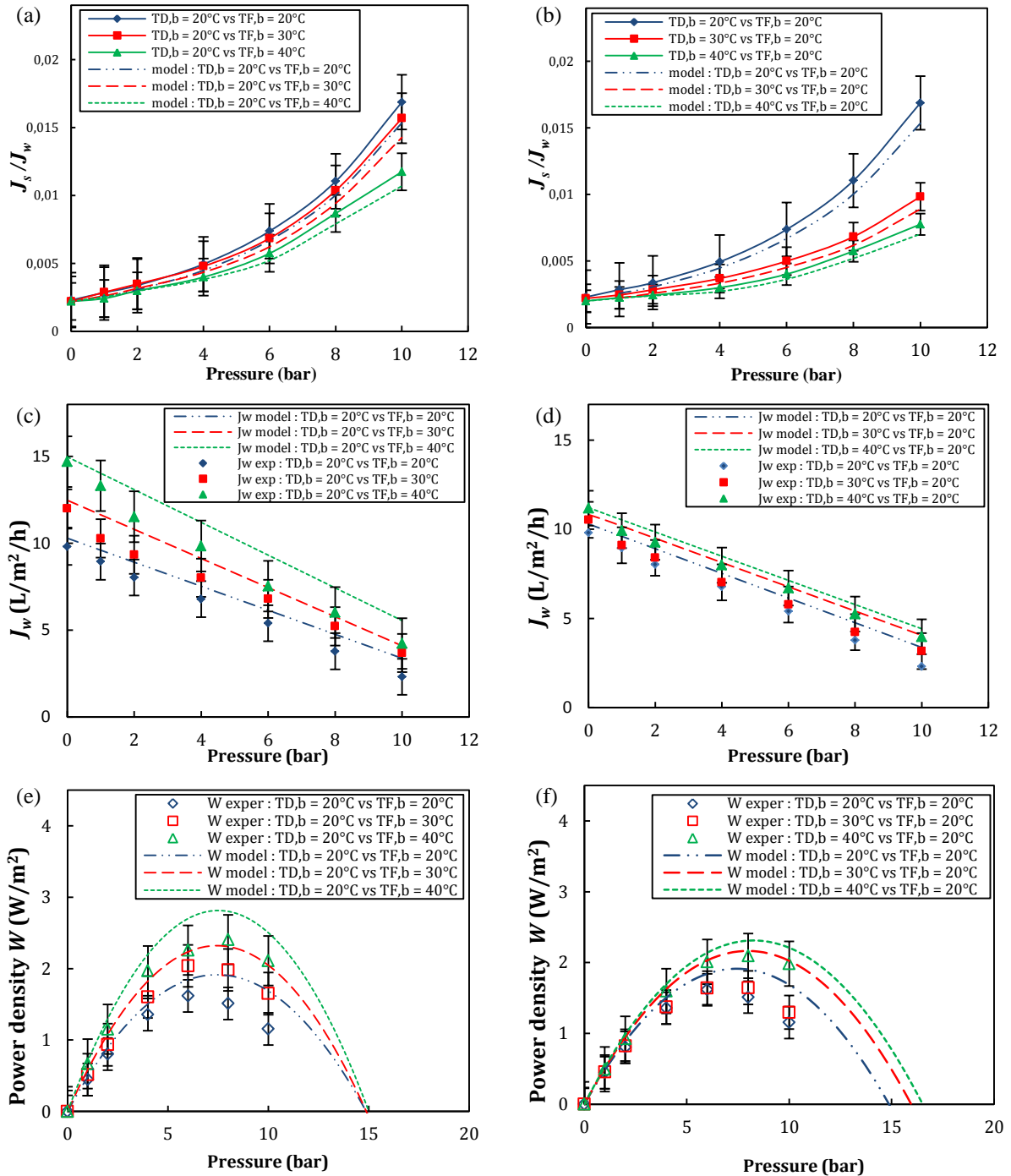


Fig. 3.13: Experimental and simulated water flux, salt flux and power density for the IGB membrane at different operation cases following Table 3.8 (Experimental conditions: 8.55mM NaCl feed solution, 0.35 M NaCl draw solution, FR = 50 ml/min.)

## 5. Conclusions

In the current chapter, models reproducing the water and the power density in PRO for a flat sheet membrane were developed. These models were verified using experimental data, showing a good capability to predict the responses of the process. The effects of operating conditions were investigated: The effect on PRO performance of the solution concentrations, flow rates and temperatures were well predicted by the models.

In particular, the impact of the bulks temperature on PRO performance was studied. It has been experimentally noted that the effect of the feed solution temperature is more important than the draw solution temperature: the water and salt permeability coefficients showed a higher dependency on the feed solution temperature, and the structure parameter  $s$  significantly decreased with the temperatures. Finally, it was observed that the high water flux resulting from the increase of feed solution temperature induced a drastic draw solution diffusion which generated a severe ICP.

**REFERENCES OF CHAPTER 3**

- [1] Logan BE, Elimelech M. Membrane-Based Processes for Sustainable Power Generation using Water and Wastewater. *Nature* 2012;488:313–319.
- [2] Achilli A, Childress AE. Pressure retarded osmosis: from the vision of Sidney Loeb to the first prototype installation – review. *Desalination* 2010;261(3):205–211.
- [3] Phillip WA, Yong JS, Elimelech M. Reverse draw solute permeation in forward osmosis: modeling and experiments. *Environ Sci Technol* 2010;44:5170–5176.
- [4] Han G, Zhang S, Li X, Chung T-S. High performance thin film composite pressure retarded osmosis (PRO) membranes for renewable salinity gradient energy generation. *J Membr Sci* 2013;440:108–121.
- [5] Loeb S, Van Hessen F, Shahaf D. Production of energy from concentrated brines by pressure retarded osmosis. II. Experimental results and projected energy costs, *J. Membr Sci* 1976;(3)1:249-69.
- [6] Brian P. Mass transport in reverse osmosis, in: Merten (Ed): *Desalination by reverse osmosis*, Cambridge, MA, MIT Press, 1966.
- [7] Skilhagen SE, Dugstad JE, Aaberg RJ. Osmotic power—power production based on the osmotic pressure difference between waters with varying salt gradients, *Desalination*. 2008;220:476–482.
- [8] Achilli A, Tzahi YC, Childress AE. Power generation with pressure retarded osmosis: An experimental and theoretical investigation. *J Membr Sci* 2009;343:42–52.
- [9] Sivertsen E, Holt T, Thelin W, Brekke G. Modelling mass transport in hollow fibre membranes used for pressure retarded osmosis. *J Membr Sci* 2012;417–418:69–79.
- [10] Li X, Zhang S, Fu FJ, Chung T-S. Deformation and reinforcement of thin-film composite (TFC) polyamide-imide (PAI) membranes for osmotic power generation, *J Membr Sci* 2013;434: 204–217.
- [11] Peinemann K-V, Gerstandt K, Skilhagen SE, Thorsen T, Holt T. Membranes for Power Generation by Pressure Retarded Osmosis, in *Membranes for Energy Conversion*. 2008, Volume 2 (eds K.-V. Peinemann and S. Pereira Nunes), Wiley, Weinheim, Germany.
- [12] Yip NY, Tiraferri A, Phillip WA, Schiffman JD, Hoover LA, Chang Kim Y, Elimelech M. Thin-Film Composite Pressure Retarded Osmosis Membranes for Sustainable

- Power Generation from Salinity Gradients. *Environ Sci Technol* 2011;45:4360–4369.
- [13] She Q, Hou D, Liu J, Tan KH, Tang CY. Effect of feed spacer induced membrane deformation on the performance of pressure retarded osmosis (PRO): Implications for PRO process operation. *J Membr Sci* 2013;445:170–182.
- [14] McCutcheon JR, Elimelech M. Influence of concentrative and dilutive internal concentration polarization on flux behavior in forward osmosis. *J Membr Sci* 2006;284: 237–247.
- [15] Gray G, McCutcheon JR, Elimelech M. Internal concentration polarization in forward osmosis: role of membrane orientation. *Desalination* 2006;197:1-8.
- [16] Chou S, Wang R, Shi , She Q, Tang C, Fane AG. Thin-film composite hollow fiber membranes for pressure retarded osmosis (PRO) process with high power density. *J Membr Sci* 2012;389:25–33.
- [17] Lee KL, Baker RW, Lonsdale HK. Membrane for power generation by pressure retarded osmosis. *J Membr Sci* 1981;8:141– 171.
- [18] Dumée L, Lee J, Sears K, Tardy B, Duke M, Gray S. Fabrication of thin film composite poly(amide)-carbon-nanotube supported membranes for enhanced performance in osmotically driven desalination systems. *J Membr Sci* 2013;427: 422–430.
- [19] Carbonell G. Mass transfer coefficients in coiled tubes. *Biotechnology and Bioengineering*. 1975;17:1383–1385.
- [20] Tan CH, Ng HY. Modified models to predict flux behavior in forward osmosis in consideration of external and internal concentration polarizations. *J Membr Sci* 2008;324:209–219.
- [21] Gruber MF, Johnson CJ, Tang CY, Jensen MH, Yde L, Hélix-Nielsen C. Computational fluid dynamics simulations of flow and concentration polarization in forward osmosis membrane systems. *J Membr Sci* 2011;379:488–495.
- [22] Nield DA, Bejan A. *Convection in Porous Media*, 3<sup>rd</sup> edition, Springer, New York, 1992.
- [23] Tiab D, Donaldson EC. *Petrophysics*, 3<sup>rd</sup> edition, 2012, pp 420.
- [24] Bourantas GC, Skouras ED, Loukopoulos VC, Burganos VN. Heat transfer and natural convection of nanofluids in porous media. *European Journal of Mechanics B/Fluids* 2014;43: 45–56.

- [25] Prante JL, Ruskowitz JA, AE Childress, Achilli A, RO-PRO, desalination: An integrated low-energy approach to seawater desalination. *Appl Energy* 2014;120:104–14.
- [26] van der Zwana S, Pothofa IWM, Blankert B, Bara JI. Feasibility of osmotic power from a hydrodynamic analysis at module and plant scale. *J MembrSci* 2012;389: 324– 333.
- [27] Herron J. Two-Layer Membrane. U.S. Patent, 12 July 2012.
- [28] Hänel C, Touati K, Tadeo F, Schiestel T. A Parameter Study with Cellulose Acetate Membranes for Pressure Retarded Osmosis, International Membrane Science & Technology Conference, Melbourne, 2013.
- [29] Cath TY, Childress AE, Elimelech M. Forward osmosis: Principles, applications, and recent developments. *J Membr Sci* 2006;281:70–87.
- [30] Geankoplis CJ. Principles of Mass Transfer, Transport Processes and Separation Process Principles, Prentice Hall, Upper Saddle River, NJ, 2003, pp. 410–456.
- [31] Loeb S. Energy production at the Dead Sea by pressure-retarded osmosis: challenge or chimera? *Desalination* 1998;120:247-262.
- [32] Zhao S, Zou L, Tang CY, Mulcahy D. Recent developments in forward osmosis: opportunities and challenges. *J MembrSci* 2012;396:1–21.
- [33] She Q, Wong YKW, Zhao S, Tang CY. Organic fouling in pressure retarded osmosis: Experiments, mechanisms and implications. *J Membr Sci* 2013;428:181–89.
- [34] Zhang M, Hou D, She Q, Tang CY. Gypsum scaling in pressure retarded osmosis: Experiments, mechanisms and implications. *Wat Res* 2014;48:383–95.
- [35] She Q, Jin X, Tang Chuyang Y. Osmotic power production from salinity gradient resource by pressure retarded osmosis: Effects of operating conditions and reverse solute diffusion. *J Membr Sci* 2012;401– 402:262–73.
- [36] Touati K, de la Calle A, Tadeo F, Roca L, Schiestel T, Alarcón-Padilla DC. Energy recovery using salinity differences in a multi-effect distillation system. *DesalWatTreat* 2014;1–8.
- [37] Palacin LG, Tadeo F, Prada C, Touati K. Evaluation of the recovery of osmotic energy in desalination plants by using pressure retarded osmosis. *DesalWater Treat* 2013;51:360–365.





# Chapter 4: Effect of the Reverse Salt Flux on PRO

## 1. Introduction

A main difference between solute flows in RO and PRO is that in RO the solute (i.e., the salts dissolved in the draw solution) flows in the same direction as the water flux, whereas in PRO the solute in the draw solution diffuses into the feed solution in the reverse direction to the water flux [2, 3], due to the concentration gradient.

Although an ideal semi permeable membrane would prevent this so-called reverse salt flow, no membrane is perfect, and a small amount of dissolved solute is always transported across the membrane. This phenomenon has been investigated in several studies, such as [4,5,6]: it is considered a significant impediment to the application of osmotically driven membrane processes, as it creates Internal Concentration Polarization, which reduces the performance, as it was shown in Chapter 3.

Significant efforts to improve PRO process have focused on tailoring the membrane structure to decrease the effects of limiting factors such as the Internal Concentration Polarization (ICP) [7,8], but further developments are still needed for successful commercial exploitation of these technologies. One area that has received limited attention, but could be a significant impediment to the viability of osmotically driven membrane processes is the reverse salt flux [9,28].

Thus, in this chapter, a mathematical model is developed to reproduce the reverse salt flux in PRO, following the same steps used to develop the water flux model in Chapter 3. Again, the model is developed trying to use the minimum number of assumptions, by taking explicitly into consideration the effect on this flow of the Internal Concentration Polarization (ICP), of the External Concentration Polarization (ECP) on both sides of the membranes, and of pressure. The proposed model is then validated and tested at lab scale, and the effect of the operating conditions on the reverse salt flux is investigated. It is shown that if the reverse salt flux is not controlled the PRO performance would be reduced, and the energy costs

could be much higher than expected. As this phenomenon is non-avoidable, the control of the salt diffusion is studied. Further, the implications of the reverse salt flux on the performance of PRO power plants are discussed and some suggestions to improve the operation of the process by controlling the reverse salt flux are proposed.

## 2. Theory

### 2.1 Modeling the reverse salt flux

As shown previously in Chapter 3, the water flux across a semi-permeable membrane in PRO is related to the water permeability, the effective osmotic pressure difference  $\Delta\pi_m$  and the transmembrane hydraulic pressure difference  $\Delta P$  [11]:

$$J_w = A (\Delta\pi_m - \Delta P) \quad (4.1)$$

where

$$\Delta\pi_m = \pi_{D,m} - \pi_{F,m} \quad (4.2)$$

With  $\pi_{D,m}$  and  $\pi_{F,m}$  the osmotic pressure at the surfaces of the active, and support layers, respectively.

In PRO, the power that can be generated per unit membrane area is equal to the product of the water flux and the hydraulic pressure differential across the membrane:

$$W = J_w \Delta P = A (\Delta\pi_m - \Delta P) \Delta P \quad (4.3)$$

The maximum of energy generated by PRO is reached when the applied pressure difference  $\Delta P$  is half of the effective osmotic pressure difference between the draw and the feed solutions:  $\Delta P = \frac{\Delta\pi_m}{2}$ ; then, the theoretical maximum power that can be produced is [12]:

$$W_{max} = A \frac{\Delta\pi_m^2}{4} \quad (4.4)$$

The Internal and External Concentration Polarizations are now characterized for flat sheet membranes (at bench scale); a parallel approach can be followed for other kind of membranes.

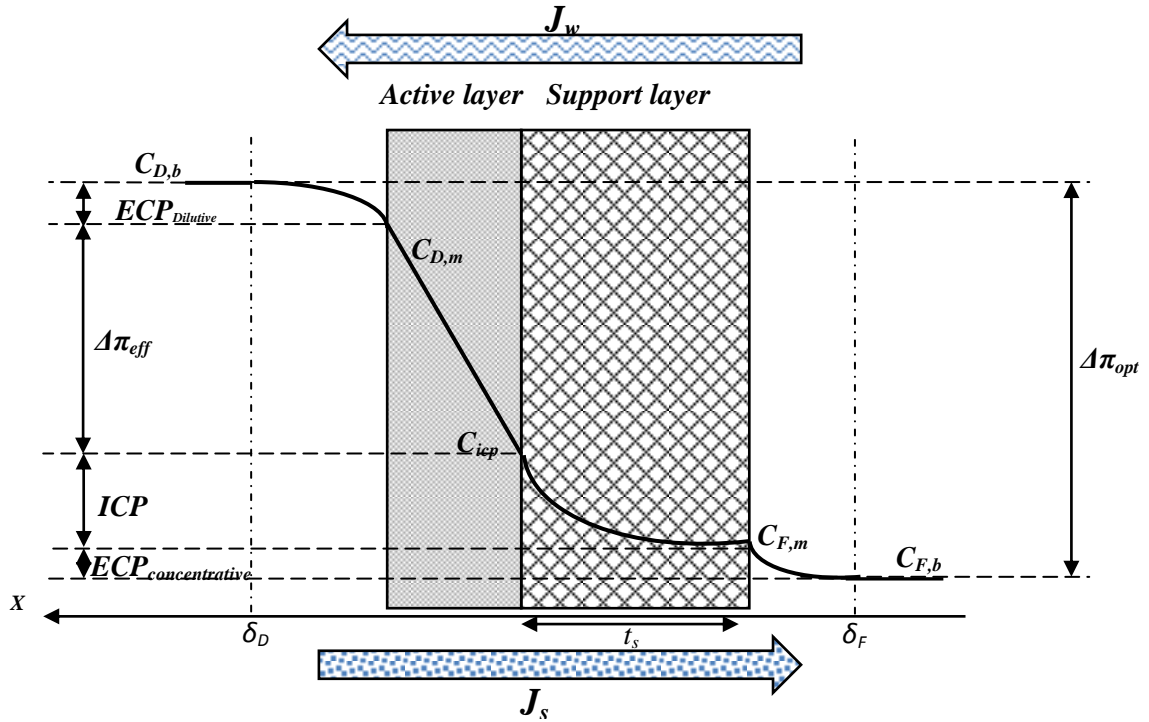


Fig.4.1: Concentration profile over the PRO membrane and directions of the water flux  $J_w$  and salt flux  $J_s$ .  $C_{D,m}$  and  $C_{F,m}$  are the solute concentrations at the interface of the active and support layers, respectively.  $C_{icp}$  is the solute concentration at the interface between the support and active layers.  $C_{D,b}$  and  $C_{F,b}$  are the draw and feed bulk concentrations, respectively.

a. *The Internal Concentration Polarization (ICP)*

The ICP is an important factor affecting the water flux since it cannot be mitigated by enhanced shear stress [13]. ICP occurs when the thin film is supported by a porous substrate. In order to reveal the effects of ICP on the permeate flux, the solute mass balance within the porous media can be calculated from a mass balance:

$$D_{s,l} \frac{dC(x)}{dx} - J_w C(x) = J_s \tag{4.5}$$

where  $C(x)$  is the salt concentration at position  $x$  and  $D_{s,l}$  is the diffusion coefficient of in the support layer, defined as:

$$D_{s,l} = \frac{\varepsilon}{\tau} D \quad (4.6)$$

where  $\varepsilon$  and  $\tau$  are the porosity and tortuosity of the support layer, respectively, and  $D$  is the bulk diffusion coefficient, that can be calculated as follows [14]:

$$D = 6.725 \times 10^{-6} \times \exp\left(1.546 \times 10^{-4} \times C - \frac{2.513}{T}\right) \quad (4.7)$$

Eq. (4.5) can be integrated over the support layer, respecting the following boundary conditions:

$$\begin{cases} C(x=0) = C_{F,m} \\ C(x=t_s) = C_{icp} \end{cases}$$

where the distance  $x$  is measured from the interface between the support and active layers,  $C_{icp}$  is the solute concentration at the interface between the support and active layers, and  $t_s$  is the thickness of the support layer (Fig. 4.1). This integration gives:

$$C_{icp} = \left(C_{F,m} + \frac{J_s}{J_w}\right) \exp(J_w K) - \frac{J_s}{J_w} \quad (4.8)$$

where  $K$  is the solute resistivity for diffusion within the support layer, defined as:

$$K = \frac{\tau t_s}{\varepsilon D} = \frac{s}{D} \quad (4.9)$$

where  $s$  is the structure parameter of the support layer.

*b. External Concentration Polarization (ECP)*

ECP appears on both sides of the membrane surface and can inhibit water permeation due to decreased effective osmotic pressure on the draw solution side [15]. The boundary conditions for the ECP on the draw solution side are:

$$\begin{cases} C(x = 0) = C_{D,m} \\ C(x = \delta_D) = C_{D,b} \end{cases}$$

where the distance  $x$  is now measured from the membrane surface of the active layer side and  $\delta_D$  is the thickness of the draw boundary layer. Integration of Eq. (4.5) over the thickness of the draw boundary layer using the boundary conditions gives:

$$C_{D,m} = \left( C_{D,b} + \frac{J_s}{J_w} \right) \exp\left(-\frac{J_w}{k_D}\right) - \frac{J_s}{J_w} \quad (4.10)$$

where  $k_D$  is the mass transfer coefficient in the draw solution calculated using:

$$k_D = \frac{Sh D_D}{d_h} \quad (4.11)$$

where  $D_D$  is the diffusion coefficient of the solute in the draw solution,  $d_h$  is the hydraulic diameter of the flow channel, and  $Sh$  is the Sherwood number, experimentally determined from measurements at different flow conditions, as follows [13]:

$$Sh = 0.04 Re^{0.75} Sc^{0.33} \quad (\text{Turbulent flow}) \quad (4.12)$$

$$Sh = 1.85 \left( Re \cdot Sc \frac{d_h}{L} \right) \quad (\text{Laminar flow}) \quad (4.13)$$

where  $Re$  is the Reynolds number,  $Sc$  is the Schmidt number and  $L$  is the length of the channel. The Reynolds and Schmidt numbers are calculated as follows:

$$Re = \frac{u.d.\rho}{\eta} = \frac{u.d}{\mu} \quad (4.14)$$

$$Sc = \frac{\mu}{\rho D} \quad (4.15)$$

where  $u$  is the velocity of the water,  $d$  is the diameter of the channel,  $\rho$  is the density of the water,  $\eta$  the dynamic viscosity of the water and  $\mu$  is the cinematic viscosity of the water, that can be obtained from [15]:

$$\mu = 1.234 \times 10^{-6} \exp\left(0.00212 \times C + \frac{1965}{T}\right) \quad (4.16)$$

*c. External Concentration Polarization on the feed solution side*

We define the boundary conditions for the ECP on the feed solution side as:

$$\begin{cases} C(x = 0) = C_{F,b} \\ C(x = \delta_F) = C_{F,m} \end{cases}$$

where the distance  $x$  is now measured from the feed boundary layer and  $\delta_F$  is the thickness of the feed boundary layer. Integration of Eq. (4.5) over this thickness of the layer using the boundary conditions gives:

$$C_{F,m} = \left(C_{F,b} + \frac{J_s}{J_w}\right) \exp\left(\frac{J_w}{k_F}\right) - \frac{J_s}{J_w} \quad (4.17)$$

where  $k_F$  is the mass transfer coefficient in the feed solution, which is calculated using:

$$k_F = \frac{Sh D_F}{d_h} \quad (4.18)$$

where  $D_F$  is the diffusion coefficient of the solute in the feed solution.

As it has been already mentioned, the salts permeate across the membrane in the opposite direction of the water flux, from the draw solution into the feed solution. The effective reverse salt flux  $J_s$  is then [16]:

$$J_s = B(C_{D,m} - C_{icp}) \quad (4.19)$$

where  $B$  is the salt permeability coefficient of the membrane active layer and  $C_{F,m}$  is the solute concentrations at the interface of the active layer. The effective osmotic pressure across the membrane is defined as the osmotic pressure along the active layer, described as follows:

$$\Delta\pi_{eff} = \Delta\pi_{opt} - \Delta\pi_{ICP} - \Delta\pi_{ECP} \quad (4.20)$$

where  $\pi_{opt}$ ,  $\pi_{ICP}$  and  $\pi_{ECP}$  are the osmotic pressure difference between the feed and draw bulks, the osmotic pressure loss caused by ICP, and the osmotic pressure loss caused by ECP, respectively. The osmotic pressures are calculated using van't Hoff equation [29]:

$$\Delta\pi_{opt} = (C_{D,b} - C_{F,b})\beta RT \quad (4.21)$$

$$\Delta\pi_{ICP} = (C_{icp} - C_{F,m})\beta RT \quad (4.22)$$

$$\Delta\pi_{ECP} = (C_{D,b} - C_{D,m})\beta RT + (C_{F,m} - C_{F,b})\beta RT \quad (4.23)$$

where  $\beta$  is the van't Hoff coefficient ( $\beta=2$  for NaCl),  $R$  is the gas constant and  $T$  is the absolute temperature.

The specific salt flux in PRO, defined as the ratio of salt flux to water flux,  $J_s/J_w$ , is affected by the intrinsic transport properties of the membranes, as follows [17]:

$$\frac{J_s}{J_w} = \frac{B}{A\beta RT} \left( 1 + \frac{A\Delta P}{J_w} \right) \quad (4.24)$$

2.2 Reverse salt flux  $J_s$ 

Substituting  $C_{D,m}$  and  $C_{icp}$  in Eq. (4.19) by their expressions in Eqs (4.8) and (4.10), the reverse draw solute can be described as:

$$J_s = B \left[ \alpha \left( C_{D,b} + \frac{1}{\phi} \left( 1 - \frac{A\Delta P}{J_s} \right)^{-1} \right) \exp \left( -\phi \frac{J_s}{k_D} \right) - \alpha' \alpha'' \left( C_{F,b} + \frac{1}{\phi} \left( 1 - \frac{A\Delta P}{J_s} \right)^{-1} \right) \exp(\phi J_s K) \exp \left( \phi \frac{J_s}{k_F} \right) \right] \quad (4.25)$$

where  $\alpha, \alpha'$  and  $\alpha''$  are constants that depend on the operating conditions, and can be easily calculated using the following relations:

$$\phi = \frac{A}{B} \beta RT \quad (4.26)$$

$$\alpha = \exp \left( \phi \frac{A\Delta P}{k_D} \right) \quad (4.27)$$

$$\alpha' = \exp \left( \phi \frac{A\Delta P}{k_F} \right) \quad (4.28)$$

$$\alpha'' = \exp(-K\phi A\Delta P) \quad (4.29)$$

It should be pointed out that Eq. (4.25) expresses the reverse salt flux in terms of experimentally accessible quantities, and it incorporates some performance-limiting phenomena of ICP and ECP which are generally neglected. In fact, in several PRO cases studied [14,15,16], the concentration of the feed solution is necessarily considered low so that the ECP is negligible. However, this assumption is not valid for feed solutions with high concentration, such as RO brine versus seawater. In addition, the model takes into consideration the difference between the mass transfer coefficients in both sides of the membrane, that in the literature are frequently considered to be the same, which does not reflect the reality: according to Eq. (4.18), the difference can be pronounced at certain solution characteristics and operating conditions (concentrations, temperature, laminar or turbulent flow, etc.).

### 3. PRO bench-scale and membranes

To evaluate the reverse salt flux using the model in Eq. (4.25) and study its effect on produced power, some laboratory equipments were carried out. A flat-sheet cellulose acetate membrane is used in the experiments, developed by Fraunhofer Institute for Interfacial Engineering and Biotechnology [10]: it is called here IGB membrane, and has similar characteristics to other commercially available semi-permeable membranes. Certified ACS-grade NaCl (Fisher Scientific) was used to prepare both feed and draw solutions using deionized water.

The laboratory equipment was reported in Chapter 3: The test unit had a channel on the feed side of the membrane to allow the feed solution to flow tangentially to the membrane. This channel was 170mm long, 70mm wide and 0.7mm deep, providing an effective membrane area of 0.013m<sup>2</sup>. Mesh spacers placed in the feed channel supported the membrane and enhanced the turbulence in the feed stream. A high-pressure positive displacement pump was used to recirculate the feed solution at selected velocities, with the temperature of the solutions controlled by electronic thermostats and the salt concentration been determined by conductivity sensors.

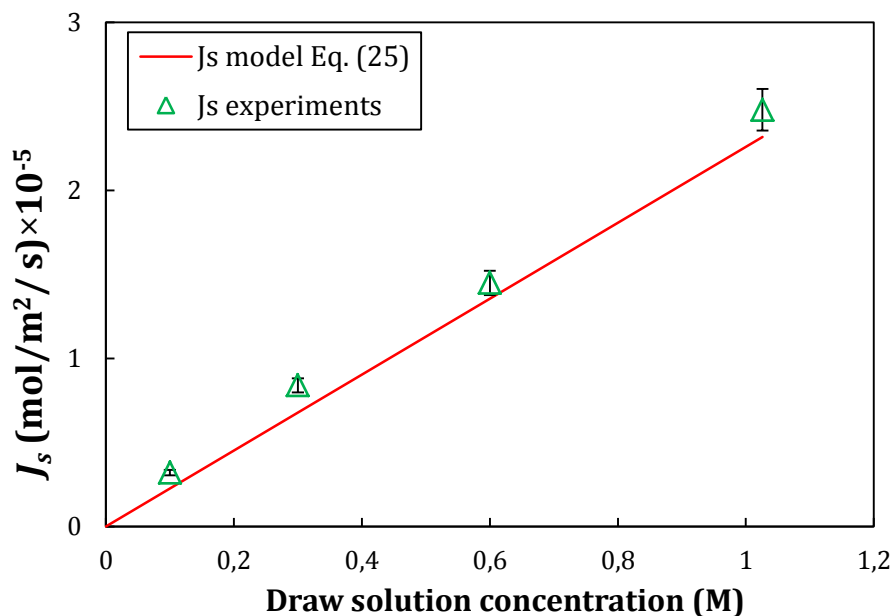


Fig.4.2: Comparison of the results predicted by the model developed in Eq. (4.25) with the experimental results for various NaCl concentrations. Feed solution is considered fresh water ( $C_{F,b} = 0.0\text{M}$ ,  $T = 20^\circ\text{C}$ ).

#### 4. Effect of the operating conditions on the reverse salt flux

##### 4.1 Effect of the osmotic pressure difference

In this section, the effect of the concentrations of the feed and draw solutions on the reverse salt flux is studied. It is normally assumed that the increase of the draw solution concentration leads to the increase of the water permeation enhancing the performance of PRO. Effectively, the difference of the osmotic pressures between solutions is key in the PRO process (See Eq. (4.4)): in fact the maximum of power produced is directly proportional to the square of this difference. However, the concentration affects also the salt flux as presented in Eq. (4.25). To study this effect, four feed solutions with different concentration were tested (8.55mM, 55mM, 0.2M, and 0.3M of NaCl) against four different draw solutions (0.6M, 0.7M, 0.8M and 1.026 M of NaCl). To reduce the number of experiments, when testing feed solutions, the draw solution was always 0.6M. For draw solutions tests, the feed solution was equal to 8.55mM. All solutions were tested under the same flow rate ( $u=50\text{ml}/\text{min}$ ).

The model in Eq. (4.25) was also solved numerically to determine the theoretical salt flux  $J_s$  in the range of concentrations chosen, keeping the other parameters in similar values which are summarized in Tables 3.2 and 3.3 of the previous chapter. Fig. 4.3-a shows that the increase of the feed solution concentration leads to a decrease of the water flux. This result is logical, as the increase of the feed solution concentration decreases the osmotic pressure difference, and therefore, decreases of the water flux and the power generated. This result was demonstrated in several previous studies [17,18]. To determine whether the flux decline was due simply to the decreased osmotic driving force, or whether there is another factor that contributed to this behavior, several different feed solutions were used. When increasing the feed solution concentration, the salt flux decreased remarkably in the same manner as the water flux. This behavior can be explained by Eq. (4.24): the salt flux is then directly proportion to the water flux.

Fig. 4.4 shows the proportion of the cause of osmotic pressure drop calculated from Eqs. (4.20), (4.21), (4.22) and (4.23). The contribution of each part on the optimum osmotic pressure difference  $\pi_{opt}$  is well defined in Fig. 4.1. The effective driving force  $\pi_{eff}$  is the osmotic pressure along the active layer. It can be clearly

seen that the proportion of the ICP increases with the increase of the feed solution concentration (from 2% at  $C_{F,b} = 8.55\text{mM}$  to 27% at  $C_{F,b} = 0.3\text{M}$ ). In fact, the salt in the feed solution enters the porous structure of the support layer as it is transported by the water flux. When reaching the support layer side, the salt cannot penetrate more due to it is rejected by the dense active layer of the PRO membrane. Therefore, the accumulation of the salt in that location induces an increase in concentration within the porous layer; hence, the new feed solution created presents a concentration higher than the feed bulk concentration, which reduces the effective osmotic driving force. On the other hand, the ECP decreases with the increase of the feed solution concentration (from 4% to 2%) which means that the concentration on the surface of the active layer tends to reach the draw bulk concentration. This observation could be explained as follows: firstly, the increase of the ICP plays the role of repulsive force to the draw solute to maintain the effective draw concentration near the draw bulk concentration; secondly, the decrease of the water flux induces the decrease of the ECP since the water flux is the transporter of the salt from the feed solution to the active layer surface.

In PRO, the driving force is directly related to the draw solution concentration, which explains the enhanced water flux when this concentration increases, as shown in Fig. 4.3-b. It can also be seen that the salt flux increases with the increase of the draw solution concentration. The proportion of the osmotic pressure drop due to the dilutive ECP also increases, which means that the concentration at the surface of the active layer  $C_{D,m}$  tends to be smaller than at the draw bulk. The ECP became more important at high water flux. It could be said that dilutive ECP acts as a barrier to the draw solute permeating into the support layer; hence, decreasing ECP means that the draw solute can more easily diffuse into the feed solution, which explains the increase of the salt flux diffusion. In the experiments, the effective osmotic pressure was reduced from 6% to 9% when the draw concentration was raised from 0.6M to around 1M.

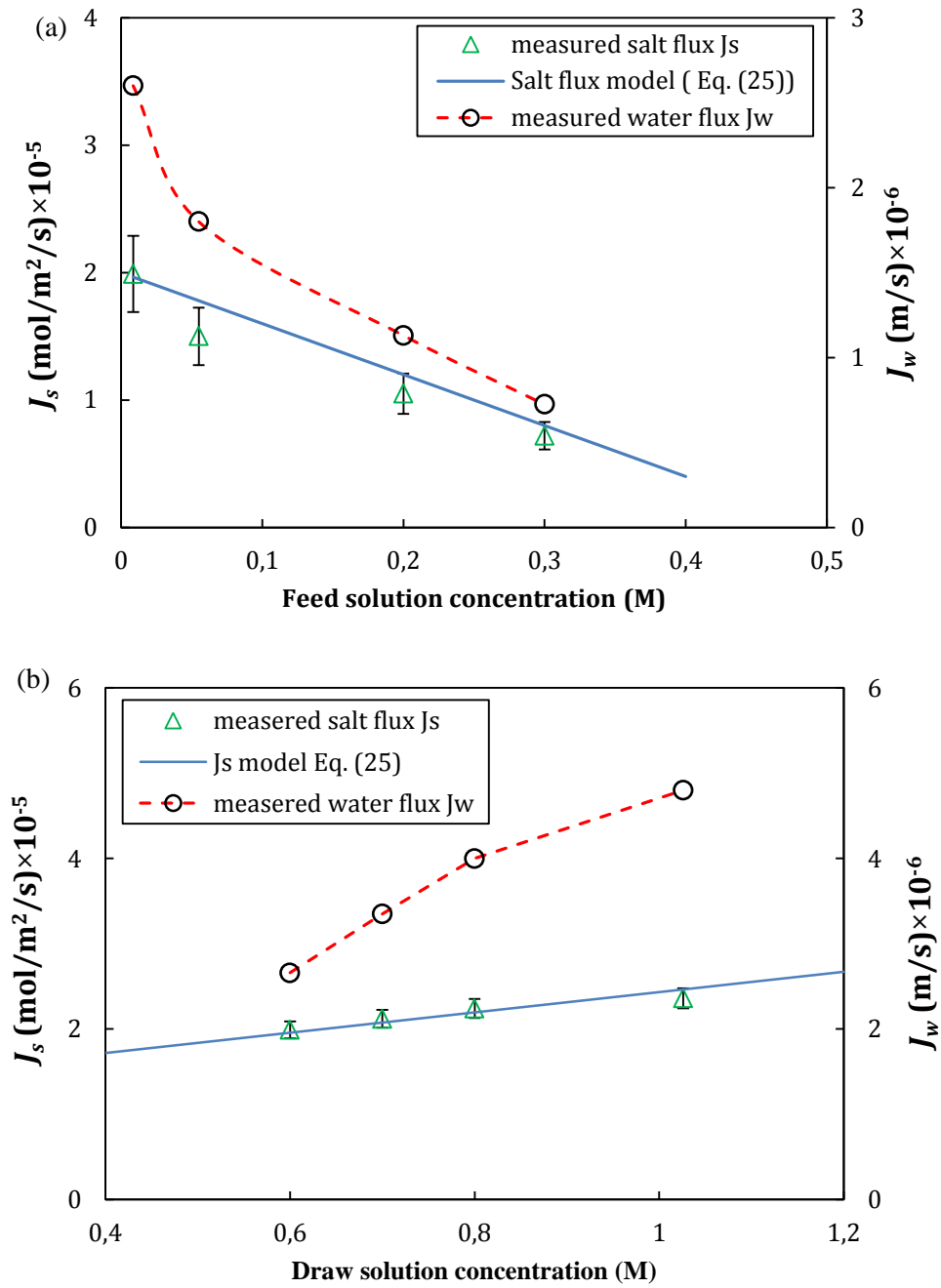


Fig. 4.3: Experimental Effects of the concentration of draw (b) and feed (a) solutions on the water flux  $J_w$  and the salt flux  $J_s$ , and comparison with the predicted  $J_s$ .

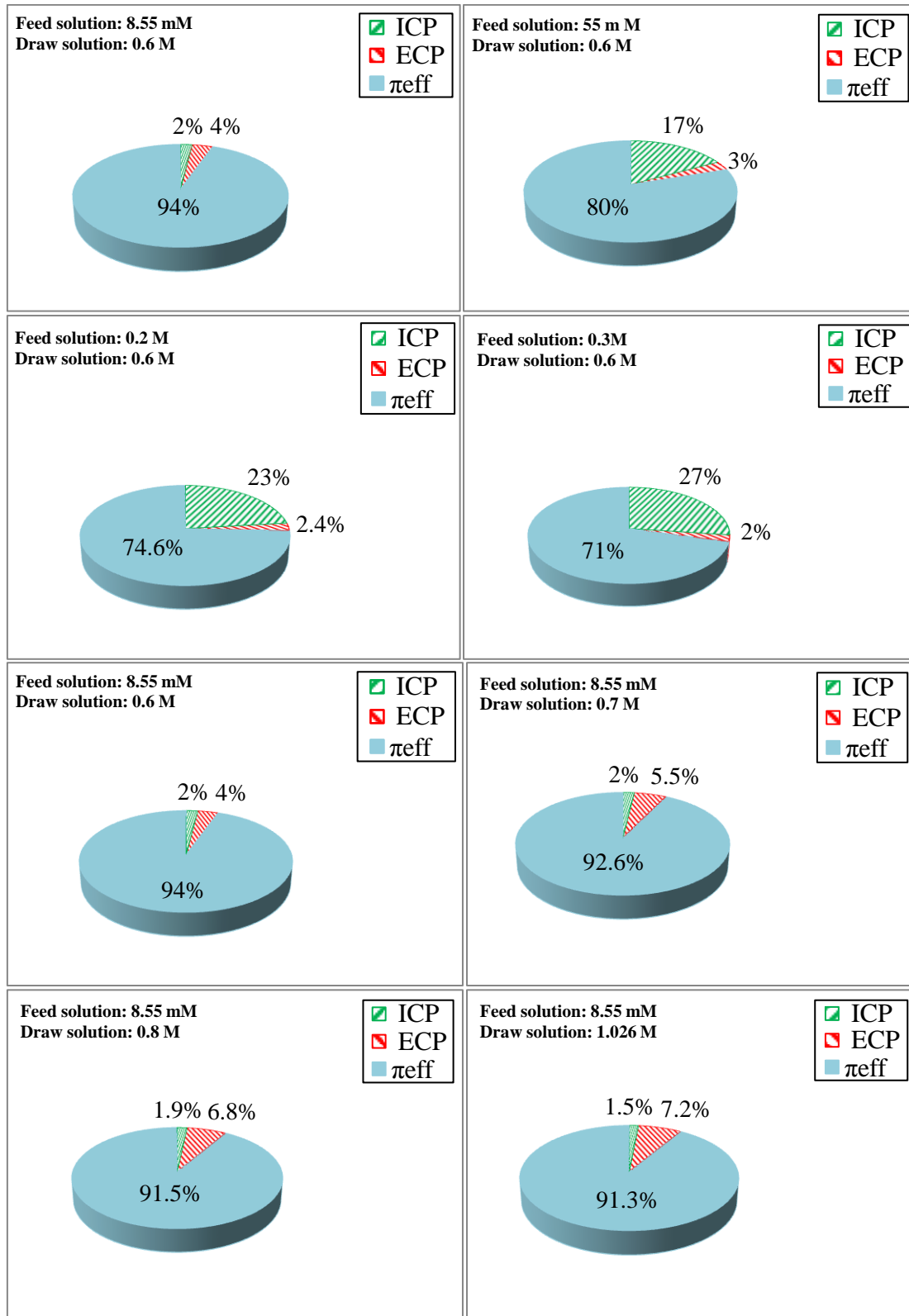


Fig. 4.4: Experimental proportion of the cause of osmotic pressure drop, as a function of the draw and feed concentrations. (Operating parameters in Table4.1).

#### 4.2 Effect of the cross flow velocity

The next study is the effect of the cross flow velocity: The velocities of draw and feed solutions affect the external CP, and the draw solution velocity may indirectly affect internal CP; therefore, both may impact the water flux. To study this effect the process was operated under four cross-flow velocities varying from 0.00535 m/s to 0.0321 m/s (that is, 25, 50, 100 and 150 ml/min): Under those conditions, the flow is considered to be laminar. During all the experiments the feed and draw solution flow rates were the same, the concentration of the draw was 1.026 M and the concentration of the feed was 8.55 mM. The experiments were carried out using the IGB membrane.

Fig. 4.5 shows clearly that the increase of the cross-flow velocity increases the water and salt fluxes. This behavior can be explained as follows:

- The first reason is given by film theory: the cross-flow velocity contributes to changing the thickness of the mass transfer boundary layer at the surface of the membrane. The boundary layer becomes thinner when the cross flow velocity is higher, which results in a higher rate of mass transfer.
- The second reason is that permeated water is mixed faster in the bulk draw solution. However, the increase rate of  $J_s$  is significantly higher than that of  $J_w$  (the salt flux was almost tripled when the water flux was increased 50%), which means that solute flux has increased more drastically at higher applied cross flows.

Fig. 4.6 presents the proportion of the osmotic pressure at different cross-flow velocities calculated from Eqs. (4.20), (4.21), (4.22) and (4.23). At low cross-flow velocities, the contribution of the dilutive ICP in the pressure drop is higher. When the velocity increases the ECP decreases, so ECP is more pronounced at high water fluxes if PRO is operated at low cross-flow velocities. ECP can be minimized by increasing the cross-flow velocity and the turbulences at the membrane surface. On the other hand, it can be seen that the ICP increases slightly with the decrease of the ECP (increase of the velocity). This result means that the feed solute can more easily diffuse into the support layer when the barrier effect of the ECP is mitigated. The effect of the ICP, as mentioned in the previous section, is more important at high feed solution concentration. This effect can be more severe if the PRO is operating under high velocity and high feed solution concentration.

However, The results showed that increasing the velocity increases the salt flux diffusion,so, to design a power plant with low velocity may reduce the salt diffusion, but it will decrease the performance of the PRO (because the power density increases with the increase of the velocity and also the ECP decreases with the velocity). Moreover, it was shown in the previous paragraph that the salt flux diffusion affects the concentration polarization (ICP and ECP). Consequently, the influence of the cross-flow velocity on specific reverse salt flux provides helpful information in PRO design and optimization.

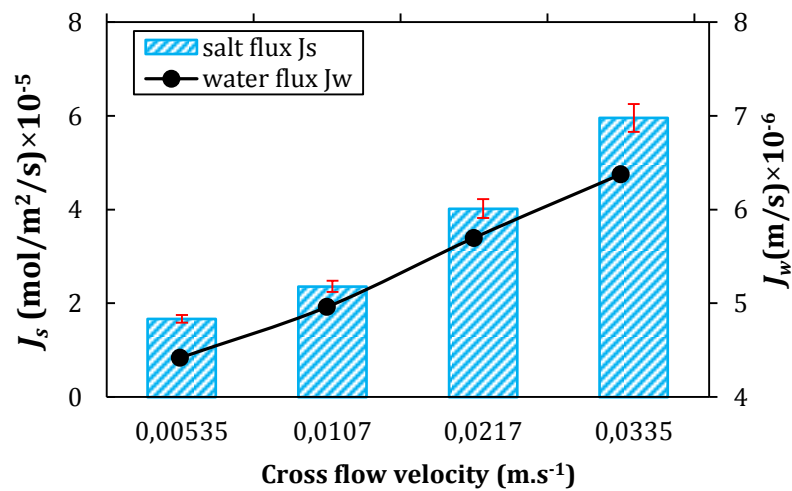


Fig. 4.5: Effect of the cross-flow velocity on the salt flux  $J_s$  and on the water flux  $J_w$ .  $\Delta P = 23$  bars.

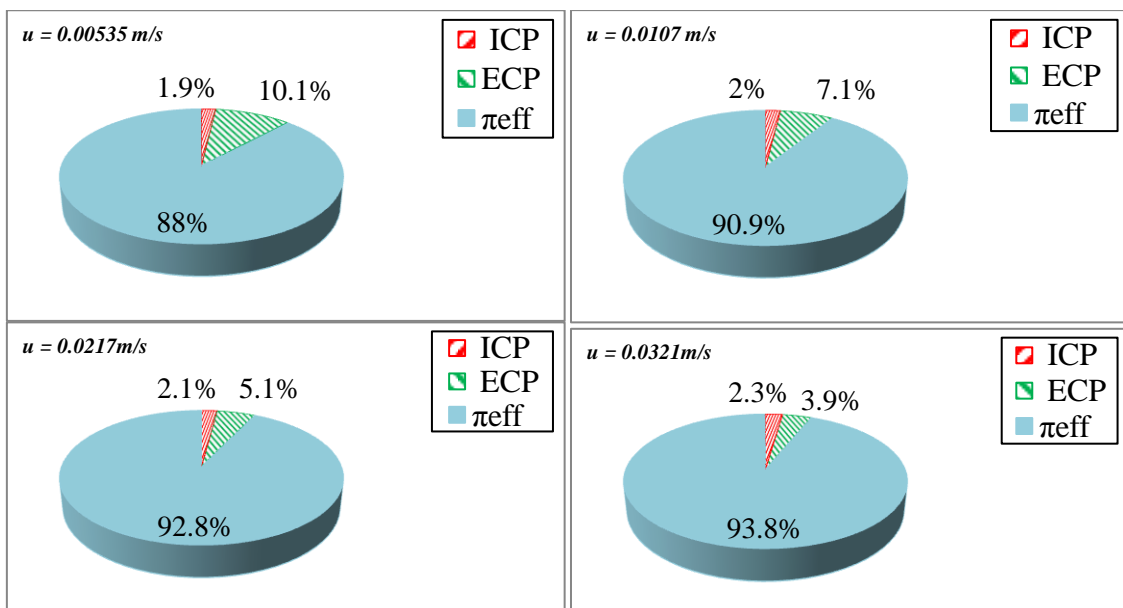


Fig. 4.6: Experimental proportion of the cause of osmotic pressure drop as a function of the cross flow velocity.

### 4.3 Effect of the membrane orientation

In PRO, two membrane orientations are normally used (See Fig. 4.7):

- the active layer facing the draw solution (denoted here AL-DS),
- the active layer facing the feed solution (denoted here AL-FS).

In fact the orientation AL-DS is most widely assumed in the literature, due to the fact that the performance and the stability of the membrane are significantly better.

The effect of ICP can be modeled by adopting the classical solution-diffusion theory for the dense rejection layer coupled with convection and diffusion transport of the solute in the porous support layer [34]. Concentrative ICP appears under AL-DS orientation, whereas the dilutive ICP appears under AL-FS. According to Lee et al [35], the water flux for PRO can be expressed as follows:

$$J_w = K \frac{(A\pi_{D,b} - A\Delta P - J_w) + B((A\Delta P/J_w) + 1)}{A\pi_{F,b} + B((A\Delta P/J_w) + 1)} \quad (\text{AL - DS})$$

$$J_w = K \frac{A\pi_{D,b} + B((A\Delta P/J_w) + 1)}{(A\pi_{F,b} + J_w + A\Delta P) + B((A\Delta P/J_w) + 1)} \quad (\text{AL-FS})$$

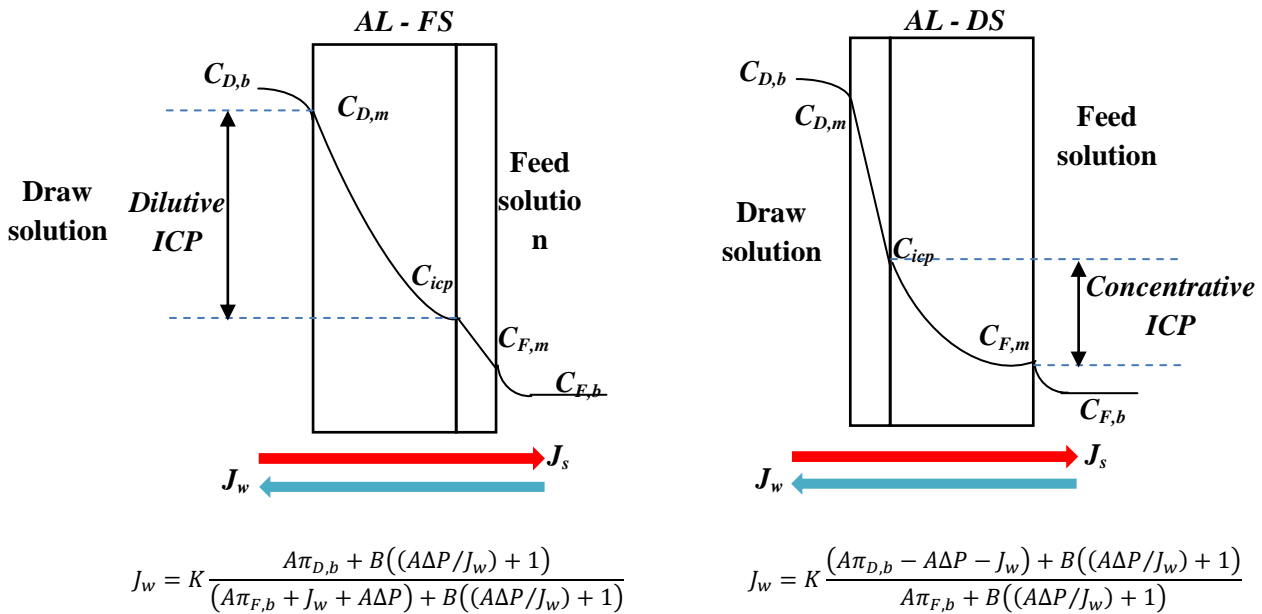


Fig. 4.7: Schematics of membrane orientations in PRO process. The concentrative and dilutive ICPs are also shown.

In this section, the effect of the membrane orientation on the reverse salt flux and the power output is studied. For that, a 1M NaCl draw solution and two feed solutions (8.55 mM and 55 mM) were tested under both membrane orientations. From Fig. 4.8, it can be seen that the performance of PRO operated under AL-DS is better at high pressure and using low feed solution concentration: the water flux and the power density are much higher and the membrane seems to be more stable under these conditions (Fig. 4.8-a, -b, -e and -f). This is due to the severe ICP that occurs in the support layer when it is facing the draw solution, which proves that the dilutive ICP in AL-FS orientation is more severe than the concentrative ICP in AL-DS orientation. However, the reverse salt flux for PRO under AL-FS is lower than PRO operated under AL-DS for the two studied feed solutions because of the remarkable difference between concentrative and dilutive ICPs in both cases. When the feed solution was 55 mM, the difference of PRO performance for the two orientations was not significant. Moreover, when operating at low pressure and under AL-FS orientation, the membrane seems to be stable in terms of water flux and reverse salt flux (Fig. 4.8-b and 4.8-d).

These results explain the tendency of using the AL-DS orientation in PRO experiments, especially at high pressure to guarantee a high power density. However, it should be pointed out that the AL-FS orientation is stable at low pressures. On the other hand, it has been shown in a previous study that AL-FS orientation resist better to fouling [32]. Moreover, it was shown here that the salt diffusion is lower for AL-FS, which means that the contribution of  $J_s$  in membrane scaling and fouling is lower than AL-DS, especially using feed solutions that contain fouling and scaling precursors. As an example, the “Mega-ton RO-PRO” project in Fukuoka City- Japan is operating under AL-FS orientation, and seems to have good results [36].

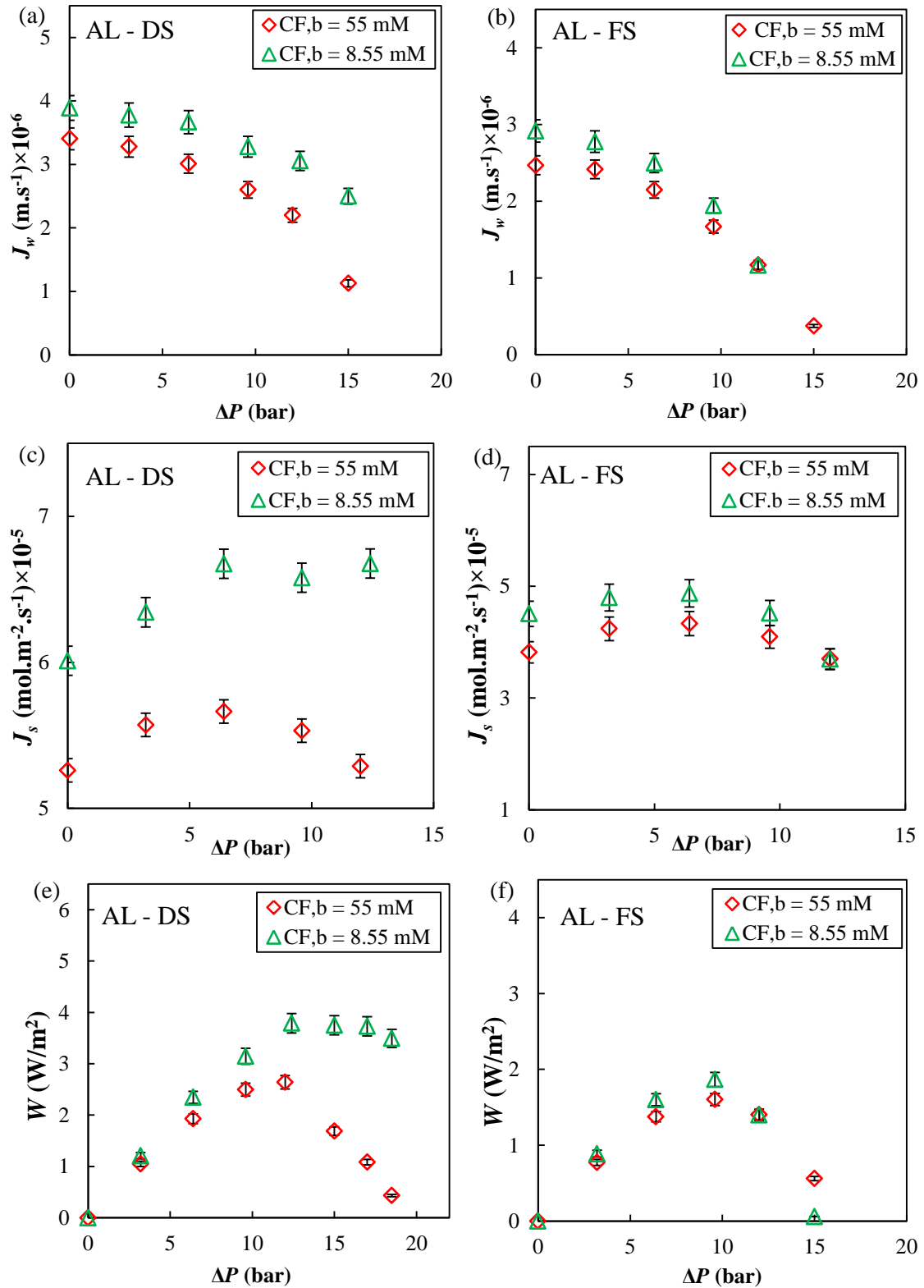


Fig. 10: Effect of the membrane orientation on the water flux ((a) and (b)), the salt flux diffusion ((c) and (d)), and the power density ((e) and (f)). 1 M NaCl draw solution,  $T = 20^\circ\text{C}$  for both feed and draw solution, cross-flow velocity of 50ml/min on both side of membrane.

#### 4.4 Effect of the draw solution composition

In this section, the effect of the of draw solution composition is investigated. Six draw solutions were tested (sodium chloride, potassium chloride, magnesium sulfate, calcium chloride, calcium nitrate and glucose). These were prepared using concentrations that correspond to the osmotic pressure of sea water ( $\approx 27$  bar). Fig. 4.9 shows the variation of the reverse salt flux and the water flux for each case tested.

It can be clearly seen that the performance of PRO drastically changes with the type of chemicals composing the draw solution. The highest salt flux was found when the draw solution was based on potassium and sodium chlorides, and the lowest was for the calcium chloride and magnesium sulfate. This distinct behavior of the salt diffusion can be attributed to the ion size in aqueous solution.

Since the ionic radius changes in aqueous solutions, it is necessary to take into account the hydrated radius. Table 4.1 shows the hydrated radius of the tested ions in aqueous solutions. From Fig. 4.9-a, it can be seen that there is a strong relationship between the salt diffusion and the hydrated ions: Sodium chloride and potassium chloride revealed a high passage through the membrane due to their small radius compared to the other entities. The lowest reverse salt flux occurs at the measurement of the  $MgSO_4$  and  $CaCl_2$  solutions, which are characterized by the bigger radius. However,  $CaCl_2$  lowest salt passage than  $MgSO_4$  despite the fact that its radius is smaller. Possibly, this behavior can be attributed to the interaction between the surface of membrane and the calcium, forming calcium acetate, which blocks the passage of the salt.

Fig. 4.9-b shows the influence of the draw solution composition on the water flux. The highest water flux occurs with calcium salts, whereas the lowest water flux was observed with magnesium salt. As shown in Eqs. (4.10) and (4.11), the diffusion coefficient of the draw solution affects the external concentration polarization. In fact, the diffusion minimizes the difference of concentrations between the draw bulk and the draw boundary layer ( $C_{D,b}$  and  $C_{D,m}$ ); when the diffusion coefficient is high, the external concentration polarization ECP is reduced and thus the water flux increases. Moreover, a possible penetration of the salts in the membrane, which causes internal concentration polarization ICP, especially when the salt is blocked in the inner structure of the membrane and cannot be

removed due to their size. Table 4.2 shows the diffusion coefficients in aqueous solution of the different ions investigated.

The magnesium salt revealed the lowest water flux. This result can be explained by the fact that the magnesium salt has the lowest diffusion coefficient and the thickest hydrated radius, which leads to more severe internal and external concentration polarization compared to the other salts. Unexpected result for calcium salts was shown: the highest water flux was observed for calcium chloride and a good performance was shown using calcium nitrate compared to the other entities despite its thick hydrated radius. This result may be attributed large hydrated nitrate radius, which reduces the salt flux and the relatively high diffusion coefficient, which minimizes the ECP. Calcium nitrate at a very low salt passage was measured, which contributes to increase the trans-membrane flux. Potassium and sodium chloride have high diffusion coefficients which lead to decrease the effect of ECP, and thus enhance the water flux. However, these entities have small ionic hydrated radius, which causes an increase in salt flux, and thus the water flux decreases. These two simultaneous and antagonist effects explain the behavior of water flux.

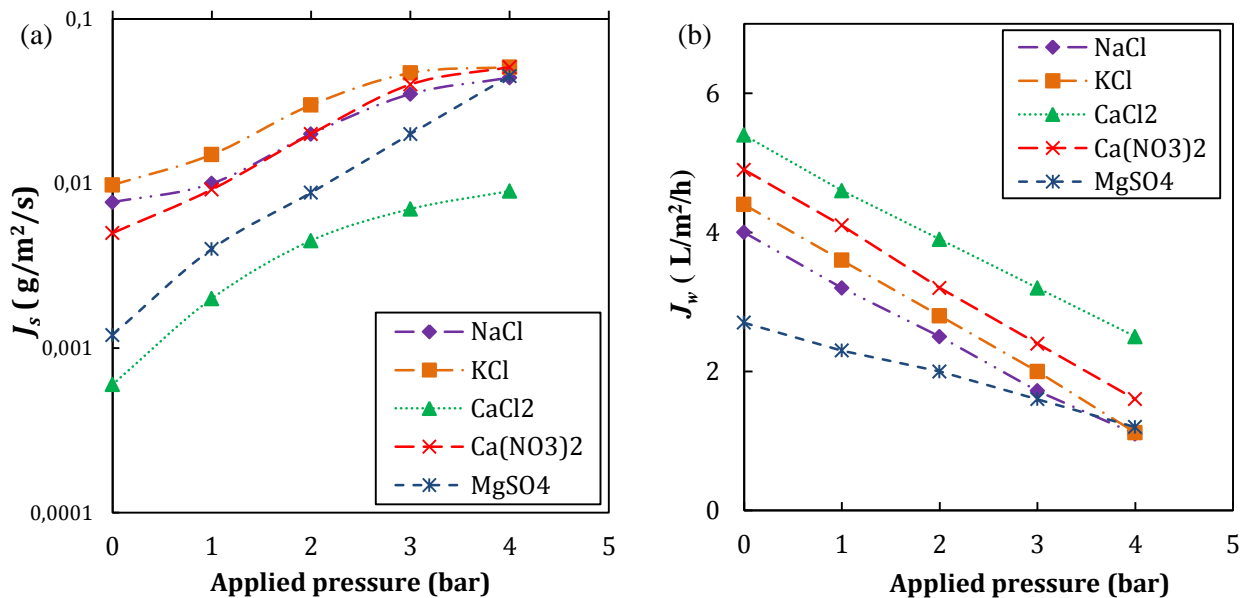


Fig. 4.9: Experimental salt flux  $J_s$  and water flux  $J_w$  for different draw solution composition as a function of the applied pressure.

Table 4.1: Hydrated radius of studied ions [21]

<i>Ion</i>	<i>Hydrated radius (<math>10^{-12}m</math>)</i>
Na <sup>+</sup>	178
K <sup>+</sup>	201
Ca <sup>2+</sup>	260
Mg <sup>2+</sup>	300
Cl <sup>-</sup>	195
NO <sub>3</sub> <sup>-</sup>	340
SO <sub>4</sub> <sup>2-</sup>	300

Table 4.2: Diffusions coefficients of tested salts [22,23,24,25,26].

<i>Salt</i>	<i>Diffusion coefficient (<math>10^{-9} m^2.s^{-1}</math>)</i>
NaCl	1.50
KCl	1.90
CaCl <sub>2</sub>	1.12
Ca(NO <sub>3</sub> ) <sub>2</sub>	1.08
MgSO <sub>4</sub>	0.74

#### 4.5 Effect of the solutions temperature

The effect of the temperatures of the solutions is now investigated. For this, a NaCl draw solution (0.35M) and a NaCl feed solution (8.55mM) were used. The experiments were realized under several temperature gradients between the two solutions.

Table 4.3 presents the results obtained in the five experiments investigated. It is clear that the increase of a solution temperature leads to the increase of its osmotic pressure, following the van't Hoff equation. Moreover, due to the heat convection and diffusion, the temperature inside the membrane depends on the temperature of the solutions in the bulks. In our study [29], a mathematical model was developed to quantify the temperature in each part of the membrane at different operating temperature. It was shown that the transport parameters ( $A$ ,  $B$  and  $s$ ) cannot be considered constants at different temperatures. In this section, the

values of  $A$  and  $B$  will be taken from [19] under the same conditions for simulation issues as described in Table 4.3. Fig. 4.10 shows the variation of the water and the salt fluxes under different bulks temperatures. As expected, the increase of the temperature leads to the increase of the water flux, which enhances the performance of the PRO, as shown in Fig. 10-a and 10-b. It can be seen that when the feed solution temperature was increased, the impact on the power density is quite significant (the power density jumps from  $1.6 \text{ W.m}^{-2}$  to  $2.4 \text{ W.m}^{-2}$ ). This result is consistent with the plots of the water flux: the performance of the PRO is higher at high feed solution temperatures. In the other case, the process shows an improvement with the increase of the draw solution temperature; however, the increase is much lower than with the feed solution temperature. Likewise, raising the temperature enhances the salt flux in both experiments.

The specific salt flux ( $J_s/J_w$ ), theoretically given by Eq. (4.24), is very useful to study the effect of the reverse salt flux on PRO. Fig. 4.10-e and 4.10-f show the variation of this specific salt flux under different operating temperature. Experimental and simulated  $J_s/J_w$  increased with temperature in both cases. The results revealed the strong relationship between the water flux and the salt diffusion: high temperature leads to a better water flux, which unfortunately induces more severe solute diffusion. We suggest that this behavior is due to a modification of the membrane structure: the temperature acts upon the pores of the membrane and tends to enlarge them which is followed by an increase of the water and salt fluxes. This seems to be consistent with the resulted water permeability coefficient  $A$  and salt permeability coefficient  $B$  presented in Table 4. Accordingly to prior studies [28,30], reverse diffusion of draw solutes can be significantly enhanced at higher applied pressure due to membrane deformation. Moreover, the proportion of the osmotic pressure drop reveals that the increase of the draw solution temperature induces more severe ICP compared to the feed solution temperature (Table 4.4). Despite the enhancement of the water flux, the increase of the solutions temperature induces a decrease of the effective osmotic pressure. This may be attributed to the penetration of the solute into the active layer because of the membrane deformation where the temperature in this location is then higher. It should be noted that the proportion of the osmotic pressure drop was calculated

respecting the Morse equation at the modeled temperature in each part of the membrane.

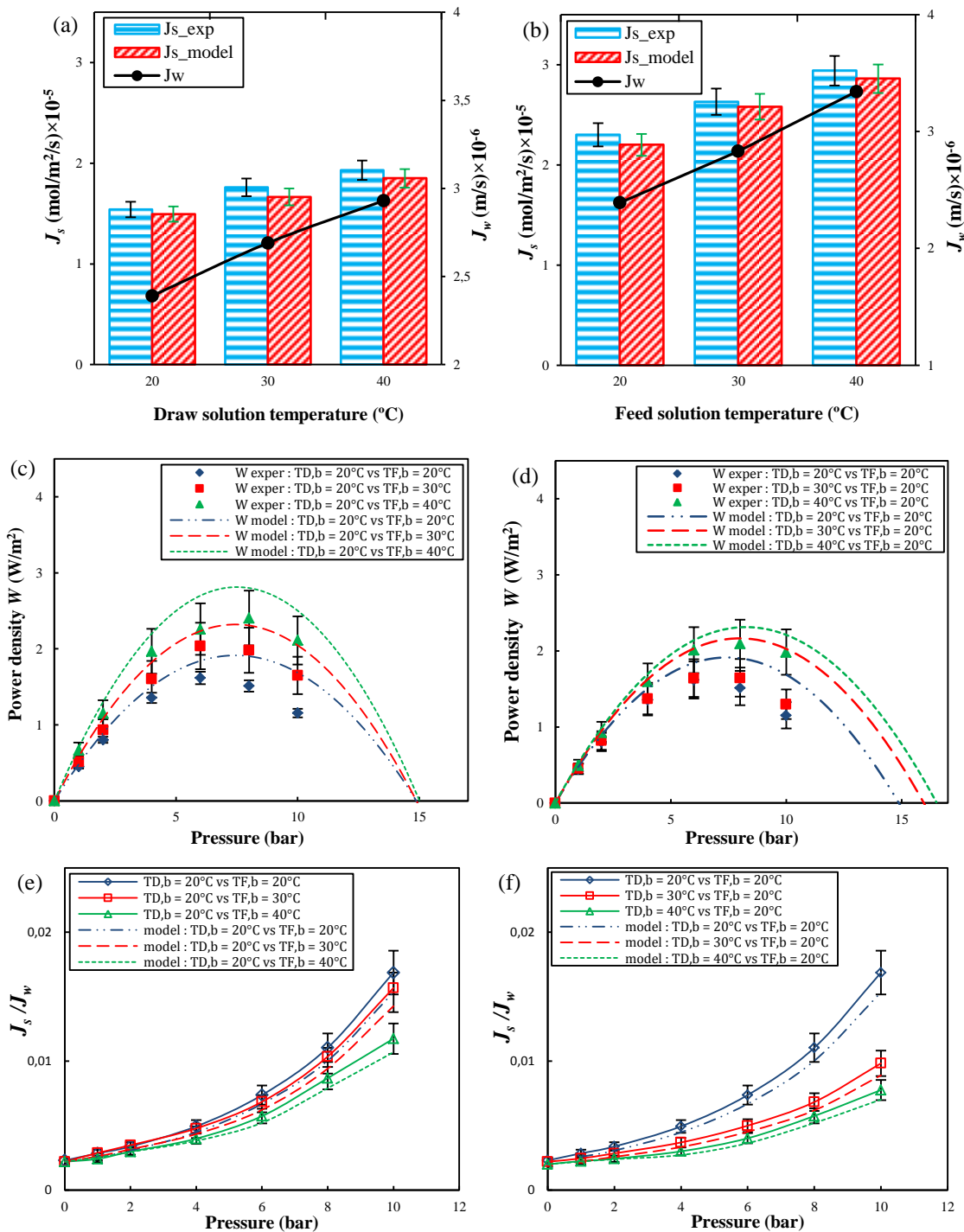


Fig. 4.10: Experimental and simulated salt and water fluxes (a, b), power density (c, d) and specific salt flux ( $J_s/J_w$ ) (e, f) under different draw and feed solution temperatures. (Experimental conditions: 8.55mM NaCl feed solution, 0.35 M NaCl draw solution,  $u = 50$  ml/min.)

Table 4.3: Temperatures, water permeability, salt permeability and proportion of osmotic pressure drop under different bulk solutions temperatures.

$T_{F,b}$ (°C)	$T_{D,b}$ (°C)	$T_{F,m}$ (°C)	$T_{D,m}$ (°C)	$T_{icp}$ (°C)	$A$ (m.s <sup>-1</sup> .Pa <sup>-1</sup> )	$B$ (m.s <sup>-1</sup> )
20.0	20.0	20.0	20.0	20.0	$1.06 \times 10^{-12}$	$2.62 \times 10^{-8}$
30.0	20.0	27.1	22.7	23.5	$1.53 \times 10^{-12}$	$4.80 \times 10^{-8}$
40.0	20.0	37.4	24.4	25.8	$1.97 \times 10^{-12}$	$5.16 \times 10^{-8}$
20.0	30.0	22.9	27.3	26.5	$1.09 \times 10^{-12}$	$2.85 \times 10^{-8}$
20.0	40.0	24.8	35.6	34.2	$1.14 \times 10^{-12}$	$3.13 \times 10^{-8}$

Table 4.4: Effective osmotic pressure and proportion of osmotic pressure drop under different bulk solutions temperatures.

$T_{F,b}$ (°C)	$T_{D,b}$ (°C)	$\pi_{eff}$ (%)	$ICP$ (%)	$ECP$ (%)
20.0	20.0	92.9	3	4.1
30.0	20.0	88.8	5.5	5.7
40.0	20.0	88.1	5.8	6.1
20.0	30.0	88.6	7.1	4.3
20.0	40.0	86.3	9.2	4.5

### 5. Theoretical discussion of the ratio $J_s/J_w$

As it has been mentioned the specific salt flux  $J_s/J_w$  can be useful to study the effect of the reverse salt flux on PRO. This is theoretically given by Eq. (4.24), where the reverse salt flux depends on two main parameters: the water flux and the applied pressure (water and the salt permeability coefficients can be considered constants in short time scales). The factor  $1 + \frac{A\Delta P}{J_w}$  is fundamental to study the contribution of the pressure and the water permeability to the salt flux. Eq. (4.24) can be rearranged based on the operating conditions:

- At high water flux and low pressure, the quantity  $\frac{A\Delta P}{J_w}$  is much smaller than 1.0, so Eq. (4.24) can be rearranged and the salt flux is approximately:

$$J_s \approx J_w \frac{B}{A\beta RT} \quad (4.30)$$

- At low water flux and high pressure, the quantity  $\frac{A\Delta P}{J_w}$  is much bigger than 1.0, so Eq. (4.24) can be rearranged as follows:

$$J_s \approx \frac{B}{\beta RT} \Delta P. \quad (4.31)$$

Eq. (4.30) shows that the salt flux is directly proportional to the water flux, which means that the increase of  $J_s$  is mainly due to the water flux permeation when operating at high water flux and low pressure. In fact, Fig. 4.11 shows that more than 90% of the salt flux at low pressure is caused the water flux.

In the other case, Eq. (4.31) shows that the salt flux is mainly caused by the applied pressure; this is consistent with the experimental results presented in Fig. 4.10-e and 4.10-f of the previous Section, where the  $J_s/J_w$  ratio increased drastically at high pressures (A similar observation has already been presented in [27]).

This result is valid as long as  $A$  and  $B$  are constant during the process. Unfortunately, several studies mentioned that  $A$  and  $B$  are modified during PRO process because of membrane modification that depended on the operating conditions [17,27,31]. According to the study reported in [29], the increase of the temperature enhances the salt permeability  $B$ , which means that the PRO process can suffer from high salt flux when operating at high pressure. She Q. et al suggest that high pressure is an important cause of membrane deformation [17]. These results confirm that, with non-ideal membrane, the reverse salt flux is inevitable because it is mainly caused by primordial factors of PRO process: the water flux and the applied pressure. Consequently, salt diffusion should be well controlled and the variation of  $B$  should also be minimized. To mitigate this, rigid membrane and well developed spacers can help to minimize the effect of the pressure and limit the risk of membrane modification.

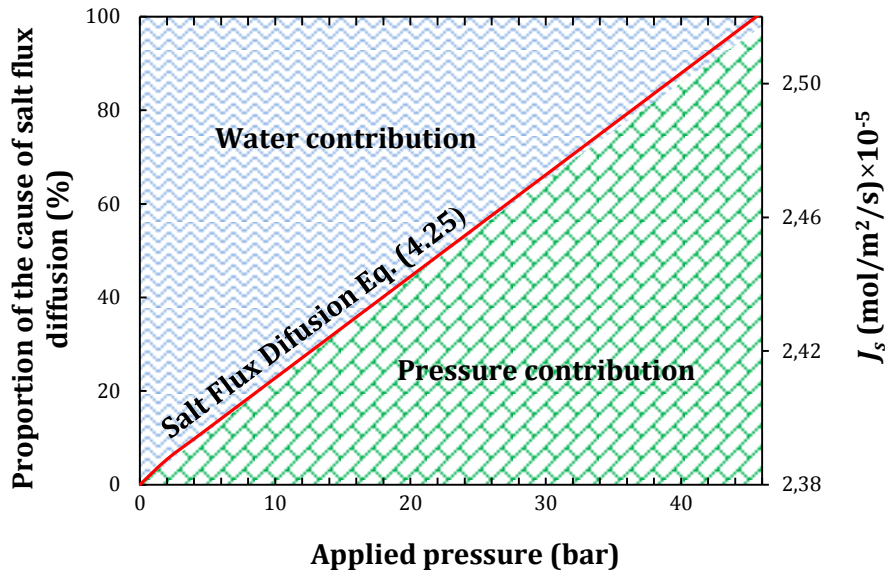


Fig. 4.11: Distribution of the cause of the reverse salt flux in PRO as function of the applied pressure (The draw solution concentration is 1M; the feed solution concentration is 8.55 mM. The continuous line is the modeled salt flux under conditions presented in Table 4.1).

## 6. Implications of the Reverse salt flux for full-scale power plants

The results shown in the previous section were for a lab-scale PRO system using synthetic solutions with non-complex matrix (absence of bivalent ions). Prior studies mentioned that any full-scale osmotic power plant is not viable if the power density produced is under  $5\text{W/m}^2$  [27]. Experimental results clearly demonstrate that the reverse salt flux has a strong adverse effect on PRO performance. Draw solutes diffusing through the membrane accumulate in the porous substrate due to the water flux. This leads to a buildup of draw solute concentration within the porous support layer in addition to the ICP caused by the accumulation of feed solutes in the support layer. Therefore, the optimal hydraulic pressure is reduced due to the new built concentration gradient.

Moreover, a recent study [32] showed that the presence of scaling precursor ions (i.e.  $\text{Ca}^{2+}$ ,  $\text{Mg}^{2+}$  and  $\text{SO}_4^{2-}$ ) on the draw solution may trigger the gypsum precipitation because of the migration of these ions from the draw solution to the feed solution by means of reverse solute diffusion. Hence, the increase of operating pressure leads to the increase of salt reverse diffusion; therefore, the risk of

gypsum precipitation increases. On the other hand, the bivalent ions reverse salt flux contributes to membrane fouling. In fact, the diffusion of calcium and magnesium from the draw solution to the feed solution increases the fouling process due to the fact that those ions form interactions with organic foulants which enhance the membrane fouling [33].

In summary, the effects of the reverse flux diffusion are:

- to enhance ICP,
- to cause membrane scaling, and
- to aggravate membrane fouling.

Therefore, those consequences will reduce the performance of PRO membrane in foul-scale power plants, and limit its durability. It should be noted that it is estimated that membranes account for up to 80% of total capital costs [6]; then, the durability of the membrane directly affects the viability of power plant. Consequently, the use of chemical cleaning and backwashing becomes a necessity to mitigate the effect of fouling and scaling, which increase the energy costs and affect the environmental impact of the process. It is also pointed out that pre-treating the water to avoid fouling and scaling requires a relatively large amount of energy and has a high cost.

The optimization of the membrane can be very beneficial to avoid the problem of the solute diffusion. In fact, inhibiting the migration of the solute from the draw solution to the feed solution can avoid the induced ICP and limit the contribution of the bivalent ions in the processes of scaling and fouling. Thus, an active layer with very high rejection is recommended. As demonstrated in the previous section, increasing the flow rate velocity increases the water flux and has a relative low impact on the ICP, and also can be useful to remove the foulant deposits from the membrane surface. Suitable operating conditions and a well-designed membrane can, then, but control its effect on power produced.

## 7. Conclusion

In this chapter, a model reproducing the reverse salt flux for a flat sheet membrane flux in PRO power plant has been developed and validated at lab scale. The effects of feed and draw solution concentrations, the cross-flow velocity, and temperature on this salt flux were investigated. The following conclusions can be made from the current study:

- The increase of the feed solution concentration decreases the rate of reverse salt flux because of the reduced concentration gradient between the two membrane sides. However, this leads to a severe concentrative ICP due to the penetration of the solute in the support layer and blocked at the surface of the active layer which reduces the performance of the PRO.
- The increase of the draw solution concentration enhances the PRO process by increasing the osmotic driving force. However, it simultaneously increases the reverse salt flux.
- The PRO process presents better performance when operating at high cross-flow velocity. However, this velocity exacerbate the effect of the ICP.
- Operating under AL-DS orientation is more suitable for high pressures. However, the AL-FS is recommended when feed solutions contain fouling precursors.
- The increase of the operating temperature leads to a better performance of the PRO. However, the salt flux also increases due to increase of the salt permeability coefficient and the diffusivity of the salt in the inner of the membrane.
- The water flux and the pressure are mainly the experimental parameters that control the salt flux evolution. PRO membranes with better rigidity and optimized spacer are required to guarantee a better performance of the PRO process.

The results of this chapter were submitted in Renewable Energy Journal as: KhaledTouati, Christopher Hänel, Fernando Tadeo, Thomas Schiestel, Effect of the operating conditions on the losses caused by Reverse Salt Diffusion in osmotic

power plants, *Renewable Energy Journal*, submitted February 2015 (under revision)

**REFERENCES OF CHAPTER 4**

- [1] Hancock NT, Cath TY. Solute Coupled Diffusion in Osmotically Driven Membrane Processes. *Environ SciTechnol* 2009;43:6769-6775.
- [2] Helfer F, Lemckert C, Anissimov, YG. Osmotic power with Pressure Retarded Osmosis: Theory, performance and trends – A review. *J MembrSci* 2014;453:337-358.
- [3] Post JW, Veerman J, HVM Hamelers, Euverink GJW, Metz SJ, NymeijercBuisman JNC. Salinity-gradient power: Evaluation of pressure-retarded osmosis and reverse electrodialysis. *J MembrSci* 2007;288:218–230.
- [4] Phillip WA, Yong JS, Elimelech M. Reverse Draw Solute Permeation in Forward Osmosis: Modeling and Experiments. *Environ SciTechnol* 2010;44:5170-5176.
- [5] Achilli A, Cath TY, Childress AE. Power generation with pressure retarded osmosis: An experimental and theoretical investigation, *J Membrane Sci* 2009;343: 42-52.
- [6] Suh C, Lee S. Modeling reverse draw solute flux in forward osmosis with external concentration polarization in both sides of the draw and feed solution. *J Membrane Sci* 2013;427:365–374.
- [7] Loeb S, Titelman L, Korngol E, Freiman J. Effect of porous support fabric on osmosis through a Loeb-Sourirajan type Asymmetric membrane. *J MembrSci* 1997;129:243–249.
- [8] Gray G, McCutcheon JR, Elimelech M. Internal concentration polarization in forward osmosis: role of membrane orientation. *Desalination* 2006;197:1-8.
- [9] McCutcheon JR, Elimelech M. Influence of concentrative and dilutive internal concentration polarization on flux behavior in forward osmosis. *J MembrSci* 2006; 284:237–247.
- [10] Hänel C, Touati K, Tadeo F, Schiestel T. A Parameter Study With Cellulose acetate Membranes For Pressure Retarded Osmosis. *International Membrane Science & Technology Conference, Melbourne, 2013.*
- [11] Lee KL, Baker RW, Lonsdale HK. Membrane for power generation by pressure retarded osmosis. *J Membr Sci* 1981;8:141– 171.
- [12] Naguib MF., Maisonneuve J, Laflamme C.B, Pillay P. Modeling pressure-retarded osmotic power in commercial length membranes. *Renew Energy* 2015;76:619–627.

- [13] Gray G, McCutcheon JR, Elimelech M. Internal concentration polarization in forward osmosis: role of membrane orientation. *Desalination* 2006;197: 1–8.
- [14] Maisonneuve J, Pillay P, Laflamme CB. Pressure-retarded osmotic power system model considering non-ideal effects. *Renew Energy* 2015;75:416–424.
- [15] Xu Y, Peng X, Tang CY, Fud QS, Nie S. Effect of draw solution concentration and operating conditions on forward osmosis and pressure retarded osmosis performance in a spiral wound module. *J MembrSci* 2010;348:298–309.
- [16] Yip NY, Tiraferri A, Phillip WA, Schiffman JD, Hoover L, Chang Kim A, Elimelech M. Thin-Film Composite Pressure Retarded Osmosis Membranes for Sustainable Power Generation from Salinity Gradients. *Environ Sci Technol* 2011;45: 4360–4369.
- [17] She Q, Hou D, Liu J, Tan KH, Tang CY. Effect of feed spacer induced membrane deformation on the performance of pressure retarded osmosis (PRO): Implications for PRO process operation. *J Membr Sci* 2013;445:170–182.
- [18] Achilli A, Tzahi YC, Childress AE. Power generation with pressure retarded osmosis: An experimental and theoretical investigation. *J Membr Sci* 2009;343: 42–52.
- [19] Yip NY, Tiraferri A, Phillip WA, Schiffman JD, Elimelech M. High performance thin-film composite forward osmosis membrane. *Environ Sci Technol* 2010;44: 3812–3818.
- [20] Phillip WA, Yong JS, Elimelech M. Reverse draw solute permeation in forward osmosis: modeling and experiments. *Environ Sci Technol* 2010;44: 5170–5176.
- [21] Tansel B, Sager J., Rector T., Garland J., F. Strayer R., Levine L., Roberts M., Hummerick M, Bauer J. Significance of hydrated radius and hydration shells on ionic permeability during nanofiltration in dead end and cross flow modes. *Sep Purif Technol* 2006;51: 40–47.
- [22] Vitagliano V, Lyons PA. Diffusion Coefficients for Aqueous Solutions of Sodium Chloride and Barium Chloride, *Riley ibid.* 1954;76(5216):1549–52.
- [23] Lobo VMM, Ribeiro ACF, Verissimo LMP. Diffusion Coefficients in Aqueous Solutions of Potassium Chloride at High and Low Concentrations, *J Mol Liq* 1998;78:139–49

- [24] Ribeiro ACF, Barros MCF, Teles ASN, Valente AJM, Lobo VMM, Sobral AJFN, Estes MA. Diffusion coefficients and electrical conductivities for calcium chloride aqueous solutions at 298.15K and 310.15K. *Electrochim Acta* 2008;54:192–196.
- [25] Gammell PM, Meister R. Measurement of the self-diffusion constant of aqueous calcium nitrate solutions by an NMR spin-echo technique. *J Chem Phys* 1976;64:4287.
- [26] Harned HS, Hudson RM. The Diffusion Coefficient of Magnesium Sulfate in Dilute Aqueous Solution at 25°. *J Am Chem Soc* 1951;73 (12):5880–82
- [27] Chang Kim Y, Elimelech M. Potential of osmotic power generation by pressure retarded osmosis using seawater as feed solution: Analysis and experiments. *J Membr Sci* 2013; 429:330–337.
- [28] She Q, Jin X, Tang Chuyang Y. Osmotic power production from salinity gradient resource by pressure retarded osmosis: Effects of operating conditions and reverse solute diffusion. *J Membr Sci* 2012;401– 402:262– 273.
- [29] Touati K, Hänel C, Tadeo F, Schiestel T. Effect of the feed and draw solution temperatures on PRO performance: theoretical and experimental study. *Desalination* 2015;365:182–195.
- [30] Kim YC, Elimelech M. Adverse impact of feed channel spacers on the performance of pressure retarded osmosis. *Environ. Sci Technol* 2012; 46 (8):4673–4681.
- [31] Skilhagen SE, Dugstad JE, Aaberg RJ. Osmotic power—power production based on the osmotic pressure difference between waters with varying salt gradients. *Desalination* 2008; 220:476–482.
- [32] Zhang M, Hou D, She Q, Y Tang C. Gypsum scaling in pressure retarded osmosis: Experiments, mechanisms and implications. *Wat Res* 2014;48:383–395
- [33] She Q, Wong YKW, Zhao S, Y Tang C. Organic fouling in pressure retarded osmosis: Experiments, mechanisms and implications. *J Membr Sci* 2013; 428:181–189.

- [34] McCutcheon JR, Elimelech M. Influence of concentrative and dilutive internal concentration polarization on flux behavior in forward osmosis. *J Membr Sci* 2006;284: 237–247.
- [35] Lee KL, Baker RW, Lonsdale HK. Membrane for power generation by pressure retarded osmosis. *J Membr Sc* 1981;8:141– 171.
- [36] Altaee A, Sharif Adel. Pressure retarded osmosis: advancement in the process applications for power generation and desalination. *Desalination* 2015;356:31–46





# Chapter 5: Effect of the temperature on hydrodynamics and PRO membrane parameters

## 1. Introduction

Laboratory experiments have already shown that PRO performance is affected by such parameters as the operating pressure or the characteristics of the draw and feed solutions. However, most of the existing publications have focused on the study of water flux and power density [1,2,3,4,5,15], with the impact of temperature being less studied [12,13]. However, in any osmotic membrane, the operating temperature affects the performance of the system, as it affects the membrane's permeability, the reverse salt diffusion and some structural parameters.

In practice the solution temperature in PRO processes may vary over a wide range, depending on the nature of the sources of the solutions, the location and its surrounding climate, etc. [10]. For example, the expected temperature of seawater would range from 12 to 35 °C [11]. If brine were used, the temperature of brines discharged from desalination plants is higher than that of raw seawater [6]; as most desalination plants are located in hot regions, the seawater temperature is over 25°C, whereas the brines are over 30°C.

The temperature accounts for a key factor that not only affects the solution's physic-chemical properties, such as the osmotic pressure, viscosity, density, and diffusion, but it also represents an important measure of the amount of energy input during operation. If the temperature of raw seawater is below a lower limit, the water flux may be too low unless temperature control strategies are actively implemented (for example, using external sources of heat). Therefore, to optimize the solution temperature for maximizing water flux yield, it is important to understand the temperature-induced interaction between solute, water and membrane [12].

Thus, in the current chapter, the effects of the temperatures of the feed and draw solutions on the structural parameters of the membrane, and the hydrodynamics

are investigated. The results provided by this study may give an interesting insight into the PRO operating conditions and PRO membrane design

## 2. PRO background

The ideal osmotic process can be described by thermodynamic equations for the water and salt fluxes. The general equations of transport are [8]:

$$J_{w,ideal} = A (\Delta\pi - \Delta P) \quad (5.1)$$

$$J_{s,ideal} = B(C_{D,b} - C_{F,b}) \quad (5.2)$$

where  $J_{w,ideal}$  is the ideal water flux,  $J_{s,ideal}$  is the ideal salt flux,  $A$  is the water permeability coefficient of the membrane,  $B$  is the salt permeability coefficient of the membrane,  $C_{D,b}$  and  $C_{F,b}$  are the solute concentrations in the bulks,  $\Delta\pi$  is the osmotic pressure difference between the bulks, and  $\Delta P$  is the hydraulic pressure applied on the draw water side.

As an asymmetric membrane is generally used in PRO, internal concentration polarization (ICP) occurs in the porous layer of the membrane, which reduces the osmotic driving force across the active layer, and thus the water flux. In PRO, the orientation Active dense Layer facing the Draw Solution (AL-DS) is considered to be mechanically more stable, as the external hydraulic pressure is applied on the draw side [6,7]. In this case, concentrative ICP occurs in the porous layer of the membrane.

Without perfect hydrodynamics in the draw solution flow channel, dilutive External Concentration Polarization (ECP) occurs in the mass transfer boundary layer of the draw solution, reducing the local concentration at the active layer from  $C_{D,b}$  to  $C_{D,m}$ , which lowers the  $\pi_{D,m}$  (the osmotic pressures of the draw active layer surface membrane). A schematic of the salt concentration profile across a membrane operating in PRO mode (active layer facing the draw solution) is shown in Fig. 5.1.

Thus, a more realistic water flux expression is:

$$J_w = A (\pi_{D,m} - \pi_{F,m} - \Delta P) \quad (5.3)$$

where  $\pi_{D,m}$  and  $\pi_{F,m}$  are the osmotic pressures at the surface of the active and support layers, respectively.

Based on the model developed in Chapter 3, and assuming that the concentrative ECP on the feed solution side is negligible in this case ( $C_{F,m} = C_{F,b}$ ), the expressions of the concentrations through the membrane are as follows:

$$C_{icp} = \left( C_{F,b} + \frac{J_s}{J_w} \right) \exp(J_w K) - \frac{J_s}{J_w} \quad (5.4)$$

$$C_{D,m} = \left( C_{D,b} + \frac{J_s}{J_w} \right) \exp\left(-\frac{J_w}{k}\right) - \frac{J_s}{J_w} \quad (5.5)$$

Assuming that the osmotic pressure is proportional to the concentration and the temperature ( $\pi = \beta CRT$ ), the osmotic pressures over the active layer are expressed as:

$$\pi_{icp} = \left( \pi_{F,b} + \frac{B}{A} \left( 1 + \frac{A\Delta P}{J_w} \right) \right) \exp(J_w K) \quad (5.6)$$

$$\pi_{D,m} = \left( \pi_{D,b} + \frac{B}{A} \left( 1 + \frac{A\Delta P}{J_w} \right) \right) \exp\left(-\frac{J_w}{k}\right) \quad (5.7)$$

Thus, the water flux  $J_w$  is defined as follows:

$$J_w = A \left[ \left( \pi_{D,b} + \frac{B}{A} \left( 1 + \frac{A\Delta P}{J_w} \right) \right) \exp\left(-\frac{J_w}{k}\right) - \left( \pi_{F,b} + \frac{B}{A} \left( 1 + \frac{A\Delta P}{J_w} \right) \right) \exp(J_w K) - \Delta P \right] \quad (5.8)$$

where  $\pi_{D,b}$  is the bulk osmotic pressure of the draw solution near the surface of the active layer,  $\pi_{F,b}$  is the bulk osmotic pressure of the feed solution near the surface of the support layer,  $\beta$  is the van't Hoff coefficient,  $R$  is the universal gas constant, and  $T$  is the absolute temperature. The mass transfer coefficient ( $k$ ) is defined as [7]:

$$k = \frac{ShD}{d_h} \quad (5.9)$$

where  $D$  is the diffusion coefficient of the solute in the draw solution,  $Sh$  is the Sherwood number and  $d_h$  is the hydraulic diameter of the flow channel defined as:

$$d_h = \frac{4S}{P_w} \quad (5.10)$$

where  $S$  is the area of the flow section and  $P_w$  is the hydrated perimeter. For a flat channel with spacer, the hydraulic diameter is [21]:

$$d_h = \frac{4\varepsilon}{\frac{2}{h_{sp}} + (1-\varepsilon)S_{vsp}} \quad (5.11)$$

where  $h_{sp}$  is the thickness of the spacer,  $S_{vsp}$  the specific surface of the spacer ( $S_{vsp} = S_{sp}/V_{sp}$ ,  $S_{sp}$  is the surface area of the spacer and  $V_{sp}$  the volume of the spacer), and  $\varepsilon$  is the porosity. The Sherwood number calculation is discussed in Section 5.1. The solute resistivity  $K$  is defined as [9]:

$$K = \frac{\tau t_s}{\varepsilon D} = \frac{s}{D} \quad (5.12)$$

where  $\tau$ ,  $t_s$  and  $s$  are, respectively, tortuosity, thickness and structure parameter. The specific salt flux in PRO, defined as the ratio of salt flux to water flux,  $J_s/J_w$ , is affected by the intrinsic transport properties of the membranes, as follows [10]:

$$\frac{J_s}{J_w} = \frac{B}{A\beta RT} \left( 1 + \frac{A\Delta P}{J_w} \right) \quad (5.13)$$

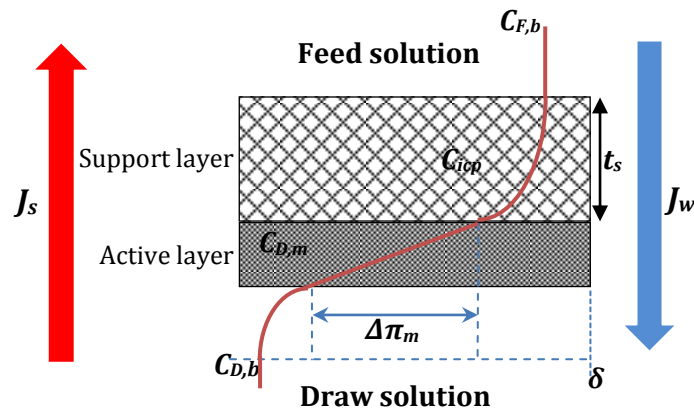


Fig. 5.1: Schematic representation of the salt concentration profile, salt and water fluxes across a membrane in PRO at steady state.

### 3. Experimental

#### 3.1 Membranes

Results from experiments with cellulose acetate flat-sheet PRO membranes (IGB membrane), developed by Fraunhofer Institute for Interfacial Engineering and Biotechnology, are used to validate the models and analyze the effect of temperatures on the PRO process. Parameters used for the calculations are summarized in Table 5.1.

#### 3.2 PRO bench-scale

A schematic diagram of the laboratory scale unit used in this study was provided in Chapter 3. The test unit had a channel on the feed side of the membrane to allow the feed solution to flow tangentially to the membrane. Mesh spacers placed in the feed channel supported the membrane. A high-pressure positive displacement pump was used to recirculate the feed solution at selected velocities. Each container was placed on an analytical balance. The fluxes were calculated based on the change of weight of the solutions in the graduated containers. The salt flux was determined based on conductivity measurements.

The temperature was maintained constant using a thermostatic bath for each bulk, with the temperature of the solutions controlled by an electronic thermometer for each side.

### 3.3 Chemicals

The feed and draw solutions were prepared using certified ACS-grade NaCl (Fisher Scientific). Osmotic pressures, viscosities, and diffusion coefficients of solutions were calculated using the equations developed in the current study.

Table 5.1: Main characteristics of the IGB Membrane

<b>Parameter</b>	<b>Values</b>
Water permeability coefficient $A$	$1.06 \times 10^{-12}$ m/s/Pa (at 20°C)
Salt permeability coefficient $B$	$2.62 \times 10^{-8}$ m/s (at 20°C)
Porosity of the support layer $\epsilon$	80 %
Thickness of the active layer $e$	100 nm
Thickness of the support layer $t_s$	12 $\mu$ m
Length of the channel	0.17 m
Effective surface of the membrane	0.013 m <sup>2</sup>
Depth of the channel	0.007 m
Width of the channel	0.07 m
Hydraulic diameter $d_h$	$9.4 \times 10^{-4}$ m
Flow velocity $u_0$	0.0107 m/s
$\tau t_s / \epsilon$	$5.06 \times 10^{-4}$ m

## 4. Effect of the operating temperature on the feed and draw solution chemistry

### 4.1 The Osmotic Pressure

The difference in osmotic pressure between bulks has been shown, in Chapter 3, to be an important parameter in PRO: In fact, the driving force of the process is the difference in osmotic pressure over the active layer, which is directly affected by the osmotic pressures in the bulks. The temperature has significant impact on these osmotic pressures: In fact, referring to the van't Hoff equation ( $\pi = \beta CRT$ ), the osmotic pressure is directly proportional to the temperature. Although the osmotic pressure is not proportional to the concentration for solutions with a very

high concentration, the assumption of proportionality between the osmotic pressure and the temperature is still applicable: for example, following the results in [11], the expression of the osmotic pressure at a given temperature  $T$ , as a function of the concentration  $C$  for a NaCl solution, can be approximated by:

$$\pi = T_R(3.805C^2 + 42.527C + 0.434) \quad (5.14)$$

where  $T_R$  is the normalized temperature:

$$T_R = \frac{T}{273.15} \quad (5.15)$$

For simplicity, NaCl solutions are now considered: Fig.5.2 shows the expected effect of the temperature on the osmotic pressure of the draw solution for different concentrations.

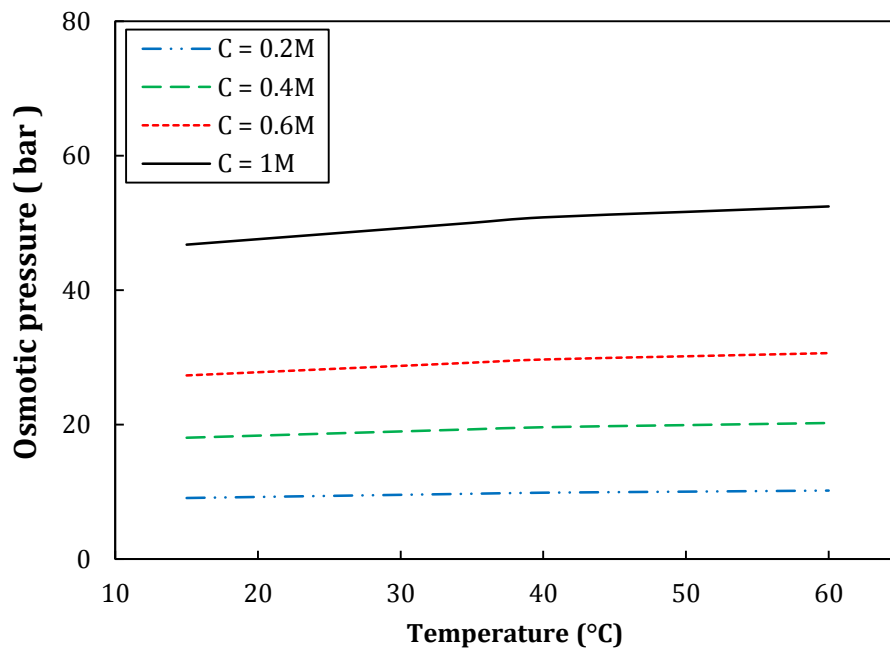


Fig. 5.2: Osmotic pressure of NaCl solutions at different temperatures and concentrations following Eq. (5.14).

It can be seen in Figure 5.2 that the osmotic pressure increases when the temperature of the solution increases. However, the effect of the temperature on the osmotic pressure is more significant when the concentration of the solution is high: When the concentration is 0.2 M, the pressure gain is around 1.5 bar when

the temperature is raised from 15 to 60°C; whereas the gain is around 7 bars for 1M. Referring to Eq. (5.1), as the water flux through the membrane is proportional to the difference of osmotic pressures, then, using a high temperature clearly leads to a better driving force to the process. In PRO processes, the driving force is directly related to the draw solution concentration, which explains the enhanced water flux at higher draw solution concentrations: as expected, the highest power densities are obtained using brines of high osmotic pressures (such as seawater RO brine, MED brine, the Dead Sea water) [24].

#### 4.2 The diffusion coefficient $D$

The Diffusion coefficient  $D$  is an important parameter in PRO as the mass transfer of feed solution  $k$  and the solute resistivity  $K$  are proportional to  $D$  (see equations 3.9 and 3.11 of Chapter 3). This coefficient has a strong dependence on the temperature and concentration of the solution. This diffusion coefficient can be calculated empirically using the Stokes-Einstein relationship [12]:

$$D = \frac{k_b T}{6\pi r \rho \mu} \quad (5.16)$$

where  $k_b$  is the Boltzmann constant,  $\mu$  is the kinematic viscosity of the solution,  $T$  is its temperature,  $r$  is the ion radius and  $\rho$  is the density of the solution.

Empirical equations have been proposed to estimate the kinematic viscosity, such as [13]:

$$\frac{\mu}{\mu_w} = 1 + e C_s \exp\left(\frac{C_s^f}{g T_R + i}\right) \quad (5.17)$$

where  $\mu_w$  is the water's kinematic viscosity at temperature  $T$ ,  $e = 0.12$ ,  $f = 0.44$ ,  $g = 3.713$ , and  $i = 2.792$  are fitting parameters (values given for NaCl solutions), and  $C_s$  is the molar concentration.

The temperature also affects the dynamic viscosity  $\eta$ . For example, this dependence was described in [14, pp. 17-18] for NaCl solutions as follows:

$$\eta(T) = 2.414 \times 10^{\left(\frac{247.8}{T-140}-5\right)} \quad (5.18)$$

Using Eqs. (5.16)-(5.18), Fig. 5.3 shows the effect of the temperature on the diffusivity of the water through the membrane. It can be seen that, in the range of temperatures studied, the value of the diffusion coefficient is almost tripled. At low temperatures (from 15°C to 20°C), the effect of the solution concentration on the diffusivity is not significant, as compared to high temperatures, where it becomes more considerable. This is due to the fact that, in NaCl solutions, interactions took place between particles within the solvent. When the temperature goes up, the viscosity of the solution decreases and the interaction between the particles is reduced due to thermal agitation. Thus, the diffusion coefficient tends to decrease as the concentration increases.

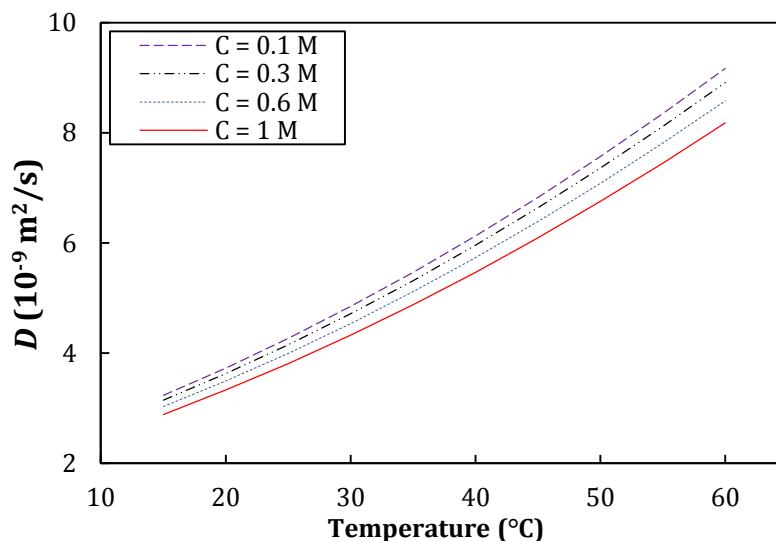


Fig. 5.3: Diffusion coefficient of NaCl solutions at different temperatures and concentrations.

## 5. Effect of the operating temperature on the hydrodynamic parameters

### 5.1 Reynolds, Schmidt and Sherwood numbers

The mass transfer coefficient  $k$  depends on the relevant physical properties of the fluid, the geometry used, and the velocity of the fluid. Dimensional analysis can be used to express this dependence: The dimensionless version of the mass transfer coefficient is the Sherwood number  $Sh$ , which depends on the Reynolds number  $Re$ , and the Schmidt number  $Sc$ .

Generally, in PRO, the flow is considered to be laminar due to the low flow velocities ( $Re < 2100$ ). In fact, in several publications, the Sherwood number is determined using the following relations, obtained from experiments at different conditions [27]:

$$Sh = 0.04 Re^{0.75} Sc^{0.33} \quad (\text{Turbulent flow}) \quad (5.19)$$

$$Sh = 1.85 \left( Re \cdot Sc \frac{d_h}{L} \right) \quad (\text{Laminar flow}) \quad (5.20)$$

These empirical relations are derived from UF and RO experiments and are correlated to the frictional factor of each membrane [28]. However, the structure of PRO membranes is quite different from RO and UF membranes. In fact, the RO membrane support layer is much thicker than the PRO support layer, and UF membranes are considered as porous structures, with higher roughness than PRO membranes. Thus, Eqs. (5.19) and (5.20) seem inadequate for PRO. Moreover, for laminar flow, Eq. (5.20) is valid where the channel length is significantly larger than hydrodynamic flow development length, or, in other words, when the length of the developing region is not significant. However, in the lab-scale PRO test, this condition is not valid due to the fact that the channel length affects the calculations. In fact, in PRO bench scale, the geometry of the pipes and the low velocity used give laminar flow. However, a recent study [22] showed that the feed spacers used to maintain the feed channel geometry and improve mass transfer near the membrane surface induce turbulent flow near the membrane surface at low Reynolds numbers. Consequently, the Sherwood number was described in [22] as follows:

$$Sh = 0.2 Re^{0.57} Sc^{0.4} \quad (5.21)$$

In Eq. (5.21),  $Re$  and  $Sc$  numbers are assumed to be homogenous over the length of the membrane. However, the pressure applied in PRO mode might modify the geometry near the membrane surface, which means that the  $Re$  and  $Sc$  are no longer considered homogenous. Therefore, we proposed the use of local values of the Reynolds and Sherwood numbers to estimate the mass transfer across the

boundary layer. Thus, we adopt the calculations for the local Sherwood developed in [23] (pp. 554–559) for the hydrodynamic boundary layer of a fluid that flows parallel to a smooth, flat, and non-porous surface:

$$Sh_x = 0.332 Re_x^{0.5} Sc^{0.66} \text{ (Laminar flow for } Re_x < 2.10^5) \quad (5.22)$$

$$Sh_x = 0.0292 Re_x^{0.8} Sc^{0.66} \text{ (Turbulent flow for } Re_x > 2.10^5) \quad (5.23)$$

The local Reynolds number and the Schmidt number are calculated as follows [28]:

$$Re_x = \frac{u_0 \rho x}{\mu} = \frac{u_0 x}{\eta} \quad (5.24)$$

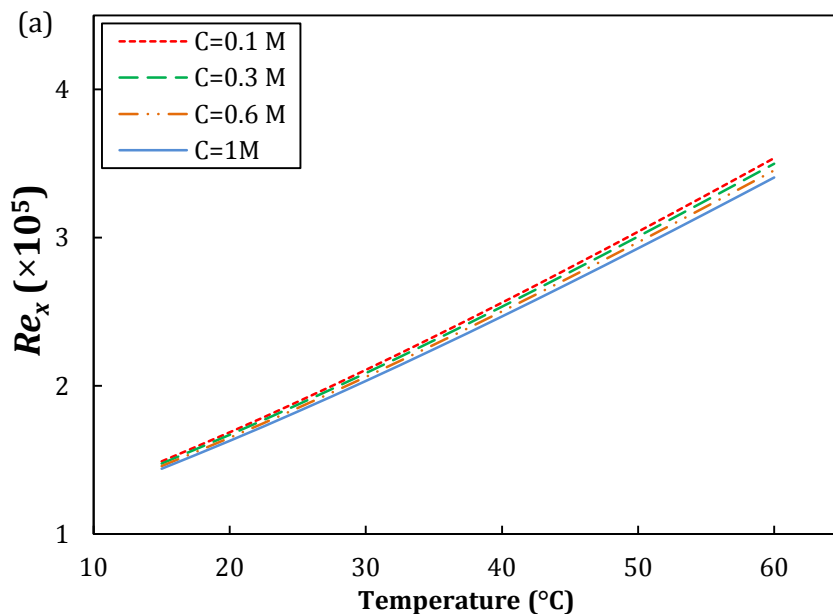
$$Sc = \frac{u_0}{\rho D} \quad (5.25)$$

where  $u_0$  is the velocity of the water,  $x$  is the distance from the start of the boundary layer (see Fig. 5.5),  $\rho$  is the density of the water,  $\eta$  the dynamic viscosity of the fluid,  $\mu$  is the cinematic viscosity, and  $D$  is the diffusion coefficient, calculated in Eq. (5.16).

As shown in Eqs. (5.24) and (5.25), the dimensionless numbers  $Re_x$  and  $Sc$  depend on parameters which also depend on the temperature, such as the viscosities  $\mu$  and  $\eta$ , and the diffusion coefficient  $D$ . Fig. 5.4 shows the variation of the dimensionless parameters  $Re$ ,  $Sc$ , and  $Sh$  with the temperature. Table 5.2 presents the parameters used for calculations for 1M NaCl solution. It can be seen that the increase of the temperature leads to an increase of the local Reynolds number, regardless of the concentration of the solutions. Moreover, the local Reynolds number exceeds the critical value ( $Re_x > 2 \times 10^5$ ) for a temperature value around 30°C, which means that the regime of the flow changes from laminar to turbulent. This result can be clearly seen in Fig. 5.4-c, where an inflection point of the curves is observed for temperatures around 30°C. As shown in Fig. 5.4-b, the effect of the concentration on  $Sc$  is negligible at high temperatures, which is due to the inverse of the diffusivity ( $1/D$ ) present in Eq. (5.25). Contrary to the  $Sc$  number, the concentration effect seems to be non-significant at low temperatures for the local

Reynolds number. Raising the temperature of the process leads to the modification of the flow regime from laminar to turbulent, because of the strong effect of the temperature on the  $Re_x$  value. This leads to the enhancement of the mass transfer coefficient ( $k$ ); therefore, the effect of the ECP is also reduced.

It must be pointed out that using NaCl solutions, the effect of the concentration is not significant. In fact, the variation of the viscosity and density of the water, within the range of concentrations studied, does not affect the local  $Re$ . For real salty fluids (seawater, brine wastewater, etc.), the result should be similar, due to the fact that the local Reynolds number is not strongly affected by the concentration, as shown in Fig. 5.4-a. Although the matrix complexity of real fluids can affect the viscosity for seawater and brine, these effects should be negligible, as more than 75% of the matrix is NaCl; however, for wastewater, the composition of the matrix is generally uncontrollable as it contains organic matter, dissolved polymeric waste, etc., which strongly affect the viscosity of the flows and their velocities.



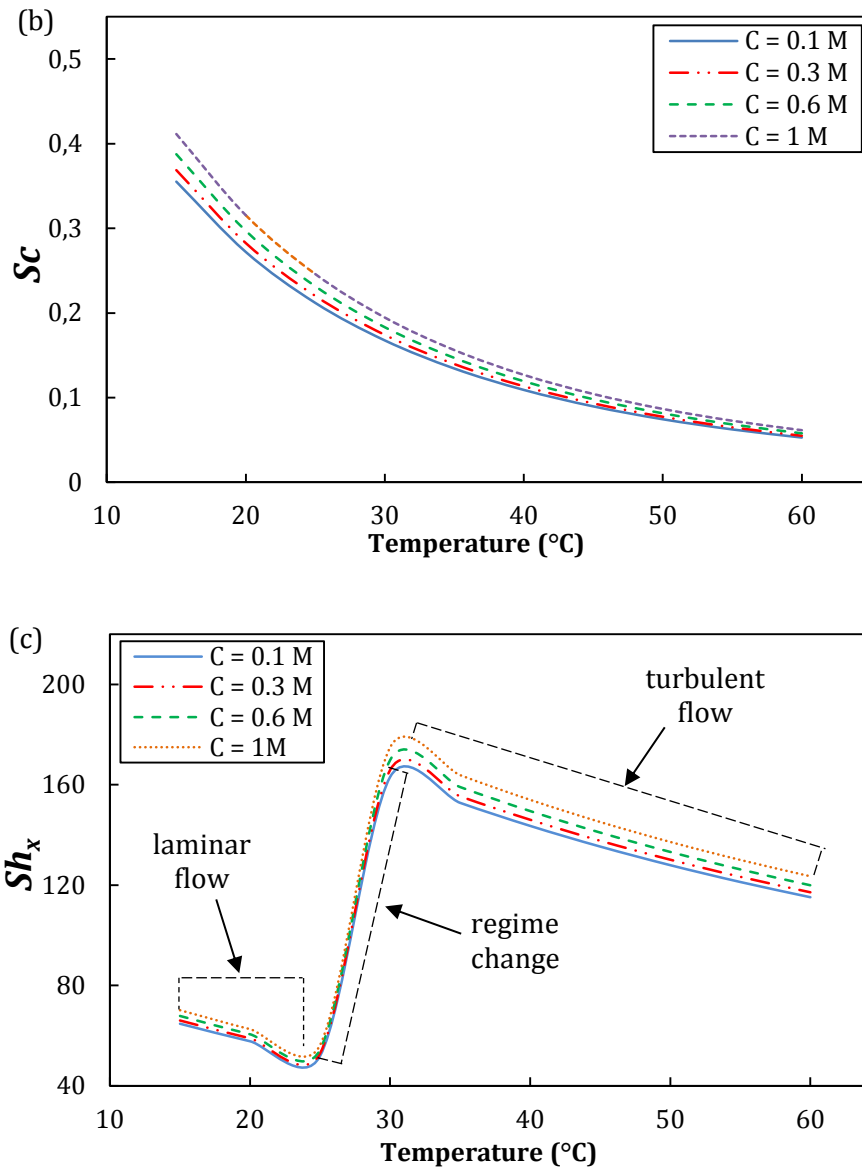


Fig. 5.4: (a) Reynolds, (b) Schmidt and (c) Sherwood numbers of NaCl solutions at different temperatures, following Eqs. (5.22) to (5.25).

Table 5.2: Characteristics of 1M NaCl draw solution at different temperatures.

$T(^{\circ}C)$	$u_0$ (m/s)	$\rho$ (kg/ m <sup>3</sup> )	$\mu$ (m <sup>2</sup> /s) $\times 10^{-6}$
20	0.0214	1042.8	1.095
30	0.0214	1039.4	0.875
40	0.0214	1035.5	0.718
50	0.0214	1030.9	0.602
60	0.0214	1025.9	0.515

### 5.2 The boundary layer thickness $\delta$

It is well known that when a viscous fluid flows along a fixed impermeable wall or past the rigid surface of an immersed body, the velocity at any point on the wall or other fixed surface is zero. The extent to which this condition modifies the general character of the flow depends upon the value of the viscosity. If the body is of a streamlined shape, and if the viscosity is small, the effect appears to be confined within (narrow regions adjacent to the solid surfaces) boundary layers. A boundary layer may be laminar or turbulent: A laminar boundary layer is one where the flow takes place in layers, with each layer sliding past the adjacent layers: they are found when the Reynolds numbers are small. A turbulent boundary layer, on the other hand, is marked by mixing across several layers, creating an exchange of mass, momentum and energy on a much bigger scale than in a laminar one. A turbulent boundary layer is only obtained at larger Reynolds numbers. Eqs. (5.26) and (5.27) describe the thickness of the boundary layer for different flow regimes [17]:

$$\delta = \frac{4.91 \times x}{\sqrt{Re_x}} \quad (\text{Turbulent flow}) \quad (5.26)$$

$$\delta = x \frac{0.382}{(Re_x)^{\frac{1}{5}}} \quad (\text{Laminar flow}) \quad (5.27)$$

where the distance  $x$  is along the membrane (see Fig. 5.5).

It has been shown in [16] that when the thickness of the boundary layer is small, the mass transfer is higher. The effect of the temperature on the thickness of the boundary layer was then studied for two specific values of  $x$  ( $x = L$  and  $L/2$ ). Fig. 5.6 shows that the effect of the concentration on the boundary layer thickness is not really comparable to the effect of the temperature. The parameter  $\delta$  has an important dependence on the regime of the flow: a laminar boundary layer is thicker than a turbulent one, which means that the mass transfers are not similar. In fact, the boundary layer is comparable to “a resistance layer” that prevents the passage of the solute to the surface of the active layer, which induces the external

concentration polarization. With turbulent flow, this resistance is mitigated by the decrease of the boundary thickness.

According to Elimelech et al. [26], ECP is characterized by its modulus  $C_{D,m}/C_{D,b} = \exp(-J_w/k) = \exp(-J_w\delta/D)$ . Consequently, the decrease of  $\delta$  induces the increase of  $k$ , which drives the concentration value  $C_{D,m}$  closer to that of  $C_{D,b}$ . The viscous effects are not as important at the front of the boundary layer, but become much more important near the end of it. Thus, when the temperature of the water becomes important, the viscosity of the solution is reduced, which leads to an increase in the value of the Reynolds number. In summary, the increase of the operating temperature leads to a thinner boundary layer and a higher mass transfer across it.

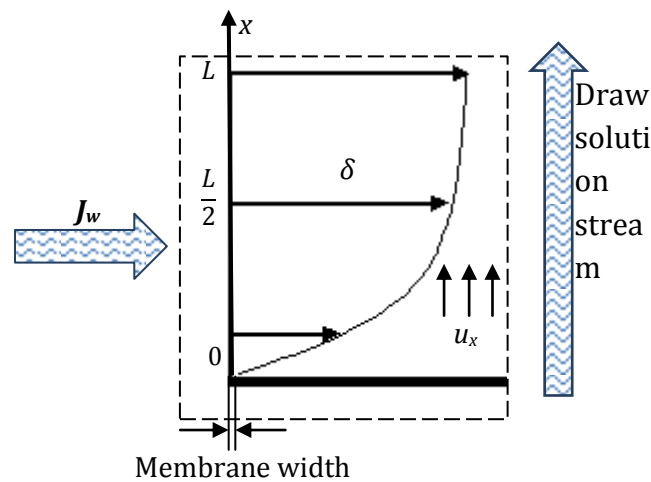


Fig. 5.5: Schematic of the boundary layer at the draw solution side.

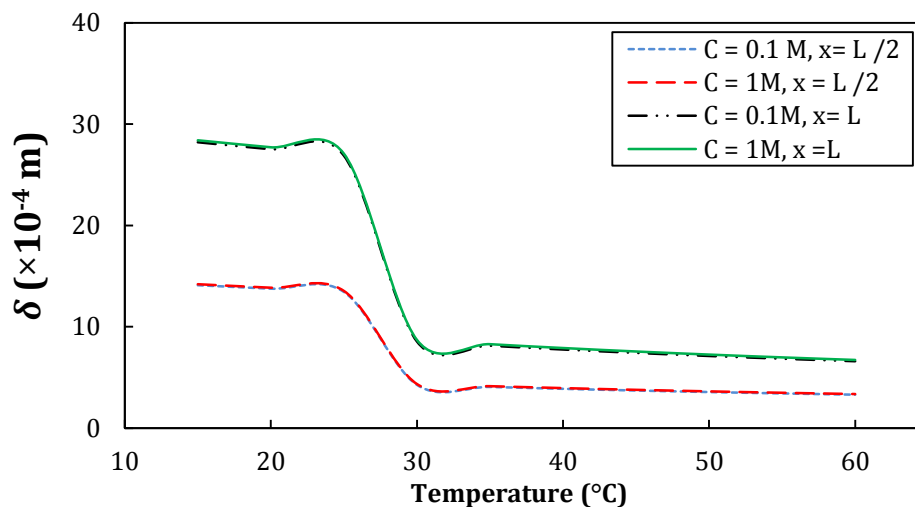


Fig. 5.6: Thickness of the boundary layer for NaCl solutions at different temperatures, following Eqs. (5.24), (5.26) and (5.27). ( $u = 0.0104$  m/s,  $L = 0.17$  m).

### 5.3 Effect of the temperature on the mass transfer coefficient $k$

The process of mass transfer across an interface in the bulk of a phase is the result of a chemical potential driving force, expressed in terms of concentrations of the species. The flux of a given species (rate of transfer per unit area normal to the interface), depends on physical properties of the system and on the phases involved. As the relationships between the flux and these parameters are not easily developed from fundamentals of mass transfer, coefficients have been defined that lump them all together. These definitions are of the form: Flux = coefficient  $\times$  (Concentration difference) [18].

In the PRO case, the mass transfer coefficient  $k$  characterizes the transport of water from the feed solution to the draw solution through the active layer. The mass transfer coefficient described in Eq. (5.9) depends on parameters that also depend on the temperature.

In this section, the effect of the temperature on the mass transfer coefficient is studied experimentally. Four draw solutions with different concentrations were tested (0.1M, 0.3M, 0.6M and 1M of NaCl).

The local mass transfer coefficient  $k_x$  can be described using Eqs. (5.22) and (5.23) as follows:

$$k_x = \frac{0.332 Re_x^{0.5} Sc^{0.66}}{d_h} D \text{ (Laminar flow)} \quad (5.28)$$

$$k_x = \frac{0.0292 Re_x^{0.8} Sc^{0.66}}{d_h} D \text{ (Turbulent flow)} \quad (5.29)$$

The overall mass transfer coefficient  $k_{overall}$  can be calculated by the integration of Eqs. (5.28) and (5.29) along the membrane. Thus,  $k_{overall}$  is described as:

$$k_{overall} = \frac{0.332 Sc^{0.66}}{d_h} D \int_0^L Re_x^{0.5} dx = \frac{0.664 Re_L^{0.5} Sc^{0.66}}{d_h} D \text{ (Laminar flow)} \quad (5.30)$$

$$k_{overall} = \frac{0.0292 Sc^{0.66}}{d_h} D \int_0^L Re_x^{0.8} dx = \frac{0.0365 Re_L^{0.8} Sc^{0.66}}{d_h} D \text{ (Turbulent flow)} \quad (5.31)$$

where  $Re_L$  is the local Reynolds number at  $x = L$ .

From Fig. 5.7, it can be seen that the mass transfer coefficient is drastically affected by the temperature. In fact, when the flow is considered laminar, the effect of the temperature is non-significant between 15°C and 25°C. However, the behavior of  $k_{overall}$  changed drastically above 30 °C. This result can be attributed to the change of the flow regime from laminar to turbulent. As shown in Sections 4.2 and 5.1, the increase of the temperature leads to a decrease in the boundary layer thickness and an increase of the diffusivity: thus, the mass transfer increases. In fact, according to film theory, a high diffusivity with a thin boundary layer enhances the rate of mass transfer (See [25], pp. 410–456).

At low temperatures, the effect of the concentration on  $k_{overall}$  is negligible, and seems to be significant at high temperatures. This behavior is similar to that of the diffusion coefficient  $D$  presented in Section 4.2. Consequently, operating at high temperatures can reduce the effect of the external concentration polarization ECP by “pushing”  $C_{D,m}$  to a value close to  $C_{D,b}$ .

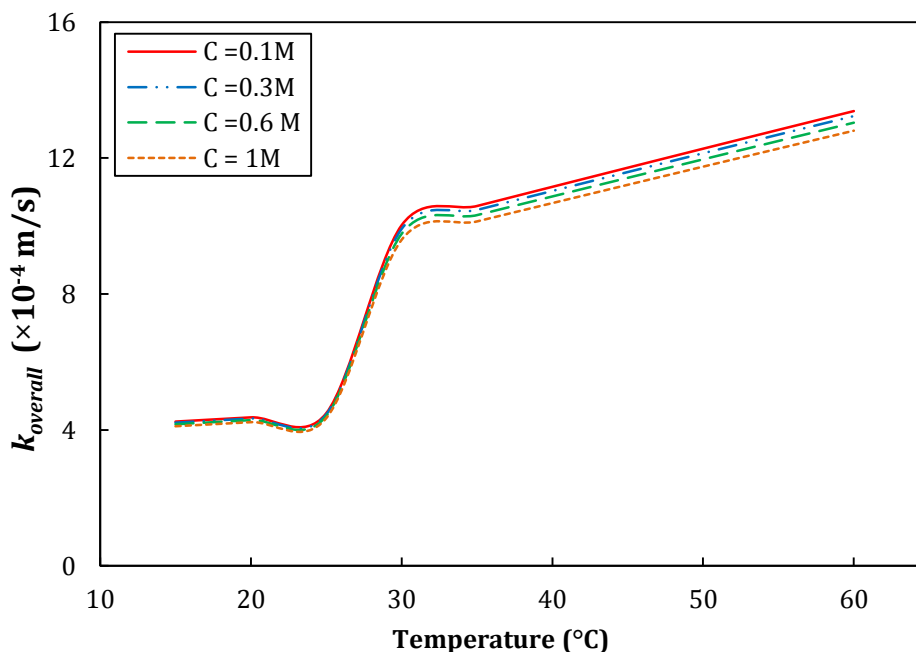


Fig. 5.7: The overall mass transfer coefficient ( $k_{overall}$ ) for NaCl solutions at different temperatures, following Eqs. (5.30) and (5.31).

## 6. Effect of the operating temperature on the membrane parameters

### 6.1 Effect of the temperature on the solute resistivity $K$

The solute resistivity  $K$ , described in Eq. (5.12), is a parameter used to determine the influence of the internal concentration polarization on the water flux. Small  $K$  values mean less ICP, resulting in higher water flux across the membrane. To determine  $K$  experimentally for different operating temperatures, a rearrangement of Eq. (5.8) is used:

$$K = \frac{1}{J_w} \ln \left( \frac{\pi_{D,b} \exp\left(-J_w/k\right) + \frac{J_w - B}{A} + \Delta P \left(1 - \frac{B}{J_w}\right)}{\pi_{F,b} + B \left(\frac{1}{A} + \frac{\Delta P}{J_w}\right)} \right) \quad (5.32)$$

Experimental results were carried out for two draw solutions (0.6M and 1M of NaCl) and one NaCl feed solution (8.55mM). The parameters were calculated using experimental results, performed in the range of temperatures from 20°C to 60°C with the applied pressure  $\Delta P = 10$  bars.  $A$  and  $B$  are considered variables with the temperature and their values were taken from our previous work in [20]. The osmotic pressures were calculated using Eq. (5.14).  $\tau$ ,  $t_s$  and  $\varepsilon$  are presented in Table 5.1, and the diffusion coefficient  $D$  is given by Eq. (5.16).

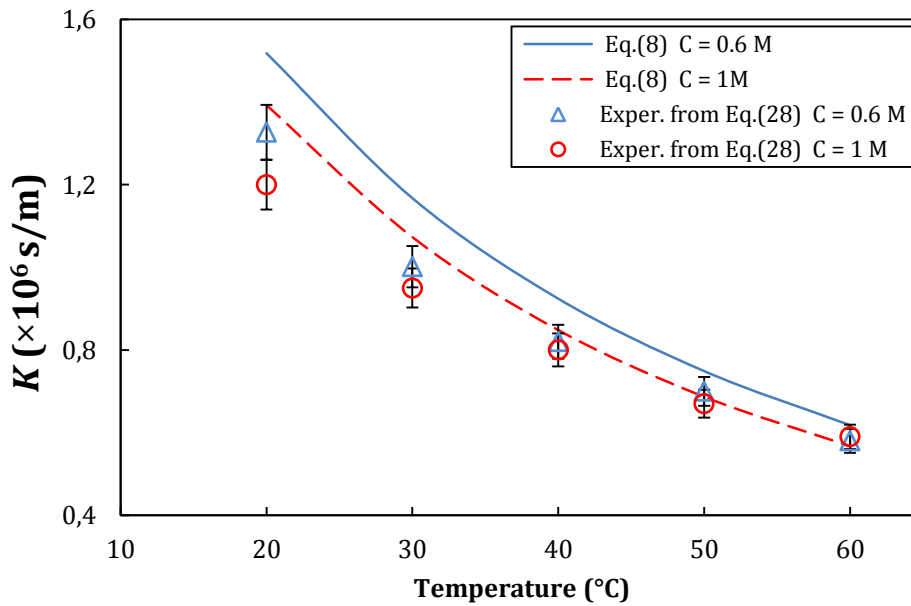


Fig. 8: The solute resistivity ( $K$ ) for NaCl solutions at different temperatures and concentrations. ( $K$ ) is calculated using Eq. (5.12) (lines), and Eq. (5.32) using experimental data (symbols).

Fig. 5.8 shows the variation of  $K$  under different temperatures, where  $K$  is firstly calculated using Eq. (5.12) (lines), and then using Eq. (5.32) (symbols). It can be seen that, at a low temperature,  $K$  calculated using Eq. (5.12) is noticeably higher than that of Eq. (5.32) for both tested concentrations. This result might be attributed to the effect of the pressure. In fact, Eq. (5.12) does not take into consideration the effect of the applied pressure on the support layer. It was shown previously in [29] that, for a given temperature, the increase of  $\Delta P$  reduces the structure parameter  $s = KD$ . In our case, two parameters are considered; the temperature and the pressure. Fig. 5.8 reveals that, at low temperatures,  $K$  is high, and the effect of the concentration of the draw solution on  $K$  is clearly considerable. In fact, Eq. (5.32) shows that  $K$  is inversely proportional to the water flux of the membrane. Thus, to reach the best performance, the solute resistivity should be as low as possible.

Fig. 5.9 shows the variation of the water flux with the solute resistivity. The modeled  $J_w$  (line) is obtained by fitting Eq. (5.8), using the experimental results of  $K$  taken from Fig. 5.8.A and B are presented in Table 5.3, and  $(k)$  values were taken from Fig. 5.7. It can be seen that the solute resistivity tends to reduce the water flux of the process: when  $K$  is high, the water flux is significantly smaller. In fact,  $K$  depends on the structure parameter  $s$ : when  $s$  decreases,  $K$  decreases too, due to the fact that the membrane becomes thinner when the operating temperature increases. This is due to the simultaneous effect of the temperature and pressure: the increase in the operating temperature makes the membrane polymer softer, so tangential forces caused by the applied pressure reduce  $s$ . Thus, to reduce the effect of  $K$  on the water flux, and thus increase the energy produced using PRO, it would be better to operate with a high temperature, following the results in Figs. 5.8 and 5.9.

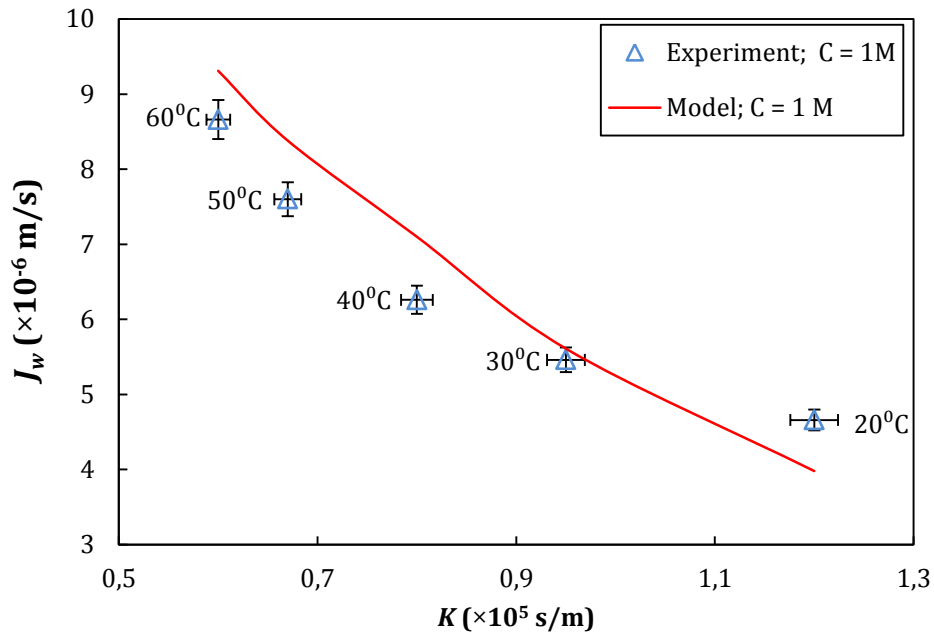


Fig. 5.9: Modeled (line) and experimental results (symbols) of the water flux  $J_w$  with the solute resistivity  $K$ . ( $C_{D,b} = 1\text{M}$ ,  $C_{F,b} = 8.55\text{mM}$ ,  $u = 0.0107$  m/s).

Table 5.3: water permeability coefficient  $A$  and salt permeability coefficient  $B$  at different temperatures

$T(^{\circ}\text{C})$	$A(\text{m/s/Pa})$	$B(\text{m/s})$
20	$1.06 \times 10^{-12}$	$2.62 \times 10^{-8}$
30	$1.43 \times 10^{-12}$	$4.25 \times 10^{-8}$
40	$1.74 \times 10^{-12}$	$5.87 \times 10^{-8}$
50	$1.98 \times 10^{-12}$	$8.00 \times 10^{-8}$
60	$2.12 \times 10^{-12}$	$8.80 \times 10^{-8}$

### 6.2 Effect of the temperature on the water flux ( $J_w$ )

The water flux ( $J_w$ ) at different operating conditions is now studied experimentally: three draw solutions were tested (0.3M, 0.6M and 1M of NaCl) at a range of temperatures varying from 20°C to 60°C. The temperatures of the feed and draw solutions were kept equal during the experiments. The feed solution concentration

was 8.55mM of NaCl and the applied pressure was  $\Delta P = 10$ . Fig. 5.10 shows the comparison between the experimental results and the model obtained by fitting Eq. (5.8). Clearly, both experimental and simulated  $J_w$  increased with temperature for all the tested solutions. The experimental results are coherent with the simulated data, except for the solution of 1M at a high temperature when the model slightly overestimates the water flux, probably due to the high salt flux diffusion caused by the temperature and the relatively high draw solution concentration, which decrease  $J_w$ .

This 1M solution concentration case is now studied separately: The variation of the water flux  $J_w$  and the salt flux  $J_s$  of 1M NaCl solutions as a function of  $\Delta P$  for different temperatures is presented in Fig. 5.11-a and b.

As expected, the increase in the temperature leads to the enhancement of the water flux. This result can be attributed to the variation of the transport parameter of the membrane due to the temperature. In fact, this increase in the water flux is caused the improvement of the water permeability of the membrane ( $A$ ), which depends strongly on the temperature, the improvement of the mass transport coefficient  $k$ , as discussed in Section 4.3, the decrease of the solute resistivity  $K$ , and the decrease of the ECP because of the decrease of the boundary layer thickness and the increase of the mass transfer coefficient. This impact is clearly seen in the power density (Fig. 5.11-c); at 60°C, the power produced is around 5.8W/m<sup>2</sup> for an applied pressure of 10 bars. This value is higher than the critical value that makes the PRO process commercially viable [1]. The brine of thermal desalination processes can provide these high temperatures (for example, the brine of a multi-effect distillation process can reach 65°C) [24].

Fig. 5.11-b shows the experimental variation of the salt flux  $J_s$  as a function of the temperature. It can be seen that the salt flux also increases when the temperature increases. This is a limiting effect to the performance of PRO, as the reverse solute diffusion induces a significant reduction in both the PRO water flux and the power density when the draw solutes diffuse through the membrane and accumulate in the porous substrate due to the water flux that has the opposite flow direction. This leads to a buildup of a draw solute concentration within the porous support layer, contributing to the increase of the ICP at the surface of the support layer, and thus, the effective osmotic pressure difference decreases.

The reverse solute diffusion occurs simultaneously with the forward water permeation in the reverse direction. A useful quantity is the specific solute flux ( $J_s/J_w$ ), which describes the amount of draw solutes permeating through the membrane normalized by the volumetric water flux. The study of the ratio ( $J_s/J_w$ ) at different temperatures (Fig. 5.11-d) reveals that the flux ratio increases with temperature, and it is also affected by the applied pressure. At low  $\Delta P$  (<4 bars), the rate of increase of the flux ratio is low compared to the higher  $\Delta P$  (>8 bars). In addition, the effect of the temperature is quite visible at low pressure, although this effect seems much smaller (even negligible) at  $\Delta P$ . This result shows that the temperature effect is dominated by the pressure at relatively high  $\Delta P$ . Consequently, an adequate choice of the applied pressure and the temperature reduces the salt diffusion through the membrane.

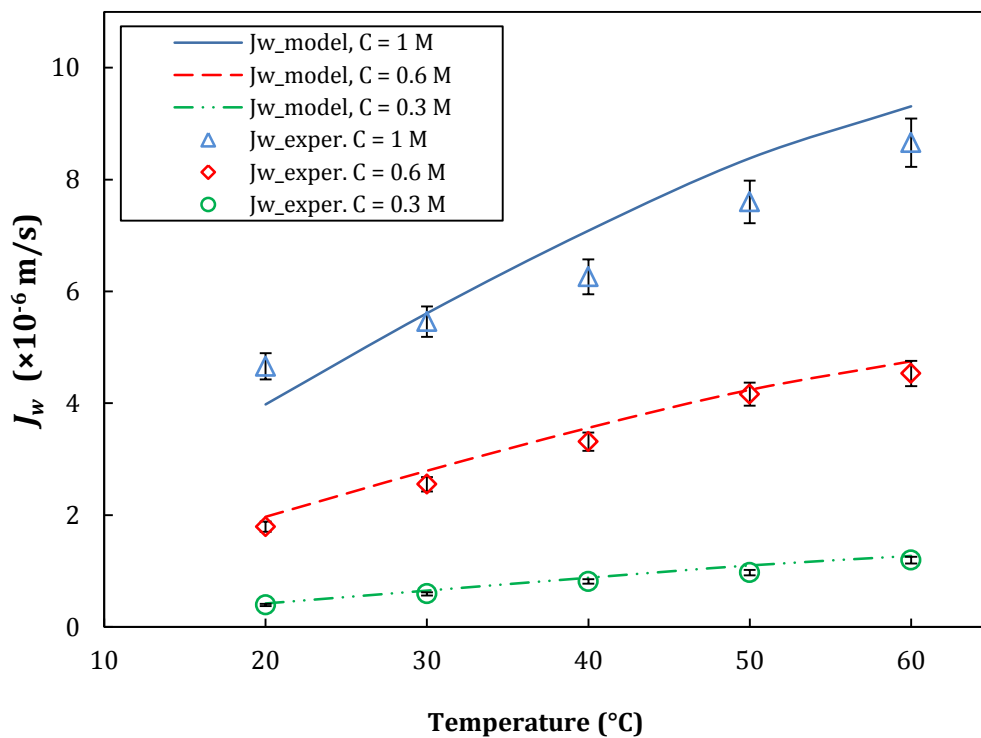


Fig. 5.10: Modeled (lines) and experimental results (symbols) of the water flux  $J_w$ .

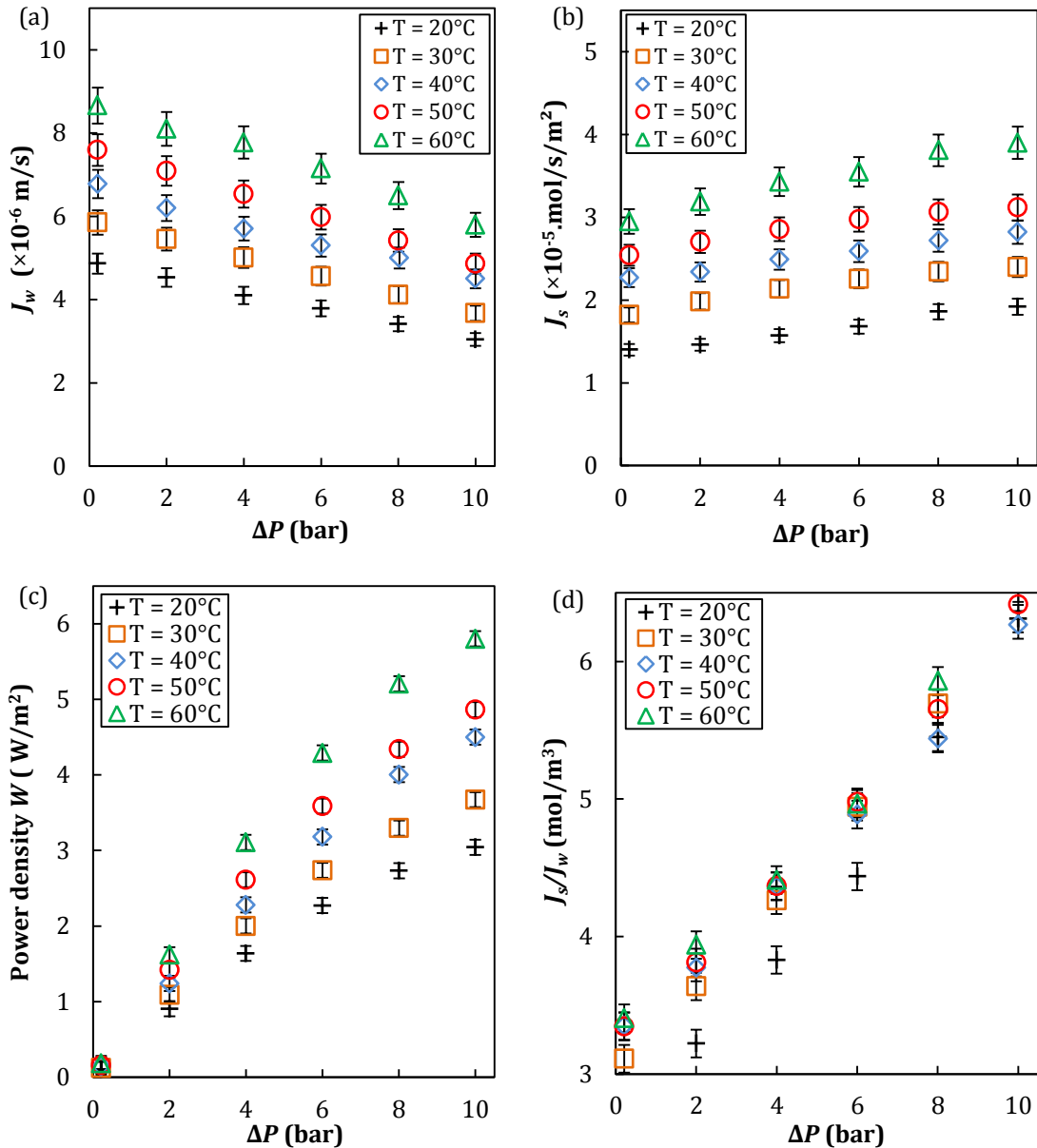


Fig. 5.11: Variation of the water flux  $J_w$  (a), the salt flux  $J_s$  (b), the power density  $W$  (c), and the specific solute flux  $J_s/J_w$  (d) with the temperature.  $C_{D,b} = 1M$ ,  $C_{F,b} = 8.55mM$ ,  $u = 0.0107m/s$ .

## 7. CONCLUSION

The effect of the temperature on the Pressure Retarded Osmosis process has been investigated. It has been theoretically and experimentally shown that the temperature affects parameters such as the diffusion coefficient, the solute resistivity, the diffusion coefficient and the osmotic pressure.

In general, working at high temperatures enhances the water flux of the process, and consequently the power recovery. The disadvantages of high temperatures are

the risk of accumulation of salt at the surface of the membrane support layer, due to the fact that raising the temperature also leads to the increase in the salt reverse flux ( $J_s$ ), and the degradation of the membrane. These can be overcome by the development of specific high-temperature membranes with a high resistance to reverse salt flux.

As further work, this study could be extended to real fluids (i.e. waste water, effluents, high concentrated brines, etc.) to investigate the effect of the matrix complexity. Moreover, the effect of the water flux  $J_w$  on the boundary layer using commercial length scale PRO membranes can also be studied following the approach of the current study.

**REFERENCES OF CHAPTER 5**

- [1] Simen B, Skråmestø Ø, Stein S, Skilhagen E. Osmotic Power From prototype to industry – what will it take? 3<sup>rd</sup> International Conference on Ocean Energy, Bilbao, October 2010.
- [2] Achilli A, Cath TY, Childress AE. Power generation with pressure retarded osmosis: An experimental and theoretical investigation. *J Membr Sci* 2009;343:42–52.
- [3] Jia Z, Wang B, Song S, Fan Y. Blue energy: Current technologies for sustainable power generation from water salinity gradient. *Renew Sustainable Energy Rev* 2014;31:91–100.
- [4] She Q, Jin X, Tang CY. Osmotic power production from salinity gradient resource by pressure retarded osmosis: Effects of operating conditions and reverse solute diffusion. *J Membr Sci* 2012;401–402:262–273.
- [5] Xu Y, Peng X, Tang CY, Fu QS, Nie S. Effect of draw solution concentration and operating conditions on forward osmosis and pressure retarded osmosis performance in a spiral wound module. *J Membr Sci* 2010;348:298–309.
- [6] Environmental Professionals, Pollution Control Study for Tuas Desalination and Power Plant Project, Final report, August 2011. [http://www.agaportal.de/nachhaltigkeit/eia/eia\\_singapur\\_meer1.pdf](http://www.agaportal.de/nachhaltigkeit/eia/eia_singapur_meer1.pdf)
- [7] Chou S, Wang R, Shi L, She Q, Tang C, Gordon Fane A, Thin-film composite hollow fiber membranes for pressure retarded osmosis (PRO) process with high power density. *J Membr Sci* 2012;389:25–33.
- [8] Peinemann KV, Gerstandt K, Skilhagen SE, Thorsen T, Holt T. Membranes for Power Generation by Pressure Retarded Osmosis, in *Membranes for Energy Conversion*. Volume 2 (eds. K.-V. Peinemann and S. Pereira Nunes), Wiley, Weinheim, Germany (2008).
- [9] Tang CY, She Q, Lay WCL, Wang R, Fane AG, Coupled effects of internal concentration polarization and fouling on flux behavior of forward osmosis membranes during humic acid filtration. *J Membr Sci* 2010;354:123–133.
- [10] She Q, Hou D, Liu J, Hai Tan K, Tang CY. Effect of feed spacer induced membrane deformation on the performance of pressure retarded osmosis (PRO): Implications for PRO process operation. *J Membr Sci* 2013;445: 170–182.

- [11] Phuntsho S, Hong S, Elimelech M, Shon HK. Osmotic equilibrium in the forward osmosis process: Modelling, experiments and implications for process performance. *J Membr Sci* 2014;453: 240–252.
- [12] Collura JS, Harrison DE, Richards CJ, Kole TK, Fisch MR., The Effects of Concentration, Pressure, and Temperature on the Diffusion Coefficient and Correlation Length of SDS Micelles. *J Phys Chem B* 2001;105: 4846–4852.
- [13] You SJ, Wang XH., Zhong M, Zhong Y-J, Yu C, Ren NQ. Temperature as a factor affecting transmembrane water flux in forward osmosis: Steady-state modeling and experimental validation. *Chem Eng J* 2012;198–199: 52–60.
- [14] Al-Shemmeri T, *Engineering Fluid Mechanics*. Ventus Publishing, Holland, 2012.
- [15] Carbonell G. Mass transfer coefficients in coiled tubes. *Biotechnology and Bioengineering*, 1975;17:1383–1385.
- [16] Wong MCY, Martinez K, Ramon GZ, Hoek EMV, Impacts of operating conditions and solution chemistry on osmotic membrane structure and performance. *Desalination* 2012;287:340–349.
- [17] Pritchard PJ. *Introduction to Fluid Mechanics*, Wiley, 2011.
- [18] Skelland AHP. *Diffusional Mass Transfer*, Wiley, 1974.
- [19] Touati K, de la Calle A, Tadeo F, Roca L, Schiestel T, Alarcón-Padilla DC, Energy recovery using salinity differences in a multi-effect distillation system. *Desal Wat Treat* 2014;1–8
- [20] Touati K, Hänel C, Tadeo F, Schiestel T. Effect of the feed and draw solution temperatures on PRO performance: theoretical and experimental study. *Desalination* 365;2015:182–195
- [21] Costa A-R, Fane AG, Wiley DE. Spacer characterization and pressure drop modeling in spacer-filled channels for ultrafiltration. *J Membr Sci* 1994;87: 79–98.
- [22] Koutsou CP, Yiantsios SG, Karabelas AJ, A numerical and experimental study of mass transfer in spacer-filled channels: effects of spacer geometrical characteristics and Schmidt number. *J Membr Sci* 2009;326:234–251.
- [23] Welty JR, Wicks CE, Wilson RE, Rorrer G. *Fundamentals of Momentum, Heat, and Mass Transfer*. 4<sup>th</sup> ed., Wiley, 2001.

- [24] Palacin LG, Tadeo F, Prada C, Touati K, Evaluation of the recovery of osmotic energy in desalination plants by using pressure retarded osmosis, *Desal Wat Treat* 2013;51: 360–365.
- [25] Geankoplis CJ. *Principles of Mass Transfer, Transport Processes and Separation Process Principles*, Prentice Hall, Upper Saddle River, New Jersey 2003.
- [26] Elimelech M, Bhattacharjee S. A novel approach for modeling concentration polarization in crossflow membrane filtration based on the equivalence of osmotic pressure model and filtration theory. *J Membr Sci* 1998;145: 223–241.
- [27] Suh C, Lee S. Modeling reverse draw solute flux in forward osmosis with external concentration polarization in both sides of the draw and feed solution. *J Membr Sci* 2013;427: 365–374.
- [28] Gekas V, Hallström B. Mass transfer in the membrane concentration polarization layer under turbulent cross-flow. I. Critical literature review and adaptation of existing Sherwood correlations to membrane operations. *J Membr Sci* 1987;30:153–170.
- [29] Chou S, Wang R, Fane AG. Robust and High performance hollow fiber membranes for energy harvesting from salinity gradients by pressure retarded osmosis. *J Membr Sci* 2013;448:44–54.





# Chapter 6: Integration of PRO in desalination processes

## 1. Introduction

The possibility of using Pressure Retarded Osmosis to recover part of the osmotic energy in desalination plants is explored in this chapter, based on the results presented in the previous chapters. The proposal concentrates on using the brines from a Multi Effect Distillation unit (MED) and a Reverse Osmosis (RO). In both cases, the objective is to obtain the maximum energy recovery, as a function of the operating conditions and the architecture of the each technology.

## 2. Motivation

Desalination has been growing rapidly as an industry and research field, combining engineering and science to develop innovative means for water desalting [1]. Many countries, especially in the Middle East, depend on seawater desalination as source of drinking water, so they have invested considerable in these technologies [1].

Desalination plants have seen considerable expansion during the past decade as the need for potable water increases with population growth. The world production of desalination water is estimated to exceed 30 million cubic meters per day, with the market expected to reach 30 billion dollars by 2015[2].

One of the major challenges in the desalination industry, especially in those countries that depend on desalination for potable water, is the handling of reject brine, which is the highly concentrated by-product of the desalination process. For every one m<sup>3</sup> of desalinated water, an equivalent amount of brine is generated [3]. Another challenge is the use of energy to produce water: As a drinking water treatment technology, seawater desalination requires more energy than most other water treatment methods. However, the power consumption associated with seawater desalination is frequently exaggerated and inaccurately represented when compared to other treatment technologies that provide safe and reliable public water supply [4].

Table 6.1 presents the range of typical pressures, associated with feed water salinity. It is clear to see that as feed water salinity increases, so does the requirement for an increase in membrane feed pressure (and associated energy) until the practical limitation of 1200 psi (82.7 bar) for Seawater Desalination reached: at this point the actual feed water recovery is typically decreased to stay within design pressure limitations [4]. Typically, the energy consumption represents 44% of the total water cost of an RO plant [6], with the water recovery of a single-stage RO desalination system ranging from 40 to 60%.

Table 6.1: Pressure requirements for different water concentration and desalination technics [4].

Source	Salinity (mg/L)	Technique	Typical Pressure Range	
			psi	bar
Surface (Fresh) Water	<500	MF/UF	15 - 30	1 - 2
Brackish Water	500 - 3500	RO	50 - 150	3.4 - 10.3
Brackish to Saline	3500 - 18,000	RO / SWRO	150 - 650	10.3 - 44.8
Seawater • USA • Middle East	18,000 - 36,000 18,000 - 45,000+	RO	650 - 1200	44.8 - 82.7

The common practice in the dealing with brine produce is to discharge them back into the sea, where it could result, in the long run, in detrimental effects on the aquatic life as well as the quality of the seawater available for desalination in the area [5,20].

This chapter investigates the integration of PRO in desalination. For this, the brine issued from desalination plants is used as draw solution to produce or to recover energy, which is able to reduce the energy consumption of desalination processes. Moreover, this reduces the concentration of the brine, which limits its impact on the environment.

### 3. Energy consumption of the desalination processes

All desalination processes are energy intensive and share a common minimum energy requirement for driving the separation of the saline solution into water and concentrated brine. In the following paragraphs, the main energy consumption of several desalination processes is studied.

#### *a. Energy consumption in RO and ED processes*

Most of the energy consumed in Reverse Osmosis and Electro Dialysis is electrical: the energy consumption of the RO unit depends mainly on the salinity of the feed water and the recovery rate. In fact, the osmotic pressure is related to the total dissolved solutes concentration of the feed water (TDS); therefore, desalination by RO of high-salinity water requires a higher amount of energy due to higher osmotic pressure (see Table 6.1). In ED plants, the electricity is used for ED electrodes and to drive the pumps. For low salinity (2500ppm), the electricity consumption of an ED unit ranges from 0.7 to 2.5 and 2.64 to 5.5kWh/m<sup>3</sup> for a salinity range between 2500 and 5000 ppm, respectively [6,7].

RO unit sizes vary from 0.1m<sup>3</sup>/day to a 395,000m<sup>3</sup>/day plant. The average reported energy consumption for seawater desalination ranges from 3.7 to 8 kWh/m<sup>3</sup> [8], although might exceed 15kWh/m<sup>3</sup> for very small units. For a typical size of seawater RO unit of 24,000m<sup>3</sup>/day, the electricity consumption ranges from 4 to 6 kWh/m<sup>3</sup> using a hydraulic energy recovery system for seawater.

To desalinate brackish water different membranes are used, much higher recovery ratios are possible, and energy consumption is lower, thanks to the lower osmotic pressures. For a brackish water RO unit, the electrical energy consumption ranges from 1.5 to 2.5kWh/m<sup>3</sup> [8].

#### *b. Energy consumption in thermal desalination processes: MED, MSF, MVC and TVC.*

Two types of energy – low-temperature heat and electricity – are required for most distillation processes (MSF, MED, MVC and TVC). The low-temperature heat

represents the main portion of the energy input, with electricity mainly used for pumping.

The MSF process operates at a top brine temperature (TBT) in the range of 90 to 110°C. An increase of TBT increases the flash range, which, in turn, increases the production rate and improves the performance. However, the TBT is limited by the temperature to which the brine can be heated before serious scaling occurs [9].

Thus, the thermal energy consumption of a MSF plant ranges between 190MJ/m<sup>3</sup> and 282MJ/m<sup>3</sup>. The electrical energy equivalent to these values based on a power plant efficiency of 30% ranges between 5.8 and 23.5kWh/m<sup>3</sup>. The electricity consumption of the pumps ranges between 2.5 and 5kWh/m<sup>3</sup>; therefore, the total equivalent energy consumption of the MSF unit ranges between 19 and 27 kWh/m<sup>3</sup>.

The MED process also requires low-temperature heat for evaporation, and electricity for pumps. It operates at brine temperatures from 64 to 70 °C. The manufacturers of MED units provide again output ratio (GOR) ranging from 10 to 16 (Although in practice, MED plants operate at GOR values of 8 to 12 [10]). According to manufacturer's values, then the thermal energy consumption of MED plants is between 145MJ/m<sup>3</sup> (GOR=16) to 230 MJ/m<sup>3</sup> (GOR=10). The work equivalent to these values based on a power plant of 30% efficiency then ranges from 12.2 to 19.1 kWh/m<sup>3</sup>, plus the consumption of the pumps, which is between 2.0 and 2.5 kWh/m<sup>3</sup>.

For TVC, both low temperature heat and electricity are also needed: At TBT between 63 and 70°C, GOR=12 and a heat input of 227.3MJ/m<sup>3</sup> (14.56 kWh/m<sup>3</sup>), with an electricity consumption of 1.6–1.8 kWh/m<sup>3</sup> are required [11]. Therefore, the total energy consumption of the TVC process is about 16kWh/m<sup>3</sup>.

MVC does not use heat, operating at a maximum TBT around 74°C, with electrical energy consumption ranging from 7 to 12 kWh/m<sup>3</sup> [11].

### *c. Minimum energy for separation*

Thermodynamic analysis of the energy requirement of desalination processes have been published by many researchers [12, 13, 14]. The expression of the minimum

isothermal reversible work of separation  $W$ , which is applicable to any desalination process regardless of the separation mechanism, is as follows [14]:

$$-W_{desal} = \Delta H - T\Delta S = \Delta F \quad (6.1)$$

where  $\Delta H$  represents the change in enthalpy between the outlet and inlet flows,  $\Delta S$  represents the change in entropy, and  $\Delta F$  the change of the free energy. Introducing the relation of free energy with the molar concentration of the salt results in:

$$-W_{desal} = \int_{inlet}^{outlet} \Delta F dn = \int_{n_{in}}^{n_{out}} RT \ln a_w dn = \int_{n_{in}}^{n_{out}} RT \ln \frac{p}{p^0} dn \quad (6.2)$$

where  $n$  represents the number of water moles in the solution,  $R$  is the gas constant,  $a_w$  is the water activity in the solution, and  $p$  is the water vapor pressure assumed as an ideal gas. The final expression for the minimal separation energy is given by:

$$-W_{desal} = \frac{0.296T}{100-n_2} \int_{100}^n \ln \frac{p}{p^0} dn \quad (6.3)$$

The theoretical minimum separation energy of water is then directly given by Eq. (6.3): it is then possible to calculate that the energy needed per cubic meter produced from an infinite source of 35g/l seawater:

$$-W_{desal (35g/l)} = 0.296T \ln a_w \quad (6.4)$$

This value is around 0.77 kWh/m<sup>3</sup> for a temperature of 20°C, but is quite far from the values in practice. For example, the Ashkelon facility, one of the most efficient seawater RO desalination facilities, operates at approximately 40% recovery and has a maximum nominal electrical SE consumption of 3.9 kW h/m<sup>3</sup> [18].

## 4. Energy recovery from MED system

### 4.1 Methodology

According to the results presented in the previous chapter, the temperature and the concentration of the draw solution play a primordial role in PRO: high temperature and concentration are desirable, as the PRO process revealed a good performance under these conditions. The multi-effect distillation system is able to provide good values of these parameters because its rejected brine has high brine concentration and temperature. In this case, the PRO system is placed after the desalination process linking two sources of water: the brine of the MED and waste water coming, for example, from industrial rejects. To ensure the well-functioning of the membrane and to optimize the energy recovery, two heat exchangers would be used. The first one is used to reduce the temperature of the brine to the optimal value for PRO membranes (to guarantee high water flux), and to extract heat that will be used to rise the temperature of the wastewater. The second heat exchanger would be placed between the heat steam condensate and the wastewater, to rise its temperature. The two water steams reach the PRO unit at different temperatures, which depend on the brine outlet temperature and the efficiency of the heat exchangers.

### 4.2 Application to a case study

#### 4.2.1 The AQUASOL MED plant

The AQUASOL plant is a solar thermal desalination system, located at the Platform Solar of Almeria (southern Spain), which is going to be used as a case study to test our proposal. Currently, the experimental plant operates as a hybrid solar-gas plant that combines a MED process and a low temperature solar field with a Double Effect Absorption Heat Pump (DEAHP) coupled with a gas boiler [15] (Fig. 6.2). The MED plant is a 14-effect forward feed unit with a vertical arrangement. The nominal operating parameters are presented in Table 6.2. A static compound parabolic concentrator (CPC) solar field provides the thermal energy required for the MED process during sunshine hours. This thermal energy is stored in two water tanks. The gas boiler used by the DEAPH can provide heat for the MED process at variable loads from 30% to 100% when no solar energy is available. A

three-way regulating valve (V2) is used to reach the nominal first-effect inlet temperature by mixing water from the primary tank with the return flow coming back from the first effect.

It must be pointed out that although the AQUASOL MED plant currently operates with brackish well water with salinity of 3.3 g/l, in order to make the results more general, data for the expected operation with seawater is used here [15]. Table 6.3 shows the expected brine and temperature concentrations starting with different inlet seawater conditions.

To validate the proposed osmotic energy recovery technique, experiments were carried out at the Fraunhofer Institute for Interfacial Engineering and Biotechnology. Self-developed cellulose acetate membranes with an optimized internal structure [16] were studied under realistic operating conditions for a scaled-down membrane surface. More precisely, process parameters such as salt concentrations, pressures and flow rates were varied in order to validate the models and get information on the most adequate operating conditions and the expected energy production (for details see [17]).

Table 6.2: Nominal operating parameters of the AQUASOL MED system.

Number of effects	14
Feed seawater flow rate	8 m <sup>3</sup> /h
Brine flow rate from the last effect	5 m <sup>3</sup> /h
Hot water flow rate	43.2m <sup>3</sup> /h
Total distillate output	3 m <sup>3</sup> /h
Cooling seawater flow rate at 25°C	20 m <sup>3</sup> /h
Vapor production in the last effect at 35°C	159 kg/h
Heat source energy consumption	200 kW
Performance ratio	> 9
Vacuum system	Hydro-ejectors (seawater at 3 bar)
Inlet/outlet hot water temperature	75.0/71.0°C
Brine temperature (on the first cell)	68°C
Feed and cooling sea water temperature at the outlet of the condenser	33°C

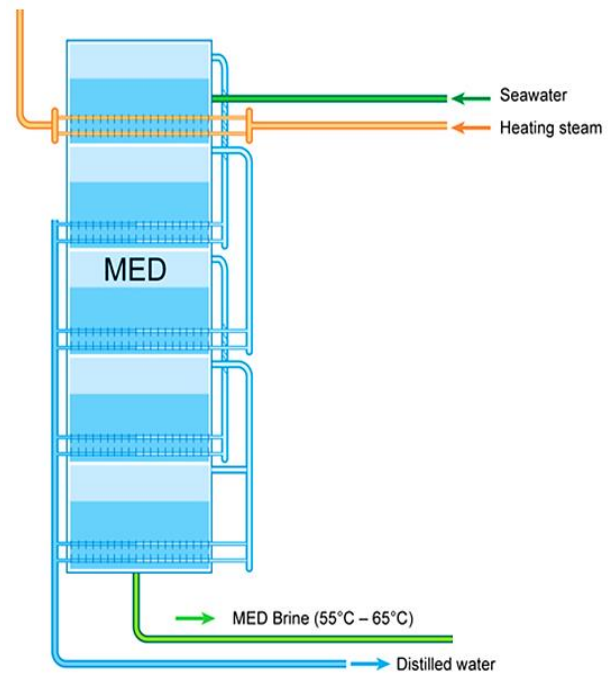


Fig.6.1: AQUASOL desalination plant.



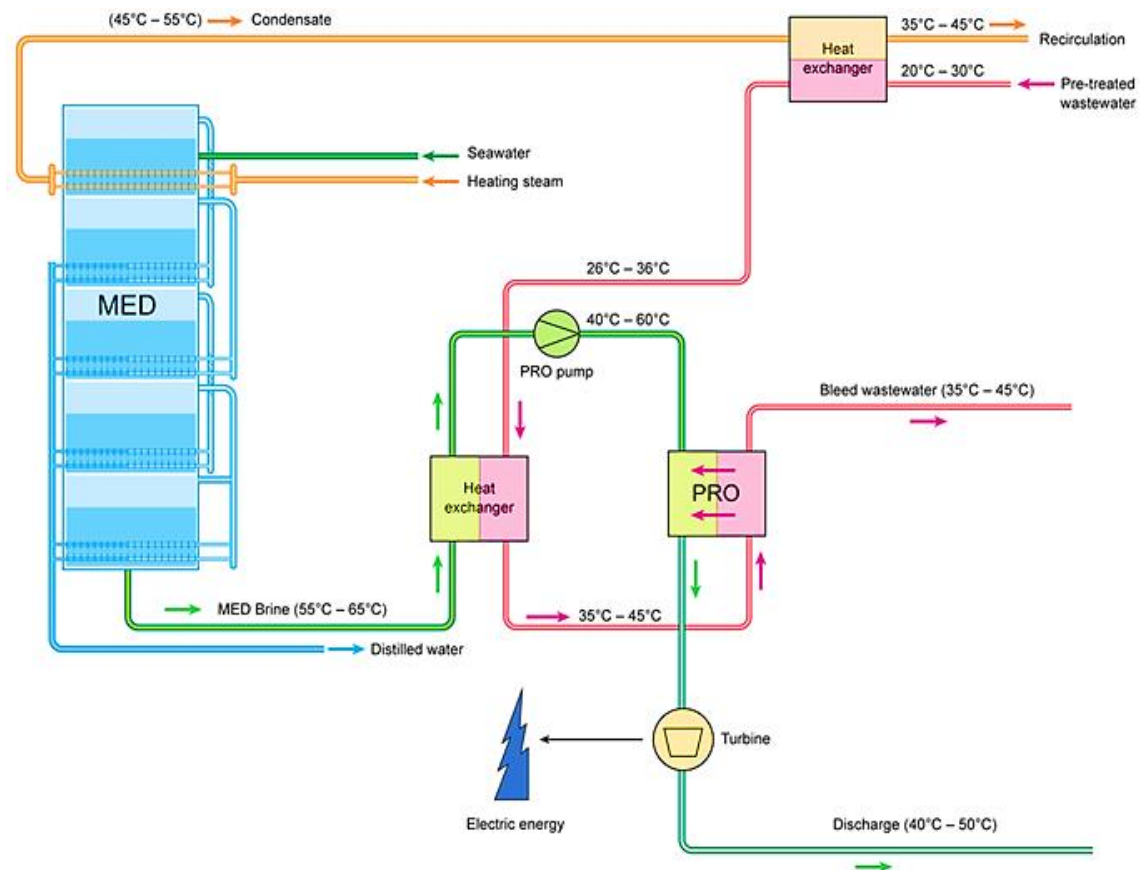


Fig. 6.3: Basic concept of the Pressure-Retarded Osmosis process for osmotic energy recovery from MED brines.

Table 6.4: expected energy recovered using the proposed system, for several combinations of seawater and feed water conditions.

Case Study	PRO Operating pressure	PRO Feed flow	PRO Feed Temperature	PRO Discharge concentration	Power recovered
#1	23.5 bars	5m <sup>3</sup> /h	20°C	39.8 g/l	14.2 kW
			30°C	35.5 g/l	19.8 kW
			40°C	33.7 g/l	<b>22.6 kW</b>
#2	22.5 bars	5m <sup>3</sup> /h	20°C	39.9 g/l	13.5 kW
			30°C	36.1 g/l	17.5 kW
			40°C	33.7 g/l	<b>21.0 kW</b>
#3	21.2 bars	5m <sup>3</sup> /h	20°C	35.7 g/l	12.8 kW
			30°C	32.5 g/l	17.1 kW
			40°C	31.1 g/l	<b>19.2 kW</b>

The experimental results obtained so far in the laboratory have shown that SG techniques depend significantly on temperature. We believe that the main effect is due to the change of fluid parameters with the temperature. For example, a preliminary evaluation of some physical parameters is presented in Table 6.5 for several typical temperature and concentration values in MED systems. To simplify the analysis, the temperatures of the streams were the same ( $T_{D,b}=T_{F,b}=T$ ). The Sherwood ( $Sh$ ), Reynolds ( $Re$ ) and Schmidt ( $Sc$ ) numbers of the feed stream were also estimated using Eqs. (3.12), (3.14) and (3.15) from Chapter 3. It can be seen in Fig. 4 that increasing the temperature leads to a better performance of the process: the changes in physiochemical properties of the membrane and the solution improve the membrane performance. This can be justified by the fact that the changes in the two streams caused by the rise of the temperature increases the water flux crossing the membrane. In fact, the rise of the temperature reduces the viscosity of the water at the surface of the membrane and increases the diffusivity of the water; thus, the internal concentration polarization (ICP) at the surface of the membrane support layer will be reduced. Also, the osmotic pressure difference increases at higher temperatures, increasing the driving force. All of this leads to higher values of  $J_w$ : Raising the temperature from 20°C to 60°C could double the amount of energy produced. This result is not only caused by the change of physico-chemical properties of the solution. In fact, membrane transport parameters are also affected by the operating temperature (see the discussion in Chapter 5).

Fig.5 shows the percentage of energy that can be recovered at different operating temperatures. It is clear that it is better to operate with inlet solutions with high temperatures to enhance PRO performance (around 10% of the energy can be recovered operating at 40°C, compared with 7% at 20°C). Dashed lines present the extrapolation of the result for non-studied values of temperature (current laboratory membranes degrade at temperatures over 50°C). Extrapolations show that using membranes that can stand high temperatures (no swelling, no collapse) can be beneficial in terms of energy recovery using PRO for these MED processes.

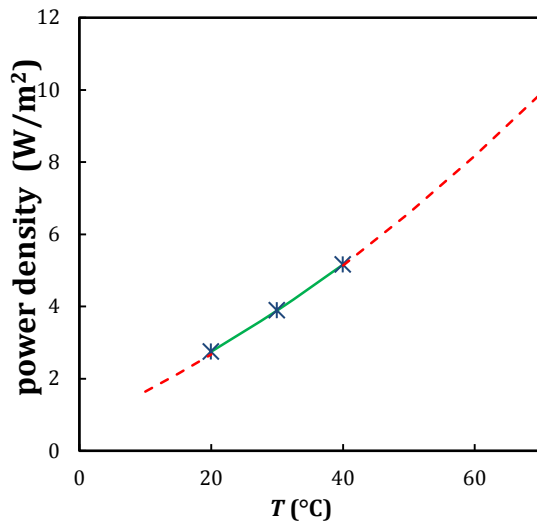


Fig.6.4: Variation of the power density with the PRO feed water temperature.

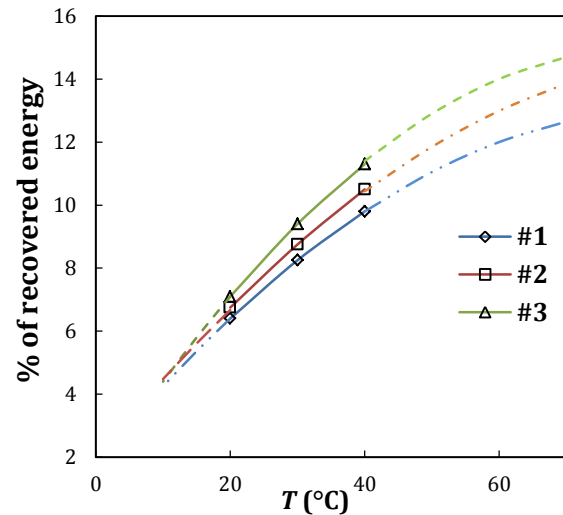


Fig.6.5: Estimated energy recovered for MED at different operating temperatures and seawater concentrations.

Table 6.5: variation of the viscosity, the diffusivity, the difference of the osmotic pressure, Sherwood, Reynolds and Schmidt numbers with the operating temperature

$T$ (°C)	$\eta_F$ (Pa.s)	$\eta_D$ (Pa.s)	$D_F$ (m <sup>2</sup> .s <sup>-1</sup> )	$D_D$ (m <sup>2</sup> .s <sup>-1</sup> )	$Sh$ (-)	$Re$ (-)	$Sc$ (-)	$\Delta\pi$ (bar)
20	$1.00 \times 10^{-3}$	$1.07 \times 10^{-3}$	$3.80 \times 10^{-9}$	$3.56 \times 10^{-9}$	25.1	99.5	265	45.0
30	$7.98 \times 10^{-4}$	$8.23 \times 10^{-4}$	$4.93 \times 10^{-9}$	$4.78 \times 10^{-9}$	26.8	125	162.4	46.6
40	$6.53 \times 10^{-4}$	$6.87 \times 10^{-4}$	$6.23 \times 10^{-9}$	$5.92 \times 10^{-9}$	28.3	150	106.7	48.1

## 5. PRO integration in Reverse Osmosis

Compared to a stand-alone PRO system (fresh water vs seawater), an RO-PRO system has already been found to have numerous advantages. For example, the brine generated during the RO process dilutes to seawater concentration values, thus minimizing any environmental impact that brine disposal can have on marine habitats [18]. It should be pointed out that the RO product water is always in a circuit separated from the waste water used for PRO, so there is no contact between impaired and drinking water: Thus, recycled water can be used as a support of the RO desalination, without health issues.

PRO energy production in the RO-PRO system is amplified by the higher concentration of the draw solution (RO brine), when compared with standard

Seawater. Moreover, a clear characteristic of the RO-PRO system is that the draw solution is already pre-treated by the well-developed pre-treatment system used in RO [19]. Thus, the brine entering the PRO sub-system is relatively free of foulants, so no additional treatment of the draw solution is needed: draw solution pre-treatment increases significantly the use of energy and chemicals in river-to-sea PRO.

### *5.1 Description of the case study*

A case study, a Reverse-Osmosis-based desalination unit intended for producing water for an electrolyzation process is used. This RO plant, composed of the elements presented in Fig. 6, was developed by SETA, S-L as a part of the H2Ocean project [29].

The desalination unit is based on two similar lines, each divided into two stages (denoted SWRO and BWRO), which can be independently operated and disconnected if required, for maintenance or operational requirements. The seawater treatment starts with a pretreatment composed of three steps: chlorination to deal with organic matter, ultrafiltration to block the metals and particles in suspension, and periodic backwash to eliminate the foulants accumulated in the filters.

The first pass of the SWRO unit starts with a chemical treatment to remove any chlorine from the pre-treatment, then bisulphite is added (to remove the oxidants dissolved in the water and provide a bacteriostatic effect) and, finally, antifouling is used to avoid salt precipitation on the membranes that would increase the energy consumption. As a safety system, a 5 microns filter is installed just in the inlet of the membranes. To feed the first-pass membranes, a high pressure pump is then used; the water produced (around 45% of the inlet seawater) is stored in a tank, whereas the brine would go to the Energy Recovery system.

In the Second Pass of Reverse Osmosis (BWRO) first antifouling is dosed to avoid salt precipitation; a micro filter is then installed with a degree of filtration of 5 microns before the high pressure pump which pressurizes the water before entering the membrane. The reverse osmosis recovery is around 70%. The water produced is stored in a DEMI water tank, whereas the brine goes to an energy

recovery system before being reused in the proposed osmotic energy recovery system or being returned to the Ultra-filtration tank.

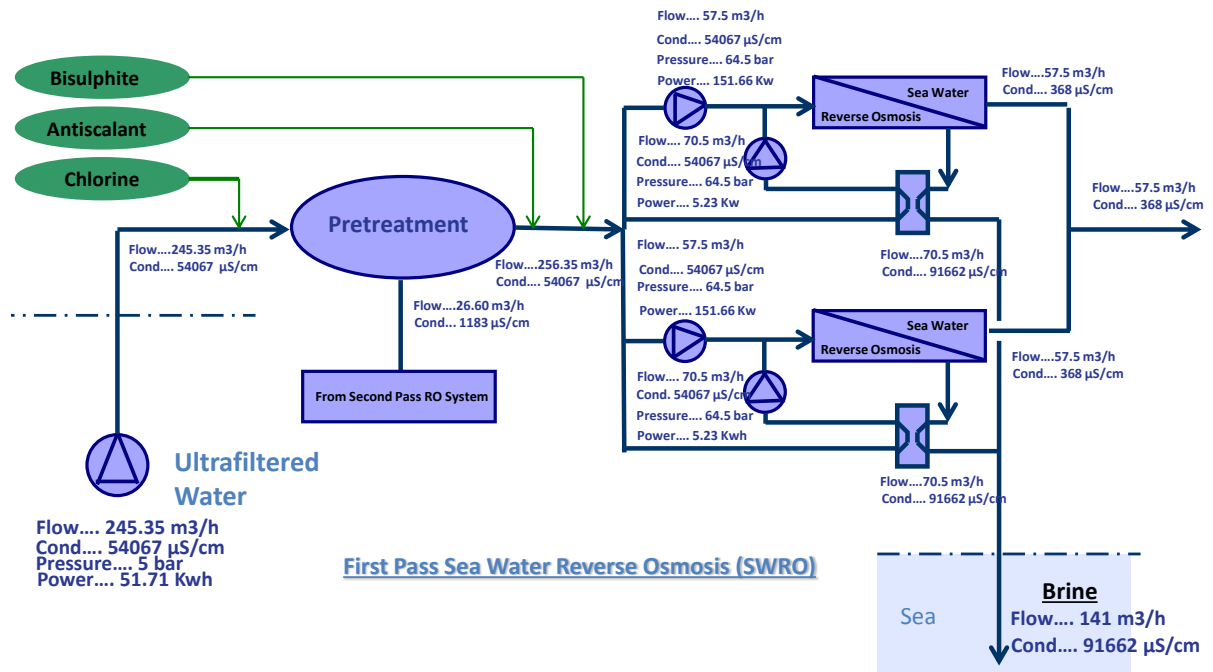


Fig.6.6: First Pass of Reverse Osmosis Desalination.

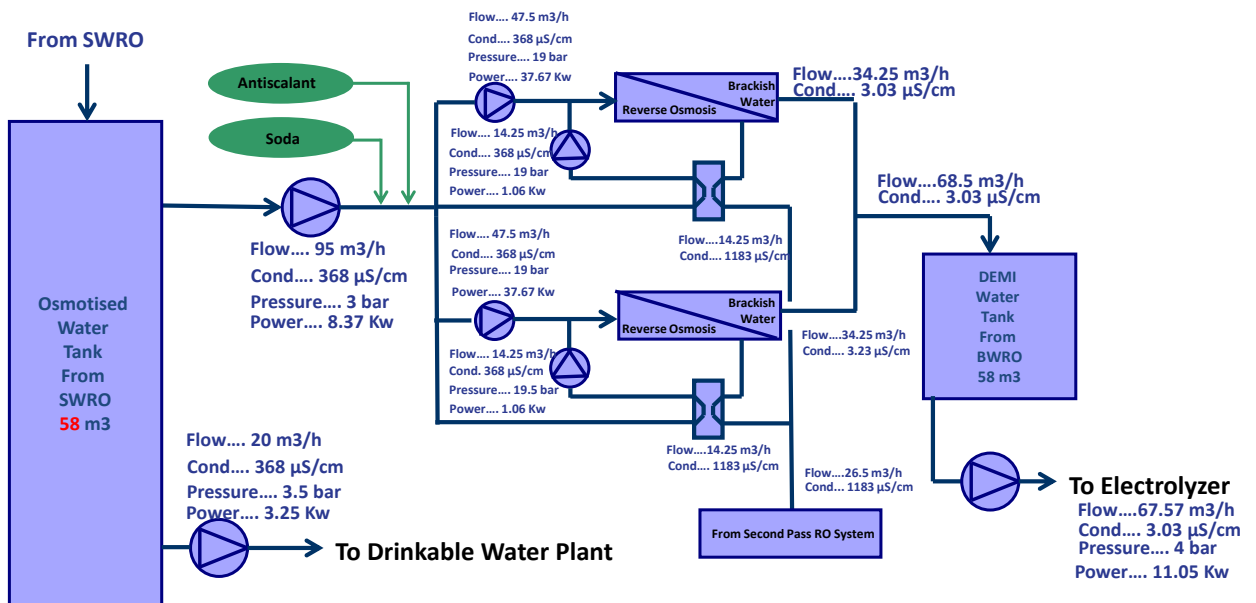


Fig.6.7: Desalination Second Pass.

Table 6.6: Power consumed by each component of the Desalination Unit

<i>Section</i>	<i>Installed Power per section</i>
<u>Pre-treatment</u>	61.27 kW
Sea Water Pressure Pump	51.71 kW
BackWash Equipment	9.56 kW
<u>Sea Water Reverse Osmosis (SWRO)</u>	356.39 kW
Ultra-filtrate Water Pump	42.61 kW
High Pressure Pump	2 x 151.66 kW
Booster Pump	2 x 5.23 kW
<u>Drinkable Water Plant (DWP)</u>	8.84 kW
Low Pressure Pump	3.25 kW
Recirculation Pump	5.59 kW
<u>Brackish Water Reverse Osmosis (BWRO)</u>	12.17 kW
Pump to Electrolyzation	11.05 kW
Pump to Services	1.12 kW
<u>Others</u>	50.0 kW
<b>Total</b>	<b>574.5 kW</b>

## 5.2 First RO-PRO configuration

### 5.2.1 Methodology

The concept of this integration is to exploit the large difference of concentration between the brines of different stages in a multi-stage RO desalination plant. Thus, PRO is placed between the retentates of the different stages: in the case of the H2Ocean desalination system, using the brines of SWRO and BWRO. Due to the high salinity of the retentate in the first stage, it contains a significant amount of energy that can be recovered by mixing with retentate from the second stage as presented in Fig 6.8. The effect of the variation of the temperature of both solutions was studied in particular: temperature of seawater normally ranges

from 12 to 35°C [20], but as most RO plants are located in hot regions, the seawater temperature is normally over 25°C; moreover, the temperature of RO brines are generally higher than that of raw seawater due to pumping and storage.

In our proposal first the brine of the first stage (with concentration around 60g/l) reduces its pressure in a pressure exchanger (that has an efficiency of up to 96%) to a value that guarantees a maximum of energy recovery according to Eq. (3.23) (see the discussion in Section 2.3), using the energy to pressurize the seawater. It should be mentioned that the brine is generated from pre-treated seawater, which improves the overall energy recovery, as fouling is reduced.

The feed water for the PRO unit is then the brine of the second stage, which has a salt concentration of around 0.5g/l. This low concentration and the RO pre-treatment make the effect of the ECP controllable. The discharge coming out of the PRO is then led to the pressure exchanger for pressure recovery.

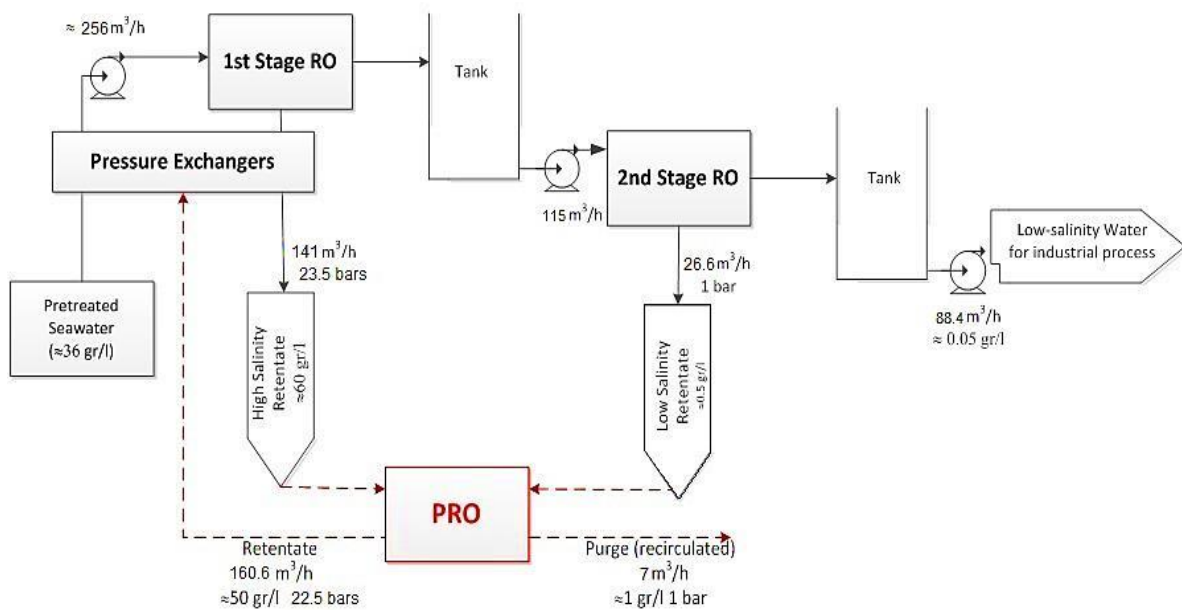


Fig. 6.8: conventional integration of PRO in the H2Ocean desalination plant.

### 5.2.2 RO-PRO modeling

A simplified presentation of the integration proposed in Fig.6.8 is illustrated in Fig 6.9: the seawater feed solution ( $V_{SF}$ ) is first pre-pressurized in the pressure exchanger PX prior to entering the desalination process. Exiting the first stage RO

sub-system ( $RO_1$ ) are two streams: a fresh water permeate stream ( $V_{p1}$ ) and a concentrated brine stream ( $V_{SR1}$ ). The concentrated brine stream is then depressurized to approximately half of its pressure (23.5bars) to reach a suitable pressure for the PRO process [5]. The permeate of the first stage RO sub-system feeds the second stage RO sub-system ( $RO_2$ ). To recover this energy, an ERD (an isobaric or turbocharged device) could be used; alternatively, a turbine could be employed to convert into electrical energy. Following this depressurization, the brine stream enters the PRO sub-system as a high salinity (draw) solution ( $V_{SR1}$ ). The feed solution for the PRO sub-system ( $V_{SR}$ ) is the low salinity retentate of the second stage. Through osmosis, the pressurized draw solution extracts water from the impaired water source under isobaric conditions, resulting in a diluted draw solution ( $V_{DR}$ ). The energy stored in the diluted draw solution is then exchanged with the seawater RO feed prior to discharge, in order to recover its potential energy and increase the energy savings of the RO-PRO system.

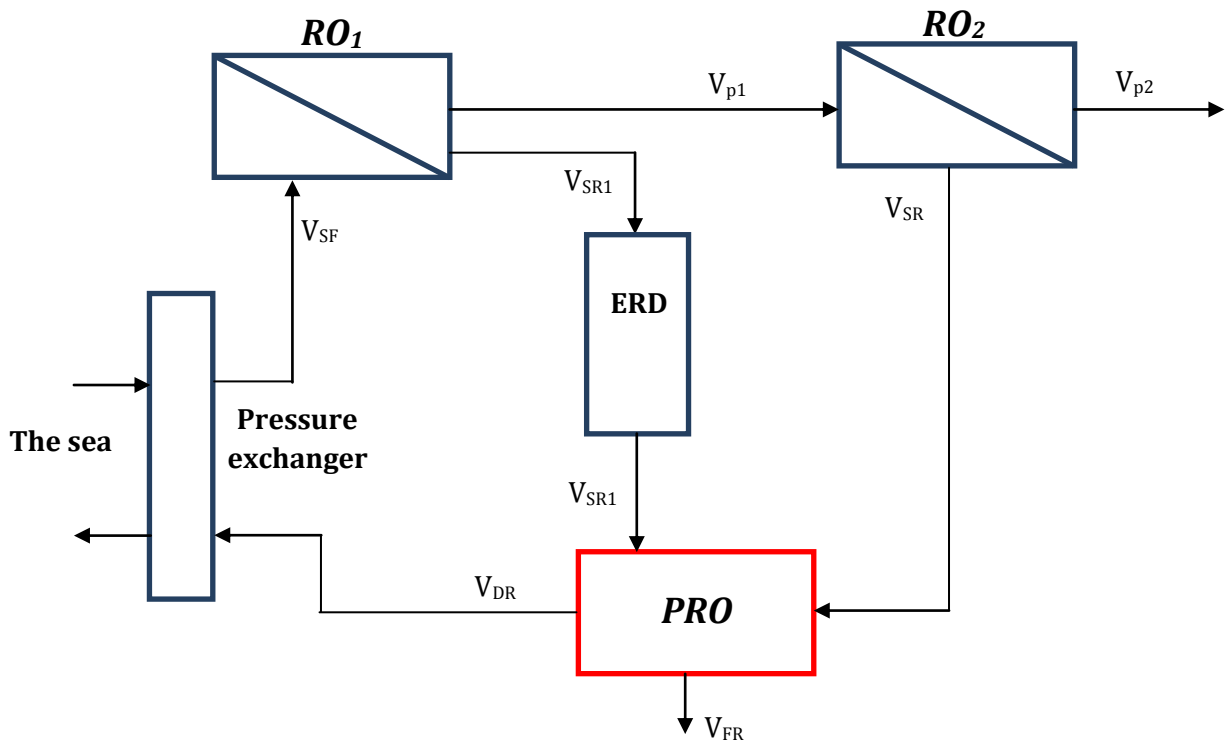


Fig. 6.9: Simplified schematic of the coupled RO-PRO system.

### 5.2.2.1 Theoretical energy consumption of the RO-PRO system.

The theoretical energy consumption is the minimum amount of energy needed to produce a desired amount of permeate. More precisely, the theoretical specific energy consumption (SEC) provides the absolute minimum amount of energy for a given recovery, assuming that the efficiency of every component (pump, ERD, motor) is 100%.

The work per volume of permeate required in a thermodynamically reversible RO desalting process can be determined based on the mole fraction of feed and brine, as presented in [7]. Assuming finite recovery in an ideal desalination process:

$$W_{RO_1,theo} = \beta RT \frac{x_{SR1}x_{SF}}{x_{SR1}-x_{SF}} \ln \left( \frac{x_{SR1}}{x_{SF}} \right) \quad (6.5)$$

$$W_{RO_2,theo} = \beta RT \frac{x_{SR2}x_{p1}}{x_{SR2}-x_{p1}} \ln \left( \frac{x_{SR2}}{x_{p1}} \right) \quad (6.6)$$

where  $x_{ds1}$  and  $x_{F,in}$  are, respectively, the salt mole fractions of the feed and draw solutions of the first stage and  $x_{ds2}$  and  $x_{p1}$  are, respectively, the salt mole fractions of the second stage feed and draw. Assuming that  $\pi = \beta RTC$ , the specific energy consumption per volume of fresh water produced ( $SEC_{RO,theo}$ ) for each stage.

$$SEC_{RO_1,theo} = \frac{\pi_{SR1}\pi_{SF}}{(\pi_{SR1}-\pi_{SF})} \ln \left( \frac{\pi_{SR1}}{\pi_{SF}} \right) \quad (6.7)$$

$$SEC_{RO_2,theo} = \frac{\pi_{SR2}\pi_{p1}}{(\pi_{SR2}-\pi_{p1})} \ln \left( \frac{\pi_{SR2}}{\pi_{p1}} \right) \quad (6.8)$$

which gives the specific energy consumption per volume of fresh water produced for each stage.

The recovery  $Y$  of each RO stage is given by:

$$Y_1 = \frac{V_{p1}}{V_{SR}} \quad (6.9)$$

$$Y_2 = \frac{V_{p2}}{V_{p1}} \quad (6.10)$$

where the subscripts 1 and 2 refer to the RO stages. The total recovery of the system is then given by:

$$Y_{total} = \frac{V_{p2}}{V_{SR}} = Y_1 Y_2 \quad (6.11)$$

For PRO, an equation similar to Eq. (6.5) can be developed. Assuming finite dilution in an ideal mixing process, the energy production can be calculated as:

$$SE_{PRO,theo} = \frac{\pi_{SR1}\pi_{DR}}{\pi_{SR1}-\pi_{DR}} \ln\left(\frac{\pi_{DR}}{\pi_{SR1}}\right) \quad (6.12)$$

where  $SE_{PRO, ideal}$  is energy production per volume of PRO permeate.  $\pi_{SR1}$  and  $\pi_{DR}$  are the entering draw solution and exiting draw solution of the PRO system, respectively. The osmotic pressure of the outlet solution can be calculated after determining the permeate volume for a predetermined PRO dilution  $\phi$ , defined as follows:

$$\phi = \frac{V_{FR}}{V_{DR}} \quad (6.13)$$

The energy consumption of the system is the combination of each part of the system; thus, the total energy consumption is:

$$SEC_{tot,th} = SEC_{RO_1,th} + SEC_{RO_2,theo} - SEC_{PRO,theo} \quad (6.14)$$

Fig (6.13) shows the  $SEC_{tot,th}$  of the system under different PRO dilutions.

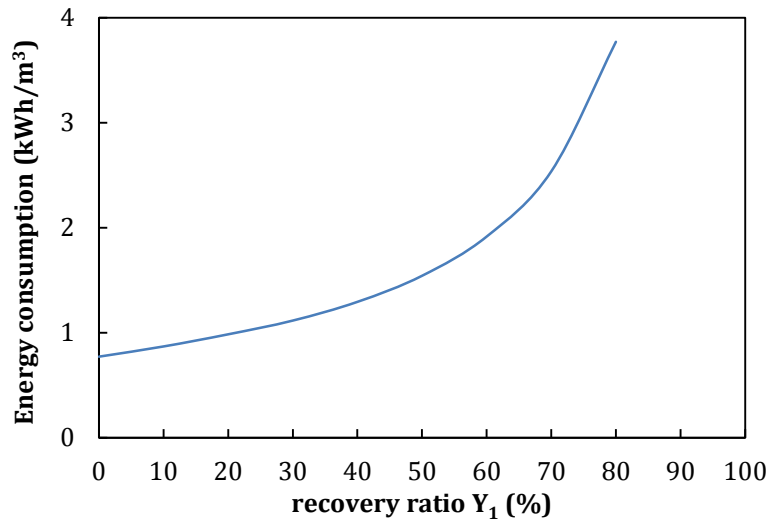


Fig. 6.10: Specific energy consumption for the first stage at different recovery ratios.

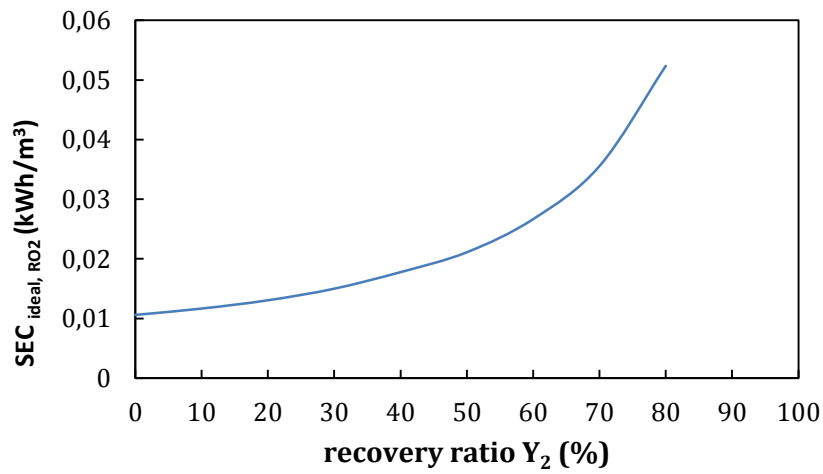


Fig. 6.11: Specific energy consumption for the second stage at different recovery ratios.

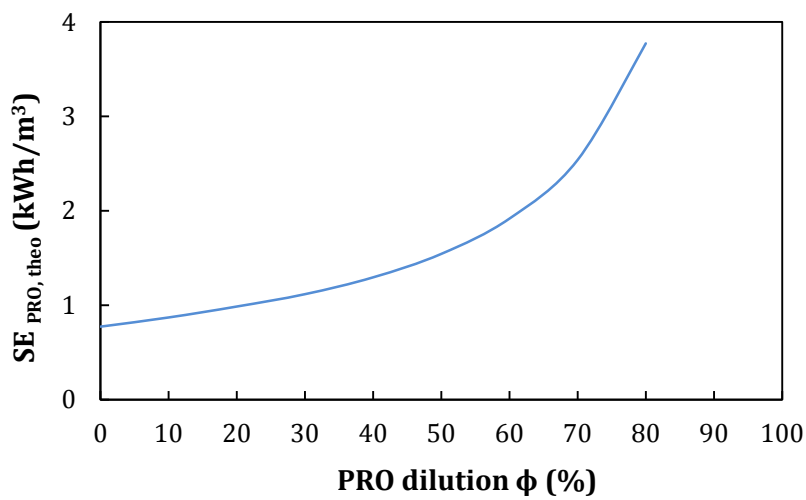


Fig. 6.12: Specific energy production for draw solution dilution in PRO at different dilution factor.

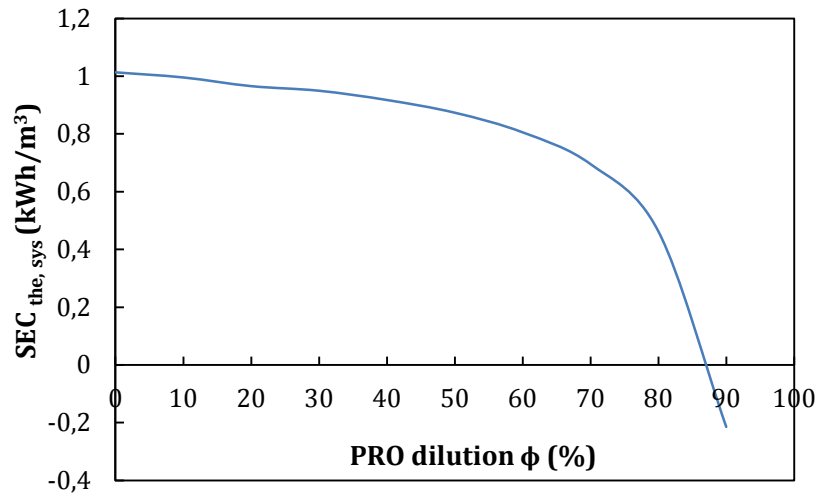


Fig. 6.13: RO-PRO specific energy for different PRO dilution factor.

To separate salts from water, it is necessary to cause the water to move in the opposite direction in the case of the reverse osmosis, by applying sufficient pressure to the seawater so that the pressure difference across the membrane exceeds  $\Delta P = 30$  bars. Therefore, As it can be seen in Fig. 6.10, theoretically the minimum work needed would be  $\Delta P \times V = 0.77$  kWh/m<sup>3</sup> of fresh water. This lower limit corresponds to a rate of production that is nearly zero. It can be also that when the recovery rate increases, the specific energy consumption would also increase. In fact, it has been shown in the literature that the optimal recovery rate for a SWRO unit is around 40 to 50% [21]. For this recovery rates, the  $SEC_{RO,theo}$  would be between 1.24 to 1.49 kWh/m<sup>3</sup> (see Fig.6.10), which clearly differs from real values [22,30,33].

Fig.6.11 shows, that for the second stage, the minimum energy required would be just 0.011 kWh/m<sup>3</sup>.

In Fig.6.12 the PRO theoretical specific energy ( $SEC_{ideal,PRO}$ ) production to dilute a brine solution upcoming from the first stage to low value of salinity solution is shown as a function of the dilution. As seen in Fig.6.12, the minimum ideal  $SEC_{PRO}$  is approximately 0.77 kWh/m<sup>3</sup> and is achieved when  $\phi = 0$ . This value of 0.77 kWh/m<sup>3</sup> is similar to the minimum energy to desalinate seawater at 0% recovery: the separation energy at 0% recovery is equal in magnitude but opposite in sign to the free energy of mixing at  $\phi = 0$ , in an other term, the equation for Gibbs free energy of mixing is achieved when entering and exiting draw solution concentrations are equal [23].

Theoretically, when flow of the PRO feed entering solution is equal to the flow of the entering PRO draw solution, the maximum of dilution can be reached which means that the concentration of the entering brine could be diluted to the value of the sea water concentration. In our case, the entering PRO feed solution flow is remarkably small compared to the the entering PRO draw solution ( $Q_{SR2}=26\text{m}^3/\text{h}$ ,  $Q_{SR1}= 141\text{m}^3/\text{h}$ ), then, the optimum therotical value of energy recovery could not be reached in this case.

### 5.2.2.2 Energy consumption of the RO-PRO system in real conditions

Real life RO+PRO plants would be less energy efficient than theoretically calculated, due to electrical conversion losses and dissipation. The amount of additional energy required depends on the specific recovery strategy, so the energy consumption of the RO-PRO under real conditions is now studied.

#### a. The Reverse Osmosis

The specific energy consumption (SEC) for a single-pass RO desalting process at the limit of the thermodynamic restriction in the absence of energy recovery (Fig. 6.10) can be derived by combining Eqs. (6.1)–(6.4) and (6.14), to obtain:

$$SEC_{RO} = \frac{R_s \pi_{SF}}{\eta_p Y (1-Y)} \quad (6.15)$$

where  $R_s$  is the salt rejection, and  $\eta_p$  is the pump conversion. Then, the energy consumption of each RO stage in a two-stage RO plant are:

$$SEC_{RO_1} = \frac{R_{s1} \pi_{SF}}{\eta_{p1} Y_1 (1-Y_1)} \quad (6.17)$$

$$SEC_{RO_2} = \frac{R_{s2} \pi_{p_1}}{\eta_{p2} Y_2 (1-Y_2)} \quad (6.18)$$

Energy recovery devices are known to be effective in many seawater and brackish water reverse osmosis installations. In the seawater desalination industry, Pressure Exchangers (PX) are extensively used to recover energy and lower operating costs: they can save half of the energy consumption.

These elements transfer the energy from brine rejection to a low-pressure incoming pretreated stream: this pressure recovery has been studied in detail in the literature [24,31]. In general, the specific energy cost for RO, in the presence of an energy recovery device (ERD) operating in the limit of the thermodynamic restriction is

$$SEC_{RO}^{ERD} = R_s \pi_f \left( \frac{1 - \eta_{ERD}(1-Y)}{\eta_{PY}(1-Y)} \right) \quad (6.19)$$

where  $\eta_{ERD}$  is the efficiency of the energy recovery device (ERD) and  $\pi_f$  is the feed water osmotic pressure. The specific energy with an ERD is for the first RO stage

$$SEC_{RO_1}^{ERD} = R_{s1} \pi_{SF} \left( \frac{1 - \eta_{ERD}(1-Y_1)}{\eta_{P1Y_1}(1-Y_1)} \right) \quad (6.20)$$

#### *b. Pressure Retarded Osmosis PRO*

As shown in Chapter 3, the water flux of the PRO system across the flat sheet membrane is

$$J_w = A \left[ \frac{\pi_{D,b} + \frac{B}{A} \left( 1 + \frac{A\Delta P}{J_w} \right)}{\exp(J_w/k_D)} - \left[ \pi_{F,b} + \frac{B}{A} \left( 1 + \frac{A\Delta P}{J_w} \right) \right] \exp(J_w K) \exp(J_w/k_F) - \Delta P \right] \quad (6.21)$$

This model was developed for a flat sheet bench-scale membrane. The variations along the membrane's length are often neglected in models designed to simulate bench scale systems because the effect is difficult to observe over very small membrane samples [25]. However, the water permeate, the salt permeate, and the friction in the membrane module, cause variations in several parameters along the length of the membrane. These include flow rates, concentrations and hydraulic pressures as well as all other variables that are dependent on them. For accurate modeling their local values should be considered. These spatial variations can be accounted for by either taking an average of inlet and outlet variables, or by considering the membrane as a finite difference model [26,32]. To develop a model for full-scale PRO applications, the flat sheet membrane area is divided into segments perpendicular to the water flow, evaluating flow conditions at specific

points along the membrane module. In this case, feed and draw solution flows are assumed to be in a co-current flow mode.

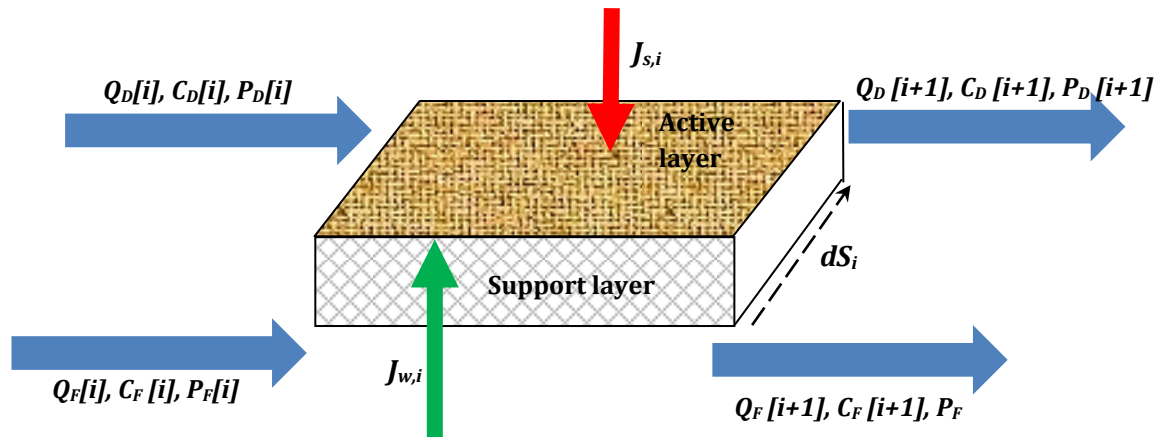


Fig. 6.14: Schematic of a single segment ( $dS_i$ ) of a flat sheet PRO membrane module.

The permeate flow through the PRO membrane  $Q_w$  can significantly dilute the draw solution concentration  $C_{SR1}$ , which results in reduced flux performance compared to small size test membrane. Such dilution effect needs to be explicitly accounted for in a flat sheet module. Due to this variation, three main parameters are evaluated at each point along the membrane: the water flux, the pressure and the concentrations.

For each segment ( $dS$ ), the exiting conditions are calculated and become the entering conditions for the next segment, until the end of the membrane module. For a single segment ( $dS$ ), the concentrations, the exit flow rates and the pressures of the draw and feed solutions are calculated as follows:

❖ **Expressions of the Flows:**

➤ *Draw solution flow*

$$Q_{D_0} = Q_{SR1} \quad (6.22)$$

$$Q_{D[i=N+1]} = Q_{DD} \quad (6.23)$$

$$Q_{D[i+1]} = Q_{D[i]} + J_w ds \quad (6.24)$$

➤ Feed solution Flow

$$Q_{F_0} = Q_{SR2} \quad (6.25)$$

$$Q_{F[i=1]} = Q_{FR} \quad (6.26)$$

$$Q_{F[i+1]} = Q_{F[i]} - J_{w1} ds \quad (6.27)$$

❖ **Expressions of the Concentrations**

➤ Draw solution concentration

$$C_{D[0]} = C_{SR1} \quad (6.28)$$

$$C_{D[i=N+1]} = C_{DD} \quad (6.29)$$

$$C_{D[i+1]} = \frac{Q_{D[i]}C_{D[i]} - J_s ds}{Q_{D[i]} + J_{w[i]} ds} \quad (6.30)$$

➤ Feed solution concentration

$$C_{F[i=N+1]} = C_{SR2} \quad (6.31)$$

$$C_{F[i=1]} = C_{FR} \quad (6.32)$$

$$C_{F[i+1]} = \frac{Q_{F[i]}C_{F[i]} + J_s ds}{Q_{F[i]} - J_{w[i]} ds} \quad (6.33)$$

❖ *Expressions of the Pressures*

The pressure losses along the membrane's length are generally ignored in bench scale PRO system because their effect is negligible. However, for a full-scale system, those losses cannot be ignored. The pressure losses do exist in both side of the membrane as:

➤ *Draw solution pressure*

$$P_{D[0]} = P_{SR1} \quad (6.34)$$

$$P_{D[N+1]} = P_{SR1} \quad (6.35)$$

$$P_{D[i+1]} = P_{D[i]} - P_{D[i],loss} \quad (6.36)$$

➤ *Feed solution pressure*

$$P_{F[N+1]} = P_{SR1} \quad (6.37)$$

$$P_{F[i-1]} = P_{FR} \quad (6.38)$$

$$P_{F[i+1]} = P_{F[i]} - P_{F[i],loss} \quad (6.39)$$

where  $S_{ds}$  is the area of the segment  $dS$ ,  $P_{D[i],loss}$  and  $P_{F[i],loss}$  are the draw and feed side pressure losses, respectively. The total water permeate flow rate  $Q_w$  at the membrane outlet is the integral of  $J_w$  over the whole membrane surface area:

$$Q_w = \sum_{i=1}^N J_{w_i} \times S_s \quad (6.40)$$

The expressions of the concentrations developed in Eqs (6.30) and (6.33) can be used to determine the draw solution concentration and the feed solution concentration anywhere in the module, and then, can be used to determine the local membrane flux  $J_w$  using its expression developed in the previous chapter. Then, the expression of the water flux in this case becomes:

$$J_w = A \left[ \frac{\pi_D + \frac{B}{A} \left( 1 + \frac{A \Delta P_{eff}}{J_w} \right)}{\exp(J_w/k_D)} - \left[ \pi_F + \frac{B}{A} \left( 1 + \frac{A \Delta P_{eff}}{J_w} \right) \right] \exp(J_w K) \exp(J_w/k_F) - \Delta P_{eff} \right] \quad (6.41)$$

where  $\Delta P_{eff}$  is the effective hydraulic pressure across the membrane, expressed as the difference between the pressures in the draw side and the feed side of the PRO, respectively:

$$\begin{aligned} \Delta P_{eff} &= P_D - P_F = \sum_{i=1}^N P_{D[i]} - \sum_{i=1}^N P_{D[i],loss} - \left( \sum_{i=1}^N P_{F[i]} - \sum_{i=1}^N P_{F[i],loss} \right) \\ &= \Delta P + \sum_{i=1}^N P_{F[i],loss} - \sum_{i=1}^N P_{D[i],loss} \end{aligned} \quad (6.42)$$

The pressure losses are [27]:

$$P_{loss} = \sum_{i=1}^N \frac{\rho \times f \times u^2}{2 \times d_h} dL \quad (6.43)$$

where  $\rho$  is the density of the solution,  $u$  is the cross flow velocity,  $d_h$  is the hydraulic diameter,  $dL$  is the length of the segment  $dL$  and  $f$  is the friction factor, given as a function of the Reynolds number [27]:

$$f = 6.23 R_e^{-0.3} \quad (6.44)$$

It was shown chapter 3 that the maximum power density is reached when  $\Delta P = \frac{\Delta \pi_{eff}}{2}$ . Then, the optimum effective pressure is:

$$\begin{aligned} \Delta P_{eff,opt} &= \frac{1}{2} \left[ \frac{\pi_D + \frac{B}{A} \left( 1 + \frac{A \Delta \pi}{J_w} \right)}{\exp(J_w/k_D)} - \left[ \pi_F + \frac{B}{A} \left( 1 + \frac{A \Delta \pi}{J_w} \right) \right] \exp(J_w K) \exp(J_w/k_F) \right] + \frac{B}{J_w} \left( \sum_{i=1}^N P_{F[i],loss} - \right. \\ &\quad \left. \sum_{i=1}^N P_{D[i],loss} \right) \left( \exp(-J_w/k_D) - \exp(J_w K) \exp(J_w/k_F) \right) \end{aligned} \quad (6.45)$$

The power density normalized by the membrane area in the module, is given by:

$$W = \Delta P_{eff,opt} \times \sum_{i=1}^N J_{W[i]} \quad (6.46)$$

where  $\sum_{i=1}^N J_{W[i]}$  is the sum of the permeate flux along the module given by:

$$\sum_{i=1}^N J_{W[i]} = \frac{Q_{w,TOT}}{S_S} = \frac{\sum_{i=1}^N Q_{w[i]}}{S_S} \quad (6.47)$$

where  $S_S$  is the entire area of the membrane. In our case, as presented in Fig.6.9 the energy is generated by a pressure exchanger, so the energy productions per volume of PRO permeate can be calculated as:

$$SE_{PRO} = \frac{W_{PRO}}{Q_w} = \frac{\Delta P_{eff,opt} \times S_S \times \sum_{i=1}^N J_{W[i]}}{S_S \times \sum_{i=1}^N J_{W[i]}} = \Delta P_{eff,opt} \quad (6.48)$$

where  $W_{PRO}$  is power produced by the PRO system. If the PRO module is supplied by a pump in the draw water side, the pressure losses reduce the net power recovered by the PRO. Those losses are compensated by the pump on the draw side of the membrane unit. The power consumed by this pump is:

$$W_{draw,Pump} = \frac{(P + P_{loss}) \times Q_{SR1}}{\eta_{P,draw}} \quad (6.49)$$

where  $\eta_{P,draw}$  is the efficiency of the pump. The net energy produced by the PRO system is, then, the difference between the power produced by the PRO unit minus the power consumed by the draw water pump:

$$W_{net} = W_{PRO} - W_{draw,Pump} = \Delta P_{eff,opt} \times Q_w \times \eta_{turbine} - W_{draw,Pump} \quad (6.50)$$

where  $\eta_{turbine}$  is the efficiency of the turbine.

Finally, the net SE of the RO/PRO process is obtained by subtracting the energy generated by the PRO unit from the SEC of the RO process:

$$SEC_{RO/PRO}^{net} = SEC_{RO} - SE_{PRO} = SEC_{RO1} + SEC_{RO2} - \Delta P_{eff,opt} \quad (6.51)$$

This energy can be rewritten regarding the productivity of the system in terms of the permeate flow in the second stage as:

$$SEC_{RO/PRO}^{net} = \frac{SEC_{RO_1} \times Q_{p,RO_1} + SEC_{RO_2} \times Q_{p,RO_2} - SE_{PRO} \times Q_w}{Q_{p,RO_2}} \quad (6.52)$$

### 5.3 Second RO-PRO configuration

#### 5.3.1 Methodology

The same RO desalination unit described in Section 4 was used in the following application. In this case, two PRO units were used (see Fig 6.8):

**The PRO unit:** was placed after the pre-treatment operation and before the first SWRO process. Thus, the pre-treated seawater will be considered as the feed solution. In this case, a part of the pre-treated seawater is conducted to the PRO as a feed solution. The amount of this part is chosen to be almost equal to the solution considered to be the draw solution of the PRO process. The retentate of the second RO stage is recirculated and conducted to be mixed with the part of the pre-treated seawater that is separated to be the PRO feed solution, then, the sum of the retentate of the second RO stage and the part of the seawater is considered as the PRO feed solution. The draw solution of the PRO is the brine of the first RO stage; this brine passes through the pressure exchanger PX to reduce its pressure to around 13.0 bars (which is theoretically the optimum value of pressure to be applied to the draw solution in PRO process). The pressure in PX will be exchanged between the brine and the combination of the non-used pre-treated seawater flow and the feed solution discharge of the PRO.

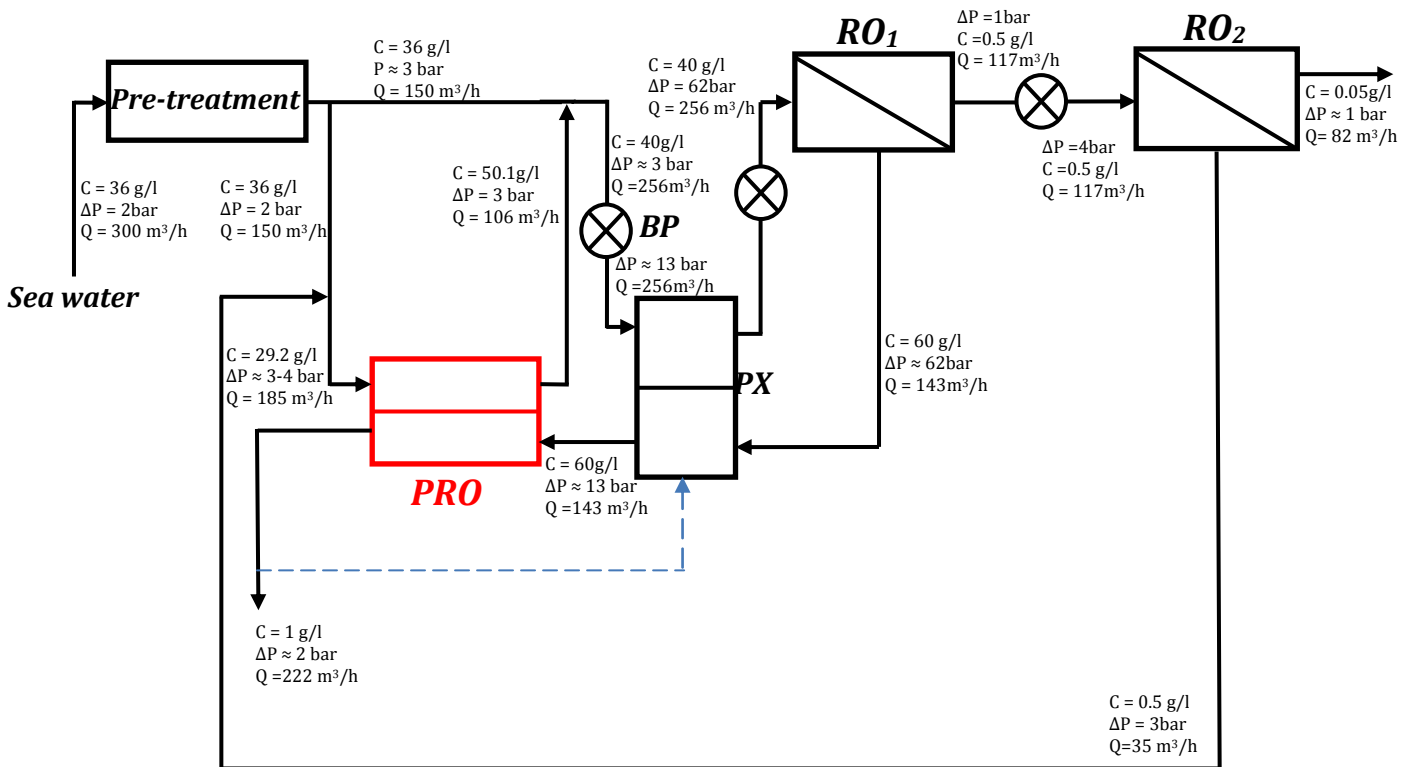


Fig. 6.15: Second integration of PRO in the RO plant.

#### 5.4 RO model results

Fig.6.16 presents the  $SEC_{RO1}$  (Eq. (6.17)) of a RO first stage without ERD as a function of recovery (pump efficiency, membrane salt rejection, and ERD efficiency were taken to be 80%, 99%, and 95%, respectively). The minimum specific energy consumption is then 3.82 kWh/m<sup>3</sup>, at 50% recovery.

As a comparison, the minimum specific energy consumption with an ERD is around 1.45 kWh/m<sup>3</sup> at 13% recovery, increasing to around 2 kWh/m<sup>3</sup> at the usual 50% recovery, so effectively the ERD reduces the SEC by almost 50%. Similar results are reported in [28].

Compared to the theoretical  $SE_{RO}$  consumption (Fig. 6.10 at 50% of recovery), the in practice two times more energy is required, as it is an irreversible thermodynamic process and the size is finite [18].

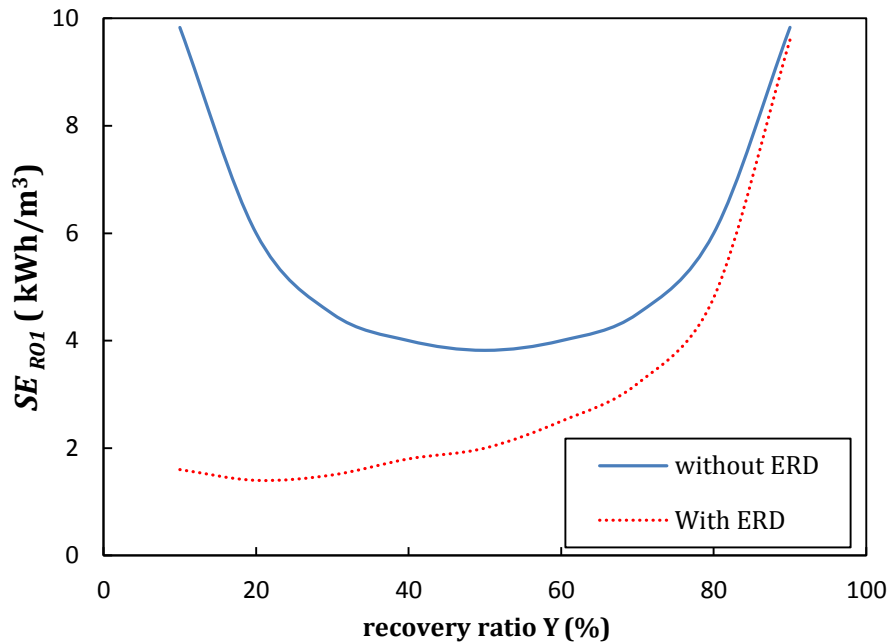


Fig. 6.16: Specific energy consumption of the first RO stage at the thermodynamic restriction, as a function of recovery (Pump efficiency, membrane salt rejection, and ERD efficiency are 80%, 99%, and 95%, respectively).

### 5.5 PRO model results

The  $SE_{PRO}$  model was investigated by studying the response of PRO sub-system after the variation of effect of operating conditions (draw and feed solution concentrations and the temperature). Modeling parameters are illustrated in Table 6.6. As it can be seen in Fig.6.17, the increase of the draw solution concentration leads to the increase of the energy recovery by the sub-system. On the other hand, the increase of the feed solution concentration is followed by the decrease of the energy. Lastly, in Fig 6.18, the increase of the draw solution temperature improves the performance of the PRO due to the improvement of the effective osmotic pressure and also the intrinsic membrane parameter such as the water permeability coefficient. These results are in agreement with the model behavior using lab-scale PRO membrane.

Fig. 6.19 illustrates the  $SE_{PRO}$  in Eq. (6.45), corresponding to the PRO system when diluting RO brine back to seawater concentration, as a function of RO recovery and PRO dilution (using the CA flat sheet membrane presented in Chapter 3): When RO recovery increases, the draw solution concentration increases, so therefore, the

PRO dilution increases. The minimum  $SE_{PRO}$  recovery is approximately 0.4 kWh/m<sup>3</sup>. This magnitude increases with RO recovery, with a maximum  $SE_{PRO}$  production of 0.72 kWh/m<sup>3</sup> at 90% of dilution. Compared to the theoretical  $SE_{PRO}$  production (Fig. 6.12), the model produces approximately half the specific energy of the ideal case, which is realistic.

Table 6.7: modeling parameters

<i>Parameter</i>	<i>IGB membrane</i>
Water permeability coefficient $A$	$1.06 \times 10^{-12}$ m/s/Pa
Salt permeability coefficient $B$	$2.62 \times 10^{-8}$ m/s
Solute resistivity $K$	$1.52 \times 10^5$ s/m
Length of the channel $L$	5 m
Width of the channel $w$	20 m
Mass transfer coefficient (draw side) $k_D$	$1.17 \times 10^{-4}$ m/s
Mass transfer coefficient (feed side) $k_F$	$1.19 \times 10^{-4}$ m/s
Diffusion coefficient in the draw solution $D_D$	$4.25 \times 10^{-9}$ m <sup>2</sup> /s
Diffusion coefficient in the feed solution $D_F$	$4.35 \times 10^{-9}$ m <sup>2</sup> /s
Porosity of the support layer $\varepsilon$	80 %
Thickness of the active layer $e$	100 nm
Thickness of the support layer $t_s$	12 $\mu$ m
Velocity average $u_0$	1 m/s
Surface of the membrane $S$	200 m <sup>2</sup>
Number of segment $N$	100

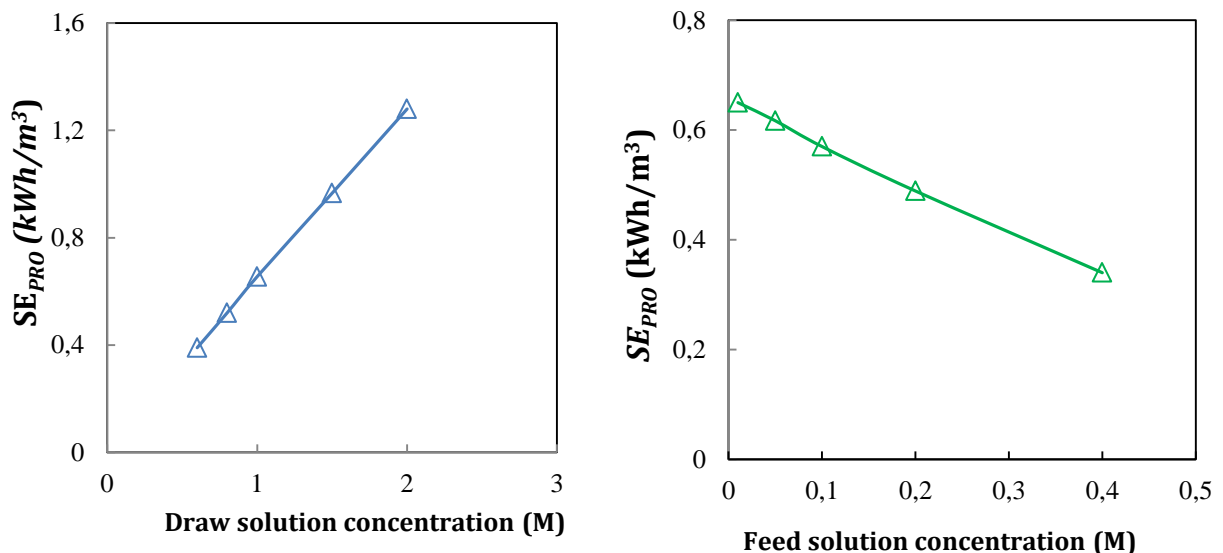


Fig. 6.17: PRO specific energy production ( $SE_{PRO}$ ) modeled as a function of feed and draw solution concentrations under optimal PRO hydraulic pressure.

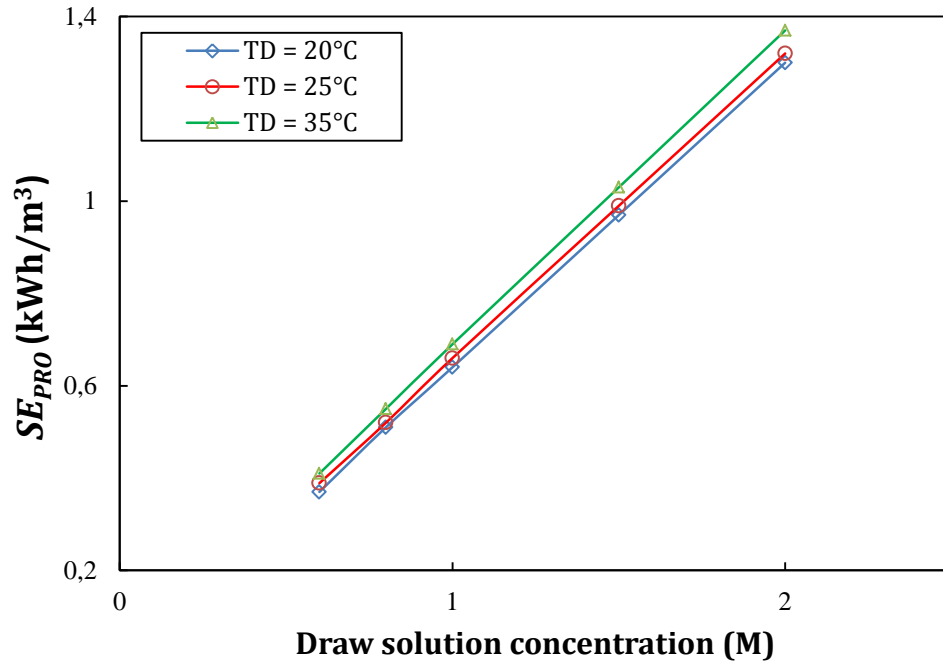


Fig. 6.18: PRO specific energy production ( $SE_{PRO}$ ) modeled as a function of feed and draw solution concentrations under optimal PRO hydraulic pressure.

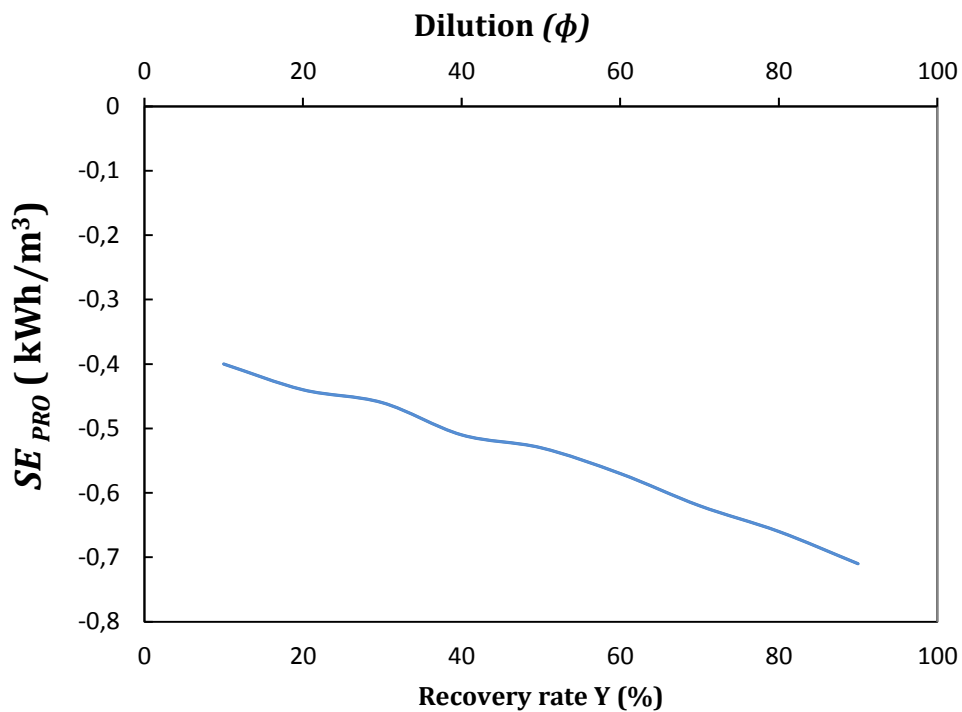


Fig. 6.19: PRO specific energy production ( $SE_{PRO}$ ) modeled as a function of dilution for the first RO-PRO integration under optimal PRO hydraulic pressure.

### 5.6 . RO-PRO model results

The total energy consumption of the RO/PRO system for both configurations is studied here. As mentioned previously, the study takes into account only the effect of the recovery ratio variation of the first RO stage, in other words, the recovery ratio of the second stage is considered constant along the study (75%).

Similarly to the RO with ERD, higher RO recoveries correspond to higher maximum  $SE_{RO}$  consumption. However, the  $SE_{RO-PRO}$  consumption decreases as PRO dilution increases, the maximum  $SE_{RO-PRO}$  consumption for the model results is remarkably very high compared to that for the ideal case. As it can be seen,  $SE_{RO-PRO}$  consumption the ideal case is much greater for the ideal case than for the model results for both configurations. This behavior is due to the fact that the ideal  $SE_{PRO}$  production is quite higher than the model  $SE_{PRO}$  production. Because of the higher starting value of the model  $SE_{RO-PRO}$  consumption and lower rate at which the model  $SE_{RO-PRO}$  consumption decreases, the model RO-PRO system is not capable to reach the energy neutrality ( $SE_{RO-PRO} = 0$ ). Consequently, operating the RO-PRO system at low RO recovery and high PRO dilution minimizes energy consumption.

The RO-PRO model results in Fig. 6.20 show a comparison of the SE values with the ideal case for the two considered RO/PRO configurations. It can be seen that for both the ideal case and the model results, the maximum  $SE_{RO-PRO}$  consumption point for each RO recovery is the point at which there is no PRO sub-system contribution (Dilution = 0). In other words, this is the maximum  $SE_{RO}$  consumption for each RO recovery. For the configuration (a), the contribution of the PRO sub-system is very limited at low  $RO_1$  recovery ratio ( $Y_1 < 20\%$ ), this is due to the low amount of rejected water issued from the second RO stage which constitutes the feed solution for the PRO sub-system. Contrary to configuration (a), the contribution of PRO is considerable at low recovery ratio because the amount of PRO feed solution is provided directly from the pretreated seawater and remains slightly constant at this range of  $RO_1$  recovery ratio ( $Y_1 < 20\%$ ).

As mentioned previously, most of the SWRO sub-systems are operating in a range of recovery ratios between 40 and 50%. In this case, the ranges of recovered energy are 11.7% to 17.9% and 16.2% to 16.5% for configurations (a) and (b),

respectively. The increase of  $Y_1$  leads to a decrease of the  $SEC_{RO-PRO}$  (case (a)). This is because a better performance of PRO due to the increase of the amount of the PRO feed solution. However, the rate of  $SEC_{RO-PRO}$  decrease in the configuration (b) seems to be slightly constant respecting to the increase of  $Y_1$ . This is due to the decrease of the amount of rejected water from  $RO_1$ . Simultaneously, the concentration of the PRO feed water decreases with the increase of  $Y_1$  because of the increase of the rejected water from  $RO_2$ , which represents a dilution factor for the PRO feed water.

For the ideal case, as presented in Fig.6.20, the increase of PRO dilution is followed by the decrease of energy consumption of the system regardless the recovery ratio  $Y_1$ . For configuration (a), the use of PX and PRO coupled to the RO sub-system, The RO-PRO system is an “energy producer system” for all rang of  $Y_1$  in the ideal case under different PRO dilutions studied. For configuration (b), the same behavior as the first configuration persists. However, when the dilution is low (e.g. 20% of dilution) the system RO-PRO system is an “energy consumer system” regardless the recovery ratio of  $RO_1$  which means that the energy produced by PRO never allows the system to reach the energy neutrality. For 50% of dilution, the system starts to produce energy near 40% of  $Y_1$ . Overall the increase of PRO dilution factor reduces the energy consumption of RO-PRO system. This result is directly related to the membrane performance. In fact, this large difference between the ideal case and the model is due to the membrane characteristics and concentration polarization. To reach high values of dilution, an improvement of the water permeability across the membrane is fundamental. Moreover, avoiding the reverse salt diffusion by reducing the salt permeability of the active layer material enhances the dilution factor. Lastly, improving the inner structure of PRO membrane support layer to reduce the effect of the internal concentration polarization and optimize the operating conditions to minimize the external concentration polarization is a challenge that can guarantee a better PRO dilution and therefore more recovered energy.

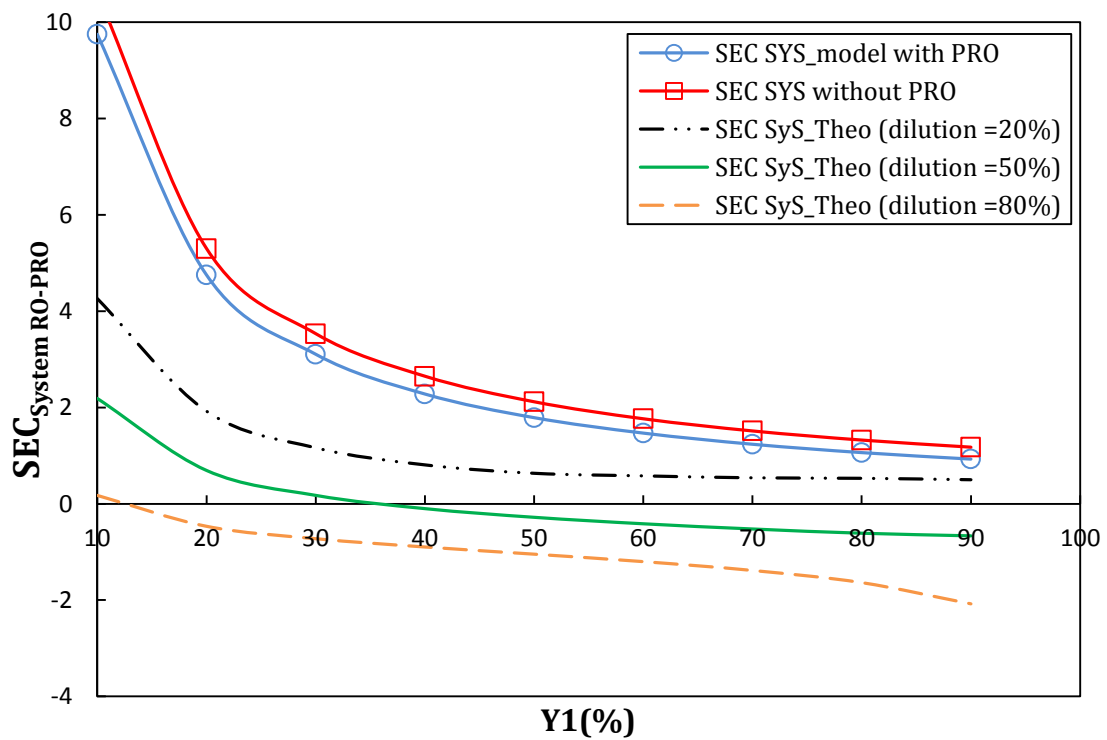
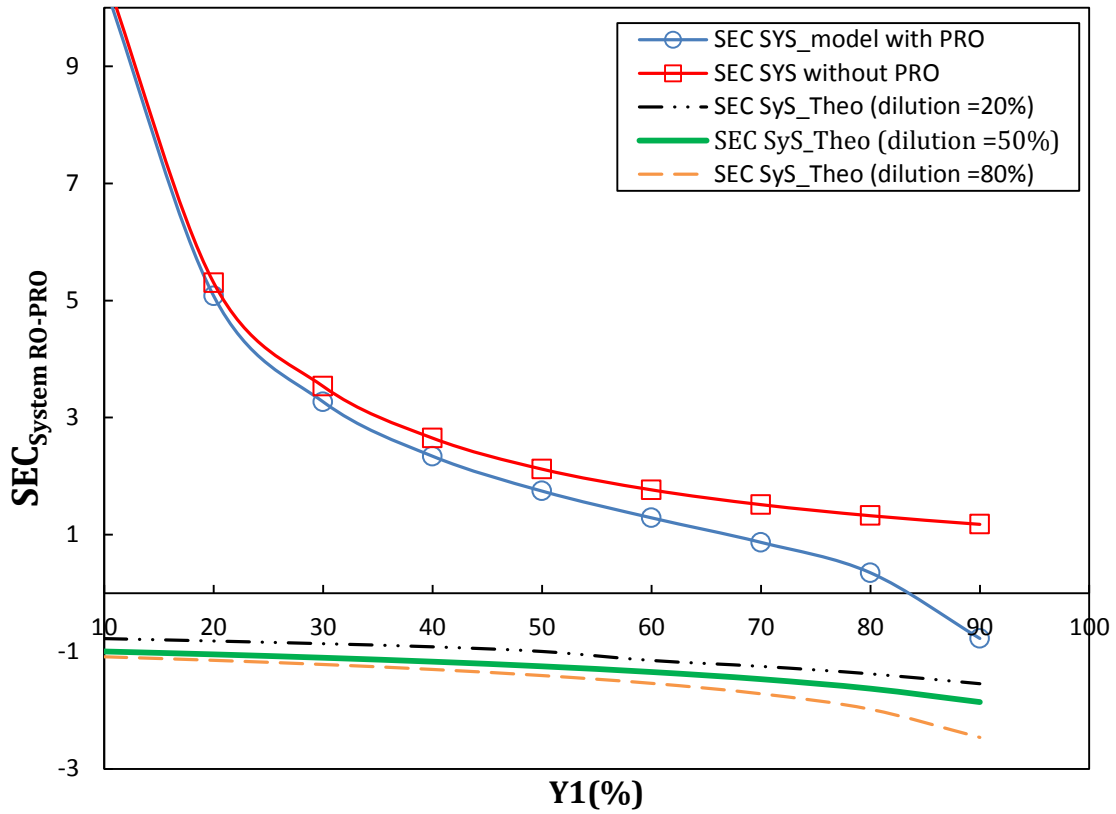


Fig. 6.20: RO-PRO specific energy as a function of RO1 recovery for different PRO dilution for both the ideal case and the model case.

## 6. Conclusions

The current chapter has studied the possibility of integrating PRO technologies for power recovery in desalination plants. Firstly, the integration of PRO within multi-effect distillation unit (MED) was investigated: Based on the Characteristics of the brine issued from the MED (high salinity and high temperature), it was seen that operating with inlet solutions with high temperatures enhances PRO performance (around 0% of the energy can be recovered at 40°C, compared with 7% at 20°C). Extrapolation of the result for non-studied values of temperatures how that using membranes that can stand with high temperature (no swelling, no collapse), the integration of PRO should be very beneficial in terms of energy production (around 14-15% at 50°C). These results, developed in Section 4, were published in *Desalination and Water Treatment Journal*: Khaled Touati, Alberto de la Calle, Fernando Tadeo, Lidia Roca, Thomas Schiestel & Diego-César Alarcón-Padilla, Energy recovery using salinity differences in a multi-effect distillation system,1-8 (2014).

The second part of this chapter deals with integration of PRO in Reverse Osmosis. Two different configurations were studied to provide adequate energy recovery. For that, a mathematical model describing the water flux in a commercial length membrane was developed. Additionally, a model reproducing the energy consumption of the system (SEC) under realistic conditions was also developed. As expected, the SEC of the RO unit using recovery energy device and PRO unit was remarkably much lower than the SEC for a stand-alone RO unit. The first RO-PRO configuration shows better performance at recommended recovery ratio for RO system (40-50%) compared to the second configuration. At low recovery ratio of the first stage, the second RO-PRO configuration achieved better performance. We expect more recovered energy for the first configuration if the feed solution is provided from outside the system due to the fact that the present feed solution is coming from the brine of the second stage which provides low amounts of water flows.

## REFERENCES OF CHAPTER 6

- [1] Muftah El-Naas H. *Reject Brine Management, Desalination, Trends and Technologies*, Michael Schorr (Ed.), ISBN: 978-953-307-311-8, (2011).
- [2] Zhou Y. *Economic Analysis of Selected Environmental Issues in China*, PhD dissertation, university of Hamburg, 2005, pp 12.
- [3] Zhang TC, Surampalli RY, Vigneswaran S, Tyagi RD, Leong Ong S, Kao CM. *Membrane Technology and Environmental Applications*, 1<sup>st</sup> ED, 2012, pp 316-317.
- [4] Schroeder E, Tchobanoglous G, Leverenz HL, Asano T. *Direct Potable Reuse: Seawater Desalination Power Consumption*, National Water Research Institute Fountain Valley, California, 2011, pp. 03.
- [5] Dawoud MA, Al Mulla MM. *Environmental Impacts of Seawater Desalination: Arabian Gulf Case Study*. *Inter. J Environ Sustainability* 2012;1(3): 22-37.
- [6] Avlonitis SA, Kouroumbas K, Vlachakis N. *Energy consumption and membrane replacement cost for seawater RO desalination plants*. *Desalination* 2003;157:151-8.
- [7] Semiat R. *Energy issues in desalination processes*. *Environ Sci Technol* 2008;42(22): 8193-8201
- [8] ARMINES. *Technical and economic analysis of the potential for water desalination in the Mediterranean region*, RENA-CT94-0063, France; 1996.
- [9] Darwish MA, Yousef FA, A-Najem NM. *Energy consumption and costs with a multi-stage flashing (MSF) desalting system*. *Desalination* 1997;109: 285-302.
- [10] Abdel-Jawad M. *Energy sources for coupling with desalination plants in GCC countries*. Report for ESCWA, September 2001.
- [11] Al-Karaghoul A, Kazmerski. *Energy consumption and water production cost of conventional and renewable-energy-powered desalination processes*. *Renew Sustain. Energy Rev* 2013;24: 343-356.
- [12] Splegler KS, El-Sayed YM. *The energetics of desalination processes*. *Desalination* 2001;134 :109-128
- [13] Dodge BF, Eshaya AM. *Thermodynamics of some desalting processes*. *Adv Chem Ser* 1960;27:7-20.

- 
- [14] Yip NY, Elimelech M. Thermodynamic and Energy Efficiency Analysis of Power Generation from Natural Salinity Gradients by Pressure Retarded Osmosis. *Environ Sci Technol* 2012;46:5230–5239.
- [15] Alarcón-Padilla DC, Blanco-Gálvez J, García-Rodríguez L, Gernjak W, Malato-Rodríguez S. First experimental results of a new hybrid solar/gas multi-effect distillation system: The AQUASOL project. *Desalination* 2008;220(1–3): 619–625.
- [16] Schiestel T. Cellulose Acetate Membranes with an Optimized Internal Structure for Pressure Retarded Osmosis. The Third Osmosis Membrane Summit, Barcelona, 2012.
- [17] Touati K, Schiestel T. Evaluation of the potential of osmotic energy as renewable energy source in realistic conditions. *Energy Procedia* 2013;42: 261–269.
- [18] Prante JL, Ruskowitz JA, Childress AE, Achilli A. RO-PRO desalination: An integrated low-energy approach to seawater desalination, *App Energy* 2014;120: 104–114.
- [19] C. Fritzmann, J. Lowenberg, T. Wintgens, T. Melin, State-of-the-art of reverse osmosis desalination. *Desalination* 2007; 216:1–76.
- [20] Danoun R. Desalination Plants: Potential Impacts of Brine Discharge on Marine Life, Technical Report, University of Sidney, 2007.
- [21] Elimelech M, Phillip WA. The future of seawater desalination: energy technology and the environment. *Science* 2011;333 : 712–717.
- [22] Peñate B, García-Rodríguez L. Energy optimisation of existing SWRO (seawater reverse osmosis) plants with ERT (energy recovery turbines): Technical and thermo-economic assessment. *Energy* 2011;36:613-626.
- [23] Lin S, Yip NY, Cath TY, Osuji CO, Elimelech M. Hybrid Pressure Retarded Osmosis Membrane Distillation System for Power Generation from Low-Grade Heat: Thermodynamic Analysis and Energy Efficiency. *Environ Sci Technol* 2014;48:5306–5313.
- [24] Zhu, A, Christofides PD, Cohen Y. Minimization of energy consumption for a two-pass membrane desalination: Effect of energy recovery, membrane rejection and retentate recycling. *J Memb Sci* 2009;339: 126–137.

- [25] Xu Y, Peng X, Tang CY, Fu QS, Nie S. Effect of draw solution concentration and operating conditions on forward osmosis and pressure retarded osmosis performance in a spiral wound module. *J Memb Sci* 2010;348: 298–309.
- [26] Banchik LD, Sharqawy MH, Lienhard JH. Limits of power production due to finite membrane area in pressure retarded osmosis, *J Memb Sci* 2014;468: 81–89.
- [27] Hoek EMV, Allred J, Knoell T, Jeong BH. Modeling the effects of fouling on full-scale reverse osmosis processes. *J Memb Sci* 2008;314: 33–49.
- [28] Gude VG, Energy Consumption and Recovery in Reverse Osmosis. *Desal and Wat Treat* 2011;36: 239–260.
- [29] [www.h2ocean-project.eu](http://www.h2ocean-project.eu).
- [30] Palacin LG, Tadeo F, De Prada C, Touati K. Evaluation of the recovery of osmotic energy in desalination plants by using pressure retarded osmosis. *Desal and Wat Treat* 2013;51(1-3):360-365.
- [31] Mbarga AA, Song L, Williams WR, Rainwater K. Integration of Renewable Energy Technologies With Desalination. *Cur Sustain/Renew Energy Reports*, 1(1), 11-18.
- [32] Wan CF, Chung TS. Osmotic power generation by pressure retarded osmosis using seawater brine as the draw solution and wastewater retentate as the feed. *J Memb Sci* 2015;479:148–158.
- [33] Palacín LG, Modelling, Simulation and advanced control of small-scale reverse osmosis desalination plants. PhD dissertation, University of Valladolid, 2014.



## Final conclusions

In this dissertation, the production of sustainable energy by Pressure Retarded Osmosis has been studied, concentrating on the development of models that make it possible to reproduce the operation of these systems in realistic conditions. These models were then verified using laboratory experiments, showing a good prediction capability. Using these models, the effects of operating conditions were investigated: in particular, concentrations, flow rates and temperatures.

In Chapter 2, the state of the art of PRO was presented. Firstly, a general theoretical background describing the different parameters affecting the process was introduced and discussed. Secondly, the evolution of the process since its inception to the present, including the PRO membrane technology progress, limitations and PRO integration, was presented and discussed. Finally, the energy production cost and the effect of the use of PRO on the environment was also studied, based on the results found during lab-scale and full-scale PRO experiments.

In Chapter 3 the impact of the temperature of the bulks on the PRO performance was studied. It has been experimentally noted that the effect of the feed solution temperature is more important than the draw solution temperature: the water and salt permeability coefficients showed a higher dependency on the feed solution temperature, and the structure parameter  $s$  significantly decreased with the temperatures. Finally, it was observed that the high water flux resulting from the increase of feed solution temperature induced a drastic draw solution diffusion which generated a severe ICP.

For the first time, a full study describing the effect of the salt flux diffusion on PRO performance was carried out in Chapter 4. For this, a model reproducing the salt flux diffusion was developed. The effects of feed and draw solution concentrations, the cross-flow velocity and temperature on this salt flux were investigated. The results showed that the increase of the feed solution concentration decreases the rate of reverse salt flux because of the reduced concentration gradient between the two membrane sides. However, this leads to a severe concentrative ICP due to the penetration of the solute in

the support layer and being blocked at the surface of the active layer, which reduces the performance of the PRO. The increase of the draw solution concentration enhances the PRO process by increasing the osmotic driving force. However, it increases the reverse salt flux. It has also been shown that operating under the AL-DS orientation is more suitable for high pressures. However, the AL-FS is recommended when feed solutions contain fouling precursors.

According to the results found in chapters 3 and 4, it was revealed that the temperature has a strong effect on the PRO process. For this, a full study of the temperature was carried out in Chapter 5 to better understand its effects. It has been theoretically and experimentally shown that the temperature affects parameters such as the diffusion coefficient, the solute resistivity, the diffusion coefficient and the osmotic pressure. Generally, operating at high temperatures enhances the water flux of the process, and consequently the power recovery. The disadvantages of high temperatures are the risk of the accumulation of salt at the surface of the membrane support layer, due to the fact that raising the temperature also leads to an increase in the salt reverse flux ( $J_s$ ), and the degradation of the membrane. These can be overcome by the development of specific high-temperature membranes with a high resistance to reverse salt flux.

The last part of this study was dedicated to evaluating the integration of PRO in desalination units for energy recovery. Two categories of desalination process were investigated; thermal desalination using a multi-effect distillation system (MED) and the membrane desalination process using a reverse osmosis unit (RO). Using MED, it was shown that the PRO is able to recover more than 15% of the energy. With RO, two integration designs were used. Both of the integration strategies showed a good performance. However, when the PRO is placed before the first stage RO, the performance was better compared to the case where the PRO is placed between the two stage brines.

As further work, several ideas should be investigated with the general aim of improving the performance of PRO:

- The existing water flux models are applicable only for “diluted” solutions (draw solutions with concentrations lower than 1.5M). These models should be modified for high concentrated solutions.
- Scaling and fouling are still not well studied in PRO. This issue should be well studied and controlled to avoid pressure losses and performance drops.
- In stand-alone PRO plants, a good pre-treatment is needed to reach the maximum performance: novel pre-treatments should be investigated.
- The use of multi -PRO stages in desalination units has not yet been investigated.

## Resumen

Ósmosis por Presión Retardada (PRO) es el proceso a través del cual la energía osmótica puede ser aprovechada para generar electricidad [6]. En un proceso típico las moléculas de agua se transportan espontáneamente a través de una membrana semi-permeable desde una corriente de baja salinidad (agua de río, agua salobre o residual) a una corriente de alta salinidad a presión (agua de mar o salmuera), con la ayuda del gradiente de presión osmótica a través de la membrana. La potencia se obtiene entonces mediante la despresurización de una porción del agua de mar diluida a través de una turbina hidráulica [7]. Se ha estimado que hasta 0,8 kWh se pueden generar usando 1 m<sup>3</sup> de agua del río y una cantidad equivalente de agua de mar.

Aunque el concepto de PRO fue mencionado por primera vez por Pattle en 1954 [9], el interés en PRO para la generación de energía comenzó en la década de 1970. El método ha mejorado significativamente en los últimos años, sobre todo después de la inauguración de la primera planta prototipo por la empresa estatal noruega Statkraft, en 2009. La planta siguió la planta propuesta por Loeb y fue diseñado para generar 10 kW [10]. La operación de la planta demostró la factibilidad de la tecnología, y los aspectos a mejorar como el rendimiento de la membrana y su durabilidad en diferentes condiciones de operación, y los efectos de la polarización de la concentración y la fuga de sal a través de la membrana.

### **Objetivos de la tesis**

Los principales objetivos del trabajo de tesis son:

1. Desarrollar un modelo del flujo de agua a través de una membrana PRO que incluya los factores limitantes del proceso, tales como la polarización de la concentración y el efecto de la fuga de sal. Este modelo se validará mediante experimentos a escala de laboratorio.

2. Desarrollar un modelo para la difusión de de sal en PRO que reproduzca el comportamiento de la difusión inversa a través de la membrana. El objetivo es caracterizar la disminución de rendimiento, y sugerir soluciones para mejores membranas PRO. Éste modelo será también validado utilizando experimentos a escala de laboratorio
3. Desarrollar un modelo para cuantificar la distribución de la temperatura en el interior de una membrana PRO, como función de las temperaturas de las soluciones, con el fin de mejorar las predicciones obtenidas a partir de los modelos de flujos de agua y sal.
4. Estudiar el efecto de condiciones realistas de funcionamiento (concentraciones, temperatura, presión, etc.) sobre el rendimiento global del proceso, realizando predicciones para el proceso global.
5. Estudiar la viabilidad de integrar PRO dentro de diferentes unidades de desalación, con el fin de mejorar su rendimiento.

### **Organización de la tesis**

Este documento consta de los siguientes capítulos:

1. El primer capítulo contiene una breve introducción que presenta la motivación, una breve discusión sobre el proceso de PRO (que será extendido en el segundo capítulo), y los objetivos de esta tesis.
2. El segundo capítulo presenta el estado del arte de PRO, desde el descubrimiento del proceso hasta la actualidad.
3. El tercer capítulo se ocupa de la elaboración de un modelo que reproduce el flujo de agua. El modelo también se valida y se utiliza para estudiar el efecto de

las condiciones de funcionamiento en el flujo de agua y, posteriormente, en la densidad de potencia.

4. El cuarto capítulo propone un modelo matemático para reproducir el flujo inverso de sales en PRO. El modelo toma explícitamente en consideración el efecto de la presión y la polarización de la concentración, tanto interna (ICP) como externa (ECP) en ambos lados de las membranas. El modelo propuesto es entonces validado y probado a escala de laboratorio. Se muestra que el rendimiento PRO se reduciría, y los costos de la energía podría ser mucho mayor de lo esperado si el flujo inverso no se controlara. Se discuten entonces las mejores condiciones del proceso.
5. En el quinto capítulo los efectos de las temperaturas de los fluidos se estudian, en particular sobre los parámetros estructurales de la membrana, y la hidrodinámica. Los resultados proporcionados por este estudio proporcionan informaciones interesantes sobre las condiciones de funcionamiento y el diseño de las membranas.
6. El sexto capítulo contiene un estudio de la integración de PRO dentro de unidades de desalación térmica (MED) y basada en membranas (RO). Especial énfasis se aplica a estudiar la viabilidad de esta integración mediante diferentes configuraciones.

## List of Acronyms

AL-DS: Active Layer facing the Draw Solution

AL-FS: Active Layer facing the Feed Solution

CA: Cellulose Acetate

CO: Carbon monoxide

CPC: staticCompound Parabolic Concentrator

CTA: Cellulose Triacetate

DEAHP: Double Effect Absorption Heat Pump

ECP: External Concentration Polarization

ERD:Energy Recovery Device

FC: Feasible Condition number

FR: Flow Rate

FO: Forward Osmosis

GHGs: Greenhouse gases

GOR: Gain Output Ratio

HTI membrane : Hydration Technologies Inc. membrane

ICP:Internal Concentration Polarization

IGB membrane:Institute for Interfacial Engineering and Biotechnology membrane

IPC: Isophthaloyl Chloride

LCOE:Levelized Cost OfEnergy

MD: Membrane Distillation

MED: Multi-Effect Distillation

MPD: m-phenylenediamine

MSF: Multi Flash Stage distillation

MVC: Mechanical Vapor Compression distillation

MVMD: Multi-stage Vacuum Membrane Distillation

NOM: Natural Organic Matter

NO<sub>x</sub>: Mono nitrogen oxides

PAN: Polyamide /Polyacrylonitrile

PES:polyethersulfone

PEI:Polyethyleneimine

PRO: Pressure Retarded Osmosis

PX: Pressure Exchanger

RED: Reverse Electrodialysis

RO: Reverse Osmosis

SEC: Specific Energy Consumption

SEM: Scanning Electron Microscope

TFC: Thin-Film Composite

TBT: Top Brine Temperature

TMC:Trimesoylchloride

WERR: Water and Energy Return Rate

WWTP:Municipal Waste Water Treatment Plant

## List Of Tables

<b>Table 2.1:</b> Theoretical extractable energy from the mixing of fresh water with saline water from different sources. ....	8
<b>Table 2.2:</b> Summary of experimental results in the literature using flat-sheet PRO membranes. ....	30
<b>Table 2.3:</b> Summary of experimental results in the literature using hollow fiber PRO membranes. ....	31
<b>Table 2.4:</b> Estimated energy production cost for different PRO power plants. ....	51
<b>Table 3.1:</b> Characteristics of 8.55 mM NaCl feed solution at different operating temperatures. ....	78
<b>Table 3.2:</b> Characteristics of two NaCl draw solutions at different operating temperatures. ....	78
<b>Table 3.3:</b> Parameters used for modeling. ....	78
<b>Table 3.4:</b> Experimental conditions. ....	78
<b>Table 3.5:</b> Comparison of the proposed PRO water flux model with previous models. ....	81
<b>Table 3.6:</b> Thermal conductivities of feed and draw solutions and IGB membrane. ....	85
<b>Table 3.7:</b> Thermal conductivity coefficients of feed and draw solutions and IGB membrane. ....	86
<b>Table 3.8:</b> Different cases of bulk temperatures and operating scenarios. ....	86
<b>Table 4.1:</b> Hydrated radius of studied ions. ....	120
<b>Table 4.2:</b> Diffusions coefficients of tested ions. ....	120
<b>Table 4.3:</b> Temperatures, water permeability, salt permeability and proportion of osmotic pressure drop under different bulk solutions temperatures. ....	123
<b>Table 4.4:</b> Effective osmotic pressure and proportion of osmotic pressure drop under different bulk solutions temperatures. ....	123
<b>Table 5.1:</b> Main characteristics of the IGB Membrane. ....	140
<b>Table 5.2:</b> Characteristics of 1M NaCl draw solution at different temperatures. ....	147
<b>Table 5.3:</b> water permeability coefficient and salt permeability coefficient B at different temperatures. ....	154
<b>Table 6.1:</b> Pressure requirements for different water concentration and desalination technics. ....	165
<b>Table 6.2:</b> Nominal operating parameters of the Aquasol MED system. ....	170
<b>Table 6.3:</b> Concentrations and temperatures of the brine in the PSA AQUASOL plant for different inlet seawater conditions. ....	171

---

<b>Table 6.4:</b> expected energy recovered using the proposed system for different seawater and feed water conditions.....	172
<b>Table 6.5:</b> Variation of the viscosity, the diffusivity, the difference of the osmotic pressure, Sherwood, Reynolds and Schmidt number.....	174
<b>Table 6.6:</b> Installed Power in each component of the Desalination Unit. ....	176
<b>Table 6.7</b> Modeling parameters.....	194

# List Of Figures

<b>Fig. 2.1:</b> Theoretically available amount of energy (MJ) from mixing 1m <sup>3</sup> of a diluted and 1m <sup>3</sup> of a concentrated sodium chloride solution (T = 293 K) .....	10
<b>Fig. 2.2:</b> Representation of water flow in FO, PRO, and RO .....	11
<b>Fig. 2.3:</b> Schematic of a PRO power plant.....	12
<b>Fig. 2.4:</b> Schematic representation of the concentration profile over the membrane .....	15
<b>Fig. 2.5:</b> Magnitude and direction of $J_w$ for FO, PRO, and RO .....	18
<b>Fig. 2.6:</b> Schematic diagram of the pilot PRO plant, constructed by Statkraft.....	22
<b>Fig. 2.7:</b> Scanning Electron Microscope photos of Cellulose acetate PRO membrane. ....	26
<b>Fig. 2.8:</b> SEM cross-section of the Polyamide/polyacrylonitrile (PAN) substrates .....	28
<b>Fig. 2.9:</b> SEM of the cross-section and surface morphologies of the PES hollow fiber .....	30
<b>Fig. 2.10:</b> Schematic of Mega-ton RO-PRO hybrid. ....	32
<b>Fig. 2.11:</b> Schematic of four RO-PRO hybrid systems proposed by Kim et al.....	33
<b>Fig. 2.12:</b> Schematic of RO-PRO hybrid adopted by Achili et al.....	35
<b>Fig. 2.13:</b> Schematic diagram of a PRO-MD hybrid system.....	36
<b>Fig. 2.14:</b> Schematic diagram of the PRO-RO system studied by Altaee et al. ....	37
<b>Fig. 2.15:</b> Schematic diagram of the FO-PRO system for combined power generation.....	38
<b>Fig. 2.16:</b> Schematic diagram of a RO-PRO hybrid system adopted by He et al.....	39
<b>Fig. 2.17:</b> Schematic diagram of the configurations proposed by He et al.....	40
<b>Fig. 2.18:</b> Schematic of the hybrid MVMD-R-PRO system proposed by Lee et al.....	42
<b>Fig. 2.19:</b> NOM Cake layer formation in the surface of PRO membrane porous layer.....	44
<b>Fig. 2.20:</b> Effect of the backwashing on reducing the NOM fouling in PRO membrane.....	45
<b>Fig. 2.21:</b> PRO scaling mechanisms. The subscript (i) refers to the precursor (i) .....	46
<b>Fig. 2.22:</b> Decrease of membrane price.....	50
<b>Fig. 3.1:</b> Concentration profile through the membrane .....	46
<b>Fig. 3.2:</b> Temperature profile over the membrane.....	46
<b>Fig. 3.3:</b> Schematic of laboratory bench-scale PRO system .....	46
<b>Fig. 3.4:</b> Simulation using Eq. (3.22) and experimental results of the water flux ( $J_w$ ). ....	80
<b>Fig. 3.5:</b> Simulation using Eq. (3.23) and experimental results of the power density ( $W$ ). ....	81
<b>Fig. 3.6:</b> Modeled and experimental power density for different Feed concentrations. ....	83
<b>Fig. 3.7:</b> Modeled and experimental power density for different Draw concentrations. ....	83
<b>Fig. 3.8:</b> Modeled and experimental power density .....	84
<b>Fig. 3.9:</b> Variation of the IGB membrane temperature with the water bulk temperature.....	86

<b>Fig. 3.10:</b> Variation of the water permeability coefficient $A$ with the bulk temperatures. ....	88
<b>Fig. 3.11:</b> Variation of the salt permeability coefficient $B$ with the bulk temperatures .....	89
<b>Fig. 3.12:</b> Variation of the structure parameter $s$ with the bulk temperatures.....	91
<b>Fig. 3.13:</b> Experimental and simulated water flux, salt flux and power density for the IGB membrane at different operation cases. ....	93
<b>Fig. 4.1:</b> Concentration profile over the PRO membrane.....	102
<b>Fig. 4.2:</b> Comparison of the results predicted by the model developed in Eq. (4.25) with the experimental results for various NaCl concentrations. ....	108
<b>Fig. 4.3:</b> Experimental Effects of the concentration of draw (b) and feed (a) solutions on the water flux $J_w$ and the salt flux $J_s$ , and comparison with the predicted $J_s$ .....	111
<b>Fig. 4.4:</b> Experimental proportion of the cause of osmotic pressure drop, as a function of the draw and feed concentrations. ....	112
<b>Fig. 4.5:</b> Effect of the cross-flow velocity on the salt flux $J_s$ and on the water flux $J_w$ .....	114
<b>Fig. 4.6:</b> Experimental proportion of the cause of osmotic pressure drop as a function of the cross flow velocity. ....	114
<b>Fig. 4.7:</b> Schematics of membrane orientations in PRO process. ....	115
<b>Fig. 4.8:</b> Effect of the membrane orientation. ....	117
<b>Fig. 4.9:</b> Experimental $J_s$ and $J_w$ for different draw solution composition.....	119
<b>Fig. 4.10:</b> Experimental and simulated salt and water fluxes (a, b), power density (c, d) and specific salt flux ( $J_s/J_w$ ) (e, f) under different draw and feed solution temperatures.....	122
<b>Fig. 4.11:</b> Distribution of the cause of the reverse salt flux in PRO as function of the applied pressure.....	125
<b>Fig. 5.1:</b> Schematic representation of the salt concentration profile, salt and water fluxes across a membrane in PRO at steady state.....	139
<b>Fig. 5.2:</b> Osmotic pressure of NaCl solutions at different temperatures and concentrations. ....	141
<b>Fig. 5.3:</b> Diffusion coefficient of NaCl solutions at different temperatures. ....	143
<b>Fig. 5.4:</b> (a) Reynolds, (b) Schmidt and (c) Sherwood numbers of NaCl solutions at different temperatures.....	147
<b>Fig. 5.5:</b> Schematic of the boundary layer at the draw solution side. ....	149
<b>Fig. 5.6:</b> Thickness of the boundary layer for NaCl solutions at different temperatures .....	149
<b>Fig. 5.7:</b> The overall mass transfer coefficient ( $k_{overall}$ ) for NaCl solutions at different temperatures.....	151
<b>Fig. 5.8:</b> The solute resistivity ( $K$ ) for NaCl solutions at different temperatures and concentrations.....	152
<b>Fig. 5.9:</b> Modeled and experimental results of the water flux $J_w$ with $K$ .....	154

<b>Fig. 5.10:</b> Modeled (lines) and experimental results (symbols) of the water flux $J_w$ .....	156
<b>Fig. 5.11:</b> Variation of the water flux $J_w$ (a), the salt flux $J_s$ (b), the power density $W$ (c), and the specific solute flux $J_s/J_w$ (d) with the temperature. ....	157
<b>Fig. 6.1:</b> AQUASOL desalination plant.....	170
<b>Fig. 6.2:</b> Schematic diagram of the AQUASOL plant.....	171
<b>Fig. 6.3:</b> Basic concept of the Pressure-Retarded Osmosis process for osmotic energy recovery from MED brines.....	172
<b>Fig. 6.4:</b> Variation of the power density with the PRO feed water temperature.....	174
<b>Fig. 6.5:</b> Estimated energy recovered for MED at different operating temperatures.....	174
<b>Fig. 6.6:</b> First Pass of Reverse Osmosis Desalination. ....	176
<b>Fig. 6.7:</b> Desalination Second Pass. ....	176
<b>Fig. 6.8:</b> conventional integration of PRO in the H2Ocean desalination plant. ....	178
<b>Fig. 6.9:</b> Simplified schematic of the coupled RO-PRO system. ....	179
<b>Fig. 6.10:</b> Specific energy consumption for the first stage at different recovery ratios. ....	182
<b>Fig. 6.11:</b> Specific energy consumption for the second stage at different recovery ratios.....	182
<b>Fig. 6.12:</b> Specific energy production for draw solution dilution in PRO at different dilution factor. ....	182
<b>Fig. 6.13:</b> RO-PRO specificenergy for different PRO dilution factor.....	183
<b>Fig. 6.14:</b> Schematic of a single segment (dSi) of a flat sheet PRO membrane module).....	186
<b>Fig. 6.15:</b> Second integration of PRO in the RO plant. ....	192
<b>Fig. 6.16:</b> Specific energy consumption of the RO <sub>1</sub> stage at the thermodynamic restriction. ....	193
<b>Fig. 6.17:</b> PRO specific energy production ( <i>SEPRO</i> ) modeled as a function of feed and draw solution concentration. ....	194
<b>Fig. 6.18:</b> PRO specific energy production ( <i>SEPRO</i> ) modeled as a function of feed and draw solution concentrations under optimal PRO hydraulic pressure. ....	195
<b>Fig. 6.19:</b> PRO specific energy production ( <i>SEPRO</i> ) modeled as a function of dilution for the first RO-PRO integration under optimal PRO hydraulic pressure. ....	195
<b>Fig. 6.20:</b> RO-PRO specific energy as a function of RO1 recovery for different PRO dilution for both the ideal case and the model case.....	198

---

## LIST OF PUBLICATIONS

The results arising from this thesis have been published in several journal articles and international conferences, which are summarized now:

### **ARTICLES**

**Khaled Touati**, Christopher Hänel, Fernando Tadeo, Thomas Schiestel, Effect of the feed and draw solution temperatures on PRO performance: Theoretical and experimental study, *Desalination*, 365(2015)182–195. (IF=3.96)

**Khaled Touati**, A. de la Calle, F. Tadeo, L. Roca, T. Schiestel, D.C. Alarcón-Padilla, Energy recovery using salinity differences in a multi-effect distillation system, *Desalination and Water Treatment*, (2014) 1–8. (IF=1.173)

**Khaled Touati**, Fernando Tadeo, Christopher Hänel, Thomas Schiestel, Effect of the operating temperature on hydrodynamics and membrane parameters in Pressure Retarded Osmosis, *Desalination and Water Treatment*, (2015) 1–13doi:10.1080/19443994.2015.1039600. (IF=1.173)

**Khaled Touati**, Fernando Tadeo, Study of the Reverse Salt Diffusion in Pressure Retarded Osmosis: influence on concentration polarization and effect of the operating Conditions. *Desalination Journal*, submitted 2015 (IF=3.96)

**Khaled Touati**, Fernando Tadeo, Pressure Retarded Osmosis for power generation: Evolution and State of the art, *Desalination*, submitted manuscript 2015 (under revision). (IF=3.96)

**Khaled Touati**, Fernando Tadeo, Theoretical investigation of the feasibility of energy recovery from two-Stage desalination system using PRO: study of two RO-PRO configurations. *Chemical Engineering Science*, 2015 (IF=2.33)

**Khaled Touati**, Fernando Tadeo, Thomas Schiestel, Impact of temperature on power recovery in osmotic power production by pressure retarded osmosis, *Energy Procedia* 50 (2014) 960 – 969.

Luis G. Palacin, Fernando Tadeo, Cesar de Prada, ***Khaled Touati***, Evaluation of the recovery of osmotic energy in desalination Plants by using pressure retarded osmosis, *Desalination and Water Treatment*, 51(2013)360–365. (IF=0.99)

***Khaled Touati***, Thomas Schiestel, Evaluation of the potential of osmotic energy as renewable energy source in realistic conditions, *Energy Procedia* 42 (2013) 261 – 269.

### **CONFERENCES**

***Khaled Touati***, FernandoTadeo, Thomas Schiestel, Pressure Retarded Osmosisto improve energy recovery in multi-stage reverse osmosis plant, *IDA World Congress 2013*, Tianjin, China, 20-25 October 2013. (Oral presentation)

***Khaled Touati***, Thomas Schiestel, Evaluation of the potential of osmotic energy as renewable energy source in realistic conditions, *The Mediterranean Green Energy Forum, MGEF-13*, Fes, Morocco, 16-20 June 2013.(Oral presentation)

***Khaled Touati***, Fernando Tadeo, Thomas Schiestel, Impact of temperature on power recovery in osmotic power production by pressure retarded osmosis,*The International Conference on Technologies and Materials for Renewable Energy, Environment and Sustainability, TMREES14*, Beirut Lebanon, 9-13 April 2014. (Oral presentation)

***Khaled Touati***, Alberto de la Calle, Fernando Tadeo, Lidia Roca, Thomas Schiestel, Diego César Alarcón, Energy recovery using salinity differences in a multi-effect distillation system, *The European Desalination Society:Desalination for the Environment, Clean Water & Energy*,Limassol, Cyprus, 11-15 May 2014. (Oral presentation)

***Khaled Touati***, Fernando Tadeo, Thomas Schiestel, Impact of temperature in pressure retarded osmosis, *1<sup>st</sup> International Symposium on Innovative Desalination Technologies with INES meeting*, Seoul, South Korea, 1-3 September 2014. (Oral presentation)

Christopher Hänel, ***Khaled Touati***, Fernando Tadeo, Thomas Schiestel. A Parameter Study with Cellulose Acetate Membranes for Pressure Retarded Osmosis,

International Membrane Science & Technology Conference, Melbourne, 2013. (Oral presentation)

Fernando Tadeo, ***Khaled Touati***, Integration of pressure retarded osmosis in energy recovery systems, *IDA World Congress 2013*, Tianjin, China, 20-25 October 2013.(Poster)

***Khaled Touati***, Fernando Tadeo, Thomas Schiestel, David Torrijos, Osmotic Energy Recovery in a multistage RO plant, *10<sup>th</sup>AEDyR International Congress*, Seville, Spain, 26-28 November 2014. (Poster)